

**Investigating the Thermal Regime of Proglacial  
Lakes and the Influence on Mass Loss of  
Glaciers in Arctic Sweden**

**Adrian Richard Dye**

Doctor of Philosophy

University of York

Environment and Geography

December 2019

# Abstract

Glaciers in contact with proglacial lakes show accelerated mass loss rates through mechanical and thermal processes (Carrivick and Tweed, 2013). An inventory of 108 proglacial lakes in Arctic Sweden is presented, results show they have increased in number and area with glacier recession since the 1950s/60s. The retreat of 24 glaciers was mapped from satellite imagery between 2010 and 2018, with the largest retreat being 126 m at a lake terminating glacier.

A common assumption persists that smaller proglacial lakes remain at a uniform 1°C. Analysis of ASTER satellite surface temperature product (AST08) data demonstrate that 11 out of the 12 largest proglacial lakes in Arctic Sweden had daytime skin surface temperatures (SST) of >4°C in August 2014. The spatial pattern of SSTs was analysed for these 12 lakes and used to form a conceptual classification of proglacial lake thermal regime by stage of deglaciation. Thermistor data of lake surface temperatures is also presented, which shows a relatively strong validation ( $n = 8$ ,  $R^2 = 0.9365$ ) of AST08 temperature data.

This thesis presents some of the first recorded proglacial lake temperatures from the front of a calving Arctic glacier, which lost 10,523 m<sup>2</sup> of ice (0.67% of area in Randolph Glacier Inventory, 2008) between 2014 and 2018. The innovative use of thermal infrared imagery at the ice front in July 2017 was supplemented with thermistor temperature surveys (using an ASV) that recorded ice proximal maximum water temperatures of 3°C and distal temperatures of 8°C. Maximum temperatures of 5°C are reported directly from the ice front during a 12 day period from July 2019, with frequent calving activity. Combined with evidence of rapid thermal undercutting and associated calving, this study provides some of the first direct evidence of proglacial lake temperatures directly impacting the retreat of an Arctic glacier.



# Contents

1. Investigating the Temperature of Proglacial Lakes and Influence on Glacier Mass Loss in Arctic Sweden .....	17
1.1 Motivation for the study .....	17
1.1.1 Thermal Evolution of Proglacial Lakes .....	19
1.1.2 The Spatial Extent and Persistence of Proglacial Lakes .....	21
1.2 Focus of the study .....	23
1.2.1 Research Aims and Objectives; .....	23
1.3 Structure of the thesis .....	24
1.3.1 Chapter 1: Introduction and Literature review .....	24
1.3.2 Chapter 2: Investigating the spatial extent of proglacial lakes and glacier retreat rates in Arctic Sweden .....	25
1.3.3 Chapter 3: Investigating Proglacial Lake Temperature in Arctic Sweden from the ASTER Satellite Temperature Product .....	25
1.3.4 Chapter 4: Quantifying Proglacial Lake Temperatures and Terminus Change of Kaskapakteglaciaren in Arctic Sweden .....	25
1.3.5 Chapter 5: Discussion and Conclusions .....	26
1.4 The Study Area in Arctic Sweden .....	27
1.4.1 Glaciers in the Study Area of Arctic Sweden .....	30
1.4.2 Climate .....	34
1.5 The Lacustrine Terminating Glacier system .....	35
1.6 Literature Review .....	39
1.6.1 Lake Terminating Glacier Evolution across Mountain Ranges .....	39
1.6.2 Influence of Proglacial Lakes on Glacier Dynamics at the Regional Scale .....	42
1.6.3 Proglacial Lake Influence on Glacier Dynamics and Calving from Field Studies .....	45
1.6.4 Studies Investigating the Thermal Regime of Proglacial Lakes .....	51
1.6.5 Proglacial Stream and Non-ice Contact Proglacial Lake Thermal Regime .....	52
1.6.6 Vertical Temperature Profile in Non-ice Contact Proglacial Lakes Regime .....	54
1.6.7 Ice Contact Proglacial Lake Thermal Regime .....	55
1.6.8 Vertical Temperature Profile in Ice contact Proglacial Lakes .....	59
1.6.9 Glacial Lake Thermal Regime on Debris Covered Glaciers in the Greater Himalaya .....	64
1.7 Summary .....	70

2	Investigating the Spatial Extent of Proglacial Lakes and Glacier Retreat Rates in Arctic Sweden .....	73
2.1	Introduction .....	73
2.2	Methodology .....	76
2.2.1	Manual Mapping of Proglacial Lake Extent from ASTER Satellite Imagery .....	78
2.2.2	Sources of Uncertainty with Manual Mapping from ASTER Satellite Imagery .....	79
2.2.3	Manual Mapping of Proglacial Lakes from Aerial Imagery .....	81
2.2.4	Mapping Glacier Terminus Change from Rapid Eye Imagery (2010 to 2018) .....	83
2.3	Results .....	84
2.3.1	Glaciers in Arctic Sweden from the Randolph Glacier Inventory (2008) .....	84
2.3.2	Proglacial Lake Inventory for Arctic Sweden from ASTER 2014 imagery .....	87
2.3.3	Variation in Geometry of Proglacial Lakes between Sub-regions .....	89
2.3.4	Analysis of Differences between Proglacial Lakes in Kebnekaise and Sarek .....	91
2.3.5	Spatial Changes in Proglacial Lakes between 1950s/60s and 2014 .....	92
2.3.6	Glacier Terminus Changes 2010 to 2018 from Rapid Eye Imagery .....	97
2.4	Discussion .....	100
2.4.1	Proglacial Lake Spatial Distribution in Arctic Sweden .....	100
2.4.2	Proglacial Lake Spatial Distribution across Sub-Regions in Arctic Sweden .....	101
2.4.3	Changes in Proglacial Lake Extent since the 1950s/1960s .....	105
2.4.4	Glacier Terminus Changes in Arctic Sweden from 2010 to 2018 .....	106
2.5	Conclusion .....	108
3	Investigating Proglacial Lake Temperature in Arctic Sweden from the ASTER Satellite Temperature Product .....	111
3.1	Introduction .....	111
3.1.1	Remote Sensing of Lake Surface Water Temperatures .....	115
3.1.2	Utilisation of ASTER Thermal Imagery over Fresh Water Bodies .....	118
3.1.3	ASTER Temperature/Emissivity Separation Algorithm used in AST05 Emissivity and AST08 Surface Temperature Products .....	122
3.1.4	Uncertainties in ASTER products (AST05 and AST08) derived from TES .....	124
3.1.5	Summary of Issues for Developing the AST08 Extraction Workflow .....	127
3.2	Methodology .....	128
3.2.1	Application of Proglacial lake (PGL) polygons and margin buffer .....	129
3.2.2	ASTER Surface Temperature Product (AST08) for Proglacial Lake Skin Surface Temperature (SST <sub>L</sub> ) Analysis .....	131

3.3	Validation of AST08 SST Against Lake Near Surface Temperatures .....	134
3.4	Results .....	136
3.4.1	Validation of AST08 Skin Surface Temperatures Against Lake Near Surface Temperatures.....	136
3.4.2	Surface Air Temperatures from Tarfala AWS (1996 to 2018).....	138
3.4.3	Skin Surface Temperatures (SST <sub>L</sub> ) for Proglacial Lakes in Arctic Sweden from AST08 Temperature Product in 2014 .....	138
3.4.4	Skin Surface Temperature (SST <sub>L</sub> ) for Ice-Contact and Non-Ice Contact Proglacial Lakes in Arctic Sweden .....	140
3.4.5	Skin Surface Temperature (SST <sub>L</sub> ) for Ice Contact Proglacial Lakes .....	142
3.4.6	Skin Surface Temperature (SST <sub>L</sub> ) for Non-Ice Contact Proglacial Lakes .....	143
3.5	Discussion .....	143
3.5.1	Analysis of Spatial Pattern of Skin Surface Temperature of Ice Contact Proglacial lakes (SST <sub>L</sub> case study).....	146
3.5.2	Analysis of Spatial Pattern of Skin Surface Temperature of Non- Ice Contact Proglacial lakes (SSTL case study).....	152
3.5.3	Discussion of Proglacial Lake SST <sub>L</sub> by Stage of Deglaciation .....	159
3.6	Conclusion.....	162
4	Quantifying Proglacial Lake Temperatures and Terminus Change of Kaskapakteglaciaren in Arctic Sweden.....	164
4.1	Introduction .....	164
4.2	Study Sites .....	168
4.3	Methodology .....	172
4.3.1	Meteorology.....	173
4.3.2	Lake Water Temperature and Light Intensity.....	174
4.3.3	Lake Water Skin Surface Temperature (SST) from Thermal Infrared Surveys during Fieldwork in 2017.....	177
4.3.4	Lake Water Temperature During Fieldwork in 2019 .....	179
4.4	Results .....	180
4.4.1	Mapping of Kaskapakteglaciaren Past Terminus Positions.....	180
4.4.2	Kaskapakteglaciaren Terminus Geometry Change during Fieldwork in 2017 .....	183
4.4.3	Meteorology during 2017 fieldwork.....	186
4.4.4	Outlet Lake Water in situ Temperature during Fieldwork in 2017 .....	188
4.4.5	Outlet Lake Water Spatial Temperature Survey.....	191

4.4.6	Near Terminus Lake Water in situ Temperature and Light Intensity during 2017 Fieldwork .....	194
4.4.7	Terminus Lake Water Temperature Spatial Surveys.....	196
4.4.8	Kaskapakteglaciaren Terminus Change during Fieldwork in 2019 .....	206
4.4.9	In Situ Lake Water Temperatures from the Calving Front during 2019 .....	208
4.5	Discussion .....	209
4.5.1	Proglacial Lake Water Temperatures near the Outlet.....	209
4.5.2	Proglacial Lake Water Temperatures around Icebergs.....	211
4.5.3	Proglacial Lake Water Temperatures near Kaskapakteglaciaren Terminus.....	213
4.5.4	Changes in Kaskapakteglaciaren Terminus Position and Geometry .....	216
4.5.5	Wider Implications for Proglacial Lake Temperatures and Recommendations for Future Study.....	219
4.6	Conclusion.....	221
5	Discussion and Conclusions.....	223
5.1.1	Objective 1: Create a proglacial lake inventory for Arctic Sweden and analyse the spatial pattern of proglacial lakes (Chapter 2) .....	224
5.1.2	Objective 2; Investigate the change in proglacial lake extent through time (Chapter 2) .....	225
5.1.3	Objective 3; Investigate the patterns in glacier retreat rates in Arctic Sweden (Chapter 2) .....	226
5.1.4	Objective 4: Analyse skin surface temperatures of proglacial lakes across Arctic Sweden (Chapter 3).....	227
5.1.5	Objective 5: Assess the relationship between patterns in proglacial lake skin surface temperature and factors affecting thermal regime of each proglacial lake (Chapter 3) .....	228
5.1.6	Objective 6: Measure spatial pattern of near surface temperature across a proglacial lake (Chapter 4).....	228
5.1.7	Objective 7: Measure water surface temperatures directly at the glacier-lake contact point (Chapter 4).....	229
5.2	Conclusions .....	230
A.	Appendix .....	236
1.	Automated Mapping of Proglacial Lakes from Remote Sensing .....	236
2.	Automated Detection of Proglacial Lake Extent with Sentinel 2 Multi-spectral Satellite Imagery .....	237
3.	Proglacial Lake Inventory of Arctic Sweden.....	239
4.	Spatial changes in proglacial lakes between 1950s/60s and 2014.....	242
5.	Glacier terminus changes in Arctic Sweden from 2010 to 2018.....	243
6.	Emissivity Values over Proglacial Lakes from AST05.....	244

7.	Spatial Pattern of Skin Surface Temperature of Ice Contact Proglacial lakes.....	246
8.	Spatial Pattern of Skin Surface Temperature of Non- Ice Contact Proglacial Lakes 248	
List of References .....		250

# Figures and Tables

Figure 2.2.1 A. Schematic of proglacial lakes in basins formed as a glacier retreats. Adapted from Carrivick and Tweed (2013). .....74

Figure 2.2.2 Satellite image from ASTER of Kaskapakteglaciaren proglacial lake (PGL<sub>ID</sub>24, 132,172 m<sup>2</sup>). .....79

Figure 2.2.3 ASTER false colour composite (R,G, NIR, 15 m resolution) satellite image (8/8/2014) of Arctic Sweden, with overlay of panchromatic aerial imagery (1950s/1960s) (Lantmateriet).....82

Figure 2.2.4 Rapid Eye multispectral satellite image (5 m resolution) from 27/7/2010.....83

Figure 2.2.5 ASTER digital elevation model (GDEM) (8/8/2014) for Arctic Sweden, with hill shading 85

Figure 2.2.6 Polar plot of glacier areas (radius scale m<sup>2</sup>) against glacier aspect (angle) for 252 glaciers in the study area (Arendt et al., 2012). .....86

Figure 2.2.7 Scatter plot of Proglacial lake area (August 2014).....87

Figure 2.2.8 Frequency distribution plot of proglacial lake area (m<sup>2</sup>). .....88

Figure 2.2.9 a. Plot of glacier aspect (from RGI, 2008) for each of 104 proglacial lakes (Arendt et al., 2012).. .....89

Figure 2.2.10 Proportional bubble plot for proglacial lake area (m<sup>2</sup>) across Arctic Sweden manually mapped from ASTER satellite imagery .....90

Figure 2.2.11 Box and Whisker plot of proglacial lake area on 8<sup>th</sup> August 2014 for the Northern study area (Green) and Sarek area (red).. .....92

Figure 2.2.12 ASTER false colour composite (R,G, NIR, 15 m resolution) satellite image (8/8/2014) of Arctic Sweden.....93

Figure 2.2.13 Plot of proglacial lake area from mapping of ASTER satellite imagery (8<sup>th</sup> August 2014; light blue) and historical aerial imagery (1957 to 1963; dark blue). .....94

Figure 2.2.14 a. Aerial image (Lantmateriet, 1960) of Riukojekna plateau icefield (Sweden) showing 1960 proglacial lake outline . .....95

Figure 2.2.15 a. Aerial image (Lantmateriet, 1959) of Kaskapakteglaciaren (Sweden) showing 1959 proglacial lake outline. ....96

Figure 2.2.16 Plot of glacier terminus position change between 2010 to 2018 from Rapid Eye (5 m) multispectral satellite imagery. ....97

Figure 2.2.17 Rapid Eye multispectral satellite image (5 m resolution) from 27/7/2010.....98

Table 2.2.1 Summary statistics for retreat of 24 glaciers in Arctic Sweden from Rapid Eye (5 m) imagery mapping from 2010 and 2018.....	99
Figure 2.2.18 Satellite image from Digital Globe 30/8/2014 of Sarek area (courtesy of Google Earth). 102	
Figure 2.2.19 Satellite image from Digital Globe 25/8/2014 of corrie glaciers with prominent terminal moraine systems.....	103
Figure 2.2.20 Satellite image from Digital Globe 25/8/2014 of Marmapakte area (courtesy of Google Earth).....	104
Figure 3.1 ASTER satellite composite (Green, Red, NIR) image showing location of the 12 proglacial lakes (Arctic Sweden). ....	113
Figure 3.2 Diagram showing Earth’s global annual mean energy budget ( $W m^{-2}$ ) for the March 2000 to May 2005 period from Trenberth and Fasullo (2011).....	116
Figure 3.3 ASTER bands superimposed on model atmosphere transmission. ....	118
Emissivity of different surfaces, from Sabol et al.(2009) .....	123
Figure 3.4 The regression line used in the TES algorithm (Gillespie et al., 1998) to scale emissivities (from Sabol et al., 2009). ....	123
Figure 3.5 Diagram of workflow for extracting Skin Surface Temperatures (SST) for proglacial lakes ( $SST_L$ ) from ASTER surface temperature product. ....	129
Figure 3.6 Schematic illustrating the selection of AST08 surface skin temperatures from pixels that have a high confidence (95%) of being purely from water. ....	130
Figure 3.7 a. A composite (Green, Red and VNIR, 15 m resolution) ASTER image of proglacial lake 3, with alphanumeric numbering system for each 90 m pixel over layed across the lake. 132	
Figure 3.8 a. AST05 band 11 emissivity product image (8/8/2014) over Arctic Sweden. 133	
Figure 3.9 Satellite image (courtesy of Google Earth) over Arctic Scandinavia with location of Kilpisjarvi lake.....	134
Table 3.1 Data points compiled for this survey for validation of the AST08 temperature product. ....	136
Figure 3.10 Validation of AST08 surface skin temperatures plotted against contemporaneous near surface in situ lake water temperatures.. ....	137
Figure 3.11 Hourly average air temperatures ( $^{\circ}C$ ) at Tarfala research centre from an automated weather station (SMHI) for 1996 to 2018.. ....	138
Table 3.2 Summary table of the 12 largest proglacial lakes from the inventory .....	139

Figure 3.12 Plot of SST <sub>LAV</sub> for each proglacial lake from AST08 analysis (8/8/2014) against aspect of parent glacier (RGI) (Arendt et al., 2015)..	140
Figure 3.13 Pixel surface skin temperatures extracted from AST08 temperature product image from 10:16 AM on 8/8/2014.	141
Figure 3.14 Box and whisker plot of lake surface water temperatures extracted from AST08 temperature product pixels over Arctic Sweden on 8/8/2014.....	142
Figure 3.15 Proglacial Lake 12 a. ASTER satellite composite image and b. ASTER surface temperature product image (AST08) on 8/8/2014.	147
Figure 3.16 Proglacial Lake 6 a. ASTER satellite composite image and b. ASTER surface temperature product image (AST08) on 8/8/2014.	149
Figure 3.17 Proglacial Lake 3 a. ASTER satellite composite image and b. ASTER surface temperature product image (AST08) on 8/8/2014.	151
Figure 3.18 Proglacial Lake 7 a. ASTER satellite composite image and b. ASTER surface temperature product image (AST08) at on 8/8/2014..	153
Figure 3.19 Proglacial Lake 5 a. ASTER satellite composite image and b. ASTER surface temperature product image (AST08) on 8/8/2014.	155
Figure 3.20 Proglacial Lake 8; a. ASTER satellite composite image and b. ASTER surface temperature product image (AST08) on 8/8/2014.	156
Figure 3.21 Proglacial Lake 9 a. ASTER satellite composite image and b. ASTER surface temperature product image (AST08) on 8/8/2014.	157
Figure 3.22 Proglacial Lake 2 a. ASTER satellite composite image and b. ASTER surface temperature product image (AST08) on 8/8/2014.	158
Figure 3.23 Schematic of proglacial lake thermal regime by stage of deglaciation showing a. Emergent proglacial lake. b. Transitional proglacial lake. c. Established proglacial lake. d. Dominant proglacial lake.....	159
Figure 4.1 A. Image of Perito Moreno glacier front and proglacial lake (Brazo Rico). B. Thermally eroded notch from Minowa et al. (2017).....	165
Figure 4.2 Schematic in plan view illustrating the common assumption that proglacial lakes are a uniform 1°C.	166
Figure 4.3 Schematic in plan view illustrating the working hypotheses of near surface water temperature patterns across a proglacial lake during the melt season..	167
Figure 4.4 Location of study sites in Arctic Scandinavia	169
Figure 4.5 Satellite image (DigitalGlobe: 10/8/2013) of Kaskapakteglaciaren.....	170

Figure 4.6 Aerial image of Kaskapakteglaciaren taken from a helicopter in 1981 ( <a href="http://www.bolin.su.se">www.bolin.su.se</a> ) .....	171
Figure 4.7 Image of Norra Kaskapakteglaciaren taken from the slopes of Norra Kaskasapakte on 4/8/2017. ....	171
Figure 4.8 Satellite image (July 2016) of Kaskapakteglaciaren, Arctic Sweden.....	173
Figure 4.9 Validation of Kestrel 5500 with Campbell CR800 Automatic Weather Station (AWS) on 24/7/2017. Photo: Tom Sloan.....	174
Figure 4.10 The remote controlled boat with HOBO thermistors that was used for surface temperature surveys. ....	175
Figure 4.11 HOBO thermistor data from the 27 <sup>th</sup> July (midday) survey. ....	176
Figure 4.12 Timelapse image (GoPro Hero4) taken from the terminus survey position (Tr) showing prominent landforms used for spatial plotting of temperature data. ....	177
Figure 4.13 Conducting a preliminary thermal infrared survey from ‘Owl’s nest’ position on the eastern lateral moraine Photo: Tom Sloan (24/7/2017). ....	179
Figure 4.14 A GoPro (Hero4) image of Kaskapakteglaciaren terminus taken from an ASV survey on the proglacial lake at on 6/8/2019 .....	180
Figure 4.15 a. Aerial image (Lantmateriet, 1959) of Kaskapakteglaciaren (Sweden) showing 1959 proglacial lake width.....	181
Figure 4.16 Previous terminus positions of Kaskapakteglaciaren and proglacial lake, Arctic Sweden..	182
Figure 4.17 Time lapse image of Kaskapakteglaciaren (looking south west) taken from LtL Acorn 5210a camera on 25/7/2017. ....	183
Figure 4.18 Time lapse images of Kaskapakteglaciaren (looking south west) taken from LtL Acorn 5210a camera on 26/7/2017. ....	184
Figure 4.19 Time lapse images of Kaskapakteglaciaren (looking south west) taken from LtL Acorn 5210a camera .....	185
Figure 4.20 Image from GoPro Hero4 camera from remote controlled boat survey of Kaskapakteglaciaren, Arctic Sweden (A.Dye, 4/8/2017) .....	186
Figure 4.21 Record of air temperature from the CR800 Campbell Automatic Weather Station (AWS) installed at the outlet survey position. ....	187
Figure 4.22 Record of average incoming solar radiation from the CR800 Campbell Automatic Weather Station (AWS) installed at the outlet survey position. ....	188
Figure 4.23 Temperature data (black) and light intensity data (blue) from HOBO thermistors situated at the outlet (Ot) survey position. ....	189

Figure 4.24 Optical image (GoPro Hero4) of outlet iceberg survey at 11:09pm.....	192
Figure 4.25 Thermal images from the FLIR A65 survey conducted from the outlet survey position on 27/7/2017.....	193
Figure 4.26 Temperature data (black) and light intensity data (blue) from HOBO thermistors situated at the terminus (Tr) survey position .....	195
Figure 4.27 Plan of boat temperature survey routes and associated dates. ....	197
Figure 4.28 Plot of temperature measurements from HOBO thermistor (20156968) suspended from the remote control boat from 25/7/2017.....	198
Figure 4.29 Thermal images from the FLIR A65 survey conducted from the terminus survey position on 24/7/2017.....	199
Figure 4.30 Images taken on 25/7/2017 from the terminus survey position.....	201
Figure 4.31 Plot of temperature measurements from HOBO thermistor suspended from the remote control boat on 25/7/2017 .....	202
Figure 4.32 Plot of temperature measurements from HOBO thermistor suspended from the remote control boat on 27/7/2017. ....	203
Figure 4.33 Plot of temperature measurements from HOBO thermistor suspended from the remote control boat on 27/7/2017. ....	204
Figure 4.34 Plot of temperature measurements from HOBO thermistor suspended from the remote control boat from 3/8/2017.. ....	205
Figure 4.35 Image (Panasonic Lumix DMC-TZ57) of Kaskapakteglaciaren taken shortly (minutes) after a calving event on 6/8/2019.....	206
Figure 4.36 Series of images (Panasonic Lumix and iPod Touch) taken at the top of the subaerial ice cliff above the temperature buoy showing crack development. ....	207
Figure 4.37 Image (Panasonic Lumix DMC-TZ57) of Kaskapakteglaciaren on 11/8/2019 (10:04AM). ....	207
Figure 4.38 Temperature and light intensity record from HOBO suspended from Kaskapakteglaciaren terminus between 29/7/2019 to 10/8/2019.....	208
Figure 4.39 Image from GoPro Hero4 camera of Norra Kaskasapakte glaciär, Arctic Sweden (A.Dye, 4/8/2017). ....	218
FigA.1 Summary of initial steps used in lake classification of a Sentinel 2 image from 16/8/2016. ....	237
FigA.2 Summary of steps involved in delineating proglacial lake areas. Steps common to all imagery are combined and have a grey background. Important datasets are in bold text (modified from Hanshaw and Bookhagen, 2014). ....	238

Table A1: Proglacial lake inventory for Arctic Sweden from manual mapping of ASTER satellite (15 m) imagery from 8/8/2014. ....	241
FigA.3 Top aerial image (Lantmateriet, 1959) of Vaktposten glaciär showing 1959 proglacial lake outline (black).....	242
FigA.4 Rapid Eye multispectral satellite image (5 m resolution) from 27/7/2010 with interpretation of corrie glacier width mapping. ....	243
FigA.5 a. AST05 band 11 emissivity product image over Arctic Sweden (8/8/2014),.....	244
FigA.6 Proglacial Lake 11 ASTER satellite composite image and ASTER surface temperature product image (AST08) on 8/8/2014. ....	247
FigA.7 Proglacial Lake 4 ASTER satellite composite image and ASTER surface temperature product image (AST08) on 8/8/2014. ....	247
FigA.8 Proglacial Lake 1 ASTER satellite composite image and ASTER surface temperature product image (AST08) on 8/8/2014. ....	247
FigA.9 Proglacial Lake 10 ASTER satellite composite image and ASTER surface temperature product image (AST08) on 8/8/2014. ....	248

# Acknowledgements

Meeting the right people in life at the right times can open doors and steer you into exciting uncharted waters. I have been very lucky throughout my PhD and met a large number of people who have helped make this project what it is, as well as being fortunate enough to know the people that I call friends and family. I have also met a large number of people who have supported and inspired me, particularly the PEGRG research group. First of all I would like to thank my supervisors Dave Rippin and Robert Bryant as well as Roland Gehrels, who have supported, inspired and most of all guided me throughout the project. Dave has been fantastic throughout the project and his regular marathon meetings have provided endless support and guidance, particularly during the difficult period following badly breaking my ankle. Rob has been a pillar of inspiration on many occasions and I am forever indebted to him for coming out to Norway to develop the method for using the thermal infrared camera at cold damp times in the middle of the night.

I have been fortunate enough to have a highly dependable support team for undertaking two field seasons on a glacier that previously nobody had worked on. My main field assistant and father has been a constant source of inspiration and also perhaps my most valued critic whose insights have helped to shape the project. Thank you to my ice twin Fran Falcini, who has been so influential throughout my PhD by providing guidance and support with endless patience. Both Fran and Tom (who is worth two people in the field) endured a particularly challenging period of fieldwork (tent bound for several days), whilst still remaining up beat and driving the project on through the rain. I'm fortunate enough that my partner Amy has supported me through the project and also been prepared to dig in when it was needed despite conditions that would turn most people back, particularly through snow, ice and wind when we retrieved the equipment in September 2019. Her support has been invaluable, as has the support of my family and friends, particularly my mother who has supported me organising the field seasons. The staff at Tarfala Research Centre have also provided excellent support whenever needed. Matthew Griffin has provided inspiration on many occasions and assisted driving the equipment back through Scandinavia in my van. Emma Dodd has been an endless source of knowledge and advice on the utilisation of satellite thermal imagery. Thankfully Masahiro Minowa et al. and Georgiy Kirillin provided valuable lake temperature data for validation, as well as guidance on the wonders of lake circulation.

# **Declaration**

I declare that this thesis is a presentation of original work and I am the sole author. This work has not previously been presented for an award at this, or any other, University. All sources are acknowledged as References.

# 1. Investigating the Temperature of Proglacial Lakes and Influence on Glacier Mass Loss in Arctic Sweden

## 1.1 Motivation for the study

Glaciers are sensitive to changes in climate and have generally retreated in most mountain areas since the Little Ice Age cold period finished between 1850 to 1920 (IPCC AR5, 2013). As glacier terminus positions retreat back due to increased mass loss, topographic basins can be produced due to moraine dams and/or high rates of subglacial erosion, where proglacial lakes may form (Carrivick and Tweed, 2013). Where proglacial lakes are in contact with glacier termini, periods of enhanced mass loss rates through thermo-mechanical processes have been shown to be controlled by changes in lake conditions (Warren and Kirkbride, 2003; Haresign and Warren, 2005; Boyce et al., 2007; Tsutaki et al., 2013; Minowa et al., 2017; Mallalieu et al., 2020; Watson et al., 2020). Such elevated rates of mass loss have been observed in the Himalaya, Alaska, Patagonia and New Zealand, where glacier termini have also had thermally eroded notches (Figure 1.1) at the waterline (Skvarca et al., 1995; Warren and Kirkbride, 1998; Boyce et al., 2007; Sakai et al., 2009; Minowa et al., 2017). This thermal erosion of the glacier front suggests that proglacial lake temperatures can be high enough to enhance subaqueous melt of the terminus and also undermine the stability of the ice cliff, which leads to ice berg calving events (Kirkbride, 1993; Kirkbride and Warren, 1997; Roehl, 2006; Minowa et al., 2017).

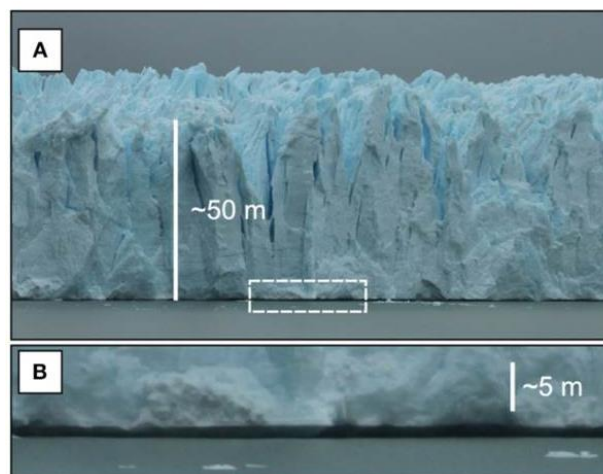


Figure 1.1 A. Photograph from 5/1/2013 showing a section of the Glaciar Perito Moreno front and proglacial lake, Patagonia. B. Thermally eroded notch, which extends back 1 to 2 m. From Minowa et al. (2017).

Despite the evidence of thermal erosion on glacier termini, constraining the thermal influence of proglacial lakes on glacier retreat has received relatively little attention, largely due to problems of accessing the hazardous ice cliff (Warren and Kirkbride, 2003; Carrivick and Tweed, 2013). There also still exists a common assumption that ‘small’ proglacial lakes remain a uniform 1°C, largely due to cooling from ice contact and meltwater (Chernos et al., 2016; Truffer and Motyka, 2016). Given the observations of thermal erosion on glacier termini and enhanced retreat rates across proglacial lakes, it is important to test this assumption that proglacial lakes remain a relatively cold 1.0°C (Chernos et al., 2016; Truffer and Motyka, 2016). Furthermore, warming trends of up to 0.1°C yr<sup>-1</sup> have been reported in large lakes in the Northern Hemisphere from satellite thermal imagery between 1985 to 2009, which suggests proglacial lake temperatures may have also increased (Schneider and Hook, 2010). It is important to test whether ice-contact proglacial lakes remain a uniform 1°C, particularly given Arctic Amplification of climate change (Serreze and Francis, 2006). Annual Arctic air temperatures have been reported to be warming at rates of 1.7 times the Northern Hemisphere average between 1971 to 2017 (Box et al., 2019). Therefore it is important to constrain Arctic proglacial lake temperatures, particularly as they may also have effects on temperature dependent species (such as salmonids) in downstream river ecosystems (Fellman et al., 2014).

It is essential to capture changes in proglacial lake surface temperatures as water is a more effective store of heat than air and more importantly water conducts heat more efficiently (Surdu et al., 2014). Consequently glaciers in contact with a body of warm water may have higher melt rates than glaciers just in contact with air, as the water stores and transmits heat to the ice surface more effectively (Sugiyama et al., 2016). Indeed both the studies of Warren and Kirkbride (2003) and Minowa et al. (2017) report a strong positive correlation between proglacial lake temperatures and rates of ice loss at calving fronts. It is important to note that water movements (e.g. waves) and currents can be a strong control on the thermal erosion rate of the glacier front (Roehl, 2006). Therefore the relationship between proglacial lake characteristics and glacier mass changes requires further investigation and is the focus of this study.

### 1.1.1 Thermal Evolution of Proglacial Lakes

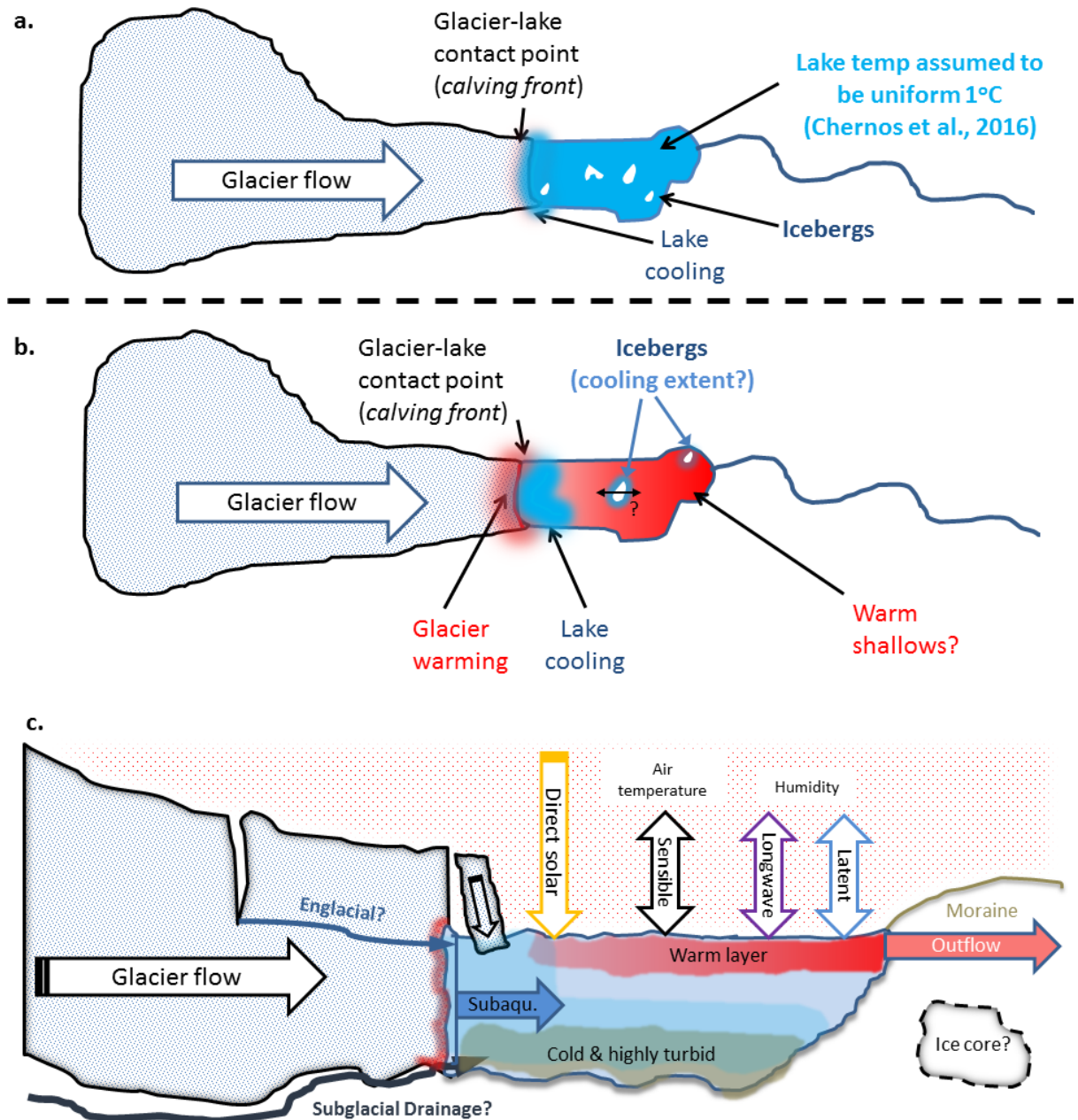


Figure 1.2 Schematic showing a. plan view of the general assumption that proglacial lakes remain a uniform 1°C (top) (Chernos et al., 2016; Truffer and Motyka, 2016). b. The working hypothesis of the proglacial lake thermal regime being in a state of dynamic equilibrium (red = warm, blue = cold). c. Side view of the main mass and energy fluxes in the proglacial lake (ice-contact) system. Where pink indicates theoretical warmer surface layers (epilimnion) and brown represents colder bottom layers (hypolimnion) with high suspended sediment load (high turbidity). There is a theoretical layer of water in between (metalimnion) and sharp boundaries (thermocline), which may be less distinct. Subaqu. = subaqueous melt derived water. Note that there will also be direct input of subaerial meltwater but this is not shown for simplicity.

When considering the thermal evolution of proglacial lakes, it is essential to consider the energy fluxes in the system, as well as mass fluxes through the system. This section will first of all introduce the warming influences acting on proglacial lakes and then the cooling influences, in order to theoretically explore the spatial pattern of each. The main drivers of the proglacial lake thermal regime situation are considered first, which could be considered to be the more spatially immobile influences, before considering the more spatially dynamic processes. Both the energy and mass fluxes in the proglacial lake system may also contribute and interact with water circulation, which may in turn change the spatial pattern of proglacial lake temperatures and is considered later on in this section. A more detailed exploration of factors controlling proglacial lake thermal regime is given in the Literature review (section 1.6.5 onwards).

The main factors controlling warming of proglacial lakes are solar radiation penetrating the water surface layers and air temperatures potentially warming the surface (Chikita et al., 1999; Richards et al., 2012; Peter and Sommaruga, 2017). The solar warming of proglacial lake water is likely to be highly influenced by surrounding topography, where mountainous relief may create substantial areas of shading and therefore reduce input of direct short wave solar radiation on some areas of the lake (for varying lengths of time) (Richards et al., 2012). The variation in warming influence (through sensible heat transfer) of air temperatures across the lake is likely to be more spatially uniform, although shading may still influence air temperature and cold air is likely to persist near the cooling influence of the glacier terminus (Aubry-Wake et al., 2015). There will also be incoming longwave radiation warming the top millimetre of lake water, as well as longwave radiation being emitted by the lake water (Aubry-Wake et al., 2015). Therefore the warming factors acting on the lake water are unlikely to be spatially uniform, thus raising the possibility that temperatures across proglacial lakes are unlikely to be uniform where they are large enough to have substantial variations in topo-climatic conditions around the perimeter.

Where proglacial lakes are long enough the distal end may be beyond this cooling influence and result in higher water temperatures due to meteorological warming, resulting in a temperature gradients across the lake (Figure 1.2)(Warren and Kirkbride, 1998). Therefore the outlet streams from proglacial lakes may represent a substantial flux of heat out of the system, particularly when there is a substantial export of mass from them during periods of high flow (Richards et al., 2012). It should also be noted that rainfall events may present substantial influxes of mass into the proglacial lake system and the heat flux associated with

this input is yet to be constrained. There will also be Latent heat fluxes occurring due to the condensation of atmospheric water vapour and also evaporation of lake water (Richards et al., 2012).

Where water bodies of different temperatures exist within proglacial lakes, they may be re-distributed through circulation processes (driven by wind or density differences) (Warren and Kirkbride, 1998; Chikita et al., 1999). This may be due to vertical mixing in the water column, as surface water that has been warmed to the density maximum (3.98°C) may sink if it is more dense than the water column below (Chikita, et al., 1999). However, crucially the suspended sediment concentration of proglacial lake water may also be sufficiently high to inhibit this vertical overturning process of the water column (Chikita et al., 1999). Water bodies may also be re-distributed horizontally through lake circulation and wind-driven processes (Chikita et al., 1999; Sakai et al., 2009). Thus a complicated temperature structure *may* exist across proglacial lakes, which is highly likely to change through time (Warren and Kirkbride, 1998).

The balance of warming and cooling factors is unlikely to remain static through the melt season, due to changing meteorological conditions affecting warming of the water and input of meltwater (Warren and Kirkbride, 1998; Chikita et al., 1999; Richards et al., 2012; Peter and Sommaruga, 2017). So not only are proglacial lake temperatures likely to change, but the spatial pattern of warmer and cooler bodies of water will change (Warren and Kirkbride, 1998; Chikita et al., 1999). This change in spatial pattern of water temperatures is particularly likely where lakes are large enough to develop circulation patterns (particularly wind driven) and may result in warmer water being advected to the glacier front, which would increase glacier melt rates (Warren and Kirkbride, 1998; Chikita et al., 1999; Chikita, 2007; Sakai et al., 2009). Consequently a better understanding of these processes is needed so as to reduce uncertainties related to future glacier retreat rate predictions, particularly given projected air temperature increases with future climate change scenarios (IPCC AR5, 2013). This study will therefore test the null hypothesis that proglacial lakes are a uniform 1°C and examine changes in proglacial lake extent associated with glacier retreat.

### **1.1.2 The Spatial Extent and Persistence of Proglacial Lakes**

The formation and persistence of proglacial lakes is also important to study as they form a store of glacial meltwater (Farinotti et al., 2016). If the proglacial lake is deep enough this can lead to the flotation of glaciers due to the buoyancy of ice, which increases crevassing

and leads to increased iceberg calving rates (Boyce et al., 2007; Tsutaki et al., 2013). The proglacial lake may also have sufficient volume to store all the water from the total melting of a glacier that disappears, then the meltwater will not contribute to sea level rise due to it being stored in the lake (Farinotti et al., 2016). However, if the proglacial lake were to drain completely, the meltwater from the lake terminating glacier would contribute to sea level rise. So quantifying the persistence of proglacial lakes is critical to understanding the input of freshwater into the ocean and influence on sea level rise (Carrivick and Quincey, 2014). It is essential to quantify the persistence of proglacial lakes in arid areas (such as the Andes, Himalaya and Canadian Arctic), as they provide a crucial store of fresh water for human populations that currently depend on dwindling resources of glacial meltwater (Farinotti et al., 2016). The recent study of Pierre et al. (2019) suggests that proglacial freshwater can act as a substantial sink and store of atmospheric CO<sub>2</sub>, through chemical weathering of suspended sediments. Moreover, they call for a global proglacial lake inventory to facilitate calculation of the amount of atmospheric CO<sub>2</sub> that may be absorbed from the atmosphere into proglacial lakes, which would help mitigate the greenhouse effect (Pierre et al., 2019).

Where proglacial lakes have formed behind unstable terminal moraine systems, it is imperative to monitor their persistence and extent as they form a potential hazard for human populations downstream. The failure of terminal moraine dams has led to glacial lake outburst floods (GLOFs) particularly in the Alps, Himalaya and South America (Buchrothiner et al., 1982; Huggel et al., 2002; Fujita et al., 2008; Somos-venezuela et al., 2014). The failure of moraine dams and sudden draining of proglacial lakes has been linked to the thermal degradation of ice cored moraine as well as avalanches and rockfalls into lakes (Wessels et al., 2002; Korup and Tweed, 2013). So monitoring the temperature, persistence and extent of proglacial lakes through time is also crucial in determining the potential hazards they pose. Ideally the presence of open water on these lakes would be monitored throughout the melt season, to constrain the time that climatological conditions can influence water temperatures.

The persistence of open water on proglacial lakes is important to constrain as winter lake ice may melt out earlier on some lakes and also freeze up later in the year (Du et al., 2017). This would suggest variations in thermal regime of proglacial lakes through the melt season, with higher lake surface temperatures delaying freeze up of the lake surface (Du et al., 2017). Furthermore, where proglacial lakes exhibit longer open water periods, the reduced period of lake ice exposes the water surface to longer periods of climate warming factors through the

melt season. Therefore as proglacial lake open water periods increase, the maximum proglacial lake surface temperatures during the melt season are also likely to increase (Surdu et al., 2014, Du et al., 2017). However, proglacial lake thermal regime is also affected by other factors, such as input of meltwater and wind driven circulation (Warren and Kirkbride, 1998; Chikita et al., 1999; Sugiyama et al., 2016), which will be discussed in section 1.58.

## **1.2 Focus of the study**

Investigating the influence of proglacial lakes on glacier retreat rates firstly requires an understanding of the spatial problem in the distribution and extent of proglacial lakes in contact with glacier termini. This enables the proportion of glaciers that may have enhanced retreat rates due to contact with proglacial lakes to be quantified, so the extent of the problem can be constrained across whole remote mountain regions. The temporal problem of how persistent these proglacial lakes are is critical in understanding their influence and also storage of freshwater through time, as well as the duration of open water through the melt season (not addressed here), which in turn affects the thermal regime. The thermal problem of how lake surface temperatures evolve through the melt season is controlled by local climatic variables (such as wind patterns) and is essential to constrain in order to quantify the influence on glacier retreat rates (Steissberg et al., 2005; Sugiyama et al., 2016; Du et al., 2017). The focus of this work is therefore on the thermal evolution of proglacial lakes and their influence on glacier retreat rates.

### **1.2.1 Research Aims and Objectives;**

The overall aim for this thesis was to investigate the temperature dynamics of proglacial lakes and the influence on glacier retreat rates in Arctic Sweden. To achieve this aim the thesis is split into three smaller projects. The specific objectives for this study are to;

- O1. Create a proglacial lake inventory for Arctic Sweden and analyse the spatial pattern of proglacial lakes.
- O2. Quantify the change in proglacial lake extent through time.
- O3. Characterise the patterns in glacier retreat rates in Arctic Sweden.
- O4. Analyse skin surface temperatures of 12 largest proglacial lakes across Arctic Sweden.

- O5. Assess the relationship between spatial patterns in proglacial lake surface temperature and factors affecting thermal regime of each proglacial lake.
- O6. Measure spatial pattern of surface temperature across a proglacial lake and analyse persistence over time.
- O7. Measure water surface temperatures directly at the glacier-lake contact point and analyse rates of change over time.

### **1.3 Structure of the thesis**

The thesis is separated into chapters, which address different aspects of the study and utilise different approaches.

#### **1.3.1 Chapter 1: Introduction and Literature review**

The first chapter is literature based which introduces the focus of the study. The study area (section 1.4) is then introduced and provides background on the climate and glaciers in the study area of Arctic Sweden. The Lacustrine Terminating Glacier System section (1.5) then briefly explores some of the interactions between the components of the system, to provide the reader with a background to the subject.

The Literature review (Section 1.6) then follows, which focuses on research into proglacial lakes across regional mountain ranges, with some discussion of the differences between neighbouring lacustrine terminating glacier systems and the response to large scale climate patterns. The influence of proglacial lakes on glacier dynamics is then reviewed to give the reader a background in the mechanical processes acting on *some* lacustrine terminating glaciers, which may also influence mass loss rates. The literature investigating the proglacial lake thermal structure and changes through time (thermal regime) will then be reviewed to explore current understanding of how the water temperatures in proglacial lakes vary between systems and over time. There is a subsection discussing research into thermal regime of glacial lakes on debris covered glaciers (supraglacial lakes) in the Himalaya, as important advances in the study of supraglacial lakes have relevance for the study of proglacial lakes despite the difference in lake bed characteristics (presence of ice).

### **1.3.2 Chapter 2: Investigating the spatial extent of proglacial lakes and glacier retreat rates in Arctic Sweden**

The second chapter uses satellite optical imagery to map the spatial extent of proglacial lakes and also glacier terminus areas in Arctic Sweden from remote sensing. The first objective is addressed through manually mapping proglacial lake extent from ASTER satellite imagery, to create an inventory of proglacial lakes in Arctic Sweden. The second objective is addressed through manually mapping proglacial lake extent from aerial imagery from the 1950s and 1960s to investigate how the number and extent of proglacial lakes has changed through time. The pattern of glacier retreat rates in Arctic Sweden is investigated through mapping of glacier terminus areas from Rapid Eye satellite imagery in 2010 and 2018.

### **1.3.3 Chapter 3: Investigating Proglacial Lake Temperature in Arctic Sweden from the ASTER Satellite Temperature Product**

The third chapter employs a remote sensing based approach to investigate the temperature of proglacial lakes in Arctic Sweden from the ASTER satellite surface temperature product (AST08). This chapter introduces the AST08 temperature product in detail and reviews the literature utilising AST08 for extraction of surface temperatures over water bodies. This then informs the development of the workflow which is used to extract surface temperatures from AST08 over proglacial lakes in Arctic Sweden, which are then analysed. The spatial pattern of temperatures from the AST08 for each proglacial lake are then analysed in relation to surrounding factors that may influence them, such as proximity to glaciers and shading from topography.

### **1.3.4 Chapter 4: Quantifying Proglacial Lake Temperatures and Terminus Change of Kaskapakteglaciaren in Arctic Sweden**

The fourth chapter presents the results of fieldwork based studies undertaken at Kaskapakteglaciaren to quantify the spatial pattern of proglacial lake temperatures and measure the proglacial lake temperature at the calving front through time (objectives 6 and 7). The changes in glacier terminus geometry are also presented from fieldwork during July/August 2017 and 2019. This chapter is based on a different approach to previous chapters and presents direct evidence of processes occurring at the ice to water interface.

### **1.3.5 Chapter 5: Discussion and Conclusions**

Chapter 5 gives a discussion of the key findings and how each objective put forward in chapter 1 was met. This chapter provides an overview of the key findings of this study and draws them all together in the conclusions section.

## 1.4 The Study Area in Arctic Sweden

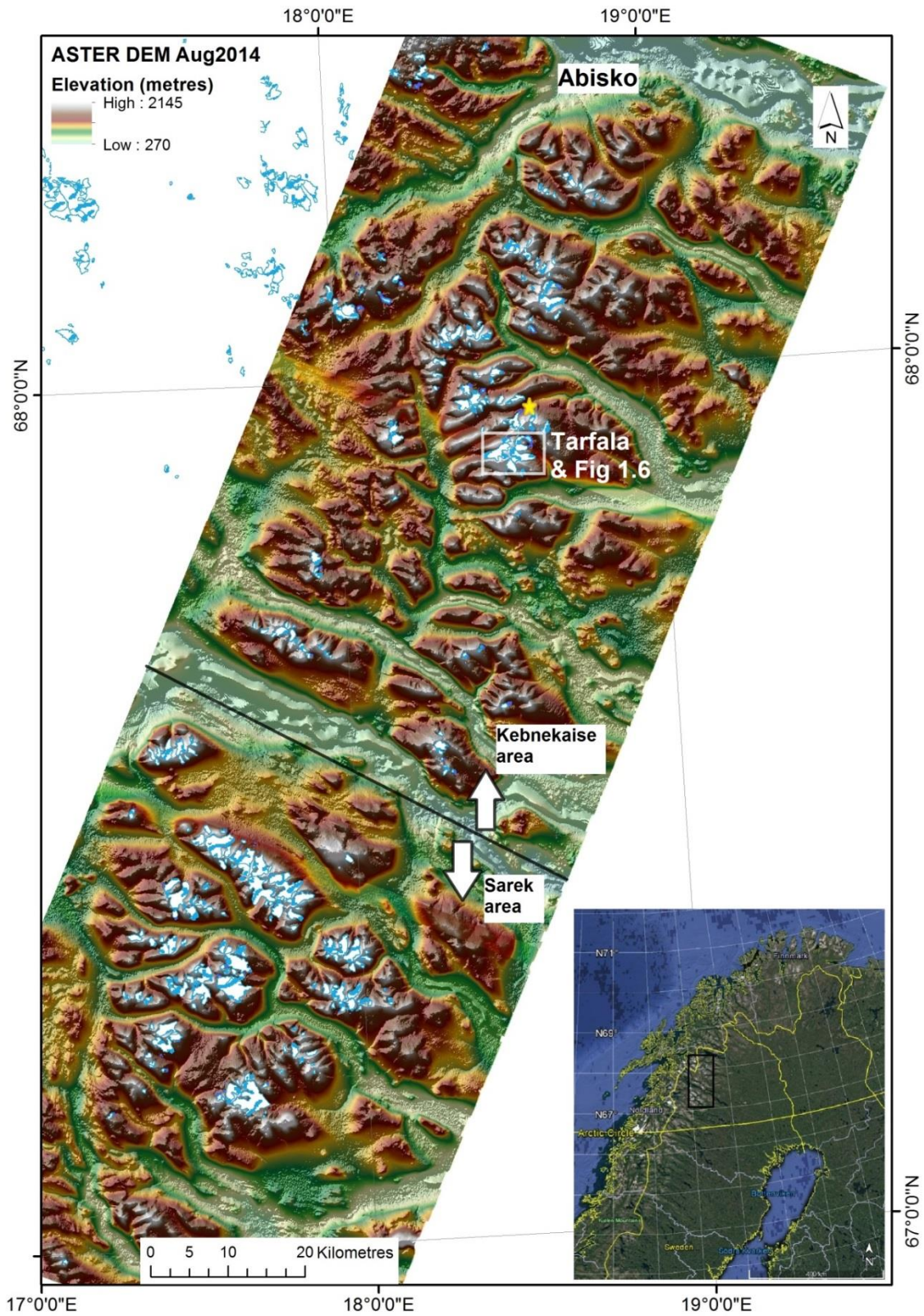


Figure 1.3 Location of proglacial lake study area in Arctic Sweden (Google Earth) (inset). Distribution of glaciers in the Kebnekaise (north) and Sarek (south) regions in Arctic Sweden with ASTER DEM from 8/8/2014. The gold star marks the location of Kaskapakteglaciaren (fieldsite).

The mountains of northern Scandinavia represent a relatively accessible area of the Arctic and an important area to study the thermal regime of proglacial lakes and relationship with climate. Arctic Scandinavia is influenced by colder Arctic weather systems, as well as warmer weather systems driven by westerly winds (Pohjola and Rogers, 1997; Bonan et al., 2019). The influence of Atlantic weather systems also means the area is subject to rain on snow events, particularly on the Norwegian side (Pall et al., 2019). There has been an increasing trend of  $0.96^{\circ}\text{C decade}^{-1}$  in mean annual air temperatures at Tarfala between 1985 to 2009 (Dahlke et al., 2012). Furthermore, the Arctic Amplification of Climate Change is likely to affect the area, although the exact nature of this climatic perturbation on Arctic Scandinavia is yet to be constrained (Kim et al., 2018). A number of substantial heatwaves have also recently (particularly the 2014 and 2018 events) affected Arctic Scandinavia and are predicted to increase in frequency in the future (Kim et al., 2018; Sinclair et al., 2019). This delicate position of Arctic Scandinavia in the climate system and recent heatwaves mean that it is imperative to study the influences of climate on proglacial lake temperatures and the relationship with glacier mass loss (Holmlund and Holmlund, 2019). This combined with the long mass balance record from Storglaciaren and relatively accessibility of the area, make it an ideal study area for investigating the influence of proglacial lake thermal regime on glacier mass loss.

There has been a long and rich history of studies into the glacial and periglacial environments of Arctic Sweden. A full review of these studies is beyond the scope of this study, but an outline of some of the most prominent studies is given. The early work of Svenonius et al., (1910) provided a good baseline for assessing the Little Ice Age maximum extent of many glaciers throughout the Kebnekaise region, through conducting logistically challenging glass plate photography surveys. Some of this historical imagery was used by Holmlund and Homlund (2019) to compare surface lowering and area reduction on Storglaciaren through comparison of digital surface models (created through surface from motion). The historical images of Kebnepakte glaciaren were also used by Kirchner et al. (2019) to recreate past calving front positions and calculate retreat rates.

There has been many studies into the mass balance, hydrology and thermal regime of Storglaciaren, facilitated through the close proximity to Tarfala research station. The nearby Rabot's glaciär has also been the focus of research and found to have a similar polythermal structure to Storglaciaren (Brugger, 2007). A long record of glacier changes also exists for Karsaglaciaren (near Abisko), which has undergone substantial mass loss but is still thought

to have remained polythermal due to a lag in response time to climatic changes and mass balance (Rippin et al., 2011; Williams et al., 2016).

The climate fluctuations and variation in glacier extent during the Holocene in Arctic Sweden have also been the subject of research, which Karlen (1973) investigated through mapping moraine geomorphology and lichenometry. The moraines of Arctic Sweden were also the focus of the seminal study of Ostrem (1964), which investigated the effectiveness of the debris cover in insulating the ice core from climatic warming influences. The ground thermal regime has also been the focus of other studies and a borehole into the permafrost has been established above Tarfala to monitor changes in ground temperature (Christiansen et al., 2010).

The study area for the regional proglacial lake mapping covers ~6,500 km<sup>2</sup> of Arctic Sweden between 67.022806°N and 68.300895° N, with predominantly Caledonian Amphibolite nappe geology (Goodfellow et al., 2008). The topography extends up to the highest point of northern Scandinavia (Kebnekaise, 2,097 m); with relief commonly of 1,000 m along the elevation axis that runs SW-NE through the study area (Goodfellow et al., 2008). There is a mixture of plateau areas and also alpine peaks up to 2,097 m (Kebnekaise North top) along the main mountain crest, with some prominent (up to 600 m high) headwalls above the glaciers (see Fig.1 and 2). The 11 year data record (2001 to 2011) from a 100 m deep borehole at Tarfalaryggen (1,550 m a.s.l.) indicates that at elevations above 1,200 m there is continuous permafrost, although there is a significant warming trend that reaches a maximum of 0.047°Cyr<sup>-1</sup> at 20 m depth (Christiansen et al., 2010; Jonsell et al., 2013). Therefore some proglacial lakes in the study area may be underlain by permafrost, although this may be degrading (Christiansen et al., 2010).



Figure 1.4 Kaskapakteglaciaren (~189 m wide calving front) with proglacial lake (1,100 m asl) and surrounding mountains (~2,000 m high) in Arctic Sweden on 19<sup>th</sup> September 2019. The headwall top left hand corner is ~600 m high and this represents the most alpine topography in the study area. The right hand moraine is mostly ice cored, although the lower sections near the lake outlet have thawed and lowered (Ostrem, 1964). Note the active wind redistribution in the right foreground, visible as a slight haze of spindrift flowing right to left.

#### 1.4.1 Glaciers in the Study Area of Arctic Sweden

The Randolph Glacier Inventory (RGI, 2008) recorded 252 glacier units across the study area. There has been considerable glacial recession since this inventory was created, but it is currently the most up to date for the study area and is therefore used in this study for glacier characteristics. The glaciers in the northern part of the study area (around Kebnekaise) tend to be of the ‘cirque’ type, which are situated in deep hollows in the mountainside and most have developed large terminal moraine systems at the rim of the cirque. In contrast, the glaciers of the Sarek area to the south tend to be larger due to higher rates of precipitation (Karlen et al., 1973). Consequently they extended beyond the cirque rims at the ‘Little Ice Age’ maximum and into the larger valley systems below, which has resulted in generally terminal moraine systems with lower crest heights (Karlen et al., 1973). The glaciers in the west of the study area tend to be of the plateau icefield type, due to the increased levels of precipitation towards Norway, resulting in ice accumulating on flat tops of mountains (Karlen, 1973; Goodfellow et al., 2008). Glaciers across the study area have been retreating since reaching the last ‘Little Ice Age’ maximum extent around 1916 (Karlen, 1973).

There is some debate as to whether the ‘Little Ice Age’ glacier advances in Scandinavia were due to lower air temperatures or a series of relatively mild winters with higher precipitation, which is discussed further below (Nesje et al., 2008). The terminal moraine systems of glaciers across Kebnekaise and Sarek areas tends to be a complex series of moraine ridges that have developed through several re-advances during the Holocene (Denton and Karlen, 1973; Karlen, 1973). The precise origins of these moraine systems are complex and not the focus of this study, but the distinct outline provides a strong spatial constraint for considering proglacial lakes within the Holocene moraine limits (Denton and Karlen, 1973; Karlen, 1973; Tonkin et al., 2017). There are many ice cored moraine systems within the study area that form prominent topography with high structural integrity (Figure 1.4) (Ostrem, 1964). These prominent moraines provided substantial barriers to glacier expansion during the ‘Little Ice Age’ and Enqvist’s images from 1910 capture bulging glacier margins due to ice cored moraine structural integrity and topography inhibiting glacier overriding (Holmlund et al., 1996). Where these terminal moraine systems have high structural integrity and prominent topography they can form substantial dams for proglacial lakes, particularly in the Kebnekaise area, although there has also been evidence of ice cored moraine lowering at Kaskapakteglaciaren (Ostrem, 1964).

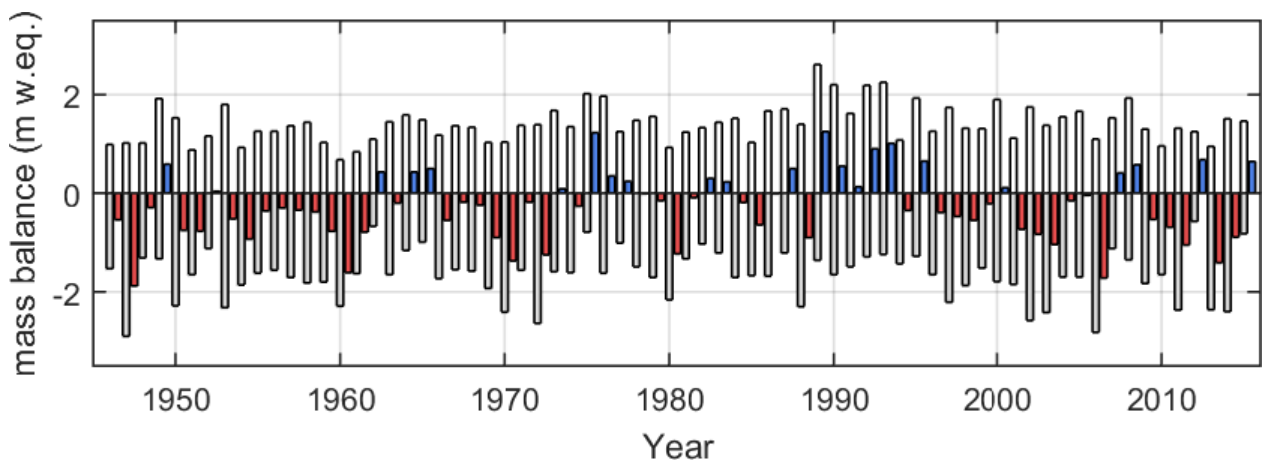


Figure 1.5 Storglaciären mass balance record from 1946 to 2015. White bars represent the winter balance and grey bars the summer balance. The net balance is given as blue for positive and red for negative. Note the period of positive mass balances during the early 1990s. <https://bolin.su.se/data/tarfala/storglaciaren.php>

The mass balance record from Storglaciären is the longest continuous annual series of records of any glacier in the world (Holmlund and Holmlund, 2019) (Figure 1.5). It dates back to 1946 and continues to the present time to provide a valuable record of how Storglaciären has responded to changes in climate over this time period (Figure 1.5). The Early Twentieth Century Warming (ETCW) that marked the end of the ‘Little Ice Age’ started around 1910 in

Arctic Sweden, with a marked 1°C warming in air temperatures (Brugger, 2007). A substantial number of historical images were taken around the Kebnekaise area to document glacier extents and reconstructions of Storglaciaren surface from using historical imagery to reconstruct a digital surface model (Surface from Motion or SfM) suggest that the glacier lost 28% of the initial ice mass between 1910 and 2015 (Holmlund and Holmlund, 2019). In 1910 the neighbouring Kebnepakte extended ~250 m into Tarfala lake (~15 m deep) and retreated at a rate of 7.9 m a<sup>-1</sup> until it terminated on land in 1945 (Figure 1.6)(Kirchner et al., 2019). Svenonius (1910) observed active calving on Kebnepakte in 1908 and estimated the calving front to be ~10 m high (Kirchner et al., 2019). The Storglaciaren mass balance record from 1946 through to 1961 is characterised by a sustained spell of negative net mass balances (with the exception of 1949) (Figure 1.5). Storglaciaren terminus retreated during this period until the 1980s when the terminus position stabilised as it is thought to have gained quasi-equilibrium with the climate (Holmlund, 1988; Brugger, 1997; as cited by Brugger, 2007).



Figure 1.6 Aerial image (Lantmateriet, 1959) of Kebnekaise (Sweden) with Tarfala valley to the east (right). Rb=Rabot's glacier Kp=Kebnepakte glacier If=Isfallsglaciaren Sg=Storglaciaren. Spatial resolution is unknown but estimated to be ~1 m.

Brugger (2007) suggests that Storglaciaren finished responding to the ETCW by the 1980s, although note that there were also some years of positive mass balance during the 1960s and

1970s (Figure 1.5). He argues the complicated subglacial topography with a prominent over-deepening (maximum ice thickness 250 m) and relatively steep surface profile of Storglaciaren results in it having a faster (125 years) response time than the neighbouring Rabot's glacier (215 years) (Figure 1.6) (Brugger, 2007). Both of these response times are calculated from numerical modelling and seem somewhat slow if Storglaciaren is thought to have reached quasi equilibrium with the climate during the 1980s, which would be 70 years after the initial climate perturbation. Nevertheless, Brugger (2007) argues that although the two glaciers have a similar hypsometry and thermal regime (both are polythermal) the flatter profile around the equilibrium line of Rabot's glacier results in a longer response time. Furthermore, glacier velocities on Storglaciaren are higher (summer maximum of  $\sim 30 \text{ m a}^{-1}$ ) than for Rabot's glacier (summer maximum of  $12 \text{ m a}^{-1}$ ) (Brugger, 2007). Consequently the retreat of Rabot's glacier in response to the ETCW was relatively slow ( $2 \text{ m a}^{-1}$ ) until  $\sim 1959$ , after which point retreat rates increased to  $11 \text{ m a}^{-1}$  until the 1980s (Brugger, 2007).

The thermal regime of Karsaglaciaren (also in the study area) was also found to be polythermal, although Rippin et al. (2011) argue that this thermal structure was likely to be out of synchronisation with the current geometry and climate. Indeed, past reconstructions of glacier extent by Williams et al. (2016) suggest that the 1926 thickness was sufficient for Karsaglaciaren to maintain a temperate core at that time. However since 1926 Karsaglaciaren has undergone substantial thinning at a rate of  $-0.23 \text{ m} \pm 0.1 \text{ m w.e yr}^{-1}$  between 1926 and 2010, which is at a similar rate as Brugger et al. (2005) reported for Rabot's glacier ( $-0.38 \text{ m w.e. yr}^{-1}$  from 1910 to 2003) (Williams et al., 2016). Williams et al. (2016) observe that Karsaglaciaren has retreated faster (1.3 km between 1926 to 2008) than any other glacier in Sweden but at a comparable rate to Norwegian glaciers, partly due to the more maritime climate. They noted that the period from 1943 to 1959 had the highest mean annual retreat rates across the glacier terminus of  $30.3 \pm 0.9 \text{ m yr}^{-1}$  and the lowest retreat rate of  $8.8 \pm 0.8 \text{ m yr}^{-1}$  between 1926 and 1943 (Williams et al., 2016).

The net mass balance of Storglaciaren during the 1980s does appear to be relatively in equilibrium across this decade (Figure 1.5) (Pohjola and Rogers, 1997). The early 1990s (including 1989) form a period of positive net mass balances for Storglaciaren. This period of positive net mass balances is associated with a period of higher winter precipitation, which is due to the intensification and more northerly track of storm systems associated with positive winter North Atlantic Oscillation (NAO) (Pohjola and Rogers, 1997; Bonan et al., 2019). Although it seems unlikely that this relatively short period of positive net mass balances (7

years) was long enough to substantially counter overall glacier retreat associated with climatic warming (Bonan et al., 2019). Particularly given observed increases in air temperature (see below) and Siccart et al. (2008) found that air temperatures correlated well with sensible heat fluxes and were the main driver of Storglaciaren mass loss. Although it should also be considered that there has been several sustained heat waves since this study (particularly July 2018) (Sinclair et al., 2018; Kim et al., 2019). These heatwaves have been characterised by high sunshine anomalies (July 2018 had 165% of monthly average) associated with high pressure systems and clear skies, which will also have resulted in higher incoming shortwave radiation fluxes and increased glacial melt (Bonan et al., 2019; Kim et al., 2019). The climatology of the area will be discussed below in section 1.4.2.

### **1.4.2 Climate**

The climate varies across the study area, which is located on the boundary between the maritime climate of Norway to the west and the continental climate of Sweden. There are meteorological stations at Tarfala (1140 m a.s.l.) in the south of the study area and Abisko (383 m a.s.l.) 5km to the north of the study area. The annual precipitation of 322 mm in Abisko and ~1,000 mm at Tarfala (Goodfellow et al., 2008) reflects the marked gradient in precipitation across the study area from SW to NE. Winter accumulation can be associated with easterly winds or westerly winds and substantial wind redistribution of snow (Figure 1.4) is evident from large numbers of perennial snow banks and geometry of accumulation deposits on some glaciers (personal communication with G. Rosquvist, Sept. 2019).

The mean annual air temperature (MAAT) at Abisko is  $-0.9^{\circ}\text{C}$  and at Tarfala is  $-3.5 \pm 0.9^{\circ}\text{C}$  (1965-2011) (Goodfellow et al., 2008; Jonsell et al., 2013). However, air temperatures above  $20^{\circ}\text{C}$  were recorded in 2003, 2007, 2014 and 2018 at Tarfala; the July 2018 average hourly air temperature was  $5.6^{\circ}\text{C}$  above the long term average (1965-2011) Swedish Meteorological and Hydrological Institute (SMHI) (Jonsell et al., 2013). Weather stations in Northern Scandinavia recorded positive sunshine anomalies hours during the July 2018 heatwave, with 165% of monthly average sunshine (Sinclair et al., 2019). These higher air temperatures and positive sunshine anomalies are likely to lead to increased lake temperatures which may affect glacier retreat rates through thermal undercutting (Kirkbride and Warren, 1997). The relationship between proglacial lake temperatures and glacier mass loss is imperative to understand given future predictions of longer and more intense heatwaves in Arctic Scandinavia (Kim et al., 2018).

## 1.5 The Lacustrine Terminating Glacier system

The development of a lake at the glacier terminus (proglacial) can occur in 2 main different situations (Carrivick and Tweed, 2013). Where high rates of subglacial erosion has created a topographic over-deepening, as the glacier retreats back from a maximum position the basin will fill with glacial meltwater and likely persist whilst there is sufficient input or there is a constriction on the output (Boyce et al., 2007). The production of prominent terminal moraine systems can provide a substantial dam that will result in a proglacial lake developing behind it from the input of meltwater (Carrivick and Tweed, 2013). The persistence of these moraine dammed lakes is not only dependent on the input of meltwater, but also the effectiveness of the dam to hold water back through time (Carrivick and Tweed, 2013). Where moraine dams have an ice core this can degrade due to the thermal erosion from lake water and lead to Glacial Outburst Floods (GLOFs) (Korup and Tweed, 2013).

The thermal degradation of ice under a debris cover on a glacier can also be spatially variable and lead to thermokarst lakes developing where debris cover is too thin to insulate the glacier from a warming climate (Kirkbride, 1993). These relatively small thermokarst ponds can coalesce to form large proglacial lakes at the terminus, however if the water temperatures rise sufficiently to thermally erode channels (or they expand into channels) then the ponds/lakes will drain (Wessels et al., 2002). Consequently, the persistence of lakes dammed by a debris covered ice core is often transient through time (Wessels et al., 2002). With projected increases in air temperatures (IPCC AR5, 2013), glacier mass loss is likely to increase and create more depressions where proglacial lakes may form. It is therefore essential to quantify how many glaciers have proglacial lakes in contact with the terminus in order to further investigate how this may influence glacier mass loss.

The dominant process driving mass loss of glaciers terminating in water is melt (surface and subaqueous) and dynamic processes of ice berg calving, as blocks of ice become detached from the glacier terminus (Boyce et al., 2007; Tsutaki et al., 2013). Quantifying each process separately is paramount to accurately determining calving rates from subaqueous melt rates and the relative contribution to glacier mass loss, which will further improve future predictions of glacier retreat rates. However, quantifying subaqueous melt rates has received relatively little attention in the literature, largely due to logistical problems of accessing the hazardous glacier to lake contact point (Eijpen et al., 2003; Roehl et al., 2006; Truffer and Motyka, 2016; Sugiyama et al., 2016). The thermal characteristics of the lake body are

particularly important, as the high specific heat capacity of water (4.2 kJ/kg °C) means the presence of a water body at the margins of a glacier can present a substantial store of heat (Schomaker, 2010). Given that water has a higher thermal conductivity than air, ice in contact with water will melt faster than ice in contact with air of the same temperature as the water (Sugiyama et al., 2016). Therefore the thermal structure of the proglacial lake water is critical in determining subaqueous melt rates across the glacier terminus, although this was not particularly emphasised until the relatively late study of Warren et al. (1995b) (as cited in Warren and Aniya, 1999).

This also raises the question as to how fluctuations in lake level influence subaqueous melt rates at the calving front, which in turn will control the position and extent of any thermally eroded notches (see Figure 1.1 and Figure 1.7) (Kirkbride and Warren, 1997; Roehl, 2006; Minowa et al., 2017). Once formed, thermally eroded notches represent a substantial weakening of the ice front where substantial amounts of ice become unsupported above the horizontal cavity of the notch (see Figure 1.1 and Figure 1.7) (Kirkbride and Warren, 1997; Roehl, 2006). The gravitational force acting on the ice above the notch can lead to fracturing and where the depth of the notch exceeds the strength of the ice this leads to large sections of ice detaching from the front in iceberg calving events (Kirkbride and Warren, 1997). Therefore, the strength of the ice structure at the terminus is a major controlling factor on calving rates into proglacial lakes (Benn et al., 2007).

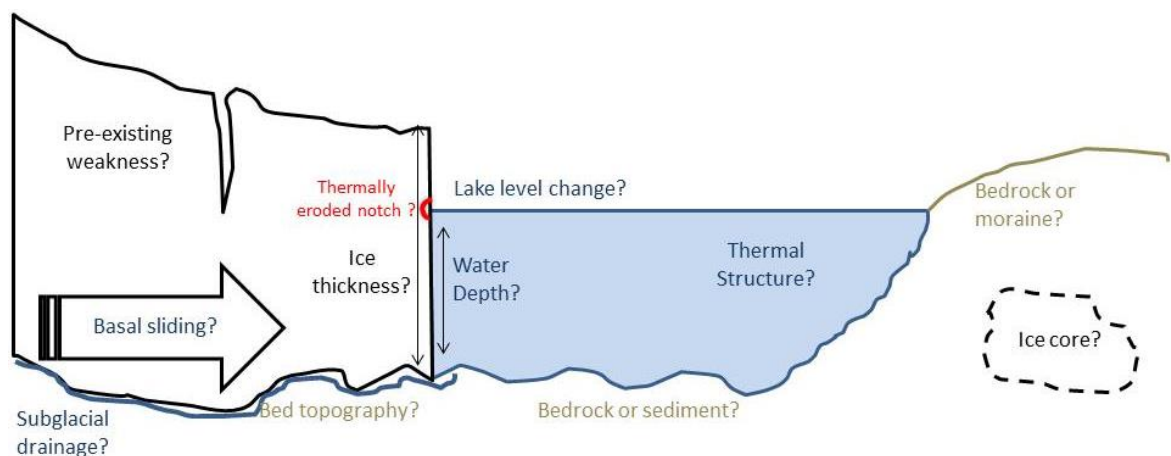


Figure 1.7 Schematic side view of the principal components of lacustrine terminating temperate glacier system. Partly modified from Carrivick and Tweed (2013).

Ice is a relatively strong material and able to resist some mechanical forces upon it, although this varies depending on the rheology and conditions of the ice (Trüssel et al., 2013).

Therefore pre-existing weaknesses within the glacier are likely to be a primary driver in iceberg calving rates in many cases where ice velocity is high, as proposed Benn et al. (2007). It

should also be noted that Geirsdottir et al. (2008) propose that grounded ice bergs in front of Sudurjokull (Iceland) provided sufficient mechanical support that it suppressed calving rates and stabilised ice flow. It should also be considered that this may also be due to suppression of water currents at the ice front due to the presence of icebergs (personal communication with D.Quincey, 2020). This observation illustrates how the terminus of glaciers in contact with proglacial lakes can be finely balanced between the processes of mass loss (e.g. calving) and mass conservation due to the inherent strength of ice.

The extent and characteristics of subglacial drainage is potentially a key component of the lacustrine terminating glacier system, as the presence of a water body at the margins of a glacier can influence subglacial water pressure (Sugiyama et al., 2011; Tsutaki et al., 2013). If the proglacial lake has sufficient depth then the hydrostatic head may be raised sufficiently to increase subglacial water pressures (Sugiyama et al., 2011). This can be sufficient to overcome glacial overburden pressure and lead to increased basal sliding, which in turn increases ice velocity and crevassing behind the ice front (Sugiyama et al., 2011). The weakening of the ice from increased crevassing pre-conditions the glacier to increased iceberg calving. Consequently the depth of the proglacial lake influences subglacial water pressure, which combined with the buoyancy of ice can result in changes to the glaciers flow dynamics and increase glacier retreat rates (Boyce et al., 2007; Sugiyama et al, 2011; Tsutaki et al., 2013). Indeed Warren et al. (1995) illustrated that iceberg calving rate can correlate strongly with depth, which is illustrated by the numbered points (1 to 14) in Figure 1.8 below.

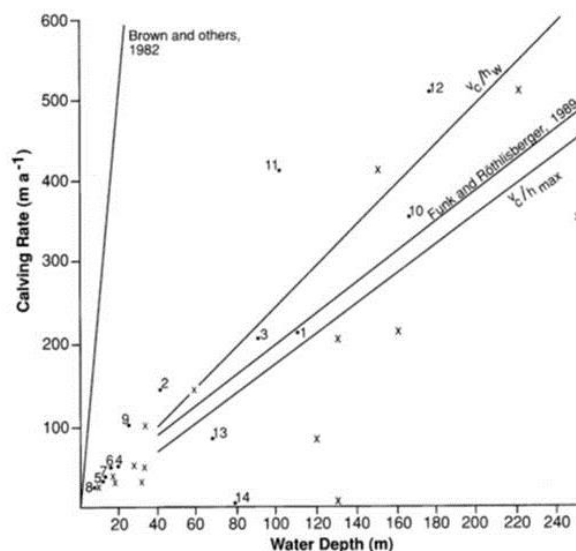


Figure 1.8 The relationship between calving rate and water depth for fresh-water lake terminating glaciers, showing the relationships for width-averaged water depth ( $h_w$ ) (dots) and maximum water depth ( $h_{max}$ ) (crosses). Relationships for tidewater terminating glaciers proposed by Funk and Rothlisberger (1989) and Brown et al., (1982) are also shown. From Warren et al., (1995)

The relatively limited dataset of 14 data points of calving and water depth has been expanded by the study of Warren and Kirkbride (2003) of 6 lake terminating glaciers in New Zealand. Whilst they also found a strong correlation between water depth and calving rate ( $r^2 = 0.83$ ) (Figure 1.8), they argue that this could be related to other processes operating in deeper water, such as circulation currents (Warren and Kirkbride, 2003). Moreover, they find a strong correlation ( $R^2 = 0.85$ ) between calving rate and ice proximal water temperature (Figure 1.9). This shows that water temperatures in proglacial lakes can be sufficiently high enough ( $>3^\circ\text{C}$ ) to weaken glacier termini and be a highly influential controlling factor of calving rates, at least for 7 out of the 10 glaciers in the dataset (Figure 1.9) (Warren and Kirkbride, 2003). They argue the influence of water temperatures on calving rates is likely to be through the mechanism of thermal undercutting of the glacier terminus resulting in iceberg detachment, particularly above thermally eroded notches (Kirkbride and Warren, 1997). It should be noted that the glaciers in the dataset from South America (Ameghino, Leones and Moreno) all have substantially higher calving rates (Figure 1.9).

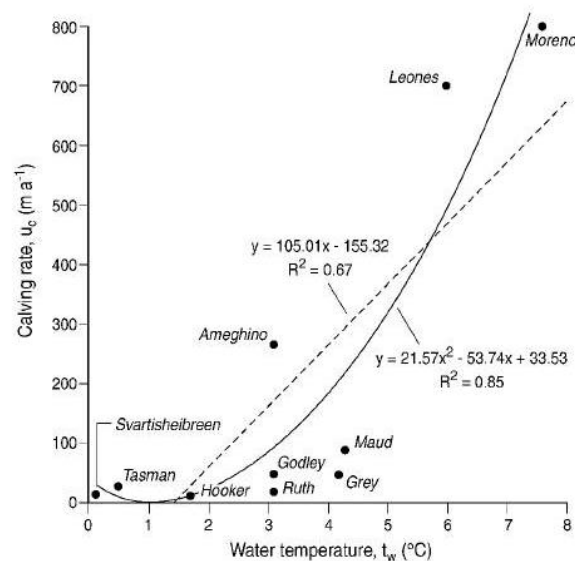


Figure 1.9 The relationship between ice proximal summer water temperature (between 10 to 200 m away from the terminus and 10 m depth) and calving rates for: Glaciar Moreno, Argentina (Rott et al, 1998; Warren, 1999); Glaciar Ameghino, Argentina (Warren, 1999); Glaciar Leones, Chile (E. Haresign and C.R. Warren, 2005); Svartisheibreen, Norway (Kennet et al., 1997) and the remaining 6 glaciers in New Zealand from Warren and Kirkbride (2003). From Warren and Kirkbride (2003).

## **1.6 Literature Review**

### **1.6.1 Lake Terminating Glacier Evolution across Mountain Ranges**

Investigating the relationship between proglacial lake systems and glaciers at the regional scale over longer temporal scales (decades), enables the evolution of neighbouring systems with different topo-climatic situations (such as aspect) to explore the response to different locational factors and changes in climate. This wider spatial scale of study became possible due to the development of satellite photography during the 1960s and particularly the development of Landsat multispectral scanner (MSS) during the 1970s. The close proximity of human settlements to moraine dammed proglacial lakes has created greater impetus to monitor and study the evolution of these systems across remote areas. This is particularly true in areas where catastrophic glacial lake outburst floods (GLOFs) have already occurred, such as the Cordillera Blanca (Peru) and especially the Himalaya (Komori, 2008).

The advancement and development of remote sensing based studies have provided notable advances in this field across remote areas and at the regional scale. These studies are briefly reviewed for methodological development below and it should be noted that this is not a fully comprehensive review of studies utilising remote sensing for detection and delineation of glacial lakes. The seminal study of Buchroithner et al. (1982) was one of the first to develop automatic identification of proglacial lakes from Landsat imagery (using normalised difference water index or NDWI) in order to understand lake evolution in the build up to the catastrophic GLOF of 2nd September 1977 in the Khumbu (Nepal) (see Appendix 2 for further details on the NDWI method). This study enabled proglacial lake development to be identified and monitored in remote areas, as well as providing a valuable insight into the causes of the flood and highlighted the need to understand moraine dam stability (Buchroithner et al., 1982). Whilst this proglacial hazard monitoring is strong rationale for developing proglacial lake automatic detection techniques, this is not the main focus for this study and the reader is referred to Huggel et al. (2002), which comprehensively investigated the use of remote sensing to monitor the hazards posed by two glacial lakes in the Swiss Alps.

The European Alps has been the focus of early studies into GLOFs (along with North America) (Emmer et al., 2018). The study of Emmer et al. (2015) on GLOFs in the European Alps appears to have been the first to create a glacial lake inventory in the range (from remote sensing) and they report expansion of proglacial lakes since 1950s. An increase in

number and area of proglacial lakes (+57% of cumulative area) between 1985 to 2000 has also been reported in the Caucasus mountains by Stokes et al. (2007).

The earlier satellite imagery can provide a useful insight into the evolution of these proglacial lake systems over longer temporal scales, but using imagery from different sensors of different resolutions (Landsat MSS 80 m, SPOT 20 m) does create substantial uncertainty (Komori, 2008). Indeed, Komori (2008) acknowledges that using imagery from multiple sensors is the likely cause of maximum horizontal errors of several tens of metres. These errors would clearly jeopardise the study of small proglacial lake systems, so Komori (2008) constrains the study of proglacial lake evolution to systems of over 0.1km<sup>2</sup> in the Bhutan Himalaya from the 1960s (using CORONA) to the early 2000's. The northern side of the range is typified by glaciers with little debris cover, which developed proglacial lakes 2 to 3 decades earlier than the debris-covered glaciers on the southern side of the range that were temporarily insulated from climatic change (Komori, 2008). Furthermore, Komori (2008) estimated that lake expansion rates were 10 to 40 m a<sup>-1</sup> on the northern side of the range in contrast to the higher rates of 35 to 70 m a<sup>-1</sup> on the southern side of the range. They note Kaab's (2005) argument that this could be due to the reduced influence of 'global warming' on the summer monsoon with increasing latitude or due to higher glacier velocities replenishing ice at the terminus. It does also seem feasible that debris cover on the southern glaciers could temporarily insulate them from changes in climate unless thermokarst ponds developed, after which point mass movements in the surrounding debris cover could lead to expansion of the ponds into larger lakes, as observed in New Zealand and Svalbard (Kirkbride, 1993; Komori, 2008; Schomaker and Kjaer, 2008). It is important to note that the topographic situation is the overall limiting factor on lake evolution, as a suitable basin is essential for lake development whether it be moraine dammed or from erosional overdeepening. This is also likely to have a strong geological control, although it receives little attention in the literature.

The study of proglacial lakes and glaciers across regions was extended to a new spatial scale by Gardelle et al. (2011) in their study of 7 areas across the Hindu Kush, Karakorum and Himalaya (HKKH), which captured 40% of the glacierised area of the 2,000 km mountain range. As with studies discussed earlier, Gardelle et al. (2011) used NDWI for automatic identification of lakes from Landsat imagery from 1990, 2000 and 2009. They found lakes with low turbidity have a similar spectral signature as shadows, which is a substantial problem in areas of such extreme relief as the HKKH. Their innovative use of DEMs to

constrain lake identification to slopes  $<10\%$  went some way to compensate for these errors, but manual inspection was still required, especially as high snow and ice cover also leads to lakes not being detected (Gardelle et al., 2011). The main innovation of Gardelle et al. (2011) was the use of glacial limits in pre-existing glacier inventories (GLIMS and ICIMOD) to classify lakes as either proglacial or supraglacial, as the different conditions in the genesis of these lakes is likely to lead to different future evolution. Indeed, they observed that supraglacial lakes tended to be smaller and more variable extent over time, whereas proglacial lakes tended to be larger and more stable. Therefore distinguishing between the two is essential in understanding the evolution of glacial lakes and especially the development of supraglacial lakes into proglacial lakes (without ice under the entire lake bed).

The paucity of high resolution climate data and mass balance data across the HKKH is a substantial limiting factor in understanding glacier and proglacial lake evolution across the mountain range, as with Patagonian studies. However, Gardelle et al. (2011) argue that remote sensing based mapping of proglacial lakes across the mountain range can provide useful insights into glacier mass balance as increased mass loss is likely to lead to increasing area of proglacial lakes. Indeed, glacial lakes in the eastern Himalaya were found to have grown by 25 to 65% between 1990 and 2009, suggesting that glaciers in these areas have retreated due to mass loss (Gardelle et al., 2011). In contrast, glacial lakes in the Karakorum and Hindu Kush shrunk by -30% and -50% respectively, suggesting that glaciers in these areas had actually advanced (Gardelle et al., 2011). The different responses of lake terminating glaciers across the largest mountain range on Earth, raises questions as to how these systems have responded to differences in climate, particularly given the number of surging glaciers in the Karakorum (Gardelle et al., 2011).

There is a substantial difference in climate and accumulation regime between these areas, as the main source of accumulation for the Himalayan glaciers is the summer monsoon, which does not affect the latter areas that predominantly accumulate during the winter months, dominated by westerly flows (Gardelle et al., 2011). Whilst the paucity of high resolution climate data substantially hinders any robust linkages being made between variations in climate and glacial lake evolution, the magnitude of the changes observed by Gardelle et al. (2011) across different climate zones suggests such remote sensing based studies can provide a useful insight into glacier mass balance at larger scales. Furthermore, Brun et al. (2018) report that lake terminating glaciers are regularly more negative (more than 1 sd) than the

regional average mass balance across the HKKH. More negative mass balances have also been reported for calving glaciers in Norway (Andreassen et al., 2020). Thus providing further impetus to understand the relationship between glacial lake evolution and glacier dynamics with changes in climate (Gardelle et al., 2011).

The majority of outlet glaciers from the Southern (SPI) and Northern Patagonian Icefields (NPI) are temperate and terminate in water, in both lacustrine and marine environments (Warren and Aniya, 1999). Whilst the ice fields of Patagonia represent the largest temperate ice mass in the southern hemisphere (covering 16,500 km<sup>2</sup>), the study of regional patterns of glacier evolution has been inhibited by the paucity of data due to their inaccessibility (Sakakibara and Sugiyama, 2014). The development of remote sensing based studies have gone some way to enabling investigations at the regional scale, although problems still exist with quantifying accumulation rates near the ice divide (Sakakibara and Sugiyama, 2014; Schaefer et al., 2015). Whilst this is problematic for quantifying the influence of proglacial lake evolution on glacier mass balances due to constraining accumulation, the change in terminus positions of these glaciers across the region provides useful insights into the influences of proglacial lakes. There has been a general pattern of glacier retreat during the 20th Century across the region, with several lake terminating glaciers experiencing accelerated retreats above this pattern (Warren and Aniya, 1999). Despite this regional pattern glacier Pio XI has also been in a period of sustained advance (as well as Perito Moreno) and glacier Calvo has maintained a long period of still stand (Warren and Aniya, 1999). This makes the insights into the influence on lake terminating glacier dynamics from Perito Moreno (discussed below in section 1.6.3) even more valuable, as it suggests that the response of the lake terminating glacier system can be out of synchronisation with regionally climate driven patterns of glacier evolution.

### **1.6.2 Influence of Proglacial Lakes on Glacier Dynamics and Mass Balance at the Regional Scale**

The development of feature tracking techniques from optical imagery has enabled studies into the variations in glacier flow speeds on the regional scale, between imagery from different dates with cloud free conditions. This approach was combined with analysis of DEMs to analyse glacier surface velocity and surface lowering in the central Himalaya between 2000 to 2015 by King et al. (2018). They found that lake terminating glaciers all retreated and showed maximum surface lowering near the terminus, whereas land terminating glaciers

thinned towards their middle reaches and tended to reduce in velocity during the study period (King et al., 2018). Crucially they observed lake terminating glaciers to be either in a phase of increasingly dynamic behaviour (increased velocities) and retreat or in a phase of relatively neutral dynamic behaviour unaffected by the lake (King et al., 2018). King et al. (2018) argue that for the glaciers observed to have increased velocities, this resulted in increased crevassing and higher retreat rates due to increased mechanical calving. Thus highlighting the potential importance of glacier dynamics on retreat rates from proglacial lakes in some cases. It should be noted that they dismiss thermo-erosional processes from having a prominent influence on glacier retreat rates in the study area, as they argue the vertical extent of thermally eroded notches would be too limited and mechanically driven forces are likely to dominate the calving regime (King et al., 2018).

Whilst deriving ice speeds in accumulation areas is problematic due to changes in snow cover (errors up to  $\pm 300 \text{ m a}^{-1}$ ), the feature tracking of Sakakibara and Sugiyama (2014) derived speeds from Landsat (1984 to 1986 and 1999 to 2011) for the ablation area of Perito Moreno were in close agreement with the GPS measured speeds from Sugiyama et al. (2011). They reported speeds of up to  $5,900 \text{ m a}^{-1}$  ( $\pm 300 \text{ m a}^{-1}$ ) up to 20km from calving fronts, although note the large error margin. During the observation period only Glaciar Pio XI advanced (both the lacustrine and marine termini), which they argue was due to the large accumulation area (Sakakibara and Sugiyama, 2014). In contrast 1 glacial fronts from the SPI retreated more than 6km during the observation period, which corresponded to large increases in velocity near the lacustrine terminus (note that 2 marine termini retreated a similar amount) (Sakakibara and Sugiyama, 2014). Notably Glaciar Uppsala changed in 2008 from a stable state to a fast flowing retreat, which they argue was most likely due to retreating beyond supporting bedrock topography at the terminus, as there was no change in climate at the nearby meteorological station (Sakakibara and Sugiyama, 2014). Also, 12 out of 17 major lake terminating glacier fronts from the SPI had terminus position changes of less than  $\pm 0.5\text{km}$ , which suggests that the rapid retreat of some lacustrine terminating glaciers observed around the SPI is due to glacier dynamics and topography rather than changes in climate (Sakakibara and Sugiyama, 2014).

Whilst it may appear that the evolution of larger and more complex systems of lake terminating glaciers in the SPI can be dominated by ice dynamics rather than changes in climate, this is difficult to quantify precisely due to the lack of local meteorological and mass balance data (Schaefer et al., 2015). This is particularly problematic in a region of

complicated maritime mountainous topography with a steep west to east gradient in precipitation driven by the strong westerly flow. Consequently taking into account the wind redistribution of snow is critical in calculating accumulation rates across the ice divide, which may have a substantial impact on the mass balance of lake terminating glaciers discussed above and also other areas, such as Arctic Scandinavia.

This lack of accounting for the effects of wind redistribution is a notable flaw in the modelling approach taken by Schaefer et al. (2015) to simulate mass balance of the SPI between 1975-2011, as well as a lack of ice cliff height data causing problems for calculating mass loss at the lacustrine terminus. Despite these caveats, Schaefer et al. (2015) argued that the regression values of 0.85 to 0.90 for temperature suggests that their reanalysis and downscaling of climate data from a cell 250km to the west has captured the influence of synoptic patterns on local variations. This is based on very limited ground observations across the region, which is likely to have distinct variations in microclimates due to the pronounced topography. This is a particularly critical factor for precipitation rates and the lower regression values (0.65 to 0.8) with a limited number of ground observations does bring in to question the capability to model precipitation and mass balance across the SPI. Despite these substantial uncertainties, Schaefer et al. (2015) argue that for 1975-2000 and 2000-2011 mass losses at the lacustrine terminus (subaqueous melt and calving) were greater than through surface ablation across the SPI.

Whilst precise quantification of the mass losses due to calving and subaqueous melt from the SPI has not yet been achieved, the high ice speeds and rapid retreat rates of some glaciers observed in this area illustrates the complex dynamic nature of these larger lacustrine terminating glacier systems. Whilst it appears that subglacial bedrock topography can at least delay lacustrine terminating glacier response to changes in climate, extensive monitoring campaigns are required to further understand the relative importance of the components of these proglacial lake systems. The linkages between air temperatures, water temperatures, meltwater fluxes, subglacial water pressure and ice flow speeds require more extensive investigation. Developing a greater understanding of these systems is essential in monitoring how they evolve with changes in climate, particularly increases in air and lake temperature, in order to predict how they may evolve in future climate scenarios. This will ultimately improve calculations of how water is stored within these catchments and the consequent contributions to sea level rise, if proglacial lakes do not effectively store all of the water

currently in these glacier systems. This will of course require greater understanding of calving rates and lake bathymetry, as well as the stability of damming moraines.

### 1.6.3 Proglacial Lake Influence on Glacier Dynamics and Calving from Field Studies

The easy accessibility of the Perito Moreno glacier (257 km<sup>2</sup>) (50°28'12"S, 73° 2'21"W) on the eastern side of the Southern Patagonian icefield (SPI) has resulted in it being one of the most studied outlet glaciers of the region (Michel and Rignot, 1999) (Figure 1.10). The glacier appears to have been in a steady state during the last century and flows from the SPI ice divide (~1,600 m) through a terminal valley (4 km wide) at rates of between 400 to 500 m a<sup>-1</sup> to a calving front that terminates into 2 freshwater lakes, where flow rates of up to 800 m a<sup>-1</sup> have been reported (Figure 1.11; Sugiyama et al., 2013). The glacier has advanced several times to form a dam between the Brazo Rico and Canal de los Tempanos (Michel and Rignot, 1999) (Figure 1.10).

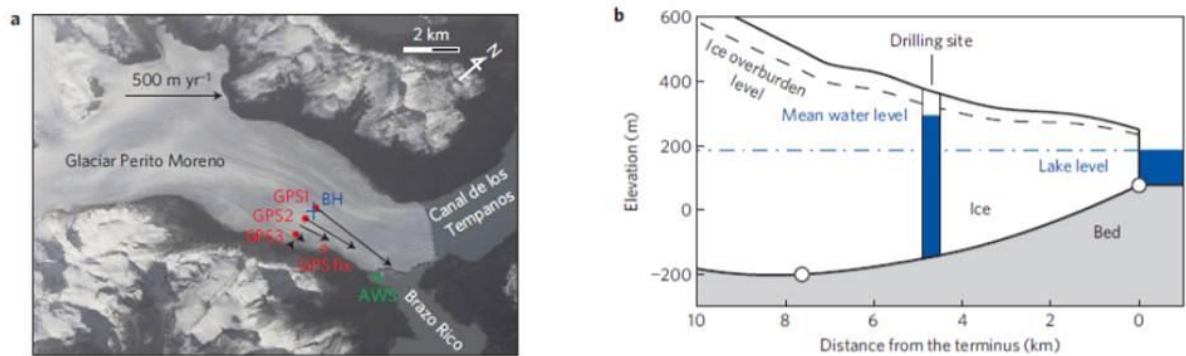


Figure 1.10 a. Satellite image of Glaciar Perito Moreno 27/3/2002 (image courtesy of NASA). GPS (filled circle, open circle), drilling (plus) and air temperature measurement (box) are indicated with ice flow vectors measured from 31/12/2008 to 7/1/2009. b. Cross section of bed profile drawn by interpolation of observational data points (open circle). Mean borehole water level during the measurement period is indicated. From Sugiyama et al. (2011).

The flow rates of Perito Moreno glacier were first measured by Raffo et al. (1953) and has been the subject of many (largely ground based) studies since then (Michel and Rignot, 1999). The most notable of which is Sugiyama et al. (2011) who conducted dGPS measurements during 2 field seasons in January 2009 and 25th February to 2nd April 2010, crucially during the second field season they were the first study in Patagonia to collect data from 2 boreholes between 4th to 13th March (Figure 1.10). Whilst this is a limited survey period, they were able to report that 40% of the changes in ice flow speed were preceded by changes in basal water pressure, which they argue was the driving factor (Figure 1.10). Sugiyama et al. (2011) found a relatively high correlation coefficient ( $r=0.76$ ) between hourly

ice speed flow and air temperature (Figure 1.11), which may have been even stronger if air temperature was actually measured on the glacier.

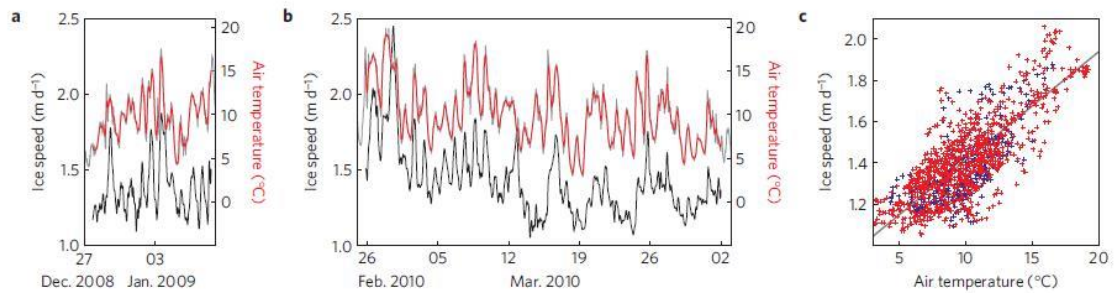


Figure 1.11 a. Ice speed at GPS1 2008/09 and 2010(black). b. Air temperature (red) from filtering hourly data (grey). c. Scatter plot of hourly ice speed and air temp. 2008/09 (blue) 2010 (red). From Sugiyama et al. (2011)

The importance of contemporaneous high precision dGPS data and borehole data is that Sugiyama et al. (2011) were able to establish that subglacial water pressure was at 94-95% of the ice overburden pressure and above the level of the proglacial lake. Therefore they were able to argue that the rapid transfer of meltwater into the system (via extensive crevassing) was sufficient to easily raise the subglacial water pressure above ice overburden level that led to increased basal sliding (Sugiyama et al., 2011). However, this argument does depend on the assumption that the subglacial drainage system was spatially uniform and in a steady state due to consistently high levels of meltwater input throughout the year (Sugiyama et al., 2011). Therefore the presence of a proglacial lake increased the subglacial water pressure which resulted in increased ice flow within 6 km of the glacier terminus.

The observed similar water level variations in the two boreholes and englacial drainage of them during drilling, does suggest some uniformity in the drainage system at least surrounding and presumably in between these two boreholes (Sugiyama et al., 2011). Whilst this is a very limited sample across a 4 km wide glacier, there is strong logic behind assuming the swift transfer of meltwater to the basal drainage system in steady state would then lead to subglacial water pressure easily reaching ice overburden level and increasing basal sliding. If this were the case then it would lead to an increase in extensional flow, with more crevassing due to increased longitudinal strain and ‘pre-conditioning for calving’ with periods of greater mass loss. Thus emphasising the relative importance of basal water pressures and also that effective pressure dependent flow laws need to be incorporated into models of lacustrine terminating glacier evolution (Sugiyama et al., 2011). This would further understanding of how proglacial lake levels at the terminus can affect subglacial water pressures, which in turn influence rates of basal sliding and ice velocity (Sugiyama et al., 2011). Although

comprehensive discussion of glacial drainage system evolution is beyond the scope of this study.

The ideal research situation for a study into the influence of proglacial lakes on glacier dynamics is to monitor the glacier before and during lake development, as this enables the changes in processes to be monitored through the change in state. The Rhonegletscher (46°34'49"N, 8°23'2"E) is a relatively small (9 km long and 16 km<sup>2</sup>) temperate valley glacier in the Swiss Alps, that formed a proglacial lake across the terminus in 2005 as a result of ongoing retreat back into an over-deepened bedrock basin (Tsutaki et al., 2013). The rate of terminus retreat remained stable initially, with an average of 7.6ma<sup>-1</sup> (2000-2005) and 6.0ma<sup>-1</sup> (2006-2010) before increasing to 50.6ma<sup>-1</sup> (2010-2011); following calving events linked to the flotation of the glacier tongue during 2009 (Tsutaki et al., 2013). This suggests that there is a lag time between proglacial lake formation and the influence on glacier dynamics, which presumably varies between glaciers largely depending on backstress from topography and the material strength of ice (Boyce et al., 2007; Tsutaki et al., 2013). The depth of the lake at the ice front is also likely to be critical, as it will have a strong control on subglacial water pressure and therefore influence basal sliding, as well as potential flotation of the terminus. Therefore calving may be terminated if the glacier retreats into shallower areas of the lake. Following proglacial lake formation the subglacial water pressure should increase as the hydraulic head rises to be level with the surface of the proglacial lake (Sugiyama et al., 2011; Tsutaki et al., 2011). If the subglacial drainage system is not efficient, then water pressure may even exceed that imposed by the proglacial lake level, as inefficient evacuation of subglacial meltwater may lead to pressure building in the system if input exceeds output (Sugiyama et al., 2011). This increase of subglacial water pressure combined with further thinning of the glacier should decrease effective pressure and lead to an increase in ice flow velocity due to an increase in basal sliding (Bindschadler, 1983; Tsutaki et al., 2013). The precise pattern of this acceleration is critical as the increase in extensional flow can cause crevassing and thus develop structural weaknesses that Benn et al. (2007) argued were the main controls on calving. Furthermore, the increased extensional flow will lead to further thinning of the glacier, further reducing effective pressure of the glacier on the bed (Tsutaki et al., 2013). Therefore capturing the precise vertical and horizontal movements of the glacier surface is essential in understanding the mechanical processes and calculating strain rates (Tsutaki et al., 2013).

An increase in retreat rate following flotation of the glacier tongue has also been observed at the Mendenhall Glacier (22 km long), Alaska (58°26'25"N, 134°33'15"W). The Mendenhall glacier starts at an ice divide at 1,600 m on the Juneau icefield and flows down through a 2 km wide valley that narrows to 0.8 km just before the glacier terminates in Mendenhall lake at 20 m a.s.l. (Figure 1.12), which formed in the 1930s. The glacier has been in recession since the Little Ice Age, with 2 rapid periods of recession during the 1940s and the second starting in the 1990s with a corresponding increase of Mean Annual Air Temperature (MAAT) of 1.6°C (Motyka et al., 2002; as cited in Boyce et al., 2007). The topographic position and bedrock ridges are particularly distinct components of the Mendenhall glacier terminus (Figure 1.12), with a prominent bedrock spur protruding across the western side of the lake. This presumably would provide substantial support, but why then did the glacier continue to retreat relatively rapidly from the 1982 terminus position whilst it still had this lateral support from the western margin? It also raises questions as to how retreat rates will change if the glacier recedes beyond the prominent pinch point where the valley width changes from ~0.8 km to ~2km (Figure 1.12).

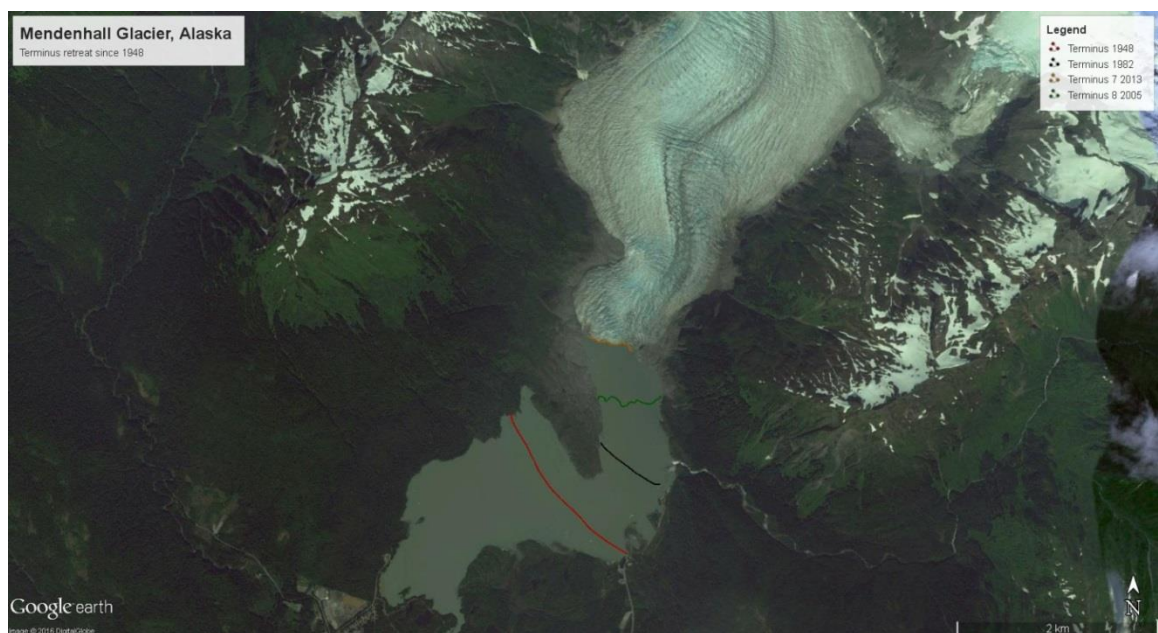


Figure 1.12 Terminus retreat of Mendenhall glacier terminus since 1948. Note that the 1948 and 1982 positions are estimated from Boyce et al. (2007), the 2005 and 2013 terminus positions were mapped in Google Earth.

The decreasing stability of the Mendenhall glacier terminus during 2000, led Boyce and others (2007) to establish an extensive monitoring campaign in which they measured; glacier mass balance, ice motion (dGPS surveys), changing terminus geometry (time lapse) , lake bathymetry (acoustic sounding) as well as establishing a weather station at the terminus and monitoring water temperature. Boyce et al. (2007) reported retreat rates of 12 m a<sup>-1</sup> (March

2002-May 2004) then increasing to  $366 \text{ m a}^{-1}$  (May 2004-August 2004) before decreasing to  $60 \text{ m a}^{-1}$  (August 2004-August 2005). Notably they argued that the observed critical thinning of the glacier was mainly from climate induced melting and also dynamic thinning due to extensional flow. As a result of this thinning subglacial water pressures exceeded over burden pressure, resulting in partial flotation of the tongue between 2002 and 2004 (Boyce et al., 2007).

Initially they propose that this flotation was stable due to ice creep accommodating the increased stresses and lateral support from the eastern margin being grounded on bedrock. This lateral support was removed by the first calving event of 25th May 2004 and by this time the ice had thinned with further weakening from small ( $\sim 1 \text{ m}$ ) changes in lake level resulting in transverse crevasses (Boyce et al., 2007). This suggests that despite the 'pre-conditioning for calving' brought about by climate induced thinning; the support from surrounding bedrock topography and capacity of the ice to accommodate increased stresses prevented the immediate onset of calving and increased mass loss. So Mendenhall glacier appears to experience periods of high retreat rates when 'topographical support' becomes ineffective (due to removal of lateral ice) and makes the glacier more susceptible to mechanical weakening associated with changes in lake level and buoyancy of ice in deep water (Boyce et al., 2007).

This 'pre-conditioning for calving' was further enhanced through thermo-erosional notches being formed on the ice cliff. Slight increases in lake level (with decreases in water temperature), following inputs of subglacial water, were then sufficient to trigger calving events on the 18th June and 23rd July (Boyce et al., 2007). The calving event on 10th July 2004 did not correspond to changes in lake level or water temperature, thus suggesting the ice had been sufficiently pre-conditioned for calving by the weakening of previous ablation, uplift and lake level fluctuations. Importantly, Boyce et al. (2007) argue that subaqueous melting was not a significant mechanism during 2004, given the cool ( $1^\circ\text{C}$ ) water temperatures and lack of convection within the lake, although it is crucial to note that temperature observations were only made below 40 m depth. Whilst these calving events increased the retreat rate of the Mendenhall glacier over a short time period, they are only 2.6% of the mass lost by surface melting between 2002 to 2005 and only represent 4% of the mean annual volume change since 1948 (Motyka et al., 2002).

Given the relatively high maximum water temperatures in the proglacial lakes of New Zealand of up to  $10^\circ\text{C}$  (compared to  $3^\circ\text{C}$  for Mendenhall lake, Alaska), it seems reasonable to

assume that subaqueous melt rates would be higher in New Zealand (Roehl, 2006; Boyce et al., 2007). Indeed, Kirkbride and Warren (1997) found distinctive geometry and evolution of the calving front of Maud Glacier (~5km long, 43°27'50.24"S, 170°30'15.49"E) from extensive field surveys. The high subaqueous melt rates and relatively stable water level resulted in distinct thermally eroded notches at the base of the subaerial ice cliff, which continued to develop into a large overhang that would eventually collapse in large and relatively rare events (Kirkbride and Warren, 1997). This process has geometric similarities to wave-cut notch erosion of sea cliffs and also leads to the development of protruding ice feet (up to 500 m long) that have some similarities to coastal wave-cut platforms (Kirkbride and Warren, 1997).

The observations from the Rhonegletscher and Mendenhall glacier suggest that ongoing retreat and glacier thinning due to climatic warming are critical (on the annual timescale) in promoting flotation of the glacier tongue, which makes it vulnerable to trigger mechanisms for calving. So glaciers become more susceptible to periods of increased mass loss through calving as proglacial lakes expand, particularly where glacier termini retreat back into deeper water and termini flotation becomes more likely.

The Yakutat glacier (337 km<sup>2</sup>) in Alaska is also experiencing strong thinning (4.76 m w.e. a<sup>-1</sup>) but maintained a floating ice tongue of 3 km in a proglacial lake for over a decade despite the calving front being over 4 km wide in water 325 m deep (Trussel et al., 2013). Trussel et al. (2013) argue that Yakutat glacier was able to maintain this floating tongue due to a lack of subaqueous melting from colder lake water (~1°C) that is less stratified, has less buoyant subglacial drainage, with less convection to transfer heat and a lack of tidal forcing to mechanically weaken the ice. They suggest that continued thinning of a terminus floating in a lake can make it susceptible to changes in water level and lead to large tabular ice bergs being calved in episodic events (2010) with long periods of stability (months-years) in between calving events. This stability can be enhanced through subglacial topography, as Trussel et al. (2013) note a relatively shallow sill (~150 m) likely supported the glacier margin between 1960-1980. This episodic nature is reflected in calving representing 7.9% of the Yakutat glacier mass loss between 2000-2007 and 16.8% between 2007-2010. Comparing the observations from the Rhonegletscher, Mendenhall and Yakutat would suggest that larger temperate glaciers are more able to sustain larger floating tongues in proglacial lakes for longer periods, but calving events then represent a higher proportion of glacier mass loss.

#### 1.6.4 Studies Investigating the Thermal Regime of Proglacial Lakes

The surface temperatures of lakes are sensitive to changes in climate, particularly changes in air temperature (Schneider and Hook, 2010). Lake surface temperature warming rates of  $0.1 \pm 0.011 \text{ } ^\circ\text{C yr}^{-1}$  (1985-2009) have been observed over Northern Europe from satellite thermal imagery, which exceeds the rate of regional air temperature warming (Schneider and Hook, 2010). This observed increase in lake surface temperatures raises the question as to whether proglacial lake surface temperatures have risen and potentially increased glacier melt rates, as well as affected ecological systems through changing water temperatures (Richards et al., 2012; Fellman et al., 2014). Given the projected air temperature increases with future climate change scenarios (IPCC AR5, 2013); this chapter will review the current understanding of factors affecting proglacial lake thermal regime.

The thermal regime of proglacial lakes and thermal processes affecting the melting of glaciers at the contact point with water has received relatively little attention. Observations have largely been constrained to point data from positioned thermistors or snap shots from thermistors lowered from boat based surveys (Chikta et al., 1999; Warren and Kirkbride, 1998; Boyce et al., 2007; Sugiyama et al., 2016, Minowa et al., 2017; Watson et al., 2020). These spatially limited studies have generally observed low proglacial lake surface temperatures of below  $3^\circ\text{C}$ , near to lake terminating glaciers in Alaska, New Zealand and Patagonia (Warren and Kirkbride, 1998; Boyce et al., 2007; Sugiyama et al., 2016). These lower proglacial lake surface temperatures have been attributed to influxes of icebergs into the lake, which tend to be during periods of enhanced calving activity (Boyce et al., 2007; Chernos et al., 2016; Sugiyama et al., 2016; Watson et al., 2020). The limited temporal sampling of these studies raises the question as to how proglacial lake temperatures evolve during periods of low iceberg calving activity. Particularly as proglacial lake surface temperatures of up to  $8^\circ\text{C}$  have been reported in Nepal, Patagonia and New Zealand, although these observations were away from the hazardous ice-water contact point (Warren and Kirkbride, 1998; Roehl, 2006; Sugiyama et al., 2016; Watson et al., 2020). It should be noted that Warren and Kirkbride (1998) made temperature observations within 10 of a glacier terminus and Roehl (2006) made temperature observations within thermal notches. The limited spatial extent of these studies also raises the question of how does the spatial pattern of proglacial lake surface temperatures vary away from the influence of icebergs. In order to explore this further, the next sections (1.6.5 and 1.6.6) will review the research into

proglacial lake thermal regime and also some of the wider literature on evolution of freshwater surface temperatures.

### 1.6.5 Proglacial Stream and Non-ice Contact Proglacial Lake Thermal Regime

As a glacier retreats back from a particular maximum position (e.g. Little Ice Age maximum) contact with a proglacial lake may be lost if the topographic basin is relatively short and the glacier retreats back up a slope (Figure 1.13). The loss of contact with the lake water will result in it having minimal influence on the glacier. However, the influx of cold glacial meltwater at inlets will have an influence on the proglacial lake thermal regime, due to differences in temperature and also density due to suspended sediment load (Richards et al., 2012). This cooling influence from the glacial meltwater input can also reduce downstream temperatures, which is likely to be ecologically significant where species, such as salmonids, depend on relatively low stream temperatures (Richards et al., 2012; Fellman et al., 2014; Peter and Sommaruga, 2017). Investigating the thermal regime of non-contact proglacial lakes is of ecological importance and can also reveal how proglacial lake temperatures may increase away from water-ice contact at glacier fronts or ice bergs (Fellman et al., 2014).

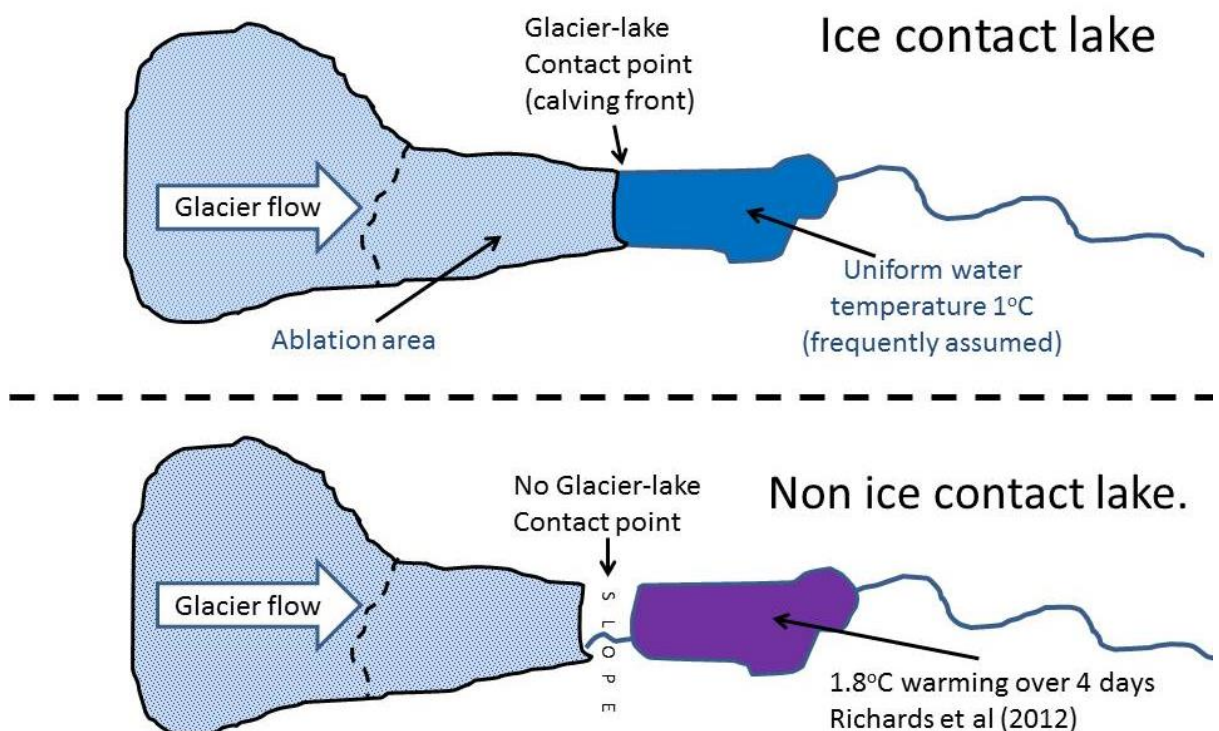


Figure 1.13 Schematic showing plan view of ice contact proglacial lake and non-ice contact proglacial lake. With typically assumed 1°C water temperatures for ice contact lake (Chernos et al., 2016) and non-ice contact warming rate of 1.8°C at Place lake (British Columbia) as observed by Richards et al. (2012) during the 4 day water residence time in the proglacial lake.

The input of glacial meltwater into a non-contact proglacial lake from a single inlet is more spatially constrained than a large (hundreds of metres) section of contact between an ice front and proglacial lake. Therefore it is easier to quantify the influence on proglacial lake thermal regime from glacial meltwater flowing through a single inlet. The water flowing through the glacial meltwater stream will be subject to climatic warming factors. Indeed, Magnusson et al. (2012) reported proglacial stream temperatures of up to 10°C within 2 km of the Damma glacier (Switzerland). These warming factors will be accentuated if the meltwater flows through other small proglacial lakes, as in the case of Place lake in British Columbia (72,000 m<sup>2</sup> in area and 1830 m asl), where Richards et al. (2012) observed inlet temperatures diurnally varying between 1 to 4°C from July to September 2007. These temperature observations emphasise the potential for proglacial water to warm away from ice-water contact points, as has also been reported by Peter and Sommaruga (2017) in the Austrian Alps. So the transfer of radiation between the atmosphere and water body, known as the surface heat flux, is discussed below.

The surface heat flux of lakes has been the focus of many studies into lake heat budgets (Richards et al., 2012). However, the surface heat flux of proglacial lakes has received relatively little attention, although Richards et al. (2012) calculated that net incoming shortwave solar radiation was the most main source of energy for short term variations of total heat content in Place lake (British Columbia). It should be noted that Richards et al. (2012) calculated the sky view factor from a high resolution DEM, in order to constrain the influence of topography on restricting incoming solar radiation. This is critical in calculating proglacial lake heat surface fluxes as the mountainous terrain can create substantial shading and so the aspect of the lake will also affect the amount of incoming solar radiation (Richards et al., 2012). The topographic situation of proglacial lakes is therefore highly likely to influence their thermal regime, as south facing lakes are likely to have higher incoming shortwave radiation than north facing lakes. Therefore, the thermal regime of proglacial lakes across a mountain area is likely to vary with topographic position and with the influence of other factors.

The inflow into non-contact proglacial lakes represents a potential input of heat into the proglacial lake system (Richards et al., 2012). Although the temperature of the inflow water will vary depending on residence time in other proglacial lakes and in the proglacial stream, as longer residence times will increase the exposure to warming factors, as Magnusson et al. (2012) report temperatures of 10°C within 2 km of the Dammagletscher terminus

(Switzerland). However, Richards et al. (2012) found that heat and water fluxes from the inflow stream (0.2 km long) and precipitation were insignificant on Place lake heat budget during summer 2007. In contrast, the biggest heat sink was found to be the outflow from the proglacial lake, which had water temperatures that were consistently similar to those recorded in the centre of the lake (Richards et al., 2012). The relatively small size of Place lake (72,000 m<sup>2</sup>) and high rates of inflow during summer 2007, led to a relatively short residence time of 4 days for water staying in the lake between inflow and outflow (Richards et al., 2012). This relatively short residence time clearly limits the potential for water to warm before leaving the proglacial lake. However, Richards et al. (2012) still observed average warming of 1.8°C for water temperatures between the inflow and outflow during summer 2007, with maximum lake surface temperatures of 6.9°C. This clearly illustrates the potential for water temperatures to increase in non-contact proglacial lakes over a short period of time. This raises the key question as to whether the distal sections of longer ice contact lakes experience similar rates of warming where they extend beyond the glacier cooling zone and whilst ice berg flux is low. However, the stratification of proglacial lake water also has to be considered, particularly where water temperatures exceed the density maximum of 3.98°C, as differences in water density can stimulate overturning in water layers and mixing may lead to lower temperatures (Warren and Kirkbride, 1998).

#### **1.6.6 Vertical Temperature Profile in Non-ice Contact Proglacial Lakes**

The vertical temperature profile of proglacial lakes is likely to vary depending on depth that solar radiation penetrates and warms surface waters; however this is likely to be countered by night time cooling (Chikita et al., 1999; Richards et al., 2012). An additional controlling factor may be the input of glacial meltwater that is high in suspended sediment, as the higher density may result in this colder (<3°C) water remaining at depth at least initially (Warren and Kirkbride, 1998; Richards et al., 2012; Sugiyama et al., 2016). Critically the concentration of suspended sediment in proglacial lake water can also control the depth of shortwave radiation penetration in the water column (Chikita et al., 1999). Indeed, Richards et al. (2012) observed water temperatures of >4°C in the upper 6 m during July/August 2007, whilst in contrast they observed temperatures of 2 to 4°C between 6 to 10 m during the same period (Richards et al., 2012). Furthermore, whilst the surface temperatures exhibited small diurnal fluctuations, temperatures at depth exhibited abrupt sub-diurnal variability (Richards et al., 2012). Richards et al. (2012) hypothesised this abrupt variability at depth was due to influx from dense turbidity flows from glacial meltwater and that these turbidity flows stopped after

August 7<sup>th</sup>. This reduction in inflow of dense sediment laden water reduced the density difference in the water column, so that water at 3.98°C (temperature density maximum) sank, which is the likely cause of the water column mixing and becoming thermally stable (Richards et al., 2012).

The change in thermal regime on August 7<sup>th</sup> resulted in lake water at all depths largely remaining around 4°C until the end of the study period, although nocturnal cooling did result in some stratification (September 2007). If the hypothesis of Richards et al. (2012) is correct, then it would suggest that the early summer warming of proglacial non-contact lake surface water can be accentuated through stratification of lake water (with denser sediment laden melt water above the lake bed) and result in notable temperatures above 4°C in surface layers. This raises the question as to how ice contact proglacial lake thermal regime evolves through the melt season in response to changes in the glacial meltwater system and meteorological conditions, which will be discussed below in section 1.6.8 (Figure 1.14).

### 1.6.7 Ice Contact Proglacial Lake Thermal Regime

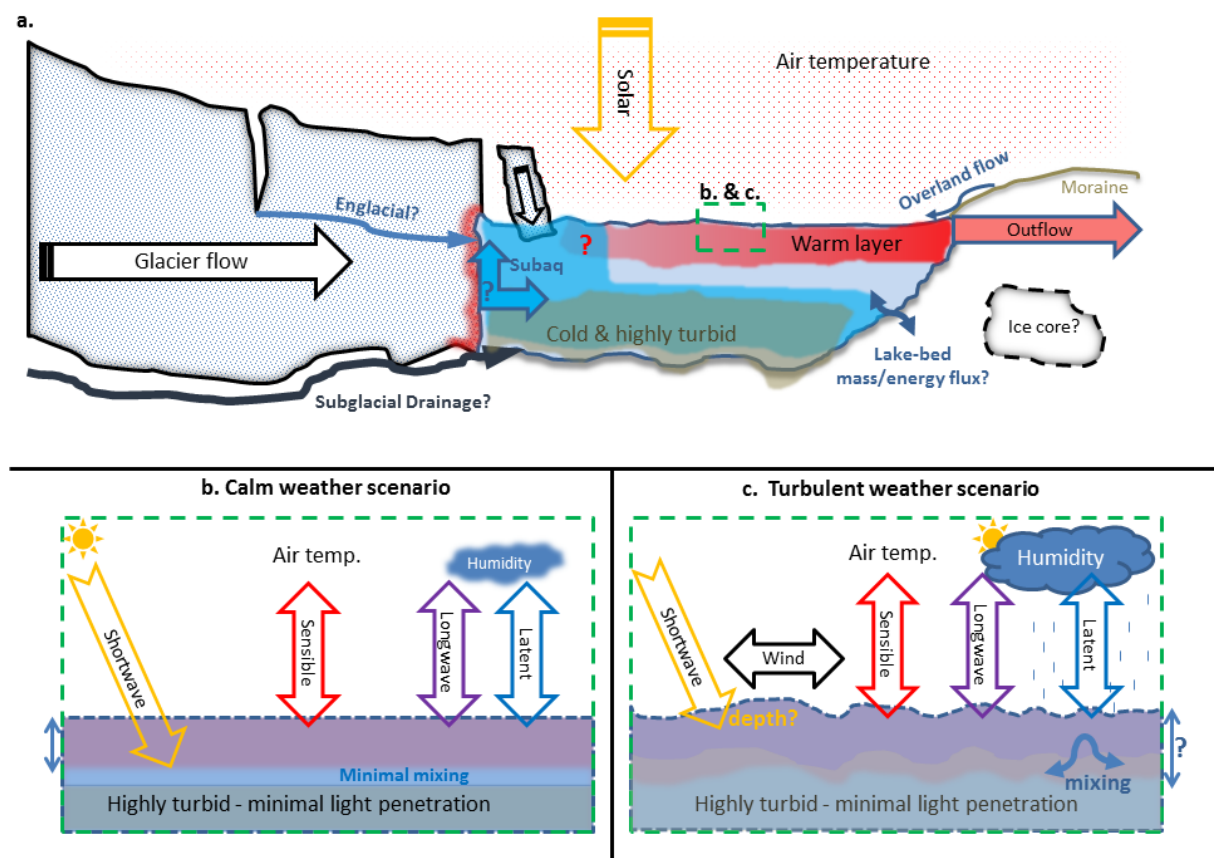


Figure 1.14 Schematic of principal components controlling ice contact proglacial lake thermal regime and potential stratification with scenarios for b. calm weather and c. turbulent weather. Partly adapted from Carrivick and Tweed (2013). With theoretical warmer surface layers (epilimnion) in pink and colder bottom layers (hypolimnion) in brown, with an intermediate layer of water (metalimnion) in between and subaqueous

meltwater shown in light blue. Boundaries between each are shown as relatively sharp, but changes in temperature (thermocline) may be less distinct. Note that proglacial lakes may also be uniform water temperatures throughout the water column. Red question mark relates to the uncertainty in horizontal extent of the warm layer (epilimnion). Solid arrows denote mass fluxes and hollow arrows denote energy fluxes (note arrows not to scale).

There are a range of factors that may control the thermal regime of proglacial lakes, with air temperature and direct solar radiation having the main warming influence on lake water (Figure 1.14) (Chikita et al., 1999; Richards et al., 2012; Peter and Sommaruga, 2017).

However, water close to the terminus will be subject to cooling from contact (with the glacier and icebergs) and meltwater input, therefore in ice contact proglacial lakes the water temperatures are likely to increase with increased distance from contact with glacier ice (Figure 1.2 and Figure 1.14) (Warren and Kirkbride, 1998). This has been observed in proglacial lakes in New Zealand, with surface (<10 m depth) temperatures of 3.0°C measured at 10 m from Maud glacier and 3.6°C 3,600 m away from the terminus between 12:30 and 15:30 respectively on 4<sup>th</sup> April 1994 (Warren and Kirkbride, 1998). On 24<sup>th</sup> March 1995 water temperatures of 3.8°C were measured ~200 m away from Maud glacier and 4.2°C at ~2,000 m away from the terminus, although note these temperatures were recorded at the later times of 17:30 and 18:00. These observations suggest that there is a zone of cooling influence near to the glacier, whilst distal sections of the lake may be beyond this direct cooling influence. This is an important observation as it demonstrates that a temperature gradient may exist across the length of a proglacial lake.

However, this temperature gradient was not observed in other proglacial lakes in New Zealand during the same period, such as Hooker lake and Tasman lake (Warren and Kirkbride, 1998). In the case of Hooker lake, Warren and Kirkbride (1998) come to the logical conclusion that the uniform cold temperatures (1.7°C to 0.21°C) across the whole lake are due to the widespread distribution of ice bergs and subsequent cooling from melt, with larger bergs becoming grounded mid-lake and smaller bergs reaching the distal section of the lake. In contrast, they attribute the cold temperatures observed in Tasman lake during the same period to lake water contact with dead ice, which makes up over half of the lake perimeter (Warren and Kirkbride, 1998). Both the cooling of proglacial lake water due to widespread ice berg distribution and contact with marginal dead ice seem highly likely and highlight the complexity of the spatial pattern of proglacial lake water temperatures. Clearly the extent and distribution of ice contact has a substantial influence on proglacial lake temperatures, although this is likely to vary through time, particularly where controlled by periods of high ice berg flux (Warren and Kirkbride, 1998).

Where glacier termini contact water the hazards surrounding ice berg calving events are usually considerable and make obtaining direct observations from the ice-water contact point highly problematic. Despite this, Warren and Kirkbride (1998) made observations as close as 10 m away from lake terminating glaciers in New Zealand. Crucially they found that surface temperatures in front of Grey glacier decreased during the day, whilst elsewhere in Maud lake surface temperatures rose by 0.2°C (from 4.5°C) between the morning and afternoon observations on the same day (Warren and Kirkbride, 1998). The spatial extent of this meltwater body is difficult to quantify from thermistor point measurements (Figure 1.14 light blue body), which hinders the interpretation of the source and also persistence through time. This raises the question of how the lake water varied in density across the vertical column, as they argue that ‘an amount’ of meltwater may have risen to the surface due to buoyancy, as there was no evidence of a meltwater overflow (Figure 1.14 light blue arrow)(Warren and Kirkbride, 1998). However, they also observed ‘interfingering’ of glacial meltwater with ambient lake water near the ice-water contact point, suggesting that the mixing of meltwater and ambient lake water is complex and partly controlled by proglacial lake thermal stratification (Warren and Kirkbride, 1998). This raises the critical issue of the horizontal extent of the warm surface layer (epilimnion) (denoted by the red question mark in Figure 1.14), as the proximity of warmer water to the glacier front will have a strong control on subaqueous melt rates. Although it should be remembered that water circulation at the ice front also has a strong control on subaqueous melt rates (Roehl et al., 2006). In order to consider the processes controlling water circulation, it is imperative to consider different meteorological scenarios, which for the purposes of simplicity are classified as the ‘calm weather’ scenario and ‘turbulent weather’ scenario (Figure 1.14). Although in reality classifying weather conditions into a continuum is problematic.

As previously discussed, the processes controlling thermal structure of proglacial lakes will largely be driven by meteorological conditions, as well as input of glacier ice and meltwater (which are also related to meteorological conditions). Therefore it is also imperative to consider how differing meteorological conditions may affect the energy and mass flux of proglacial lakes, particularly with regard to movement of mass and consequent changes in the thermal structure. Two different weather scenarios (calm and turbulent) will be discussed below in order to guide the reader further before reviewing the literature on glacial lake thermal regime in more depth (Figure 1.14).

The 'calm weather' scenario (Figure 1.14 b) might typically be associated with clear sky conditions with minimal wind. Under these conditions direct solar shortwave radiation will penetrate into the water column and lead to warming of the surface layer (Figure 1.14) (Chikita et al., 1999; Richards et al., 2012). Where proglacial lake water has a high suspended sediment concentration, this will likely inhibit the depth of solar shortwave radiation penetration into the water column and therefore control the depth (centimetres to metres) of the warm surface layer (epilimnion) under calm conditions (Chikita et al., 1999; Richards et al., 2012).

There will also be a sensible heat flux between the water body and the atmosphere, as if air temperatures are sufficiently high enough during the daytime this will warm the water surface (centimetres) (Richards et al., 2012). Counter wise if night time temperatures are sufficiently cool enough (below lake temperature) then there will be a period of night time sensible heat flux from the lake to the atmosphere (Richards et al., 2012; Watson et al., 2020). The top millimetres (skin surface) of the lake water will also be subject to incoming and outgoing longwave radiation flux during the diurnal cycle (Aubry-Wake et al., 2015). There will also be a cooling effect on lake temperatures from the latent heat flux associated with evaporation of lake water to the atmosphere, which in turn will partly be controlled by atmospheric water concentration (humidity) (Richards et al., 2012). Particularly as counter wise, condensation of atmospheric water vapour on the lake surface will have a warming effect on the lake surface water through latent heat release following the change in state from vapour to liquid (Richards et al., 2012).

The turbulent weather scenario (Figure 1.14c) is assumed to have higher cloud cover than the calm weather scenario (although this may not always be the case as high winds may also occur under clear skies in some situations). The higher cloud cover will result in a lower flux of direct solar radiation (although there will still be some diffuse solar radiation) and therefore have less warming influence than compared to the calm (clear skies) scenario (Richards et al., 2012). There will also be a greater incoming flux of downwelling atmospheric longwave radiation due to higher atmospheric water content (particularly from clouds) which will warm the skin (millimetres) of the lake water (Aubry-Wake et al., 2015).

A critical aspect of the turbulent weather scenario, is higher wind speeds, as this will drive mixing of the surface water layers (Warren and Kirkbride, 1998; Chikita et al., 1999; Sugiyama et al., 2016). Therefore redistributing heat absorbed in the upper layers further down the water column and mixing with cooler water, which may also reduce stratification of

the water column (Warren and Kirkbride, 1998; Chikita et al., 1999; Watson et al., 2020). The wind direction is crucial, as winds blowing towards the glacier will advect warmer water towards the ice front (Chikita et al., 1999). Where warmer water comes into contact with the ice front, it will increase subaqueous melt rates, particularly if combined with water circulation (Chikita et al., 1999). Therefore the vertical temperature profile of the water column is also important in determining the vertical distribution of subaqueous melt rates of the ice front and the evolving geometry of the subaqueous terminus (Sugiyama et al., 2016; Sugiyama et al., 2019).

### **1.6.8 Vertical Temperature Profile in Ice contact Proglacial Lakes**

As with non-contact proglacial lakes, the input of glacial meltwater with high suspended sediment load tends to develop as a cold layer above the lake bed (hypolimnion) (Figure 1.14) (Warren and Kirkbride, 1998; Chikita et al., 1999; Sugiyama et al., 2016). The penetration of solar radiation tends to warm the surface waters, although night time cooling can then introduce instability to produce a more turbulent warm layer below the surface (epilimnion) (Warren and Kirkbride, 1998; Chikita et al., 1999). A transition layer of varying thickness and moderate temperatures (metalimnion) can form between the epilimnion and hypolimnion (Figure 1.14). The stability of such thermal stratification largely depends on the density of water across the water column, so that if surface water remains consistently above or below the density maximum of 3.98°C then overturning will not be driven by temperature changes (Warren and Kirkbride, 1998; Chikita et al., 1999). Indeed Hooker Lake (~2.5 km long, max. depth ~136 m and 877 m asl) in New Zealand was observed to have a relatively cold surface epilimnion layer (1.7°C to 1.4°C) and also thermal stratification below that with a colder bottom hypolimnion layer (0.5°C to 0.21°C) and metalimnion layer between 55 to 65 m depth (Warren and Kirkbride, 1998). The stability of such thermal stratification depends on differences in water density through the water column to be maintained, particularly through input at depth of cold subglacial meltwater with high suspended sediment load (Warren and Kirkbride, 1998; Sugiyama et al., 2016).

In contrast during the same study period (and region) both Maud (~2.5km long and 1,035 m asl) and Godley lakes (~4 km long and 1,095 m asl) were observed to be isothermal, with very little (0.4°C) change in temperature with depth (Warren and Kirkbride, 1998). Whether Maud and Godley lakes had thermal stratification earlier on in the summer is hard to establish, but Warren and Kirkbride (1998) postulate that stratification was likely if

subglacial meltwater input with high suspended load was high enough to develop a hypolimnion and surface warming created a warm epilimnion. They argue the strong katabatic winds that are common in the study area during summer likely resulted in extensive mixing down to a depth of 100 m (both lakes have a maximum depth of 100 m), which combined with an exhaustion of sediment supply led to a break down in the thermal stratification (Warren and Kirkbride, 1998). In contrast Hooker lake (maximum depth 136 m) is at a lower altitude (877 m) and the glacier has a larger ablation area, so surface warming continues into the autumn, as does input of turbid meltwaters, which help to maintain thermal stratification for longer before becoming isothermal later in the autumn (Warren and Kirkbride, 1998). This change in thermal structure across the water column is critical as heat is redistributed from surface waters to depth and potentially controls the subaqueous melt rates acting on the glacier front (Warren and Kirkbride, 1998).

The presence of a warm ( $>3^{\circ}\text{C}$ ) surface layer (epilimnion) in contact with the glacier terminus is likely to increase subaqueous melt rates (Warren and Kirkbride, 1998; Haresign and Warren, 2005; Sugiyama et al., 2016). Where water temperatures below this epilimnion are cold ( $<1^{\circ}\text{C}$ ) subaqueous melt rates are likely to be lower and so the geometry of the glacier terminus will develop a protruding ‘ice foot’ below the warmer surface water, as has been reported in Patagonia (Sugiyama et al., 2019). Where the warm surface waters contact ice an undercut thermally eroded notch is likely to form due to high subaqueous melt rates (see section 1.6.10 for further discussion of lake evolution on debris covered glaciers) (Warren and Kirkbride, 1998; Roehl, 2006; Sugiyama et al., 2016). Indeed, Roehl (2006) observed surface temperatures of  $\sim 3^{\circ}\text{C}$ , which rapidly decreased to  $\sim 1^{\circ}\text{C}$  at 10 m depth 18 m away from the terminus of Tasman glacier and rapid thermally eroded notch formation (maximum rate of  $65\text{cm d}^{-1}$ ) in December 2001. Roehl (2006) also observed maximum surface water temperatures of  $10^{\circ}\text{C}$  135 m away from Tasman glacier terminus. This thermal undercutting of the subaerial ice cliff is likely to lead to high calving rates (Warren and Kirkbride, 2003). Indeed Warren and Kirkbride (1998) and Minowa et al. (2017) found a correspondence between lake surface temperatures and frontal ablation rates. Furthermore, Warren and Kirkbride (1998) note that it seemed probable that all the proglacial lakes studied in New Zealand were likely to have summer water temperatures of  $2^{\circ}\text{C}$  to  $4^{\circ}\text{C}$  and be highly heterogenous, with lakes in similar situations having different thermal structure. This emphasises the need for further study into proglacial lake thermal regime through the melt season and not just a snapshot of proglacial lake thermal structure at limited time points.

The evolution of proglacial lake temperatures has been observed through the austral spring with 3 separate surveys in October and November at Glaciar Leon (11 km long, 46°46' S, 73°13' W), an outlet glacier draining the eastern side of the Northern Patagonian ice field (Haresign and Warren, 2005). The proglacial lakes in Patagonia are substantially larger than those in New Zealand, with Lago Leones being 10km long, 2.5 km wide and having a maximum depth of 360 m (Haresign and Warren, 2005). Indeed, Haresign and Warren (2005) argue that the relatively warm temperatures of 5 to 8°C they observed in the lake during the spring are likely due to the large lake size diluting the cooling influence of meltwater and strong warming factors due to the low altitude (303 m) and latitude (46°S). What's more, they observed relatively warm ice proximal (~200 m away from the terminus) surface temperatures of between 7°C down to 5°C at ~5 m, below which near isothermal conditions of ~5°C existed on 19<sup>th</sup> October 2002 (Haresign and Warren, 2005). Interestingly they found similar surface temperatures across the lake, although the distal vertical temperature profile exhibited a weak thermocline (abrupt temperature gradient) at ~35 m depth (Haresign and Warren, 2005). They found that this thermocline in the water column progressed westwards towards the glacier front through the November, which suggests increased mixing of the surface waters to a greater depth as the season advanced (Haresign and Warren, 2005). This progression westwards is against the dominant westerly wind direction, from katabatic winds coming off the glacier. This suggests that proglacial lakes have a complex pattern of temperature structure that evolves through mixing processes through the melt season (Chikita et al., 1999).

The thermal structure of water in front of several glacier fronts emanating from the Southern Patagonian icefield has also been investigated through boat based surveys by Sugiyama et al. (2016) during austral summer 2013 (Figure 1.15). It should be noted that Lago Argentino (~1480km<sup>2</sup> up to ~500 m deep and 32 km wide) is substantially larger than the New Zealand proglacial lakes discussed above. Indeed the separate branches of Lago Argentino are named as lakes in their own right and are perhaps more comparable to fjord systems due to their size. The only lake to exhibit 3 clearly stratified layers during the study of Sugiyama et al. (2016) was Brazo Upsala, with a surface layer between 4.5 to 5.0 °C, metalimnion of 3.4°C between 40 m to 280 m and cold layer of 2.06 to 1.6°C between 280 m to 470 m (Figure 1.15). Although towards the glacier front they also observed a further highly turbid bottom layer of subglacial meltwater at 0.80°C to 0.56°C below 470 m (Figure 1.15) (Sugiyama et al., 2016). The 3 layer structure observed at Brazo Upsala and cool surface layer due to high iceberg flux is similar

to that observed at Hooker glacier by Warren and Kirkbride (1998). This suggests that a high input of subglacial meltwater with high suspended sediment concentration maintains density gradients across the water column and helps to maintain thermal stratification (Figure 1.15) (Chikita et al., 1999; Sugiyama et al., 2016). Furthermore, the high turbidity of cold ( $1^{\circ}\text{C}$  to  $-0.2^{\circ}\text{C}$ ) bottom water in Lago Viedma helped maintain a 2 layer thermal stratification, with a distinct thermocline at 118 m depth and surface temperatures reaching  $\sim 6.5^{\circ}\text{C}$  (Figure 1.15) (Sugiyama et al., 2016). It should be noted that these survey results represent a snapshot on 1 day and that this thermal structure may change through the melt season, particularly if subglacial sediment supply is exhausted or surface temperatures drop below the density maximum temperature of  $3.98^{\circ}\text{C}$  (Warren and Kirkbride, 1998).

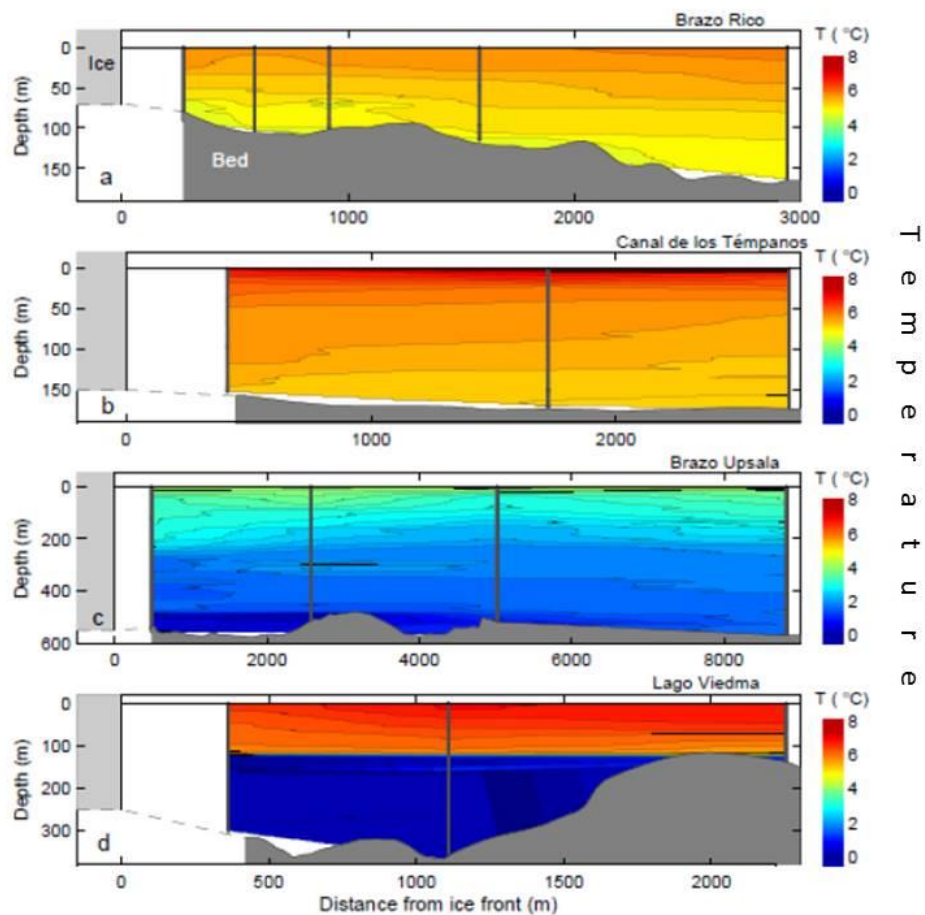


Figure 1.15 Side view of vertical temperature profiles of proglacial lakes in Patagonia during December 2013, with horizontal interpolation between survey points (grey vertical lines) and bed topography in grey. Note the white bar indicating space between the ice front and nearest survey point (grey vertical lines). Brazo Rico and Canal de los Témpanos are both in contact with glacier Perito Moreno, whilst Brazo Upsala and Lago Viedma are in contact with glaciers of their name sake. From Sugiyama et al., (2016).

In contrast to Brazo Upsala and Lago Viedma (in contact with namesake glaciers), the lakes (Brazo Rico and Canal de los Témpanos) in contact glacier Perito Moreno exhibited no

distinct thermal stratification during the survey of Sugiyama et al. (2016) (Figure 1.15). They suggest that this relatively isothermal structure is due to the effects of wind driven circulation, which effectively mixes warm surface water ( $\sim 6^{\circ}\text{C}$ ) down to depths of 200 m (Figure 1.16) (Sugiyama et al., 2016). Given the strong katabatic and westerly wind patterns on the east side of the Patagonian ice caps, this wind driven recirculation seems highly likely. These observations of wind driven remixing would suggest that wind patterns can regulate surface temperatures of proglacial lakes, which in turn will affect subaqueous melt rates and formation of thermally undercut sections of the ice front (Figure 1.16).

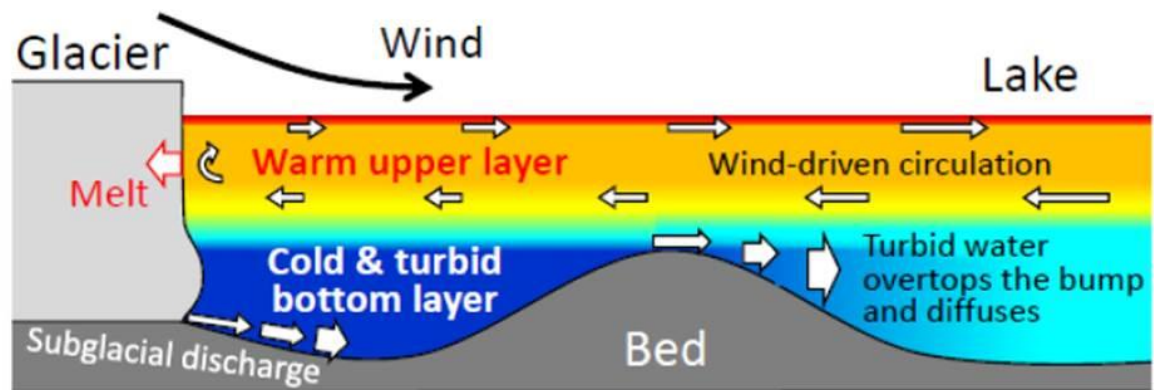


Figure 1.16 Schematic diagram from Sugiyama et al. (2016), showing proposed factors influencing Patagonian proglacial lake thermal structure. Based on observations made during the study (see Fig.12 above).

The distribution of subaqueous melt rates at the ice front is likely to vary with thermal structure (Figure 1.16). However, due to the hazards of accessing the ice-lake contact point no observations were made within 300 m of ice fronts during the survey of Sugiyama et al. (2016) (Figure 1.15). Whilst they acknowledge this limitation, they have estimated subaqueous melt rates from interpolating the nearest readings to the ice front (Sugiyama et al., 2016). This has been done using empirical relationships based on laboratory experiments and observations from ice bergs, which have been corrected to account for the difference between saline and freshwater (Sugiyama et al., 2016). However, Haresign and Warren (2005) question the application of such empirical data to calculating subaqueous melt rates at a lacustrine terminating ice front, particularly as it is unclear as to whether length ( $l$ ) should apply to the ice cliff depth or width and also do not account for forced convection. Whilst these calculations are relatively crude, Sugiyama and others (2016) would suggest that subaqueous melt rates can account for up to 19% of mass loss at the terminus of Glacier Perito Moreno, although this figure would be higher ( $\sim 70\%$ ) if currents at the ice front were constrained (Sugiyama et al., 2016; Minowa et al., 2017). Furthermore, Haresign and Warren

(2005) argue that they could not calculate accurate subaqueous melt rates for Glaciar Leon (Patagonia) due to a lack of data on upwelling rates and currents at the ice front, although they do suggest waterline melting may account for half of the mass loss at the terminus. However, it is imperative to consider the observations of proglacial lake surface cooling 10 m in front of Godley glacier, whilst the rest of the lake surface waters warmed by 0.2°C (Warren and Kirkbride, 1998), as this would call in to question the robustness of interpolating water temperatures at the ice-water contact point from observations 300 m away.

The observations of lake water cooling in front of a lacustrine terminating glacier by Warren and Kirkbride (1998) emphasises the need of high spatial resolution observations of proglacial lake temperature at the ice-water contact point. This is essential in order to constrain subaqueous melt rates, which in turn control the development of thermally eroded notches and subaqueous glacier front morphology. The development of thermally eroded notches and protruding ice feet can influence the rate of mechanical mass loss processes (iceberg calving) at the ice-water contact point. As a result changes in thermal structure of ice contact proglacial lakes can not only affect the glacier mass loss through changes in subaqueous melt rates, but also mechanical processes of mass loss as previously discussed.

### **1.6.9 Glacial Lake Thermal Regime on Debris Covered Glaciers in the Greater Himalaya**

The down wasting of debris covered glacier tongues with low profile angles resulted in the formation of supraglacial ponds through thermokarst processes (Figure 1.17) (Kirkbride, 1993). These supraglacial ponds sometimes then coalesce through retreat of ice cliffs and collapse of englacial channels to form a supraglacial lake, with a lake bed consisting of glacial ice, often with a substantial debris cover (Kirkbride, 1993). After the lake bed has become substantially ice free (through subaqueous melt and subaqueous calving) then it becomes a proglacial lake (Figure 1.17) (Kirkbride, 1993). It is imperative to distinguish (although difficult) between supraglacial and proglacial lakes as the glacier ice at the lake bed may have a substantial cooling impact on the temperature structure of the lake where there is ice contact and production of meltwater (Chikita et al., 1999). The genesis of proglacial lakes from debris covered glaciers and geometry of the calving front is also notably different from debris free systems due to the potential insulating effect of the debris cover over glacier ice, so subaqueous ice ramps may persist for longer periods of time (Kirkbride and Warren, 1997; Robertson et al., 2012). Therefore glacial lakes from debris covered glaciers in the Himalaya

are treated as a separate subcategory in this study, particularly as in many cases the presence of ice at the lake bed has not been recently confirmed from field studies to enable distinguishing whether the lake is supraglacial or proglacial. Furthermore, there is some reference to supraglacial ponds, but studies into these are not reviewed in detail due to the presence of ice at the lake bed and difference in scale to most proglacial lakes (as well as water residence time).

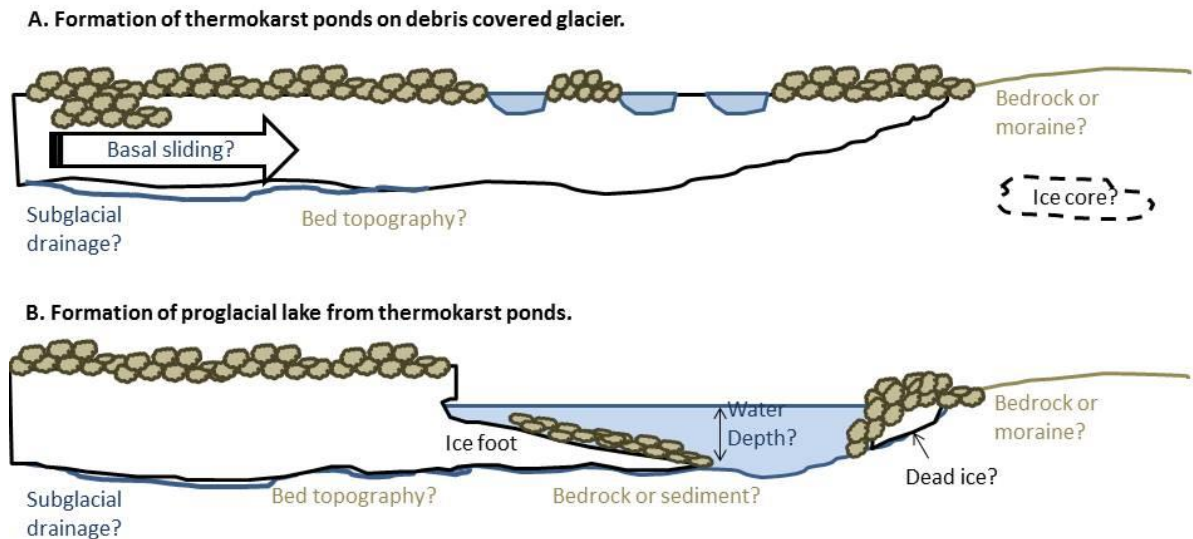


Figure 1.17 Schematic of formation of glacial lakes on debris covered glaciers. The initial formation of supraglacial ponds (A) is followed by an intermediate stage where coalescence of ponds forms a supraglacial lake with a lake bed consisting of glacier ice (likely to be debris covered). Once a substantial section of the lake bed is ice free then it becomes a proglacial lake (B). Note the presence of the ice foot (Kirkbride, 1993; Warren and Kirkbride, 1997).

The prolonged existence of large ice ramps protruding into the lake (usually with slopes of  $\sim 20^\circ$ ), would suggest that subaqueous melt rates are perhaps not as dominant in the mass loss of these lacustrine terminating glacier systems. However, Robertson et al. (2012) argue that debris covers of up to 10 m thick are sufficiently thick enough to insulate the ice foot from proglacial water temperatures. Furthermore, they argue that the debris covering the terminus and the ice foot can suppress the buoyant forces acting on the ice temporarily, with some sporadic large subaqueous calving events occurring when the buoyant forces exceed the overburden pressure (Robertson et al., 2012). Subaqueous calving from a debris covered ice foot has also been observed at Thulagi glacier in Nepal (Watson et al. 2020). The presence of ice feet protruding from calving fronts in New Zealand, Nepal and Patagonia also highlights the need for bathymetric data (Sugiyama et al., 2019; Watson et al., 2020), particularly as the plot of calving rate versus width averaged proglacial lake depth (Figure 1.8) from Warren et al. (1995), is only based on 14 data points. This is particularly important as the glacier terminus

will behave differently if the ice mass extends into the lake (subaqueously), particularly if it succumbs to buoyancy forces (Watson et al., 2020). Furthermore, Quincey and Glasser (2009) argue that constraining the presence and influence of subaqueous protruding ice feet is a priority for further research, as it would advance quantitative mechanics based predictions of mass loss at lacustrine termini. The study of thermal structure within glacial lakes in the Himalaya has received some attention due to the potential for thermal undercutting to increase iceberg calving rates and lead to lake expansion that could produce larger GLOFs (Chikita et al.; 1999; Chikita, 2007; Sakai et al., 2007). It is imperative to note that the presence of ice at the lake bed may have a cooling influence on lake water near the bed, where there is contact between the two (Chikita et al., 1999). Despite this vital difference, the input of glacial meltwater and meteorological influences acting on supraglacial lake thermal regime are likely to be similar to proglacial lakes in comparable situations (size and topographic setting). There has been more study of the influence of wind on lake water circulation and stratification for supraglacial lakes, which have implications for the study of proglacial lake thermal regime.

The recent study of Watson et al. (2020) has provided some advances in understanding of glacial lake thermal regime, particularly insights into seasonal fluctuations in temperature from thermal satellite observations (ASTER and Landsat). They report increases in average lake surface skin (top mm) temperature after the spring melt of lake ice and declines before freeze up in the autumn, with a plateau in temperatures during the monsoon, for 3 glacial lakes in Nepal (Watson et al., 2020). The average lake surface skin temperature (excluding pixels with icebergs) was extracted from ASTER and Landsat land surface temperature products (see section 3.1 for a detailed review of extracting lake surface temperatures from satellite thermal imagery) for Imja Tsho, Lower Barun, and Thulagi glacial lakes, with respective observed maximums of 9.6°C, 7.2°C and 10.8°C between 2000 to 2018. These observations suggest that the thermal regimes of these lakes are quite different, with Thulagi likely being the warmest, although it is imperative to remember that satellite thermal observations represent a temporally limited snapshot of the skin (top mm) surface temperature.

The temperature across the water column at distal part of the Thulagi glacial lake was also investigated by Watson et al. (2020) over a 48h period from 28<sup>th</sup> to 30<sup>th</sup> October 2017. During this relatively short period, they observed temperatures in the top 10m converging around midday, due to solar warming of shallower layers and mixing due to thermal

convection as well as forced convection (wind and iceberg driven) (Watson et al., 2020). Crucially they observed relatively uniform suspended sediment concentration in towards the surface and an exponential decrease in light penetration through the upper water column (Watson et al., 2020). Therefore solar penetration and heating was limited to the upper few metres, with warming below this due to convection, as is evident from warming of the water column below ~2m during the latter part of the day and into the night. In contrast the surface layers cooled ~1°C during the early night and ice formation was noted on the lake surface. Thus emphasising the importance of night time cooling on glacial lake thermal regime. Furthermore, it is likely that night time cooling is less substantial at Thulagi lake due to the higher air temperatures, given the lower altitude of 4045 m, compared to 4538 m at Imja and 5005 m at Lower Barun (O'Reilly et al., 2015). The lake water in contact with glacier ice is likely to be colder than water further away from the ice front, due to direct contact with glacier ice and the influx of meltwater from the glacier (Chikita et al., 1999; Roehl, 2006). The input of cold (<1°C) glacial meltwater with high suspended sediment concentrations (SSC) has been observed to form density currents and sediment laden underflows out from the glacier terminus into deeper zones of the lake in contact with Trakarding glacier in Nepal (Chikita et al., 1999). Critically, Chikita et al. (1999) observed that suspended sediment concentrations in Tsho Rolpa (in contact with Trakarding glacier) were sufficiently high enough to overcome the temperature density differences. Consequently they found that the stratification of Tsho Rolpa was defined by SSC rather than temperature differences (Chikita et al., 1999). As a result the lower layers of water in Tsho Rolpa had high SSC and temperatures below 2.5°C, with a prominent thermocline at ~25 m above which temperatures of >5°C were observed in the epilimnion (near surface layers) (Chikita et al., 1999). The observation of temperatures above the density maximum (3.98°C) in the epilimnion is a critical finding, as it confirms that SSC can be sufficiently high to stop water >3.98°C sinking from the surface layers and mixing to produce water with lower temperatures (Chikita et al., 1999). The development of this warm (>4°C) epilimnion has substantial implications for glacier subaqueous melt rates.

As the length of glacial lakes increases the distal zones of glacial lakes are subject to less cooling influence than ice proximal areas (if the influx of cold meltwater is not sufficient to dominate across the whole lake). This temperature gradient was observed across Tsho Rolpa, with distal temperatures of >5°C and ice-proximal temperatures of ~2.5°C, which Chikita et al. (1999) attributed to the influx of ice meltwater and glacier cooled surface water. Watson et

al. (2020) reported a significant cooling event ( $\sim 2^{\circ}\text{C}$ ) from the satellite thermal image analysis of the Thulagi glacial lake, which they argue was due to a relatively large volume of icebergs ( $\sim 500,000 \text{ m}^3$ ) following calving events during summer 2017 and subsequent melt of icebergs over several months. Crucially they observed that glacial lake skin surface temperatures ‘returned to normal’ during the melt season following the melt of these icebergs (Watson et al., 2020). This suggests that calving events can have a substantial impact on glacial lake temperatures although the temporal extent may be limited. They also observed icebergs moving back and forth across the lake, due to daytime winds being predominantly up valley and night time winds being predominantly down valley during fieldwork in 2017 (Watson et al., 2020). Therefore suggesting wind regime plays an important role in movement of icebergs and also their influence on mixing of the upper water column, as well as spatial distribution of cooling influence from iceberg melt across the lake.

Critically, Chikita et al. (1999) observed expansion of the  $>5^{\circ}\text{C}$  warm water across Tsho Rolpa towards the Trakarding glacier terminus during the afternoons, driven by valley winds blowing towards the glacier. These wind driven currents resulted in warm water ( $\sim 4.5^{\circ}\text{C}$ ) coming into contact with the glacier terminus and resulting in high subaqueous melt rates undercutting the ice cliff and leading to increased calving rates with maximum lake expansion of  $0.18 \text{ m d}^{-1}$  between September 1993 and June 1994 (Chikita et al., 1999). Thermal undercutting of Thulagi glacier terminus was also argued by Watson et al. (2020) to be the dominant driver of calving during 2017, as indicated by the distinctive crescent pattern of crevassing immediately behind the ice front. Chikita et al. (1999) also observed counter currents that were also partly driven by turbid meltwater (high SSC) emanating from englacial channels from the terminus (Figure 1.18). These counter currents resulted in uplift of colder water near the distal end of the lake, although this varied diurnally with varying wind speed (Chikita et al., 1999). This upwelling colder water was then subject to warming from incoming solar radiation, although there was some cooling due to sensible heat exchange (Chikita et al., 1999) (Figure 1.18).

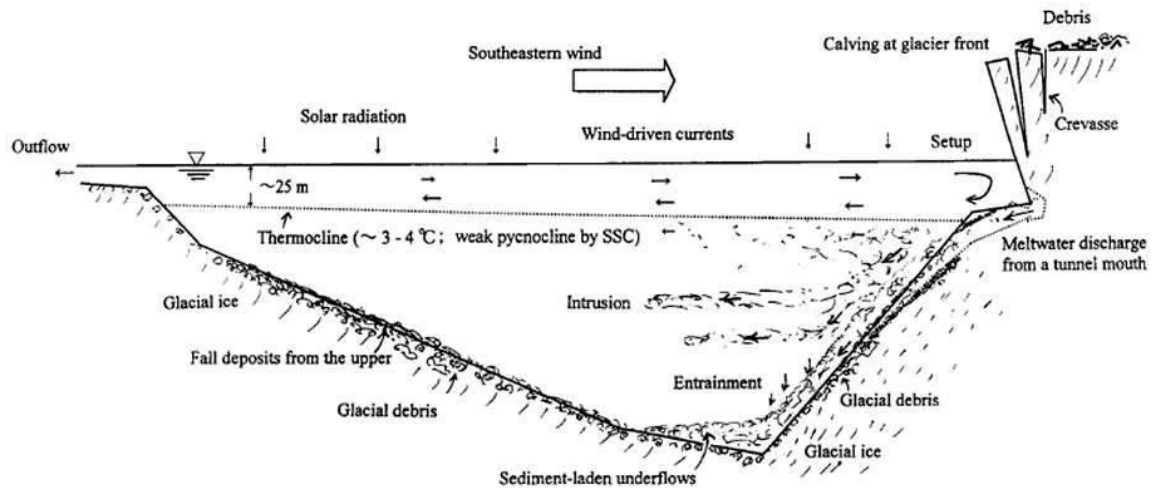


Figure 1.18 Conceptual model of supraglacial lake current system in Tsho Rolpa on Trakarding glacier (Nepal) from Chikita et al. (1999). Also illustrating sediment laden flows in the system and influence of suspended sediment concentration on lake stratification.

The observations and conceptual model (Figure 1.18) proposed by Chikita et al. (1999) present a systematic process for glacial lake circulation to result in relatively efficient transfer of heat towards the ice front and result in rapid retreat of lake terminating glacier fronts. The role of englacial drainage potentially driving water circulation at the ice front remains an open research question, but would most likely enhance subaqueous melt rates further (Roehl, 2006). The influence of wind driven currents on this process is clearly critical and dependent on topographic location, size of the glacial lake and wind patterns (Chikita, 2007; Sakai et al., 2009).

The length and topographic setting of glacial lakes will also have a strong control on wind speeds, with larger lakes experiencing greater fetch and less topographic screening resulting in greater wind speeds across the lake surface (Chikita, 2007). Indeed, Chikita (2007) found that in contrast to Tsho Rolpa, wind stress over Imja lake was insufficient to drive water currents. The lower velocity of valley winds over Imja lake surface was partly through screening from the end moraine (and dead ice zone) that was ~25 m higher than the water surface (Chikita et al., 2007). The lower wind driving stress over lake Imja resulted in less surface mixing and a shallower seasonal thermocline (4.5 m) with warmer temperatures of 6 to 8°C, in contrast to the deeper (24.2 m) thermocline with temperatures of 3 to 4°C observed in Tsho Rolpa (Chikita et al., 1999; Chikita, 2007). In both lakes colder (< 3°C) turbid meltwater occurred below the thermocline, which tended to deepen towards the glacier front (Chikita et al., 2007).

It is imperative to note that Chikita (2007) argues that the deepening of the thermocline towards the glacier in lake Imja does suggest some wind driven mixing and propose a threshold velocity of  $0.4 \text{ m s}^{-1}$  for this to occur. These observations of near surface glacial lake temperatures above  $3.98^{\circ}\text{C}$  are of critical importance for glacial lake thermal regime as they confirm that water above the temperature density maximum can persist at the surface if the water column is underlain by waters with high suspended sediment concentration and wind velocities are too low for wind driven mixing to occur. The observations from these studies were missed by Watson et al. (2020), who argued that Imja lake likely remained at or below  $4^{\circ}\text{C}$  from observations from satellite thermal imagery. Although it should be noted that Watson et al. (2020) also identify a peak average temperature of  $9.6^{\circ}\text{C}$  for Imja Tsho from satellite imagery during October 2004, which may have exceeded  $3.98^{\circ}\text{C}$  due to wind speeds being insufficient to drive surface mixing (Chikita 2007). These higher near surface water temperatures may lead to higher subaqueous melt rates where they come into contact with glaciers (Chikita, 2007).

The influence of wind driven currents of warm near surface water on ice cliff retreat rates has also been studied at other supraglacial ponds and lakes in Nepal (Sakai et al., 2009). They also found that surface wind speeds increased with greater fetch across glacial lakes up to 1,000 m long (Sakai et al., 2009). Where glacial lakes were greater than 20 m long and water temperature was 2 to  $4^{\circ}\text{C}$  subaqueous melt rate exceeded subaerial melt rate, which resulted in undercutting of the ice cliff (Sakai et al., 2009). However, Sakai et al. (2009) found that ice-cliff calving only occurred where lake length exceeded 80 m, as this fetch was required for wind driven currents (from valley winds) to advect warmer water towards the ice cliff. This resulted in high subaqueous melt rates undercutting the ice cliff and led to calving of icebergs due to collapses above thermal notches, which they argue is an key process for expansion of glacial lakes in the Himalaya (Sakai et al., 2009). This also suggests that smaller glacial lakes may also have less influence on ice cliff retreat rates due to insufficient fetch for wind driven currents to advect warmer water towards the ice cliff.

## **1.7 Summary**

The extent and distribution of ice contact (including marginal dead ice) has a substantial influence on proglacial lake temperatures, although this is likely to vary through time, particularly where controlled by periods of high ice berg flux (Warren and Kirkbride,

1998). The observations of ‘interfingering’ and the cooling influence of glacial meltwater with ambient lake water near the ice-water contact point, suggest that the mixing of meltwater and ambient lake water is complex and partly controlled by proglacial lake thermal stratification and suspended sediment concentration of meltwater input (Warren and Kirkbride, 1998, Chikita, 1999). The stability of thermal stratification in proglacial lakes depends on differences in water density through the water column to be maintained undisturbed, particularly with surface warming and through input at depth of cold turbid subglacial meltwater (Warren and Kirkbride, 1998; Chikita, 1999; Sugiyama et al., 2016). Observations of wind driven remixing in Nepal, Patagonia and New Zealand would suggest that wind patterns can regulate surface temperatures of proglacial lakes through mixing with deeper colder layers (Warren and Kirkbride, 1998; Chikita, 1999; Sakai et al., 2009; Sugiyama et al., 2016). This in turn will affect subaqueous melt rates and formation of thermally eroded notches.

This emphasises the need of high spatial resolution observations of proglacial lake temperature directly at the ice-water contact point. This is essential in order to constrain subaqueous melt rates, which in turn control the development of thermally eroded notches and subaqueous glacier front morphology (Sugiyama et al., 2016; Truffer and Motyka, 2016). The development of thermally eroded notches and protruding ice feet can influence the rate of mechanical mass loss processes (iceberg calving) at the ice-water contact point (Warren and Kirkbride, 1998; Sugiyama et al., 2019). So changes in thermal structure of ice contact proglacial lakes can not only affect the glacier mass loss through changes in subaqueous melt rates, but also as a driver of mechanical processes of mass loss (Sugiyama et al., 2016).

Comparing the observations from the Rhonegletscher, Mendenhall and Yakutat would suggest that larger temperate glaciers are more able to sustain larger floating tongues in proglacial lakes for longer periods, but calving events then represent a higher proportion of glacier mass loss. Larger glacier systems tend to have increasingly complicated glacier dynamics, as exemplified by the surging glaciers of the Karakorum and complicated advance and retreat patterns of Patagonian glaciers. The discovery of subglacial water pressures at 95% of the overburden pressure of Perito Moreno glacier illustrates how finely balanced the components of these highly dynamic systems can be (Sugiyama et al., 2011). It also emphasises the importance of subglacial drainage in ‘communicating’ changes in lake level to the glacier system, which in turn can drive changes in velocity through increased meltwater input facilitating increased basal sliding (Sugiyama et al., 2011). The complicated

pattern of advances and retreats across the Patagonian icefield outlet glaciers illustrates how complex glacier dynamics and unique topographical situation can result in large lacustrine terminating glaciers becoming out of synchronisation with climate.

The diversity of lacustrine terminating glacier systems is clearly apparent and results in the dominance of components within the system varying between different environments. These components are intertwined with climatic drivers, as increased air temperatures will increase meltwater input into the subglacial drainage system and in turn raise lake levels whilst also increasing water temperatures (at least for a period of time) (Warren and Kirkbride, 1998). Thus leading to increased subaqueous melting and mechanical weakening of the ice at the same time (Warren and Kirkbride, 1998; Minowa et al., 2017). Furthermore, the high specific heat capacity of water means that proglacial lakes become an effective store of heat that enhances disintegration of the ice margin (Due et al., 2017; Minowa et al., 2017). The systems are largely in a continual state of dynamic equilibrium, although it is apparent that relatively static states of the proglacial lake can correspond to static states of the glacier (Trussel et al., 2013). Whilst glacier termini appear to have some resistance to the mechanical and thermal processes promoting ice disintegration, it appears that no glacier can indefinitely resist changes in lake characteristics brought about by climatic warming and associated glacier thinning (Trussel et al., 2013). There is great impetus to further investigate these systems in order to understand the future contributions to sea level change and also hazard potential for neighbouring populations.

## 2 Investigating the Spatial Extent of Proglacial Lakes and Glacier Retreat Rates in Arctic Sweden

### 2.1 Introduction

Glaciers are sensitive to changes in climate so they have generally retreated since the Little Ice Age cold period finished and are predicted to retreat further with future climate change scenarios (IPCC AR5, 2013). The water stored inside glaciers makes them an important component of the hydrological system, particularly in drier areas where they are a vital water source (Jansson et al., 2003; Farinotti et al., 2016). If glacier recession continues then this store of water may eventually disappear and change local hydrological systems, which will have substantial implications for ecology and human populations downstream (Fellman et al., 2014; Farinotti et al., 2016).

It is also imperative to remember that snow that settles in the accumulation zone may be stored in the glacier as ice until it flows down to lower elevations, where it melts in the accumulation zone (Jansson et al., 2003). This process of water transfer is much slower for glaciers (decades) than most riverine catchments (years), so glaciers can also act as a longer term store of water than typical non-glacial catchments (Jansson et al., 2003; Fellman et al., 2014). Consequently water may be stored on land in glaciers due to climatic conditions (cooler or wetter) several decades (or longer) ago and provide a crucial source of water during periods of drought or in arid areas (Jansson et al., 2003; Farinotti et al., 2016). Glaciers can also act as a store of water on seasonal and also diurnal timescales (Jansson et al., 2003). Where this glacial meltwater from glacial recession is not stored on land (such as proglacial lakes), then it will contribute to sea level rise if it exceeds the snow and ice mass accumulated on glaciers (IPCC AR5, 2013). Therefore the overall aim of this chapter is to constrain the area of proglacial lakes in Arctic Sweden, as they form a substantial store of freshwater and may also be an important sink for atmospheric CO<sub>2</sub> (Pierre et al., 2019).

As glacier terminus positions retreat back due to increased mass loss, topographic basins are left where terminal moraine systems provide a dam (Fig 2.2.1 A) or where subglacial erosion into the bedrock has been high (Fig 2.2.1 B). Proglacial lakes are likely to develop in these topographic basins if meltwater input is sufficient and water storage is efficient (Carrivick and Tweed, 2013). Proglacial lake distribution and extent has been mapped at the regional scale in the Alps, Greater Himalaya, Peru and Patagonia through analysis of multi-spectral

satellite imagery (Buchrothiner et al., 1982; Huggel et al., 2002; Gardelle et al., 2011; Hanshaw and Bookhagen, 2014; Loriaux and Casassa, 2013). There is an increasing body of research which highlights the exacerbation of glacier retreat rates where they are in contact with proglacial lakes (Komori et al., 2008; Carr et al., 2017; Wang et al., 2015; King et al., 2017; King et al., 2018).

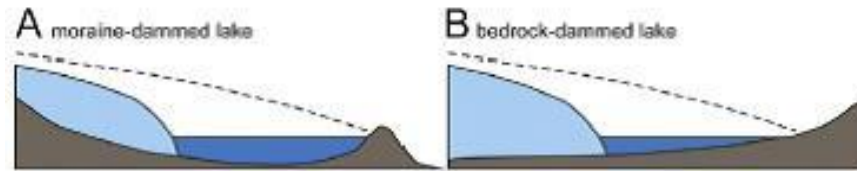


Figure 2.2.1 A. Schematic of proglacial lakes in basins formed as a glacier retreats back from a terminal moraine dam or B. where high subglacial erosion has resulted in a basin within the bedrock. Adapted from Carrivick and Tweed (2013).

Where moraine-dammed proglacial lakes are present in mountainous areas with human populations downstream (such as the Alps, Andes and Greater Himalaya) they can present a considerable hazard of glacial outburst floods (GLOFs), if the moraine dam is overtopped or becomes unstable (Liboutry et al., 1977; Buchrothiner et al., 1982; Huggel et al., 2002). Consequently proglacial lakes in these areas were the focus of early studies and the development of remote sensing technology enabled lakes to be detected across larger remote areas (Buchrothiner et al., 1982).

Where proglacial lakes are in contact with glacier termini, they have been shown to influence glacier mass loss rates through mechanical processes associated with variations in water level controlling ice flotation and increased crevassing leading to higher calving rates (Boyce et al., 2007; Trüssel et al., 2013; Tsutaki et al., 2013). The presence of thermally eroded notches cutting into glacier termini where they are in contact with proglacial lake water is evidence of mass loss through transfer of heat from the water body (Warren and Kirkbride, 1998; Roehl, 2006). Furthermore, similar high retreat rates have been reported in lacustrine and tidewater terminating glaciers on Novaya Zemlya, which have both retreated 3.5 times faster than land terminating glaciers between 1973/6 and 2015 (Carr et al., 2017). Therefore studying the evolution of proglacial lakes and the influence on glacier retreat rates across remote regions is paramount and requires remote sensing based studies to assess the wider changes, which is reviewed in the Literature Review (Section 1.6.1). Consequently it is essential to study the spatial extent of proglacial lakes individually and across regions, not only to identify where they have formed important stores of glacial melt water but also where they may be

exacerbating glacier retreat rates. Additionally, the recent study of Pierre et al. (2019) found that proglacial freshwater may act as a significant sink for atmospheric CO<sub>2</sub> through chemical reactions with silicates and carbonates in turbid meltwater. They proposed that these reactions may be a ‘globally relevant’ phenomenon with regard to atmospheric CO<sub>2</sub> and called for a global proglacial lake inventory (Pierre et al., 2019).

When considering the spatial extent of proglacial lakes, it is imperative to also consider how this may change through time. When glaciers are at the maximum extent (in this case the Holocene maximum) then proglacial lakes emerging from the Holocene period will be non-existent, as the basins will be covered in glacier ice (Figure 2.2.1). As glaciers retreat then the number of proglacial lakes is likely to increase if there are sufficient basins in areas formerly under the glacier (Figure 2.2.1). The extent of these basins will also dictate the size of proglacial lakes that may form, as well as the effectiveness of any damming (or underlying ice that may act as a barrier) (Figure 2.2.1). Consequently the pattern of subglacial erosion across glacier beds and/or regime of moraine building will dictate the possible extent of proglacial lakes (Frey et al., 2010; Cook and Swift, 2012). It is also crucial to remember that the underlying geology will have a strong control on rates of subglacial erosion and sediment supply for moraine building (Karlen, 1973; Cook and Swift, 2012). This poses the question as to whether there are particular areas where proglacial lakes are larger and more numerous, which has not been addressed in Arctic Scandinavia.

As glaciers retreat they may lose contact with proglacial lakes, which may also fill or empty at other points in time depending on the input of water or efficiency of damming the lake (Carrivick and Tweed, 2013). Consequently it is paramount to also assess how the spatial extent of proglacial lakes has changed in time and also whether the amount of contact with glaciers has changed in time (Komori, 2008; Carrivick and Quincey, 2014; Hanshaw and Bookhagen, 2014). It should also be remembered that increases in lake terminating glacier velocity have been observed in the Himalaya (King et al., 2018). These increases in glacier velocity may result in the terminus position advancing forward if sufficient ice is delivered to the front to exceed rates of mass loss (Carrivick and Tweed, 2013). Therefore it is critical to explore the relationship between proglacial lake expansion and glacier retreat. Particularly as future predictions of climate change suggest glaciers will retreat further and it is therefore vital to assess whether proglacial lakes represent a stable store of water in their place (IPCC AR5; 2013). It is also essential to assess this stability as Glacial Lake Outburst Floods have been observed in many glaciated mountain regions with severe damage and casualties

downstream (Clague and Evens, 2000; Huggel et al., 2002; Ghimire, 2004; Emmer, 2018). Further constraining the spatial extent (and persistence) of proglacial lakes and influence on glacier retreat rates at the regional scale would improve future predictions in glacier mass loss and corresponding rise in sea level (IPCC AR5, 2013).

Given that smaller glaciers are more sensitive to climate change (Rippin et al., 2011; Paul et al., 2016), this study focuses on an area of the Arctic characterised by relatively small glaciers that have been subject to recent warming trends in air temperatures (Arendt et al., 2012; Jonsell et al., 2013). This chapter will first of all present the methodology used to examine the spatial pattern of where there are proglacial lakes in Arctic Sweden to assess glacial meltwater storage, before exploring the number and size of proglacial lakes in relation with the glaciers of the region. The retreat rates of lake terminating glaciers are also examined and compared to retreat rates of nearby land terminating glaciers to see if there are differences. The creation of a proglacial lake inventory will identify how many are in contact with glaciers at a particular point in time, thus identifying how many lakes may influence the retreat rates of glaciers in Arctic Sweden.

The aims of this chapter are as follows;

- O1. Create a proglacial lake inventory for Arctic Sweden and analyse the spatial pattern of proglacial lakes.
- O2. Quantify the change in proglacial lake extent through time.
- O3. Characterise the patterns in glacier retreat rates in Arctic Sweden.

## **2.2 Methodology**

The identification of proglacial lakes first requires the identification of glacial areas and then defining the 'proglacial zone'. This is particularly problematic in an area with plateau icefield glacial systems as well as numerous perennial snow patches that regularly survive the summer season. Consequently, the 2006 mapping for the Randolph Glacier (RGI) inventory v3.2 (Arendt et al., 2012) was utilised for identifying glacial units in the study area, which were mapped in 2008. The RGI was used to extract the following characteristics; a. glacial area, b. glacial slope and c. glacier aspect. The Holocene maximum glacier extents are largely clearly identified by prominent moraine systems across the region and correspond to glacier maximum extents during the Little Ice Age and previously mapped in the MSc thesis of Dye

(2015) (Ostrem, 1964; Denton and Karlen, 1973). The extent of the proglacial zone was restricted to the Little Ice Age maximum extent in order to constrain the climatic period in which these proglacial lakes appeared to the last ~100 years, as climatic events are better known for the recent past (Karlen, 1973). This facilitates the relationship between proglacial lake changes in extent and climatic events to be explored, particularly with reference to the Storglaciaren mass balance record (started in 1946; see Chapter 1 Section 1.4 Study Area).

The increase in freely available satellite imagery has improved the study of proglacial lakes by remote sensing, through an increase in spatial resolution and also frequency of satellite over passes. The development of the Sentinel 2 satellite has resulted in readily available imagery with 10 m resolution with high frequency (every 3 days for Arctic Sweden). Sentinel 2 imagery is also relatively high radiometric resolution (16 bit) and the depth of colour associated with this has improved the results from using the Normalised Difference Water Index (NDWI) for automatically delineating areas of open water (discussed in Appendices 2). The NDWI uses differencing between different bands, the Green and NIR were utilised in a workflow for automatically identifying areas of open water (Appendix A 2) (Hanshaw and Bookhagen, 2014). The automatic glacier delineation from Paul et al., (2016) was also utilised to outline glaciers and automatically identify contact points with proglacial lakes using the 'intersect' function in ArcMAP (Appendix A 2).

The whole Sentinel 2 archive was searched between the launch in 2015 and September 2018, unfortunately due to a combination of cloud and snow/ice cover the proglacial lake open water conditions were not as extensive as in August 2014. The mapping of proglacial lakes requires imagery with relatively low cloud cover and ideally low snow cover so that the extent of open water is maximised. Moreover, shadowing from topography is problematic for proglacial lake mapping, as proglacial lakes with low suspended sediment have a similar spectral signature (low reflectance) to shadows and can be difficult to distinguish, particularly where the water body is in shadow (Gardelle et al., 2011). Therefore imagery from the ASTER satellite from 8<sup>th</sup> August 2014 was used for proglacial lake mapping (despite the lower resolution), as it is a more comprehensive inventory of maximum proglacial lake extent in Arctic Sweden. The 2014 proglacial lake inventory was then used to assess changes in proglacial lake area and glacier retreat rates for a limited area where relatively snow free aerial imagery was available from 1957 to 1963. A limited amount of cloud/snow free Rapid Eye (5 m) satellite imagery was available for Arctic Sweden for 2010 and 2018. This imagery is utilised in a different approach to assess the retreat rates of both land terminating and lake

terminating glaciers, in order to explore whether lake terminating glaciers have experienced more rapid retreat over this period. The methodology for these three different aspects of the study is discussed in detail below.

### **2.2.1 Manual Mapping of Proglacial Lake Extent from ASTER Satellite Imagery**

The relatively high resolution (15 m) and availability of ASTER (Advanced Spaceborne Thermal Emission and Reflection Radiometer) multispectral satellite imagery (8 bit) was utilised to map the extent of proglacial lakes from optical imagery. The ASTER satellite imagery was favoured over Landsat 8, as the green and red bands have higher spatial resolution (15 m as opposed to 30 m). Crucially the ASTER thermal imagery is also analysed in Chapter 3, so minimising offset between optical lake outline and thermal imagery was high priority for this study (see Chapter 3.2 Methodology). The MADAS (METI AIST Data Archive System) was used to search through the ASTER archive to select Level 1T images, that are geometrically registered and orthorectified using ASTER GDEM and supplied as calibrated radiance values. The relatively limited repeat cycle (16 days) of the ASTER satellite means selecting suitable imagery for proglacial lake mapping over the study area was limited due to the cloudy nature of the Arctic Maritime climate.

The whole ASTER archive from 2000 through to 2018 was searched, in order to select the most suitable imagery to create an inventory that would capture the maximum extent of proglacial lakes. The ASTER imagery from 8<sup>th</sup> August 2014 (10:46am) was selected for proglacial lake mapping, as the snow cover was minimal with distinct proglacial lake outlines and all glacial areas were free of cloud in the scene (cloud cover 7.0%), which is difficult to find in a maritime climate. Furthermore, the sun illumination elevation angle of 37.9° results in minimal shadow areas that are problematic for delineating proglacial lake margins. The green (band 1, 0.52 – 0.60 µm), red (band 2, 0.63-0.69 µm) and visible near infrared (NIR; band 3N, 0.78 – 0.86 µm) bands (all 15 m spatial resolution) were combined to create a composite image used to identify proglacial lakes. It should be noted that the ASTER sensor does not have a blue band.

The relatively low radiometric resolution (8 bit) of ASTER imagery resulted in the Normalised Difference Water Index (NDWI) product images being unable to distinguish between large areas of shadow and water bodies using automated techniques. Therefore water bodies were manually mapped using the green, red and NIR composite image (bands 1,2,3) by drawing polygons around the edges of pixels of water (Figure 2.2.2). Where pixels were

observed to be a mixture of land and water, the polygon was drawn to dissect such mixed pixels (Figure 2.2.2). Manual mapping of proglacial lake polygons was conducted in one batch, with comparison of delineation of lake margins to minimise subjective uncertainty.



Figure 2.2.2 Satellite image from ASTER of Kaskasapakte glaciaren proglacial lake (PGL<sub>ID</sub>24, 132,172 m<sup>2</sup>), displayed as a composite of green, red and near infrared (bands 1, 2, 3N; all 15 m resolution) showing vertices for proglacial lake manual mapping.

### 2.2.2 Sources of Uncertainty with Manual Mapping from ASTER Satellite Imagery

The geometric error associated with mapping proglacial lake polygons in a raster image with 15 m x 15 m pixels (grid) has been calculated following the method used in Hanshaw and Bookhagen (2014). They propose that ~69% of lake pixels (for a regular shaped polygon) will be subject to boundary errors due to proximity to the lake margin and whether the 15 m pixel is a mixture of lake water and land (Hanshaw and Bookhagen, 2014). The number of pixels along the lake outline is first calculated by dividing the perimeter ( $P$ ) by the grid size ( $G$ ) (15 m for ASTER VNIR) which is then multiplied by 0.6872 (Hanshaw and Bookhagen, 2014). Whilst the complicated irregular geometry of some proglacial lakes may mean this proportion is not fully representative (particularly for lakes with peninsulas and bays), this geometric simplification is adopted here for theoretical calculation of spatial errors across the whole proglacial lake inventory. It is assumed that the uncertainty for delineating a lake

margin is half a pixel and therefore the first two terms are multiplied by the area of half a pixel (Hanshaw and Bookhagen, 2014);

$$\text{Error } (1\sigma) = (P/G)*0.6872*G^2/2 \quad (1)$$

These calculations give a purely theoretical geometric indication of error. They produce a critical area threshold of 170,156.22 m<sup>2</sup> for geometric errors to be 5.00% of the overall area of the lake. Consequently proglacial lakes smaller than 170,156.22 m<sup>2</sup> have geometric errors greater than 5.00%, but are still reported here for completeness of the inventory, as the location and existence of these lakes is important to record. Note that proglacial lakes have only been mapped for pixels where there is a greater than 95% confidence of their presence on 8<sup>th</sup> August 2014. Therefore the change in area of these smaller lakes (<170,156.22 m<sup>2</sup>) over relatively short time periods (years) is impossible to report on at the 95% confidence level with the 15 m resolution of ASTER imagery.

It is also vital to remember that the proglacial lake levels and spatial extents captured by ASTER imagery at 10:46am on 8<sup>th</sup> August represent a snap shot in time. The lake level and spatial extent of proglacial lakes are likely to change through time due to variations in meltwater input, water seepage and evaporation (Fujita et al., 2009). Consequently the lack of access to higher resolution imagery taken at the same time as the ASTER imagery on 8<sup>th</sup> August 2014 meant that a more precise validation of spatial errors of proglacial lake outline mapping from ASTER imagery on 8<sup>th</sup> August could not be undertaken by this study. Therefore detailed analysis of spatial errors associated with projection of ASTER imagery, particularly the ortho-rectification process, has not been undertaken by this study but should be borne in mind as a potential source of uncertainty.

The manual delineation of proglacial lake margins is also a source of uncertainty, due to the subjective nature of drawing a boundary at the lake margin. This uncertainty was minimised through mapping all proglacial lakes in one batch, thereby ensuring the most consistent delineation of boundaries with minimal change in judgement over time. Future studies may choose to conduct manual mapping of the same lake on different occasions and compare variations in mapping extent. This would provide a quantitative assessment of error due to subjective delineation of margins. This was not conducted by this study due to the lack of high spatial resolution imagery taken at the same time as the ASTER imagery to act as a validation dataset, but should be borne in mind by the reader.

### 2.2.3 Manual Mapping of Proglacial Lakes from Aerial Imagery

The Swedish Lantmateriet historical (1957 to 1963) aerial imagery (panchromatic) catalogue for the Kebnekaise and surrounding areas was searched and 49 tiles (each 5 km x 5 km) were downloaded. These tiles were manually inspected for suitability for identifying proglacial lakes and 25 tiles were rejected due to having a substantial snow cover across the scene. This historical imagery has recently (July 2019) become freely available from Swedish Lantmateriet, but at the time of writing metadata was not available. The year of image capture is apparent from the file name, but it has not been possible to attain the exact date that each image was taken and some tiles are also a combination of images. A total of 24 aerial imagery tiles (1957 to 1963) covering  $\sim 600 \text{ km}^2$  were selected for analysis of proglacial lake extent (Figure 2.2.3). Whilst these images were taken during different years, they provide a useful benchmark for changes in proglacial lake extent and number between the 1957-63 period and 2014 (Figure 2.2.3).

The historical (1950s/1960s) aerial imagery is of higher spatial resolution ( $\sim 1 \text{ m}$ ) than the ASTER multispectral imagery (15 m) used to create the 2014 proglacial lake inventory. In order to minimise erroneous changes in lake extent being due to difference in resolution between the historical imagery and ASTER 2014 imagery, the polygons derived from the ASTER manual mapping were copied and used for the historical (1957 to 1963) dataset. The historical polygons were then only adjusted at the lake to glacier ice margin, to purely capture changes in lake size due to glacier recession. Where the 2014 proglacial lake outlines were visibly covered by glacier ice in the historical imagery, they were classed as '1960sUnbornProGL' (ProGL = Proglacial lake). Some of the proglacial lake outlines were covered by snow, which were classed as '1960sSnowConcealedProGL'. It is possible that some of the 2014 proglacial lake outlines concealed under snow were also covered glacier ice.

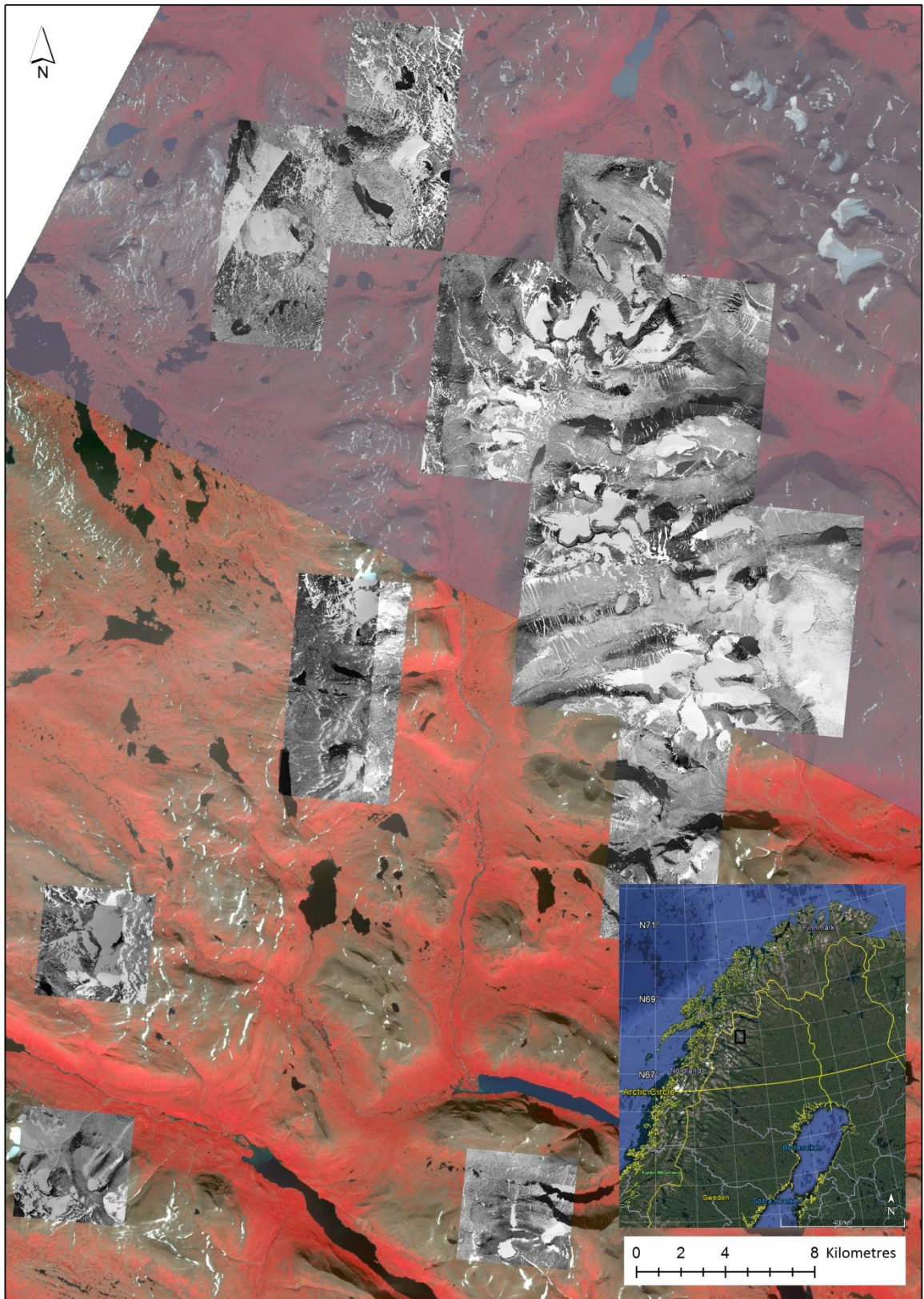


Figure 2.2.3 ASTER false colour composite (R,G, NIR, 15 m resolution) satellite image (8/8/2014) of Arctic Sweden, with overlay of panchromatic aerial imagery (1950s/1960s) (Lantmateriet). Note aerial imagery is from different dates; 1957 – 1 tile including largest lake (northwest centre) 1959 – all of central cluster (around Kebnekaise) 1960 – western images, 1963 – southern images. Inset image (Google Earth) shows location of main image (black box).

## 2.2.4 Mapping Glacier Terminus Change from Rapid Eye Imagery (2010 to 2018)

The Rapid Eye satellite imagery catalogue available through Planet imagery portal was searched extensively, but only limited spatial areas over the study area were available and cloud/snow free for contemporaneous dates. A series of 14 Rapid Eye multispectral satellite images (5 m) were downloaded for 16/8/2010 and 11 images for 27/7/2018, covering Kebnekaise and the northern sections of the study area (Figure 2.2.17). These images were manually inspected to select glaciers with minimal snow cover for analysis of terminus change, with a total of 24 glaciers being selected for analysis. The geometry of glacier termini varied, from some with more classical parallel sides with a perpendicular front to other termini with a more triangular shape with a triangular snout (Figure 2.2.4). To account for this variation in glacier termini geometry a reference point was selected on either side of the glacier where the width was consistent for 2010 and 2018 (Figure 2.2.4). The glacier terminus area was then mapped below these width reference points to create a terminus polygon for 2010 and one for 2018 (Figure 2.2.4) (Lea et al., 2014). The 2018 area was then subtracted from the 2010 polygon area to give the area of ice lost over this period. This area of ice lost was then divided by the width of the polygon reference points (purple line Figure 2.2.4) to partly account for glacier thinning and narrowing within the width averaged retreat.

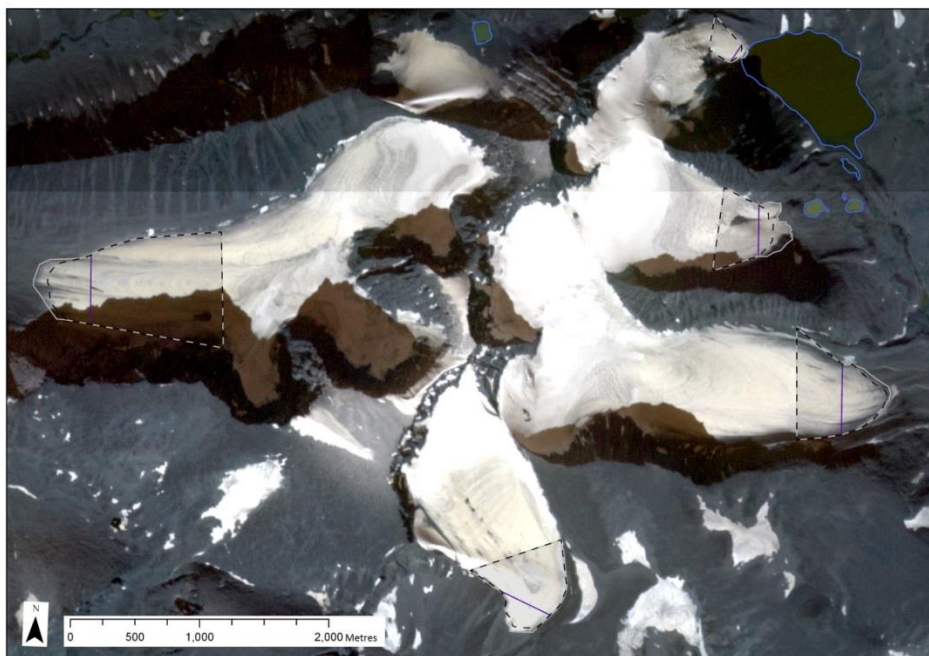


Figure 2.2.4 Rapid Eye multispectral satellite image (5 m resolution) from 27/7/2010 with; grey outline = 2010 glacier terminus area, dashed black line = 2018, purple line = width of glacier terminus area, blue polygon = Aug 2014 proglacial lake outline.

## **2.3 Results**

### **2.3.1 Glaciers in Arctic Sweden from the Randolph Glacier Inventory (2008)**

The Randolph Glacier Inventory polygons were downloaded for Scandinavia and cropped to the extent of the study area (Figure 2.2.5). There were 252 ‘glaciers’ within the study area as mapped in the RGI (2008). The main glaciated areas are focused around the mountainous areas (>1,000 m) of Sarek region in the south and the Kebnekaise region in the north, with some smaller groups of glaciers in surrounding areas (Figure 2.2.5). There are some substantial mountains (~1,800m elevation) to the east of Kebnekaise, which are currently not glaciated due to the strong precipitation gradient across the area (Figure 2.2.5) (Hock et al., 2002). There were several other glaciers in Arctic Sweden that lie to the west near the Norwegian border that were not included in this study, due to being outside the coverage of the ASTER imagery from 8/8/2014.

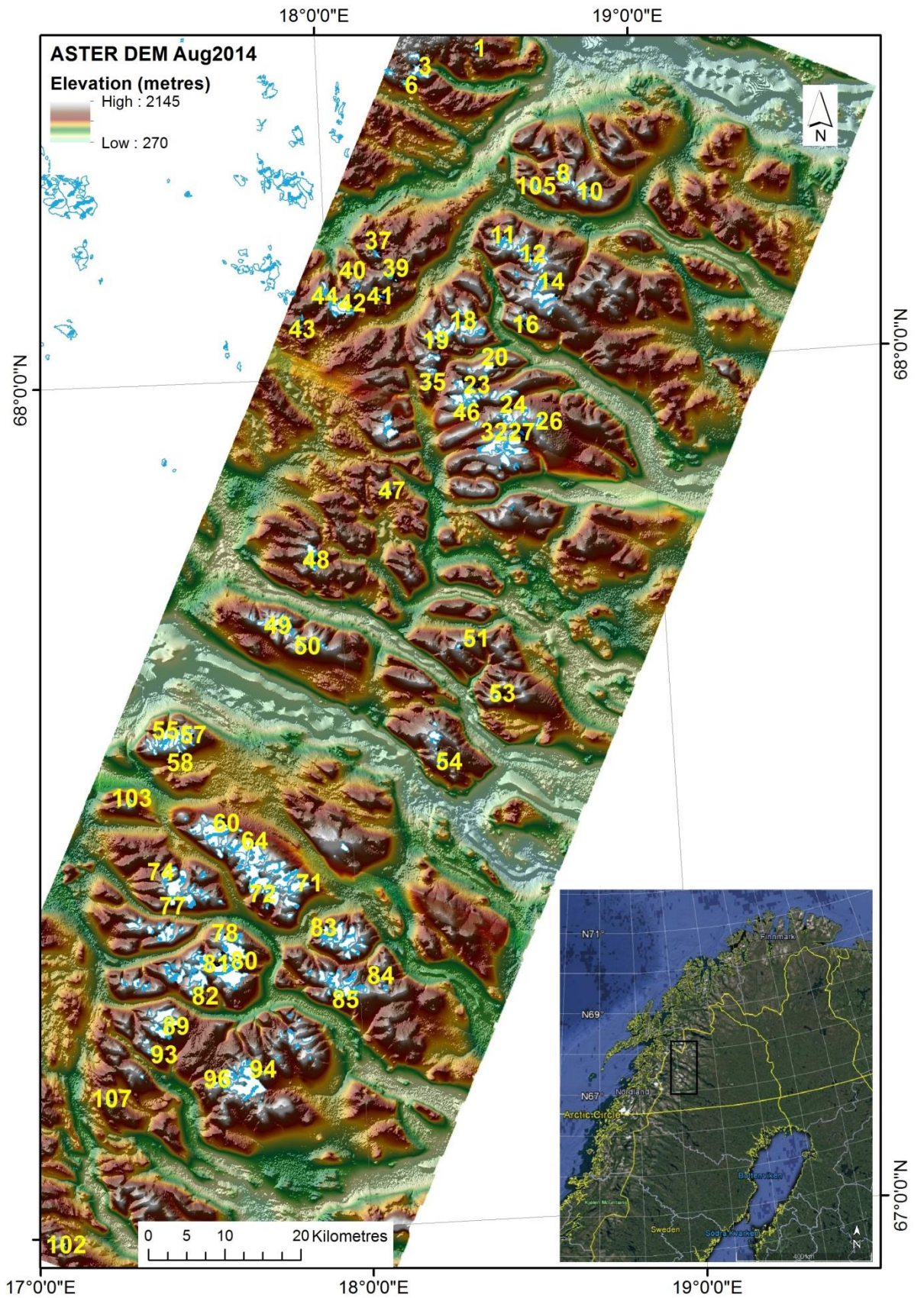


Figure 2.2.5 ASTER digital elevation model (GDEM) (8/8/2014) for Arctic Sweden, with hill shading from NW. White polygons = RGI 2008 glacier areas. Blue dots = proglacial lake 2014 locations. Inset image (Google Earth) shows location of the study area (black box).

Across the study area the 252 glaciers tend to be located on northerly through to easterly aspects and ranged in area from 51,540 to 10,200,000 m<sup>2</sup> (Figure 2.2.6). The largest glacier represents a notable outlier, as the next largest glacier area was 6,627,000 m<sup>2</sup> and only 3 glaciers were >6,000,000 m<sup>2</sup> and most (89.0%) tend to be less than 2,000,000 m<sup>2</sup> in area (Figure 2.2.6). In the Randolph Glacier Inventory (RGI), total glacier area in 2008 for Kebnekaise and the northern part of the study area was 45,099,759 m<sup>2</sup> with a mean glacier area of 850,939 m<sup>2</sup> and median of 552,809m<sup>2</sup>. In contrast total glacier coverage in Sarek was much larger, totalling 85,107,135 m<sup>2</sup> with a mean of 1,636,676 m<sup>2</sup> and median of 1,359,667 m<sup>2</sup> (Appendix A 2). Of these glacial ice bodies (covering 130,206,894 m<sup>2</sup> in total, RGI, 2008), 43 were in the Kebnekaise northern area and 32 were in the Sarek area to the south.

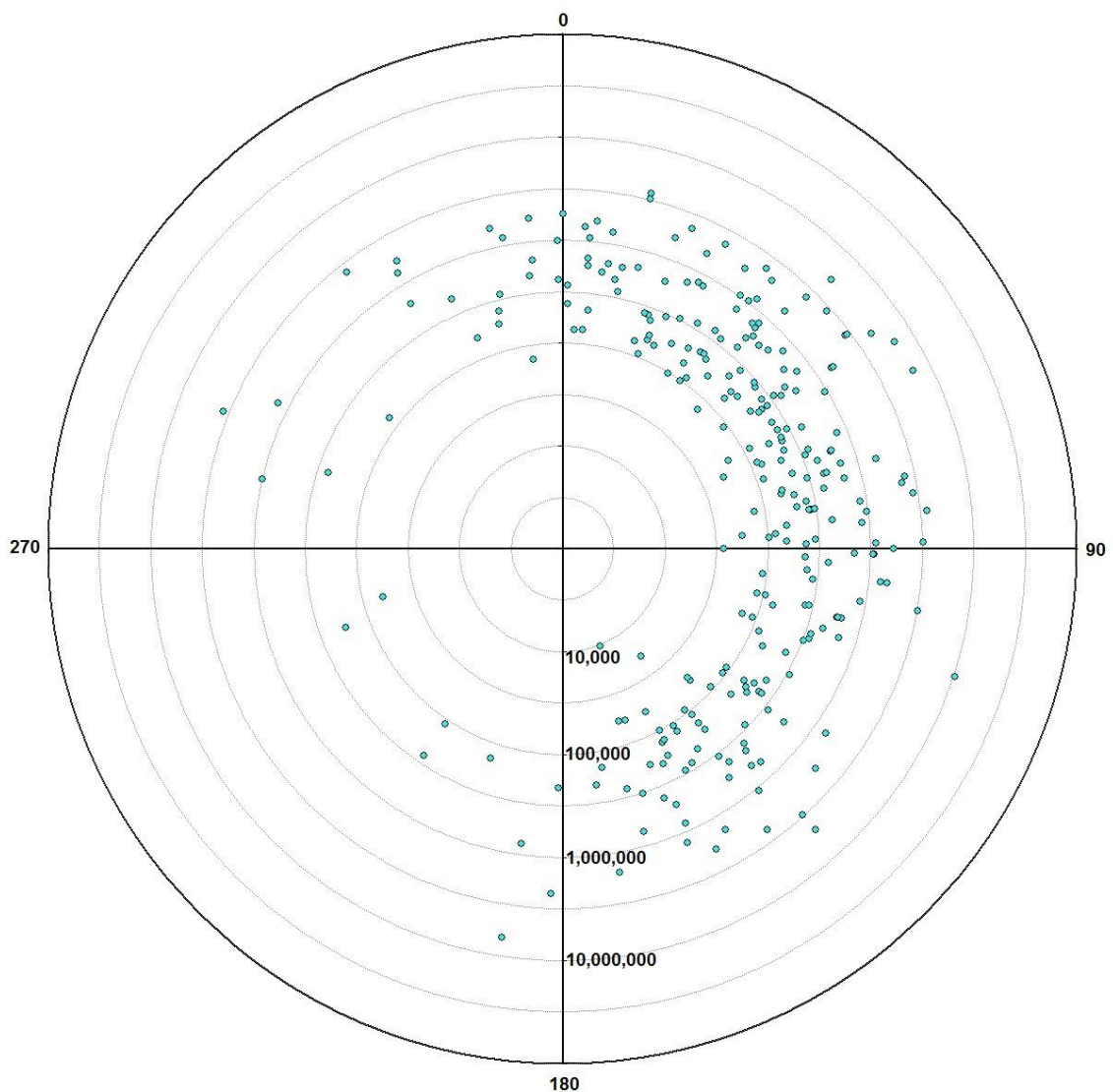


Figure 2.2.6 Polar plot of glacier areas (note the logarithmic (base 10) radius scale m<sup>2</sup> with origin at 1,000) against glacier aspect (angle) for 252 glaciers in the study area (Arctic Sweden), from the Randolph Glacier Inventory (2008) (Arendt et al., 2012).

### 2.3.2 Proglacial Lake Inventory for Arctic Sweden from ASTER 2014 imagery

The forefields of 252 glaciers (RGI, 2008) were inspected in ASTER multispectral imagery (10:46AM 8/8/2014) to manually detect proglacial lakes within the Holocene maximum limits in Arctic Sweden (Denton and Karlen, 1973; Karlen, 1973). A total of 72 glaciers from the Randolph Glacier Inventory (RGI) had proglacial lakes in the fore field on 8<sup>th</sup> August 2014 (Figure 2.2.5). There was a further 3 glacial ice bodies (visible in satellite imagery) that had proglacial lakes in the fore field, although these were not identified in the Randolph Glacier Inventory they are included here for completeness. Therefore a total of 75 out of 255 (29.4%) of glacial ice bodies had proglacial lakes in the fore field at the time of image capture. There was no correlation between glacier area and proglacial lake area ( $R^2 = 0.0286$ ) (Figure 2.2.7).

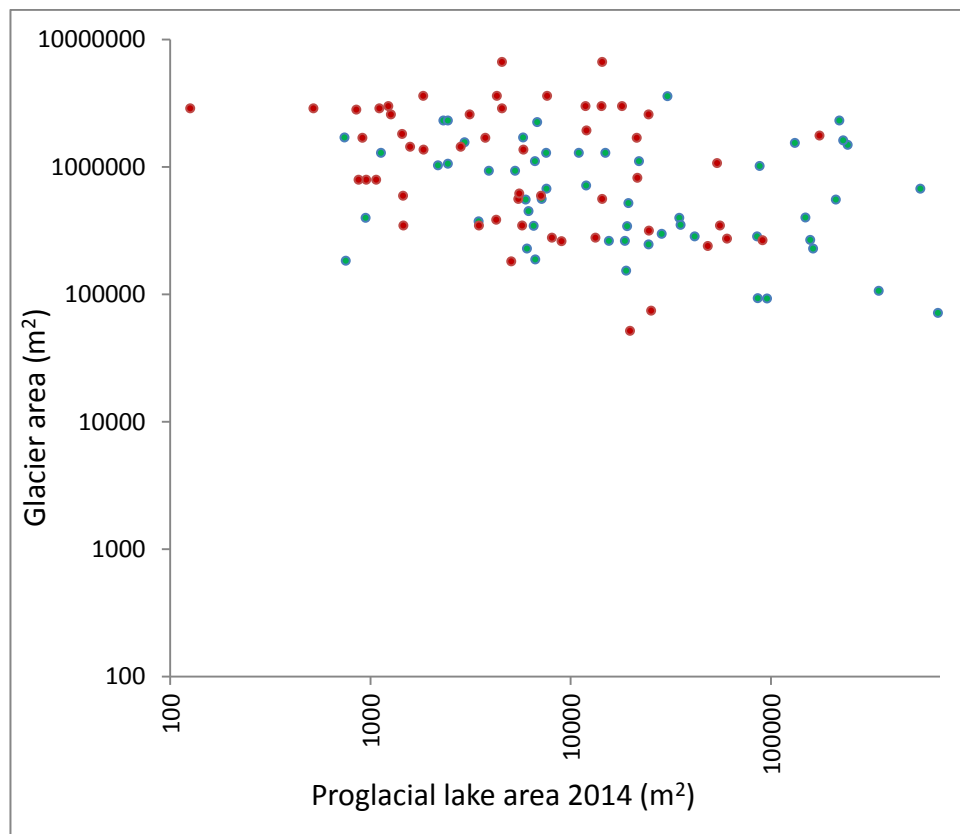


Figure 2.2.7 Scatter plot of Proglacial lake area (August 2014) against glacier area (RGI, 2008) for Arctic Sweden, note the logarithmic scale ( $n^{10}$ ) for each.  $R^2 = 0.0286$ . Green denotes Kebnekaise area and Red denotes Sarek area.

A total of 108 proglacial lakes were mapped across Arctic Sweden (Figure 2.2.5), 42% of which were in visible contact with a glacier terminus on 8<sup>th</sup> August 2014 (Appendices 2.2 for Inventory table). The total combined area of proglacial lakes mapped in ASTER imagery

(8/8/2014) was 4,767,295 m<sup>2</sup>. The minimum proglacial lake area mapped in this study was 126 m<sup>2</sup> and the maximum was 686,233 m<sup>2</sup>, with a mean of 44,187m<sup>2</sup> and median of 7,590 m<sup>2</sup> for all lakes mapped in the study area. The majority (88.9%) of proglacial lakes were <100,000 m<sup>2</sup> and 52.8% were <25,000 m<sup>2</sup>. Indeed the proglacial lake population size distribution in August 2014 was positively skewed with 71.2% of proglacial lakes being relatively small (<30,000 m<sup>2</sup>) (Figure 2.2.8).

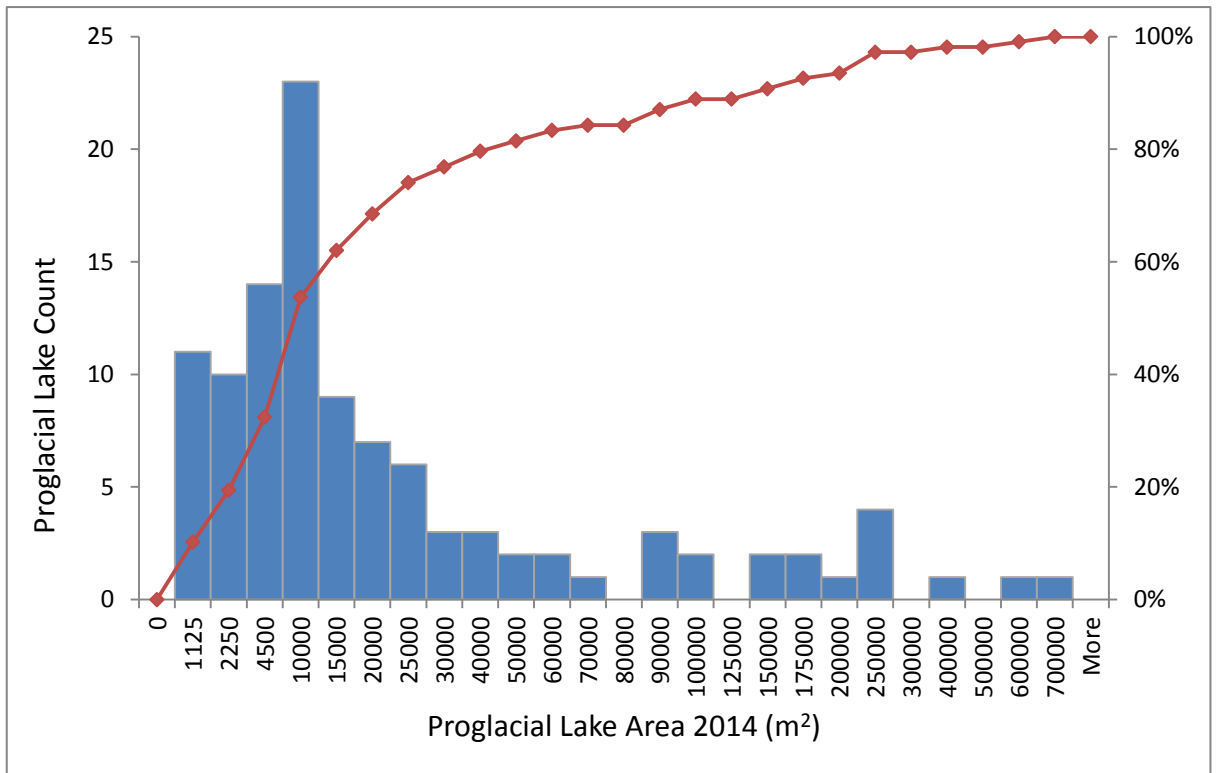


Figure 2.2.8 Frequency distribution plot of proglacial lake area (m<sup>2</sup>) on 8/8/2014, Sweden.

The aspect of the glacier associated with each proglacial lake was predominantly (76.9 %) north through to easterly aspects, with 34 lakes (32.7 %) facing east, 26 (25.0%) facing north east and 20 (19.2%) facing north (Figure 2.2.9). There were also 13 lakes (12.5%) associated with glaciers facing south east and 6 (5.8%) facing south (Figure 2.2.9). There was no proglacial lakes associated with glaciers facing south west or west and only 5 lakes (4.8%) associated with glaciers facing north west (Figure 2.2.9). Proglacial lake elevations were between 996 m and 1620 m, with the majority (95.4%) lying between 1,100 m to 1,500 m (Figure 2.2.9). There was no correlation between proglacial lake area and elevation ( $R^2 = 0.0304$ ) (Figure 2.2.9).



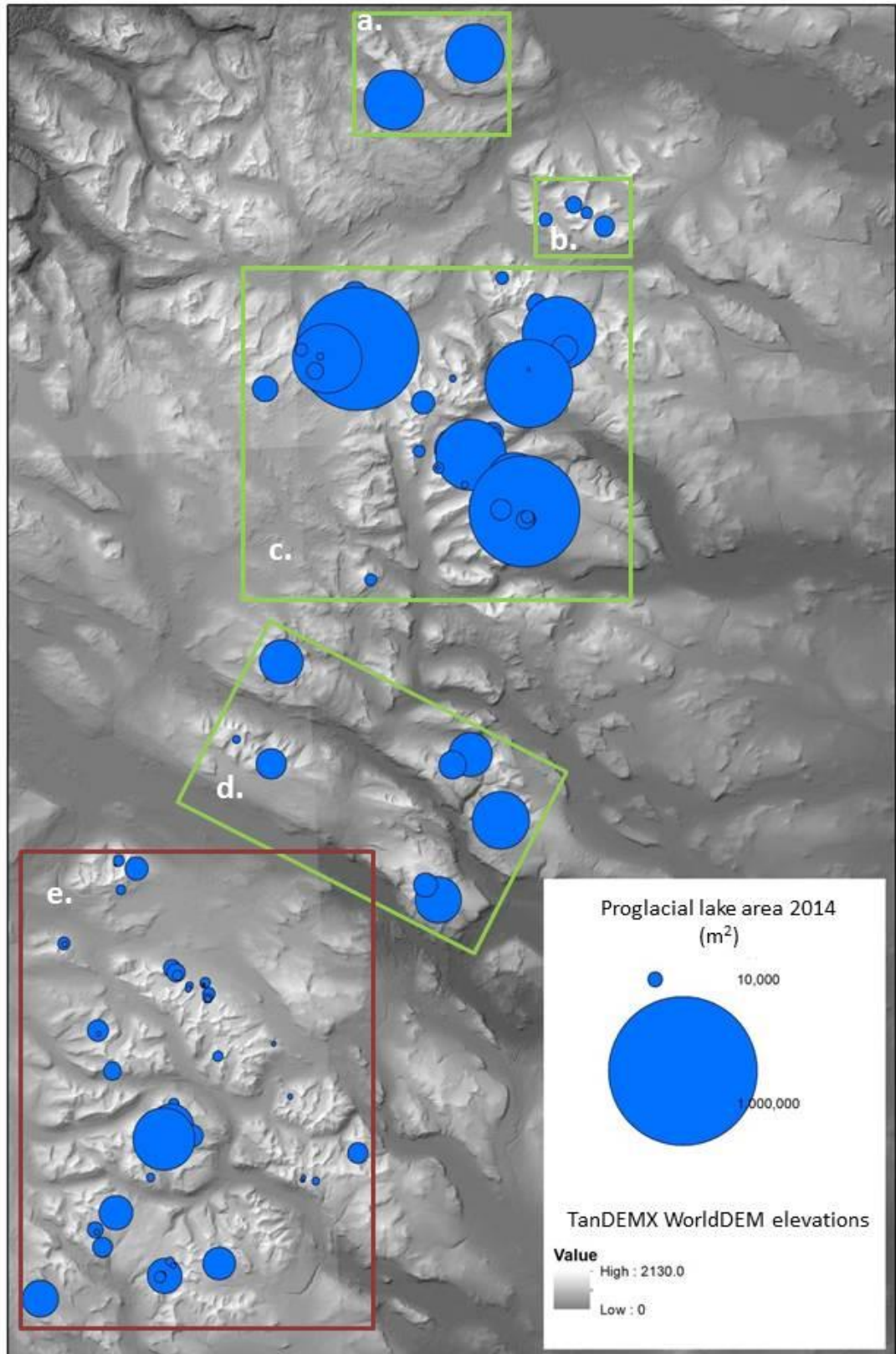


Figure 2.2.10 Proportional bubble plot for proglacial lake area ( $m^2$ ) across Arctic Sweden manually mapped from ASTER satellite imagery (15 m) (8/8/2014). Green boxes denote sub-regions (a, b, c, d) of proglacial lake populations, which are described individually but treated as ‘Kebnekaise area’ for statistical analysis. Red box (e.) denotes Sarek area.

The very northern limit of the study area (area a, Figure 2.2.10) contains 4 smaller proglacial lakes ( $<20,000 \text{ m}^2$ ) and two of the 12 large ( $>100,000 \text{ m}^2$ ) outliers, which are located close to the Norwegian border. The next group of lakes to the south (area b, Figure 2.2.10) are smaller ( $\sim 10,000 \text{ m}^2$ ) and associated with small corrie glaciers with terminal moraine systems. The Kebnekaise area (area c, Figure 2.2.10) has a large range in proglacial lake sizes, from  $744 \text{ m}^2$  to  $686,233 \text{ m}^2$  and represents a diverse population of proglacial lakes associated with corrie glaciers, some small valley glaciers and plateau icefields in the west of the region (Karlen, 1973). The central area (area d, Figure 2.2.10) are between  $\sim 50,000$  to  $150,000 \text{ m}^2$  and associated with corrie glaciers.

The areas described above are referred to as the Kebnekaise and surrounding areas. These areas are further analysed as one population of proglacial lakes due to geographical proximity and limited number of proglacial lakes in some sub-regions, making statistical analysis problematic due to the relatively small populations. It should be remembered that there are variations in climate across this wider area, with a decrease in precipitation towards the north east (Hock et al., 2002; Goodfellow et al., 2008). The southernmost population of proglacial lakes lie in the Sarek area are generally smaller, although there is 1 larger proglacial lake ( $>100,000 \text{ m}^2$ ) (Figure 2.2.10). The difference in sizes between the Sarek proglacial lake population and rest of the study area (Kebnekaise and surrounding areas) is further analysed in the next section (2.3.4).

#### **2.3.4 Analysis of Differences between Proglacial Lakes in Kebnekaise and Sarek**

In the Sarek area 23 out of the 54 (42.6%) proglacial lakes mapped in August 2014 had a contact point with a glacier and 28 (51.9%) were moraine dammed, whereas 21 out of the 54 (38.9%) in the Kebnekaise and Central region had contact with proglacial lakes and 23 (42.6%) were moraine dammed. On 8<sup>th</sup> August 2014 the mean proglacial lake size in the Kebnekaise area was  $72,873 \text{ m}^2$  and a median of  $17,129 \text{ m}^2$ . In contrast, the mean proglacial lake area in the Sarek area was  $15,502 \text{ m}^2$  and a median of  $5,283 \text{ m}^2$ . Both datasets have a positive skew and non-parametric distribution (Figure 2.2.11), due to the large range in proglacial lake area but small lakes being more numerous. So a Mann Whitney U test was performed to test whether the Sarek proglacial lake population had significantly smaller areas than the Kebnekaise population. Due to the relatively large number of observations ( $n_1=54$  and  $n_2=54$ ) the critical U value ( $U_{crit}$ ) was calculated ;

$$U_{crit} = \mu - z * \sigma - 0.5 \quad (2)$$

Where ( $\mu$ ) is the mean distribution of  $U$  values, ( $z$ ) is 1.96 for a two tailed test at the 0.05 significance level and ( $\sigma$ ) is 1 standard deviation of the distribution of  $U$  values. The calculated  $U_{crit}$  for the proglacial lake dataset was 1,138.513. As the smallest  $U$  value was lower than  $U_{crit}$  ( $U_1= 906$ ) the null hypothesis ( $H_0$ ), that there was no significant difference between the two datasets, is rejected. Therefore the proglacial lakes in the Sarek area had a statistically significant smaller area than the proglacial lakes in the Kebnekaise area (Figure 2.2.11).

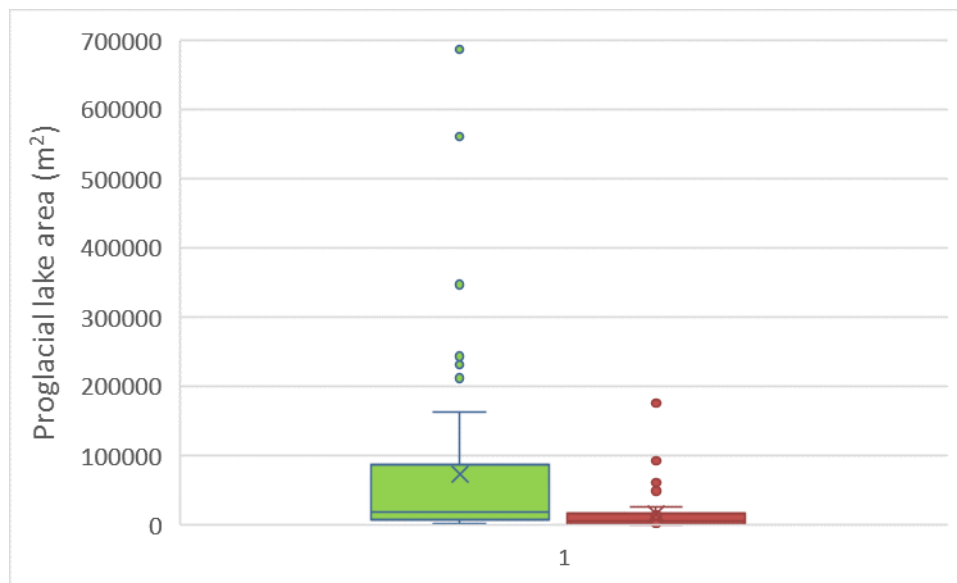


Figure 2.2.11 Box and Whisker plot of proglacial lake area on 8<sup>th</sup> August 2014 for the Northern study area (Green) and Sarek area (red). Whiskers extend to points within 1.5 times the interquartile range (IQR) from the upper and lower quartile. Points 1.5 times the IQR from the upper and lower quartile are plotted as outliers. With  $x$  = mean and central line = median.

### 2.3.5 Spatial Changes in Proglacial Lakes between 1950s/60s and 2014

A total of 33 proglacial lakes that were present in the ASTER August 2014 imagery were within the area covered by the 1950s/60s aerial imagery (1957 to 1963). Due to the relatively high presence of snow cover within the historical imagery, 7 proglacial lakes that were present in 2014 could not be clearly identified and were classed as ‘snow concealed proglacial lakes’. These ‘snow concealed’ proglacial lakes ranged in area from 2,224 m<sup>2</sup> to 24,498 m<sup>2</sup> when they were mapped in the ASTER imagery from 8th August 2014. The possible presence or absence of these proglacial lakes should be borne in mind as they form a substantial proportion (21.2%) of the total number (33) of the August 2014 proglacial lakes that are within the spatial area covered by the 1950s/60s imagery (Figure 2.2.12).

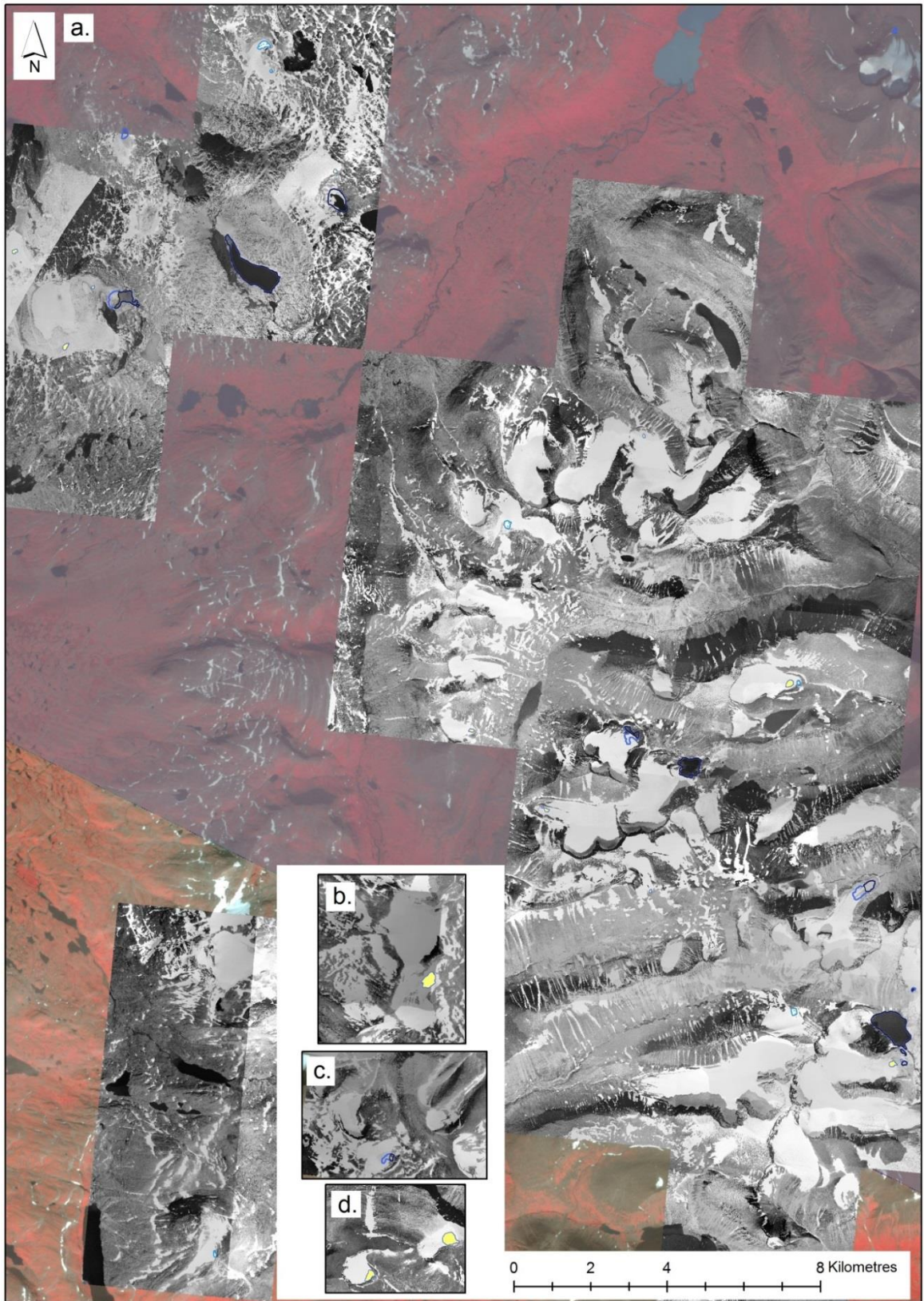


Figure 2.2.12 ASTER false colour composite (R,G, NIR, 15 m resolution) satellite image (8/8/2014) of Arctic Sweden, with overlay of panchromatic aerial imagery (1950s/1960s) (Lantmateriet). Black outline polygon = 1950s/60s lake outline. Yellow fill polygon = unborn proglacial lake. Blue outline polygon = 2014 lake outline. Blue fill polygon = snow covered proglacial lake. Inset image (same scale) shows proglacial lakes located ~20km south.

There were 15 (45.5%) proglacial lakes (PGL<sub>ID</sub>; 18, 20, 29, 30, 33, 34, 35, 38, 44, 45, 46, 48, 51, 52, 108) that were mapped in the ASTER imagery (26 lakes in total) from 8<sup>th</sup> August 2014 but were visibly covered by glacial ice in the 1950s/60s imagery (1957 to 1963) (Figure 2.2.12; Figure 2.2.13). These proglacial lakes were classed as ‘unborn’, 12 of them were from corrie glaciers (mostly easterly aspect) and 3 were from plateau icefields. No proglacial lakes that were present in the 1950s/60s imagery were observed to have a dry bed in August 2014. The 15 proglacial lakes that were classed as ‘unborn’ in the 1950s/60s imagery ranged in size from 744 m<sup>2</sup> to 86,144 m<sup>2</sup> with a mean of 19,352 m<sup>2</sup> and median of 6,072 m<sup>2</sup> at elevations between 1,178 m to 1,406 m. There were 11 proglacial lakes that were mapped in the ASTER imagery from 8<sup>th</sup> August 2014 and visibly had open water in the 1950s/60s imagery (Figure 2.2.13).

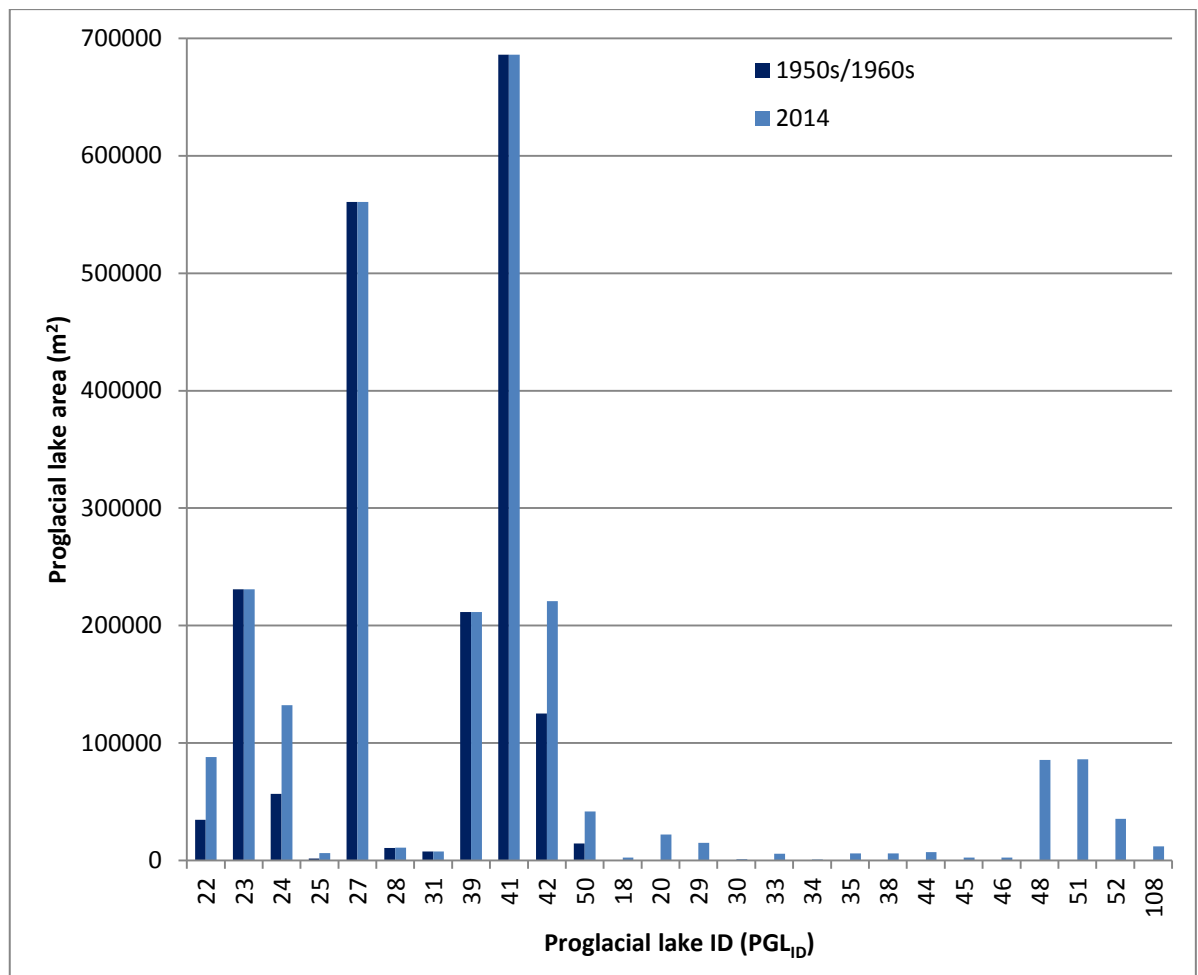


Figure 2.2.13 Plot of proglacial lake area from mapping of ASTER satellite imagery (8<sup>th</sup> August 2014; light blue) and historical aerial imagery (1957 to 1963; dark blue). Lake 41 is covered by an aerial image from 1957, lakes 48, 51 and 52 from 1963 imagery and the remaining lakes are covered in imagery from 1959 or 1960. Note that ‘snow concealed’ lakes are not plotted.

The 11 proglacial lakes present in the 1950s/60s imagery had a very large range in area from 1,695 m<sup>2</sup> to 686,233 m<sup>2</sup>, which included the largest proglacial lake in the ASTER August 2014 imagery study area (Figure 2.2.10). The mean area of the 11 proglacial lakes present in the 1950s/60s imagery was 176,091 m<sup>2</sup> with a median of 56,779 m<sup>2</sup>, indicating a large positive skew in the dataset. These same 11 proglacial lakes had a mean area of 199,701 m<sup>2</sup> and a median of 132,172 m<sup>2</sup> in August 2014. There was no change in area of the four largest proglacial lakes (in the historical imagery) over this period (lake 41; 1957 to 2014, lakes 23 and 27; 1959 to 2014 and lake 39; 1960 to 2014) (Figure 2.2.13).

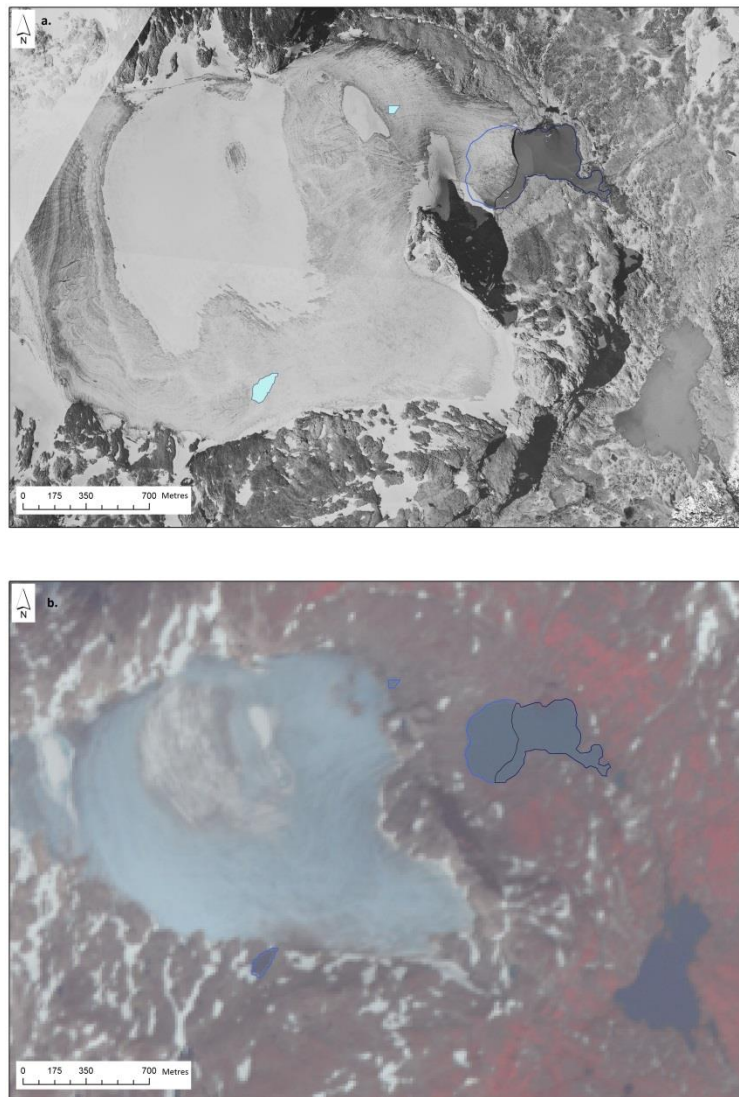


Figure 2.2.14 a. Aerial image (Lantmateriet, 1960) of Riukojekna plateau icefield (Sweden) showing 1960 proglacial lake outline (black) with August 2014 proglacial lake outline (blue) and locations of two ‘unborn’ proglacial lakes (shaded light blue). Spatial resolution is unknown but estimated ~1 m. b. ASTER satellite composite image (G,R, NIR, 15 m resolution) from 8th August 2014 (10:46am) with 1960 proglacial lake outline (black) and August 2014 outline (blue).

The remaining 6 proglacial lakes present in the 1950s/60s imagery all increased in area. The largest absolute increase in proglacial lake area occurred at lake 42 from a plateau icefield glacier (Riukojekna) receding, which increased from 125,220 m<sup>2</sup> in 1960 to 220,826 m<sup>2</sup> in 2014, an increase of 95,606 m<sup>2</sup> (+76.4% of 1960 area) (Figure 2.2.14). Only lake 28 had a smaller proportional increase in area over this period (4.6%) (Figure 2.2.13), although there is low confidence in this increase as it is only +488 m<sup>2</sup> and the reader is referred back to previous discussion of spatial errors associated with the ASTER 15 m resolution imagery (2.2.2).

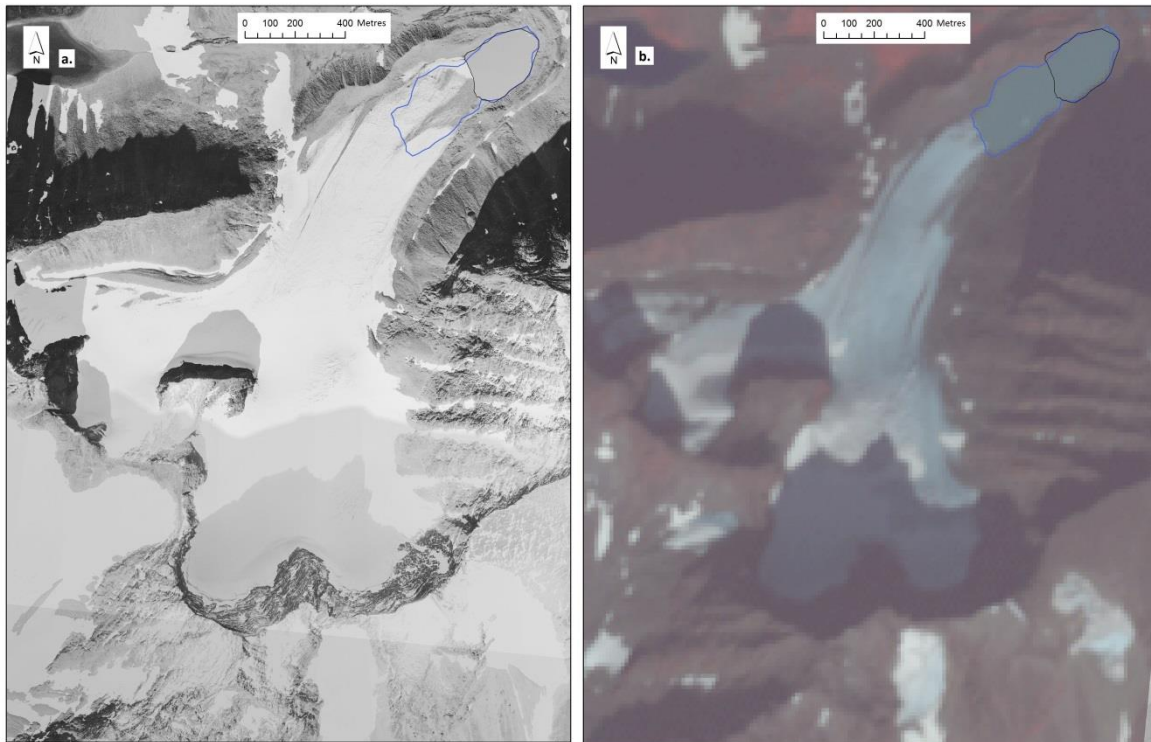


Figure 2.2.15 a. Aerial image (Lantmateriet, 1959) of Kaskapakte glacier (Sweden) showing 1959 proglacial lake outline (black) with August 2014 proglacial lake outline (blue). Spatial resolution is unknown but estimated ~1m. b. ASTER satellite composite image (G,R, NIR, 15m resolution) from 8th August 2014 (10:46am) with 1960 proglacial lake outline (black) and August 2014 outline (blue).

The next largest absolute increase (75,393 m<sup>2</sup>) in proglacial lake occurred at lake 24 from recession of an alpine/valley glacier (Kaskapakte glacier), from 56,779 m<sup>2</sup> in 1959 to 132,172 m<sup>2</sup> in 2014, which represents a 132.8% increase on the 1959 area (Figure 2.2.15). There was a comparable amount of area change for lake 22 (53,420 m<sup>2</sup>), which represented a 154.2% increase of the 1959 area (34,644 m<sup>2</sup>) associated with the retreat of a large corrie glacier (Vaktposten) (see Appendix A 4 for images). Lake 50 had a larger proportional change of 191.9% (27,467 m<sup>2</sup>) of the 1963 proglacial lake area (14,312 m<sup>2</sup>), associated with the retreat of a relatively small corrie glacier (Figure 2.2.13). The largest proportional change of a

proglacial lake occurred at lake 25 (264.6%), but there is very low confidence in the magnitude of this change due to snow covering part of the lake boundary and the lakes relatively small size (6,180 m<sup>2</sup> in 2014) (Figure 2.2.13).

### 2.3.6 Glacier Terminus Changes 2010 to 2018 from Rapid Eye Imagery

A total of 24 glaciers in the Kebnekaise and surrounding area were selected for analysis in Rapid Eye satellite images (5 m) (14 from 16/8/2010 and 11 from 27/7/2010). The 2010 and 2018 terminus areas were mapped as polygons in ArcMAP and the area change was then calculated from the difference between the two polygons. This area of ice lost was then divided by the width of the glacier between the two reference points, in order to partly account for glacier thinning and narrowing within the width averaged retreat rate (Lea, 2014). This approach was taken particularly as many of the glaciers in the area have a triangular outline in plan view (Figure 2.2.4). Out of the 24 glacier termini that were mapped, 5 had proglacial lakes in the forefield but no contact, 11 had no proglacial lakes in the fore field and 8 had direct contact with a proglacial lake (Figure 2.2.16, Figure 2.2.17). The changes in terminus area of these 24 glaciers between 2010 to 2018 are further discussed below.

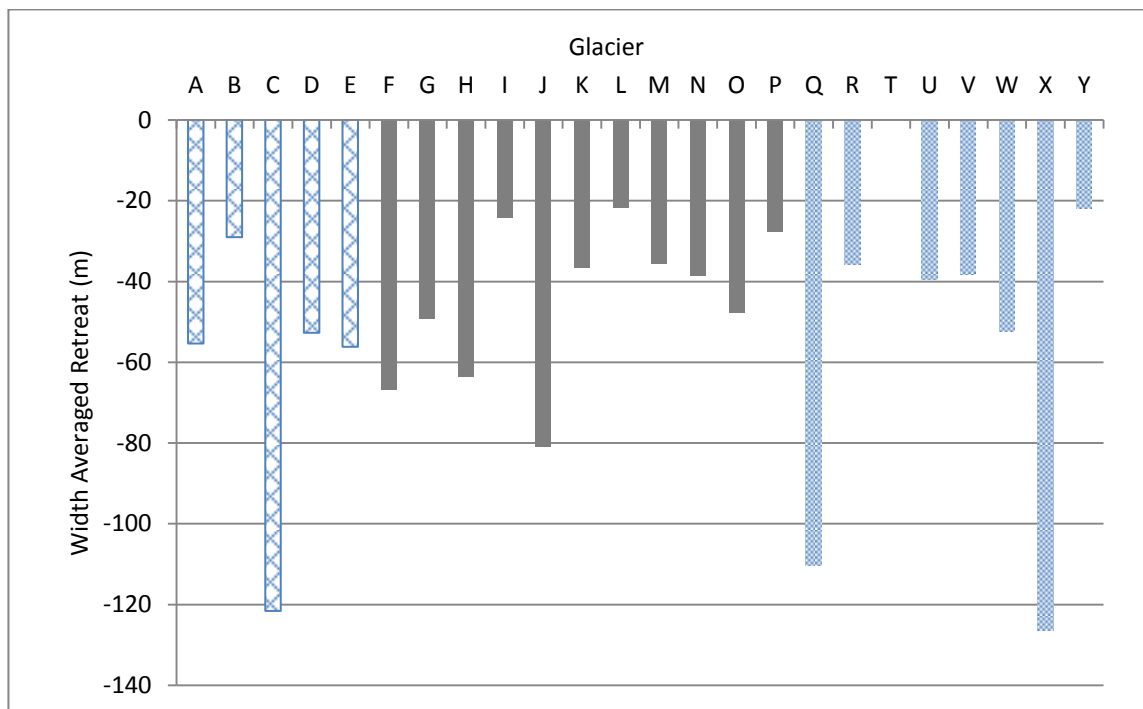


Figure 2.2.16 Plot of glacier terminus position change between 2010 to 2018 from Rapid Eye (5 m) multispectral satellite imagery. With blue crosses denoting glaciers with a proglacial lake in the forefield (non-contact), grey bars denoting glaciers with no proglacial lake in the forefield and blue hashed bars denoting glaciers with contact to a proglacial lake. See Figure 2.2.17 for map.

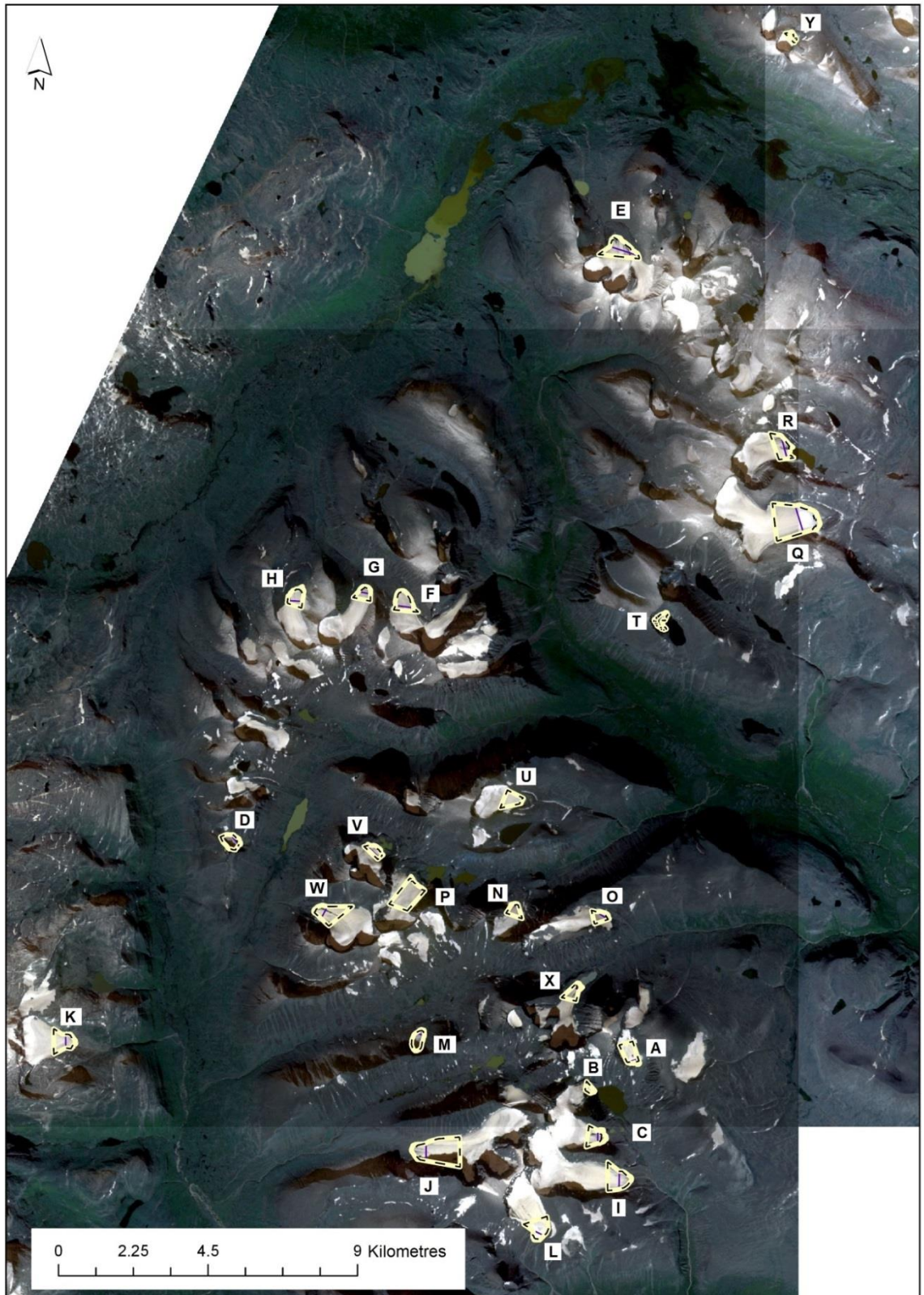


Figure 2.2.17 Rapid Eye multispectral satellite image (5m resolution) from 27/7/2010 with; yellow outline = 2010 glacier terminus area, dashed black line = 2018 glacier terminus area, purple line = width of glacier terminus area. Lettering corresponds to glacier label in Figure 2.2.16.

The width averaged retreat of 24 glaciers across the northern part of the study area ranged between 0 to 126 m between 2010 and 2018 (Figure 2.2.16, Figure 2.2.17). The mean width averaged retreat rates for glaciers with proglacial lakes over this period in the forefield (but no contact) was 63 m, with a median of 55 m. For land terminating glaciers the mean width averaged retreat was 53 m and a median of 39 m. The mean width averaged retreat rate for glaciers in contact with a proglacial lake was 53 m and a median of 39 m, which changes to a mean of 61 m and median of 39 if glacier T is excluded. The smallest of these glaciers (glacier T) had an area of 1,837 m<sup>2</sup> and was in contact with a much larger proglacial lake with an area of 346,729 m<sup>2</sup> (2014) and was the only glacier analysed that had no change in terminus position between 2010 to 2018 (Figure 2.2.16).

	Land terminating glacier retreat (m)		Lake terminating glacier retreat (m)
	Non-contact	No lake	Contact
Mean	62.98	44.70	53.05
Mean rate (ma <sup>-1</sup> )	7.87	5.59	6.63
Median	55.37	38.54	38.84
Range	92.57	59.07	126.34
SDEV	34.64	18.97	43.34
Count	5	11	8

Table 2.2.1 Summary statistics for retreat of 24 glaciers in Arctic Sweden from Rapid Eye (5 m) imagery mapping from 2010 and 2018. For land terminating glaciers with proglacial lakes in forefield (non-contact), land terminating glaciers with no lake and lake terminating glaciers with contact to proglacial lake water at the terminus.

The largest width averaged retreat of 126m occurred at Kaskapakteglaciaren (glacier X Figure 2.2.16 ), which is an alpine valley glacier that has contact with a proglacial lake (132,172 m<sup>2</sup> in 2014) across the full width (189 m) of the terminus throughout the period (2010 to 2018). A similar amount of retreat occurred at Isfallsglaciaren (glacier C; Figure 2.2.16), which retreated 122 m between 2010 and 2018 and has no contact with any proglacial lakes, although there are several smaller ones in the forefield. Marmaglaciar (glacier Q, Figure 2.2.16) retreated 110 m over this period and there was a 143 m wide proglacial lake in contact with the 412 m wide ice front in 2018. The 3 glaciers with the largest retreat rates discussed above had notably larger retreat rates than the other 21 glaciers analysed for terminus change (2010 to 2018), with the next (4<sup>th</sup>) largest retreat being 81 m at the land terminating Rabot's glaciär (Figure 2.2.16). The 5<sup>th</sup> and 6<sup>th</sup> largest retreats (67 m and 63 m) also occurred at land terminating glaciers (Figure 2.2.16). The remaining 18 glaciers all retreated less than 60 m between 2010 and 2018 (Figure 2.2.16).

## 2.4 Discussion

### 2.4.1 Proglacial Lake Spatial Distribution in Arctic Sweden

A substantial proportion (29.4%) of the 255 glaciers in Arctic Sweden had proglacial lakes in the forefield on 8<sup>th</sup> August 2014. A total of 108 proglacial lakes were mapped across Arctic Sweden from ASTER imagery taken on 8<sup>th</sup> August 2014 to produce the first proglacial lake inventory for an area in Scandinavia. There is some variation in glacier style and size across the study area in Arctic Sweden, with mean glacier size being 1,636,676 m<sup>2</sup> in the Sarek area and 850,939 m<sup>2</sup> in the northern half of the study area. Glaciers tend to be located on northerly through to easterly aspects, with virtually no glaciers on south westerly aspects. The diversity in glaciers across the study area makes it a valuable region for exploring the relationship with their spatial extent and proglacial lakes.

The previous Holocene maximum extent of glaciers across the study area is clearly visible in multispectral imagery, due to prominent moraine systems, glacial deposits and minimal vegetation cover development (Denton and Karlen, 1973; Karlen, 1973). Furthermore, historical imagery (1910) records the previous extent of some glaciers in the Kebnekaise region and provides useful validation of the interpretation of past glacier maximum extents (Svenonius, 1910; Holmlund and Holmlund, 2019). One might expect the number of proglacial lakes from the Holocene to be zero at the maximum extent. However, some glaciers (such as Kebnepakte) terminated in lakes at their 1910 maximum extent, which consequently extended beyond the Holocene glacier margin but are included here as a proportion of the lake remains within the Holocene extent (Kirchner et al., 2019). It may be reasonable to postulate that as glaciers retreated back from the 1910 maximum and decreased in area, then where they have receded there may be an increase in proglacial lake area. Consequently decreasing glacier size may be expected to correlate with increasing proglacial lake size. However, there was no correlation between glacier area and proglacial lake area ( $R^2 = 0.0286$ ). This suggests that the relationship between glacier area and proglacial lake area is more complex and will be explored further below.

The mapping of these proglacial lakes is particularly important given recent research suggesting proglacial freshwater could be a substantial sink of atmospheric CO<sub>2</sub> (Pierre et al., 2019). Moreover, at the time of mapping none of these 108 proglacial lakes were included in the Global Lakes and Wetlands Database (GLWD) (Birkett et al., 1995). Of these lakes 42%

were observed to be in contact with a glacier terminus on 8<sup>th</sup> August 2014 and therefore had the potential to directly influence processes of mass loss where they were in contact with a glacier (Carrivick and Tweed, 2013). It is also salient to analyse the spatial extent and distribution of non-ice contact proglacial lakes, as they can be an important store of freshwater and may have also previously influenced glacier retreat rates (Farinotti et al., 2016).

When exploring the relationship between glaciers and proglacial lake spatial extent it is necessary to consider a broad range of proglacial lake characteristics. The aspect of proglacial lakes will be controlled by the aspect of the parent glacier. The aspect of the glacier associated with each proglacial lake was predominantly (76.9 %) north through to easterly aspects, which follows the pattern of glacier locations across the study area (Figure 2.2.9) (Karlen, 1973). The predominance of glaciers and proglacial lakes on easterly and northerly aspects is unsurprising in an area where strong positive winter mass balances have been associated with strong westerly flows (positive phases of the NAO) (Pohjola and Rogers, 1997; Banon et al., 2019). Periods of strong westerly winter airflows would favour accumulation on leeward (easterly) aspects due to wind redistribution and deposition of snow, promoting glacier development on easterly aspects (Karlen, 1973). Furthermore, there were no proglacial lakes associated with glaciers facing south west or west and only 5 lakes (4.8%) associated with glaciers facing north west (Figure 2.2.9). There were also 13 lakes (12.5%) associated with glaciers facing south east and 6 (5.8%) facing south (Figure 2.2.9). This suggests that a greater number and extent of glaciers on northerly and easterly aspects have left behind more basins where proglacial lakes have filled after glacial recession. The majority of proglacial lake elevations were between 1,100 m to 1,500 m (Figure 2.2.7) and there was no correlation between proglacial lake area and elevation ( $R^2 = 0.0304$ ) (Figure 2.2.7). This is unsurprising as it is dictated by the extent of glaciers through the Holocene, which have tended to terminate in a relatively narrow elevation band that has been constrained by maximum elevations of ~2,000 m and valley levels around ~1000 m around Kebnekaise (Karlen, 1973).

#### **2.4.2 Proglacial Lake Spatial Distribution across Sub-Regions in Arctic Sweden**

The distribution of proglacial lakes in Arctic Sweden tends to be focused around the northern area (around Kebnekaise) and Sarek area to the south, with a small number of proglacial lakes in the central region north of lake Akkajaure (Area d; Figure 2.2.10). Whilst the

elevation in the Sarek and Kebnekaise areas is similar (maximums of 2,089m and 2,097m respectively, although 1,800m is more typical) the glaciers in the Sarek area tend to be larger and extend beyond corrie rims (Figure 2.2.18). Also, the topography in Sarek tends to be more open, with wider valleys between mountains and moraine systems extend further horizontally (Figure 2.2.18). Consequently there are less extensive topographic hollows in the Sarek area for proglacial lakes to develop in as glaciers retreat (Figure 2.2.18, Figure 2.2.19). As a result, proglacial lakes in the Sarek area are significantly smaller (mean 15,502 m<sup>2</sup>) than those further north in the central and Kebnekaise regions (mean 72,873 m<sup>2</sup>) (Figure 2.2.11). The manual mapping from 8<sup>th</sup> August 2014 showed that 43% of the proglacial lakes in the Sarek area had a contact point with a glacier. Therefore a substantial number of these lakes have the potential to influence the morphology and retreat rates of glacier termini in the Sarek region.

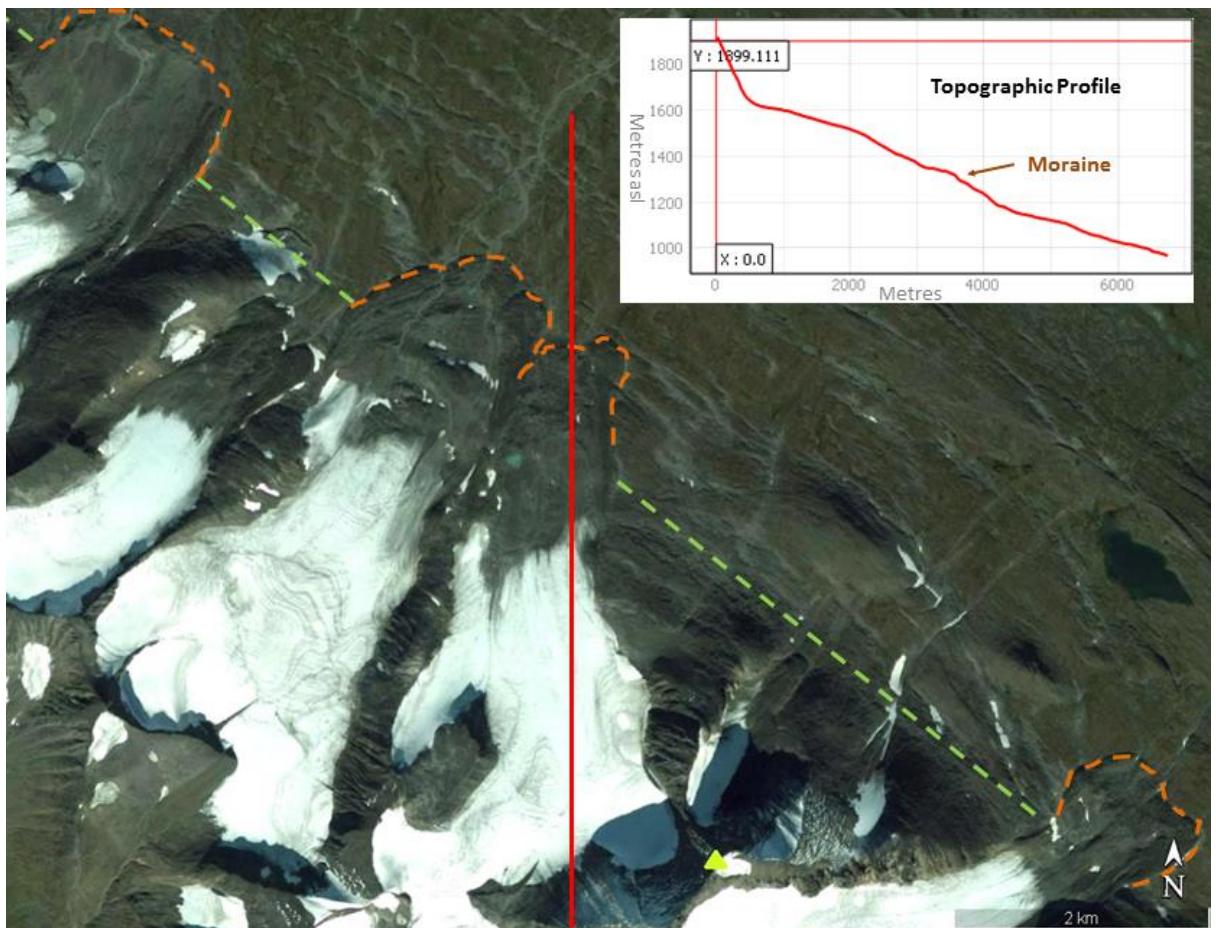


Figure 2.2.18 Satellite image from Digital Globe 30/8/2014 of Sarek area (courtesy of Google Earth). The highest peak in the area, Sarektjakka (2,089 m) is indicated by the green triangle (bottom centre left). Red line denotes the topographic profile (inset). Note the extensive terminal moraine systems extending beyond the corrie into the main valley below (orange dashed line). Green dashed line marks the valley side. Small proglacial lakes are clearly visible in the forefields due to the green colour from high suspended sediment load (Amphibolite). Note the wide vegetated valley bottom to the north east.

In contrast the glaciers in the northern Kebnekaise area tend to be more constrained by topography, with narrower high valleys and corries. The smaller glacier areas are also reflective of the decreasing amounts of precipitation further north and east (Goodfellow et al., 2008). The glaciers in the Kebnekaise and surrounding regions also tend to have terminal moraine systems with higher topography, mostly corresponding to the maximum extent of the Little Ice Age (LIA) ~1910 (Denton and Karlen, 1973; Karlen, 1973) (Figure 2.2.19). The northern and central regions (areas a, b and d Figure 2.2.10) have maximum elevations of ~1,800 m and tend to have smaller corrie glaciers (Figure 2.2.19).

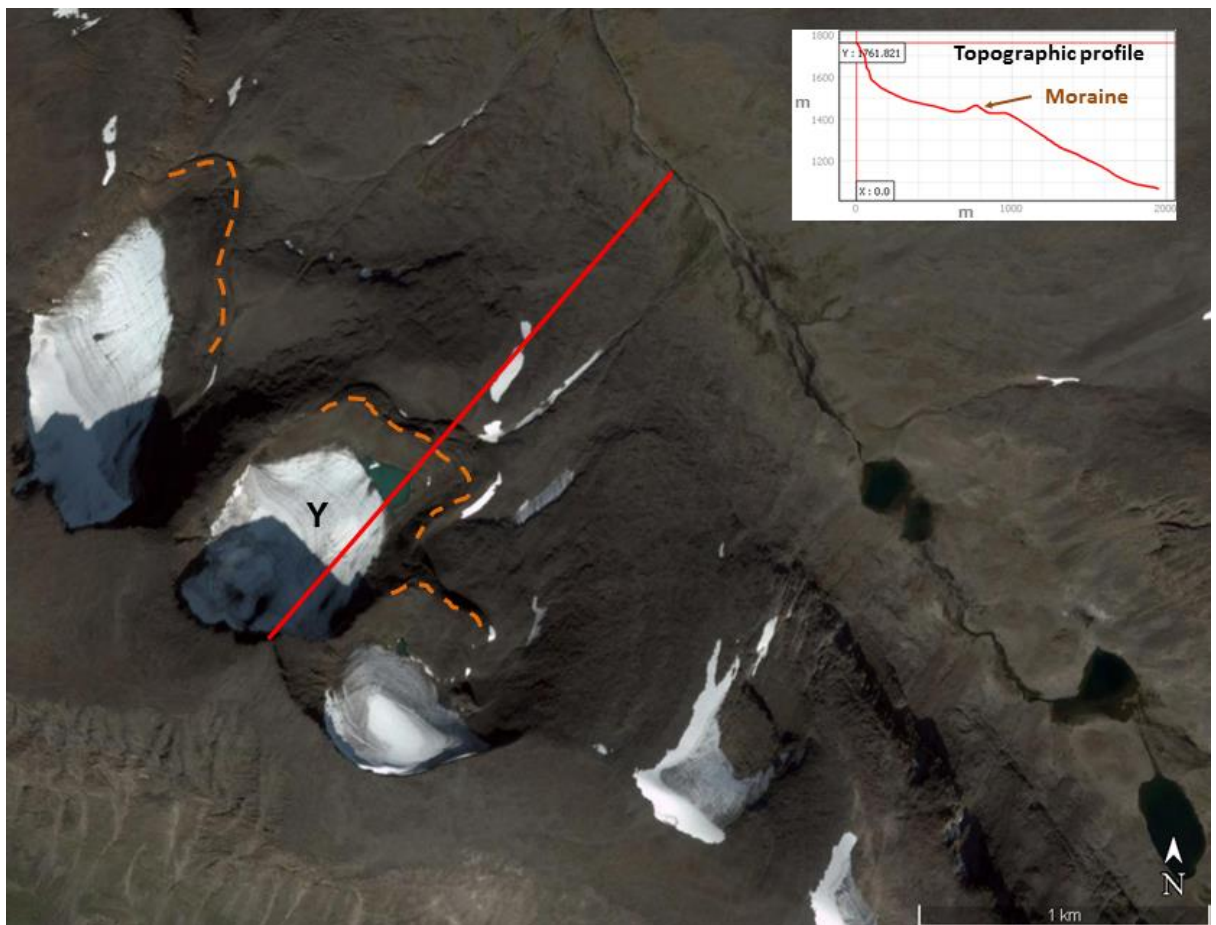


Figure 2.2.19 Satellite image from Digital Globe 25/8/2014 of corrie glaciers with prominent terminal moraine systems (orange dashed line). Red line denotes the line of topographic profile. Note the relatively narrow main valley system (in comparison to Sarek ) with minimal vegetation. Glacier Y refers to referencing system for mapping glacier terminus change (Figure 2.2.17).

The glaciers in the Kebnekaise area (area c; Figure 2.2.10) tend to be quite diverse. The increase in precipitation rates to the west of the area and plateau topography is reflected in more extensive plateau icefield glacier areas, which would have previously supported more extensive outlet glaciers (Goodfellow et al., 2008). In the main area of the Kebnekaise mountain chain, glaciers tend to be more topographically constrained due to narrower/higher

valleys and corries (Denton and Karlen, 1973) (Figure 2.0.20). This combined with more prominent terminal moraine systems (with higher crests), has created topographic niches where proglacial lakes have formed as glaciers have retreated back from their LIA maximum extents (see yellow star; Figure 2.0.20) (Karlen, 1973).

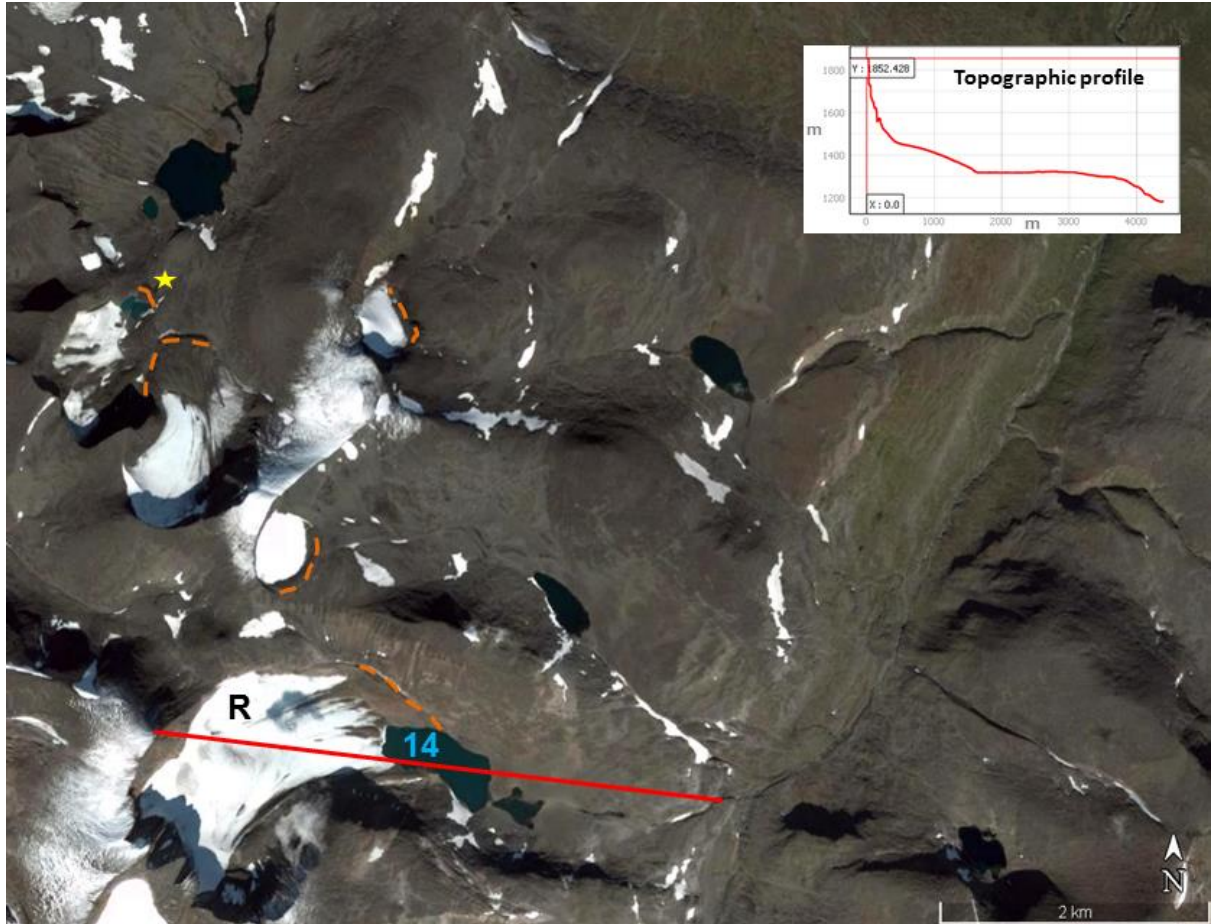


Figure 2.0.20 Satellite image from Digital Globe 25/8/2014 of Marmapakte area (courtesy of Google Earth). Red line denotes the line of the topographic profile. The highest peak in the image, Marmapakte (1,888 m) is in the lower left hand corner. Marmapakte glaciaren (R see Figure 2.2.17) flows north east from the peak to partly terminate in a proglacial lake (PGL<sub>ID</sub>:14) at 1285 m at bottom centre of image.

Proglacial lakes have also formed in the Kebnekaise region in glacial over-deepenings that have been produced through high rates of subglacial erosion on the bedrock (Kirchner et al., 2019). This is evident in Figure 2.0.20, as lake 14 extends beyond the terminal moraine from the LIA maximum (dashed orange line) and occupies a topographic depression (Karlen, 1973). Although the depth is unknown, the lack of a damming terminal moraine suggests that this lake is occupying a topographic depression excavated by glaciers previous to the LIA.

The type and extent of glaciation in Arctic Sweden controls the number and size of proglacial lakes. A substantial proportion (38%) of proglacial lakes in the Kebnekaise and surrounding

regions have contact with a glacier terminus and therefore have the potential to influence the morphology and subsequent retreat of glaciers. However, it is pertinent to consider the extent of the contact between the lake and the proportion of the glacier terminus as a whole, particularly as small lakes are unlikely to influence the glacier thermally or mechanically and may also quickly lose contact with the ice as the glacier retreats back. The extent of glacier terminus in contact with proglacial lake water and influence on terminus geometry is discussed in Chapter 4.

### **2.4.3 Changes in Proglacial Lake Extent since the 1950s/1960s**

There has been a notable emergence and expansion of proglacial lakes since the 1950s/1960s in Arctic Sweden. There were 15 (45.5%) proglacial lakes that were mapped in the ASTER imagery (33 lakes in total) from 8<sup>th</sup> August 2014 that were visibly covered by glacial ice in the 1950s/60s imagery (Figure 2.2.13). These proglacial lakes were classed as ‘unborn’ as they have emerged from underneath glacial ice since the 1950s/60s, 12 of them were from corrie glaciers (mostly easterly aspect) and 3 were from plateau icefields. Of these 15 unborn lakes 6 were >10,000 m<sup>2</sup> on 8<sup>th</sup> August 2014 in the ASTER imagery, this represents 18.2% of the overall sample of 33 proglacial lakes. It is also possible that some of the 7 ‘snow concealed’ proglacial lakes may have been underneath glacial ice, but impossible to confirm due to the snow cover in the available imagery.

There has also been a substantial increase in area of the 11 proglacial lakes that were present in the 1950s/60s imagery, with an increase in mean area from 176,091 m<sup>2</sup> (1950s/60s) to 199,701 m<sup>2</sup> (2014). The largest absolute increase in proglacial lake area over this period occurred at Riukojekna plateau icefield (Figure 2.2.14), which increased by 95,606 m<sup>2</sup>, representing an increase of 76.4% of the area in 1960 (Figure 2.2.13). There was also a substantial increase in proglacial lake area of 75,393 m<sup>2</sup> at Kaskapakteglaciaren, which was 132.8% of the 1959 lake area (Figure 2.2.13 and Figure 2.2.15) (see Chapter 4 for further discussion). There was a similar amount of expansion with an increase of 53,420 m<sup>2</sup> for proglacial lake (PGL<sub>ID</sub> 22) area at Vaktposten glaciär (Figure 2.2.13 and Figure 2.2.14). Both of these proglacial lake expansions were associated with retreat of large corrie/valley glaciers, which raises the question as to whether the respective proglacial lakes may have enhanced glacier retreat rates in this situation.

The relatively high snow cover in the 1950s/60s made precise quantification of glacier terminus area problematic (Figure 2.2.12). Therefore it was not possible to calculate width

averaged glacier retreat rates between the 1950s/60s imagery and the ASTER 2014 imagery, due to snow concealing glacier margins. Each glacier was manually inspected in both sets of imagery, but not reported in detail in this section due to the low precision of the analysis.

Whilst the sample discussed above is relatively limited, it suggests that there has been a substantial increase in number and extent of proglacial lakes in Arctic Sweden between the 1950s/60s imagery and the snapshot captured by the ASTER satellite imagery (8<sup>th</sup> August 2014). Furthermore, no proglacial lakes that were present in the historical imagery were observed to have a dry bed in August 2014, essentially no proglacial lakes were observed to have disappeared with progress through time. Therefore the number of proglacial lakes in Arctic Sweden has increased since the 1950s/60s and the extent of proglacial lakes has increased too (Figure 2.2.13). At the time of writing these findings represent the first report of changes in proglacial lake extent for an Arctic area since the 1950s/60s. Although it should be noted the study of Carrivick and Quincey (2014) reports an increase of 44% in the number ice marginal lakes on the south west margin of the Greenland ice sheet between 1987 and 2010. Therefore more mapping of proglacial lakes in the Arctic is required, ideally over a large time span to explore the relationship with proglacial lake expansion, glacier retreat and changes in climate.

#### **2.4.4 Glacier Terminus Changes in Arctic Sweden from 2010 to 2018**

The available Rapid Eye (5 m) imagery for Arctic Sweden, which was sufficiently cloud and snow free, was relatively limited in extent. The imagery extent focuses around the main Kebnekaise mountain chain, with mostly corrie glaciers and some small valley glaciers (Figure 2.2.17). Only 24 out of the 255 glacial bodies in the study area were within the area covered by the imagery and sufficiently snow free for terminus area mapping (Figure 2.2.17). Within this limited sample of 24 glaciers in Arctic Sweden, there was a wide range of terminus width averaged retreat of 0 to 126 m between 2010 and 2018 (Figure 2.2.16). This heterogeneity in terminus change suggests that individual glacier characteristics and locational factors play a prominent role on influencing changes in glacier terminus area.

Where glaciers are in contact with a proglacial lake, retreat rates may be exacerbated through mechanical and thermal processes at the water to ice contact point (Carrivick and Tweed, 2013). So the glaciers mapped for terminus change were classed as lake terminating or land terminating, which was further subdivided by presence of proglacial lake in the forefield, as this may have influenced retreat in the past. The mean width averaged retreat rate for glaciers

in contact with a proglacial lake was higher (53 m) than for land terminating glaciers without a proglacial lake (44 m) between 2010 and 2018. The annual average retreat for lake terminating glaciers in Arctic Sweden of  $6.63 \text{ m a}^{-1}$  (2010 to 2018) is substantially lower than average retreat of  $46.9 \text{ m a}^{-1}$  reported by Carr et al (2017) for Arctic lake terminating glaciers in Novaya Zemlya.

The highest retreat rates reported in this study between 2010 and 2018 are for land terminating glaciers with proglacial lakes in the fore field (but no contact), with a mean width averaged retreat of  $63 \text{ m}$  ( $7.87 \text{ m a}^{-1}$ ). This would suggest that the glaciers without contact to a proglacial lake (but present in the fore field) had higher width averaged retreat on average than those in contact with proglacial lakes or glaciers without any proglacial lakes in the forefield. However, the relatively limited sample is problematic for statistical analysis, as due to the small number of glaciers in each category the mean retreat rate may be substantially affected by a large change in 1 glacier. It should also be noted that defining the exact width of some glacier termini is problematic due to triangular snouts in some cases and therefore makes defining the proportion of proglacial lake contact problematic (Appendix A 5). Indeed there is a notable variation in width averaged retreat rates in each of these three datasets, as clearly individual glacier characteristics and situation play a prominent role in response to climate and changes in the terminus area.

The largest width averaged retreat of  $126 \text{ m}$  occurred at Kaskapakteglaciaren between 2010 and 2018 (Figure 2.2.16), which equates to  $15.75 \text{ m a}^{-1}$  over this period (glacier X Figure 2.2.17). This is an alpine valley glacier that has contact with a proglacial lake ( $132,172 \text{ m}^2$  in 2014) across the full width ( $189 \text{ m}$ ) of the terminus throughout the period (2010 to 2018) and also since at least 1959 (Figure 2.2.15). This rate of terminus retreat is substantially lower than rates for lake terminating glaciers of  $46.9 \text{ m a}^{-1}$  in Novaya Zemlya (Russian Arctic) (1986 to 2015) and  $80.8 \text{ m a}^{-1}$  in Patagonia (mid 1980s to 2010) (Sakakibara and Sugiyama, 2014; Carr et al., 2017). The smaller retreat rate of Kaskapakteglaciaren may be due to the smaller size of the glacier in comparison to glaciers in Novaya Zemlya and Patagonia, which may be due to relatively higher lateral support in proportion to the terminus width ( $189 \text{ m}$ ) of Kaskapakte (Boyce et al., 2007).

A comparable amount of retreat to Kaskapakteglaciaren occurred at Marmaglaciaren (glacier Q, Figure 2.2.17), ( $110 \text{ m}$ ) and Isfallsglaciaren ( $122 \text{ m}$ ) (glacier C Figure 2.2.17) between 2010 and 2018. Marmaglaciaren also had a  $\sim 140 \text{ m}$  wide proglacial lake in contact with the  $412 \text{ m}$

wide ice front. Isfallsglaciaren has no contact with any proglacial lakes, although there are several smaller ones in the forefield. As the name suggests there is a prominent icefall on Isfallsglaciaren, which is likely to have played a role in the large width averaged retreat of the glacier (Holmlund and Holmlund, 2019). The magnitude of the changes in these 3 glaciers is notable and will have skewed the mean for each glacier class, given the relatively small sample sizes.

The range in retreat rates of the 24 glaciers mapped in 2010 and 2018, would suggest that they have responded to climatic changes at different rates, illustrating the importance of considering the glacier response time (Brugger, 2007). The particular characteristics of each glacier are clearly paramount, as this will dictate how a glacier responds to climate change through surface melt or glacier dynamics. The 3 largest retreat rates are notably larger than the other 21 glaciers analysed for terminus change (2010 to 2018), with the next (4<sup>th</sup>, 5<sup>th</sup> and 6<sup>th</sup>) largest retreats occurring at land terminating glaciers (Figure 2.2.17). This would suggest that factors other than contact with proglacial lakes have had a substantial influence on the retreat rates of most glaciers sampled in Arctic Sweden between 2010 and 2018. However, detailed analysis and discussion of the characteristics of each glacier is beyond the scope of this study. Particularly as it would require Radar to investigate the thermal structure of these glaciers, as well as the profile and properties of the glacier bed. Glacier velocities would also need to be required to investigate the glacier response times to climatic changes (Brugger, 2007).

## **2.5 Conclusion**

The development and expansion of proglacial lakes in the Arctic has received relatively little attention to date. These proglacial lakes form a prominent aspect of the hydrological system through storing of glacial melt water, particularly as this storage may mitigate the rise in sea levels from glacier recession associated with climate change. Where glaciers continue to recede the amount of water that they store reduces and therefore the water stored in proglacial lakes is more critical for maintaining water levels in downstream catchments, which has important implications for ecology and human populations. The recent study of Pierre et al. (2019) have suggested that proglacial freshwater may act as a substantial sink and store of

atmospheric CO<sub>2</sub> and call for a global proglacial lake inventory. This study provides one of the first proglacial lake inventories for an Arctic area.

There was a substantial proportion (29.4%) of glaciers inspected in this study area of Arctic Sweden, which had proglacial lakes in the fore field. A large proportion (42%) of the 108 proglacial lakes mapped in Arctic Sweden were classed as being in contact with glacier termini and therefore had the potential to influence glacier retreat rates through enhancing mass loss. The total area of 4,767, 295 m<sup>2</sup> covered by the 108 proglacial lakes in the inventory represents a substantial area of water that was previously not included within the Global Lake and Wetland Database (GLWD) (Birkett et al., 1995). The mapping of proglacial lakes reported in this study has important hydrological implications for assessing how currently glaciated catchments will respond to climate change. Furthermore, the increase in number and extent of proglacial lakes since the 1950s/60s reported in this study emphasises the increasing prevalence and importance as part of the hydrological system in Arctic Sweden. There were also significant differences in the area of proglacial lakes between sub regions in Arctic Sweden, with proglacial lakes in the Sarek region being significantly smaller than the Kebnekaise and surrounding areas. This is due to the differing extent and characteristics of glaciers between the two regions.

This study has mapped changes in glacier terminus geometry of land and lake terminating glaciers for the limited high resolution imagery available over Arctic Sweden. The largest retreat rate of 15.75 m a<sup>-1</sup> reported in this study was for Kaskasapakteglaciaren, which terminates in a lake. This would further support the body of evidence suggesting that glacier retreat rates can be exacerbated where the terminus is in full contact with proglacial lake water, although it is only from a limited sample of glaciers in Arctic Sweden. This retreat rate is substantially lower than has been reported for lake terminating glaciers in Arctic Russia and Patagonia, which are much larger glacier systems. The mean retreat rate for lake terminating glaciers in this study was higher than for land terminating glaciers (with no lake) but lower than for land terminating glaciers with a proglacial lake in the fore field.

There was a large range in retreat rates amongst the 24 glaciers analysed between 2010 and 2018, which emphasises the heterogeneity in glacier responses to climatic changes. Future remote sensing based studies should increase the number of lake and land terminating glaciers for terminus change mapping, ideally with imagery over multiple time steps to investigate the relationship with climatic changes. This would increase the statistical

robustness of constraining the influence of proglacial lakes on glacier retreat rates at the regional scale. This is particularly important given future predictions of increased air temperatures and heatwaves, which are predicted to increase glacier retreat and also lake temperatures.

## 3 Investigating Proglacial Lake Temperature in Arctic Sweden from the ASTER Satellite Temperature Product

### 3.1 Introduction

In a changing climate it is important to assess how the physical environment changes in order to ascertain the consequences for ecological systems and human populations. There is a general view that lakes represent sentinels of climate change, which can be used to gauge their response to changes in climate and surrounding environmental conditions (Adrian et al., 2009). It is essential to constrain the responses of lakes to climate change given that they represent the major component of liquid freshwater storage on Earth and support biodiversity, as well as providing vital ecosystem services to people around the world (O'Reilly et al., 2015; Woolway et al., 2019). Lake surface water temperatures can be highly correlated with regional air temperatures, making them useful indicators of climate change (Adrian et al., 2009; O'Reilly et al., 2015). Furthermore, O'Reilly et al. (2015) report significant warming of  $0.34^{\circ}\text{C decade}^{-1}$  of 235 globally distributed lake surface temperatures (1985 to 2009) and note the 'consistency' with global increase in air temperatures of  $0.25^{\circ}\text{C decade}^{-1}$  (1979 to 2012) (Hartman et al., 2013). In light of these observed increases in lake temperatures, the overall aim of this chapter is to measure the temperature of proglacial lakes in Arctic Sweden and assess the spatial pattern of temperatures across lakes and the region.

The pattern of increase in lake surface temperatures discussed above is not homogeneous and different regional patterns have been reported (Schneider and Hook, 2010; O'Reilly et al., 2015). Indeed, there has been stronger warming trends in the mid to high latitudes of the northern hemisphere, with maximum regional rates of  $0.08^{\circ}\text{C a}^{-1}$  in lakes across Northern Europe (Schneider and Hook, 2010; O'Reilly et al., 2015). Some of the most rapid lake surface warming reported has been from seasonally ice covered lakes ( $0.72^{\circ}\text{C decade}^{-1}$ ), particularly in areas that have experienced increases in air temperature and solar radiation (O'Reilly et al., 2015). Also, a widespread reduction in lake ice has been observed across the Northern Hemisphere, with reductions in annual lake ice cover that increase the annual duration of open water and vulnerability of such lakes to climatic warming (Sharma et al., 2019). This decrease in seasonal lake ice cover is one of the earliest indicators of climatic warming and is predicted to increase, with a reduction of 29 (+/-8) ice covered days and ~25% of seasonally ice covered lakes projected to be permanently ice free by 2080 to 2100

under RCP 6.0 (Sharma et al., 2019; Woolway et al., 2019). Furthermore, surface waters of seasonally ice covered lakes are predicted to warm by  $2.3 \pm 0.6^{\circ}\text{C}$  by 2080 to 2100 under RCP 6.0 (Woolway et al., 2019). The observed increases in surface water temperature, decreases in seasonal lake ice cover and predicted future continuation of these trends makes it essential to further constrain lake surface water temperature responses to climate, particularly as this is heterogeneous and can depend on individual lake characteristics and location (Adrian et al., 2009; O'Reilly et al., 2015; Sharma et al., 2019; Woolway et al., 2019).

Within these regional patterns there is a greater complexity of lake surface water temperature response to climate, with some individual lake surface water temperature trends diverging from air temperature trends (O'Reilly et al., 2015). It is imperative to consider what factors control the response of lake surface water temperatures to climatic changes, as a range of other lake characteristics and meteorological conditions can also have a strong influence on lake surface water temperatures (O'Reilly et al., 2015). The surface water temperature of a lake is driven by absorbed solar irradiance and heat exchange with the atmosphere, which is controlled by air temperature, solar radiation, humidity, ice cover and also wind (Edinger et al., 1968; O'Reilly et al., 2015). These factors can vary substantially between lakes in different locations, particularly where distinct microclimates occur.

If these factors are taken into consideration on a regional scale, across a mountain range for instance, then one might expect to see a range in lake surface temperatures. For example south facing lakes at lower warmer elevations would experience more solar irradiance and more positive heat exchange with higher air temperatures, than higher north facing lakes shaded by topography (O'Reilly et al., 2015). Consequently it is essential to consider the topo-climatic situation of an individual lake when assessing the response of surface water temperatures to climatic changes. Furthermore, the response of lake surface water temperatures to climatic changes is also mediated by characteristics such as lake depth and surface area, which influence the cooling or warming of surface waters as well as potential mixing with deeper water (Schmid et al., 2014; O'Reilly et al., 2015). The varied warming response of lakes to changes in climate requires that detailed analysis is undertaken to assess the driving factors controlling changes at each lake (O'Reilly et al., 2015). The 12 largest proglacial lakes in the study area were selected for analysis of skin surface temperature (SST) patterns, as these lakes were sufficiently large enough for extracting pixel temperatures with minimal thermal contamination of 90m ASTER satellite thermal imagery (Figure 3.1). The use of ASTER thermal imagery for extracting SSTs is reviewed in section 3.1.2.

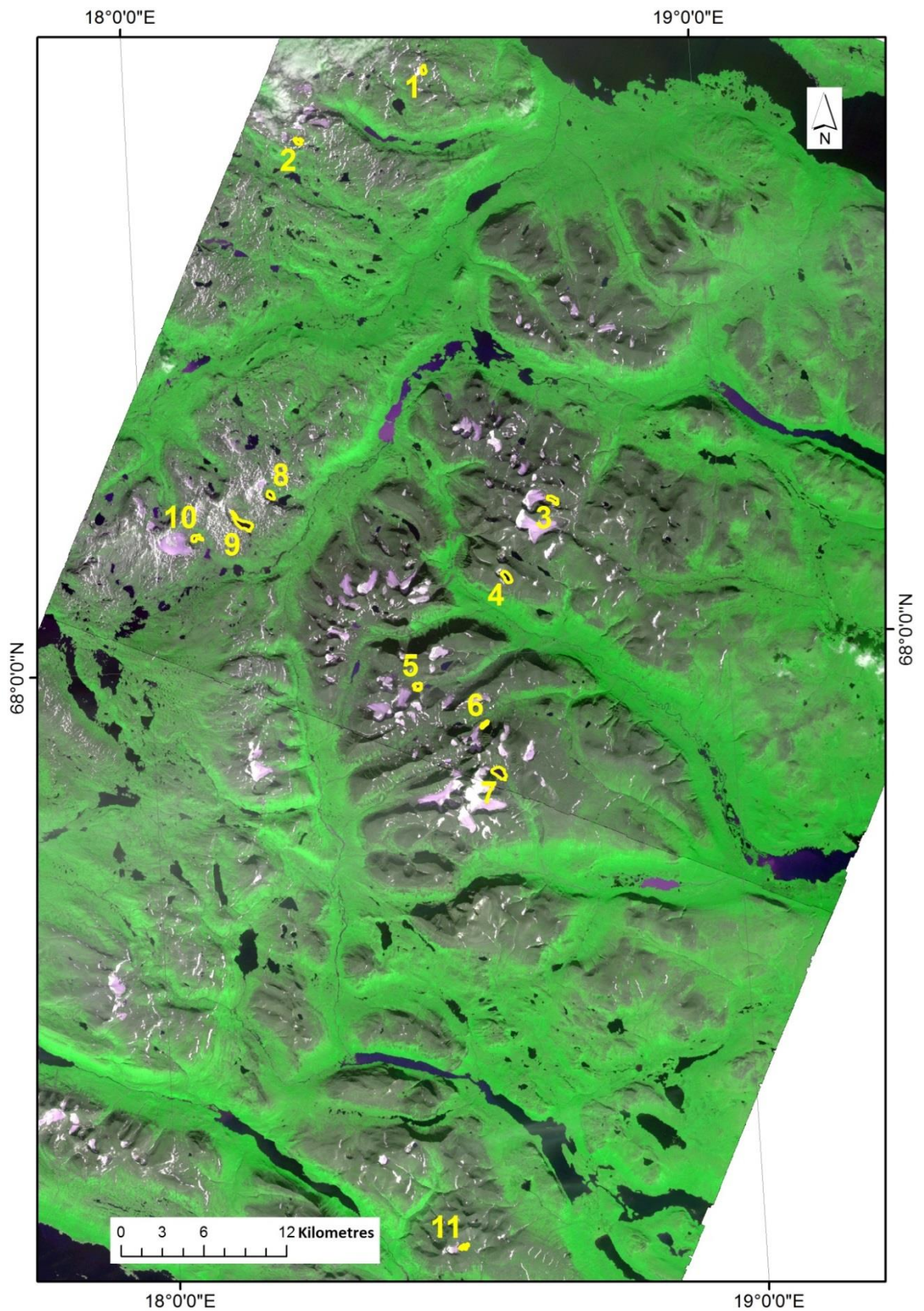


Figure 3.1 ASTER satellite composite (Green, Red, NIR) image showing location of the 12 proglacial lakes (Arctic Sweden) with large enough area to have sufficient pixels for skin surface temperature analysis from the AST08 temperature product. NOTE lake 12 is situated ~50km to the south in the Sarek area. Lakes are numbered sequentially here for simplicity, see Results section for lake

geometry/characteristics from Proglacial Lake Inventory (PGLID). Tarfala research station is located next to lake 7 (Tarfalasjon). Lakes 1, 3, 4, 6, 11 and 12 were all classed as 'ice-contact' on 8/8/2014, lakes 2, 5, 7, 8, 9, 10 were all classed as non-ice contact.

Annual Arctic air temperatures are reported to have warmed at rates of 1.7 times the Northern Hemisphere average between 1971 and 2017 (Box et al., 2019). This is likely associated with the Arctic amplification of rising global temperatures through a series of feedbacks, mostly focused around the reduction in sea ice cover leading to decreased albedo over the Arctic and decreased reflectance of incoming solar radiation (Serreze and Francis, 2006; Box et al., 2019). This study focuses on an area of Arctic Sweden where increases in air temperature of  $0.042^{\circ}\text{C a}^{-1}$  (1965-2011) have been reported for Tarfala research station, which provides a well-positioned record of meteorological conditions, as it is located at 1,130 m in a glaciated valley containing proglacial lakes (Jonsell et al., 2013).

The higher air temperatures discussed above are likely to lead to increased lake temperatures, particularly if combined with periods of cloud free conditions that result in high levels of incoming solar radiation (associated with recent heatwaves e.g. July 2018) warming surface water layers (O'Reilly et al., 2015; Kim et al., 2018; Chikita, 1999). The mean annual air temperature (MAAT) for Tarfala is  $-3.5 \pm 0.9^{\circ}\text{C}$  (1965-2011) and proglacial lakes in the area develop seasonal ice cover (Jonsell et al., 2013). The MAAT of  $-3.5 \pm 0.9^{\circ}\text{C}$  (1965-2011) at Tarfala is well below the threshold of  $8.4^{\circ}\text{C}$  for lake ice becoming intermittent as suggested by Sharma et al. (2019). The timing of ice onset and break up for proglacial lakes in the study area is largely unconstrained and requires further investigation, particularly given the decreasing trend in annual duration of ice cover as observed for global lakes by Sharma et al. (2019). It is salient to constrain annual ice cover duration as it is a major control on surface water temperatures and makes seasonally ice covered lakes more vulnerable to climatic warming (O'Reilly et al., 2015; Sharma et al., 2015). However, this is beyond the scope of this study but should be borne in mind when considering the surface water temperature of proglacial lakes.

Despite the warming trends in air and lake water temperatures discussed above, a general assumption persists that smaller lakes in contact with glacier termini have uniform temperatures of  $1^{\circ}\text{C}$  (Chernos et al., 2016; Truffer and Motyka, 2016). It is important to test whether proglacial lakes remain a uniform  $1^{\circ}\text{C}$ , especially given Arctic Amplification of climatic warming in the Northern Hemisphere (Serreze and Francis, 2006). Constraining ice-contact proglacial lake surface temperatures is essential as thermal undercutting of the glacier

may occur where water temperatures are high enough and enhance rates of glacier mass loss, which has been observed in several studies (Kirkbride, 1993; Warren and Kirkbride, 1998; Warren and Kirkbride, 2003; Roehl, 2006; Minowa et al., 2017; Watson et al., 2020). Furthermore, these proglacial lakes are a key part of the hydrological system and are increasing in number as glaciers retreat, as reported in Chapter 2 (Komori, 2008; Gardelle et al., 2011; Carrivick and Quincey, 2014; Hanshaw and Bookhagen, 2014).

The water temperatures of proglacial lakes will affect recipient river water temperatures and affect geochemistry, particularly through nutrient cycling and the solubility of gases, such as CO<sub>2</sub> (which is temperature dependent) (Caissie, 2006; Webb et al., 2008; as cited in Fellman et al., 2014). Therefore changes in proglacial water temperatures are likely to have ecological consequences, not only for temperature dependent species (such as salmonids and invertebrates) but also potential changes in geochemistry (Fellman et al., 2014). Recent research by Pierre et al. (2019) has also suggested that proglacial freshwaters are potentially a substantial sink of atmospheric CO<sub>2</sub>, through chemical weathering of suspended sediment (glacial flour). Fellman et al. (2014) found that there was a 0.9°C to 1.5°C rise in stream water temperature for every 1% change in watershed lake area coverage of catchments with <30% glaciated area in South East Alaska through May to August 2011. Given the predicted increases in future lake temperatures and glacial recession it is therefore essential to constrain the water temperatures of proglacial lakes (IPCC AR5, 2013; Woolway et al., 2019). The overall aim of this chapter is to measure surface water temperatures of proglacial lakes (ice-contact and non-ice contact) across Arctic Sweden and explore the locational factors influencing them (Figure 3.1).

The objectives for this chapter are;

- O4. Analyse skin surface temperatures of the 12 largest proglacial lakes across Arctic Sweden.
- O5. Assess the relationship between spatial patterns in proglacial lake surface temperature and factors affecting thermal regime of each proglacial lake.

### **3.1.1 Remote Sensing of Lake Surface Water Temperatures**

The outgoing longwave radiation (OLR) from the Earth will balance the absorbed solar radiation (ASR) where the climate is in equilibrium, however there is a range of fluxes between land, water bodies and atmosphere that couple OLR with ASR (Trenberth et al.,

2009). The outgoing longwave radiation from Earth occurs on wavelengths of 3 to 100  $\mu\text{m}$ , with a particular centre between 9 to 14  $\mu\text{m}$ , although this depends on the Earth's surface material and temperature and is further discussed below (Trenberth et al., 2009). This longwave radiation can be converted into imagery visible to the human eye, known as thermal infrared (TIR) imagery, which shows the temperature difference across the view from a thermal camera sensor (Kirk et al., 2016). The use of remote sensing is widely established for monitoring glacier terminus positions but has been underutilised for detecting surface temperatures of proglacial lakes, despite freely available satellite thermal infrared imagery (Wessels et al., 2002; Watson et al., 2020). It is essential to correct thermal infrared imagery for atmospheric conditions as longwave radiation detected at the satellite sensor will be a mixture of emissions from the atmosphere, as well as emissions from the Earth's surface (Figure 3.2) (Trenberth and Fasillo, 2011). Also longwave radiation emitted from the Earth's surface may also be blocked or attenuated by the atmosphere, particularly where water content is high (Gillespie et al., 1998; Gustafson et al., 2006) (Figure 3.2).

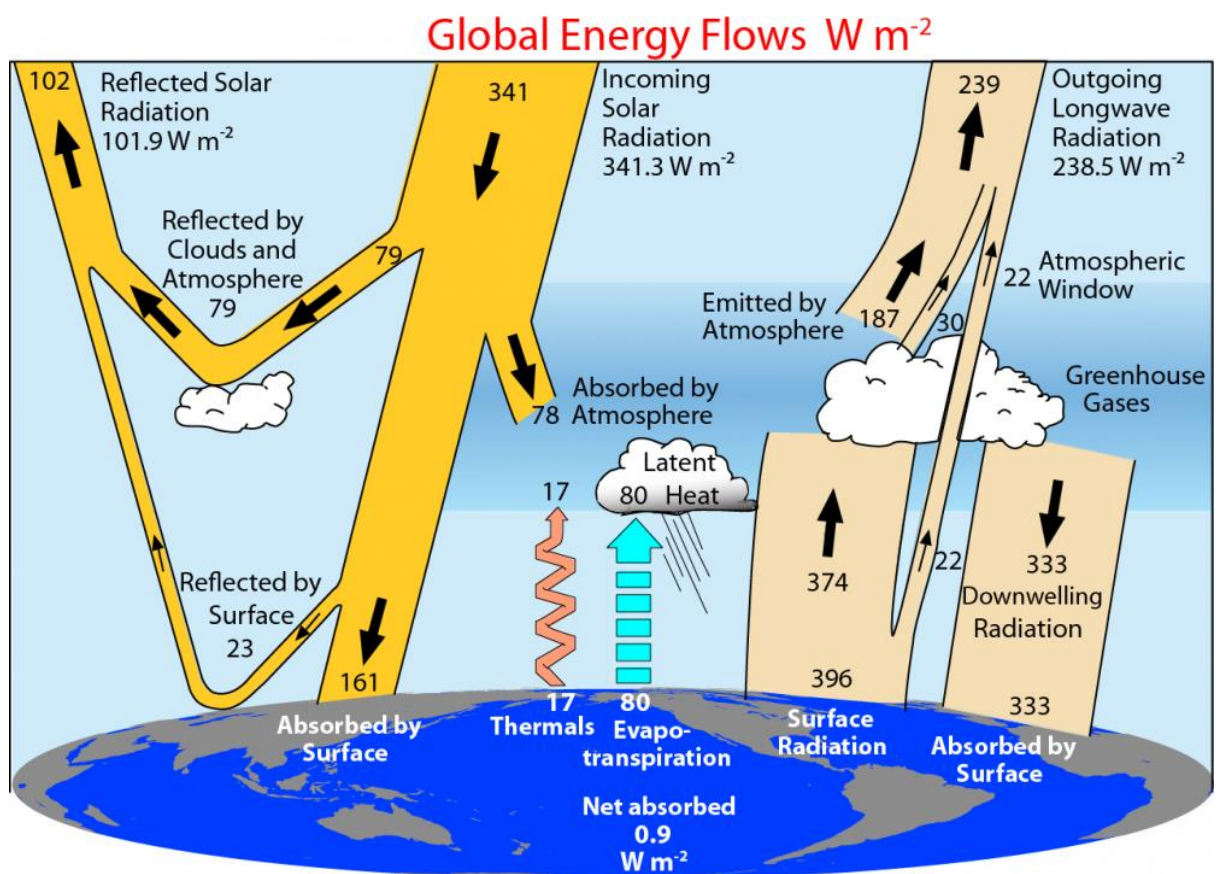


Figure 3.2 Diagram showing Earth's global annual mean energy budget ( $\text{W m}^{-2}$ ) for the March 2000 to May 2005 period from Trenberth and Fasillo (2011). The broad arrows schematically indicate more substantial flows of energy (Trenberth and Fasillo, 2011).

As with optical remote sensing, the amount of cloud cover in a scene is often the main barrier to analysis of thermal satellite imagery over proglacial lakes, as clouds effectively absorb most longwave radiation emitted by the Earth's surface and prevent it reaching the satellite sensor (Figure 3.2). Furthermore, longwave radiation is also emitted from water vapour in the Earth's atmosphere (Trenberth et al., 2009) (Figure 3.2). Thus atmospheric correction for satellite thermal imagery scenes is essential in order to distinguish between longwave radiation emitted by the atmosphere from that emitted by the surface and also to calculate how much of the surface emission is attenuated by the atmosphere (Trenberth et al., 2009). Therefore understanding the flux of longwave radiation through the atmosphere enables calculation of the amount of surface emitted longwave radiation that reaches the satellite sensor (Gillespie et al., 1998; Gustafson et al., 2006). However, characterisation of water vapour content in the atmosphere is problematic, particularly the distribution and radiative characteristics of clouds (Trenberth et al., 2009).

The radiation reaching the sensor is referred to as 'brightness temperature', as it refers to how much radiation from a surface is seen by the sensor (Planck, 1901). Brightness temperature does not take into account how efficient that surface is at emitting radiation (Planck, 1901). The skin surface temperature (SST) relates to the radiation emitted by the skin (top mm) of a surface, which is a kinetic temperature as it relates to the vibrational energy of the skin surface layer (Gillespie et al., 1998). In order to establish skin surface temperatures (SST) from longwave radiation at the satellite sensor, it is also essential to calculate how efficient a surface is at emitting radiation, which is referred to as the emissivity (Planck, 1901; Gillespie et al., 1998). The emissivity of a surface depends on the chemical composition and structure, which varies for different parts of the Earth's surface and may also be affected by moisture content (Gustafson et al., 2006; Sabol et al., 2009). Also, the spectral emissivity may vary across different wavelengths in the thermal infrared region, which results in different surfaces having spectral peaks in emissivity at different wavelengths (Sabol et al., 2009). This variation in spectral emissivity between different surfaces can be utilised to identify different surfaces, such as different rock types, which is discussed further in section 3.1.3 (Sabol et al., 2009).

The section below will first of all provide an overview of the studies using ASTER thermal imagery over fresh water bodies, before reviewing the use of the Temperature/Emissivity Separation algorithm (TES) with ASTER imagery. The TES algorithm is used iteratively to produce the ASTER land surface temperature product (AST08) from the 5 ASTER thermal

infrared (TIR) bands (90 m) (Gillespie et al., 1998). The surface kinetic temperatures (Kelvin) produced in the AST08 product are derived from the corresponding Emissivity product (AST05) for each TIR band, which are also calculated using the TES algorithm (Gillespie et al., 1998). There is a summary of uncertainties associated with the emissivity (AST05) and surface temperature (AST08) products derived with the TES algorithm. This will particularly focus on the use of these products over water, in order to inform the reader of potential sources of uncertainty in the AST08 surface temperature product. This provides a background for the development of the methodology and workflow used in this study for extracting proglacial lake surface temperatures from AST08 surface temperature product imagery.

### 3.1.2 Utilisation of ASTER Thermal Imagery over Fresh Water Bodies

The Advanced Spaceborne Thermal Emission and Reflection Radiometer (ASTER) satellite has 5 bands across the thermal infrared (TIR), with central wavelengths of 8.30  $\mu\text{m}$  (band 10), 8.65  $\mu\text{m}$  (band 11), 9.05  $\mu\text{m}$  (band 12), 10.60  $\mu\text{m}$  (band 13) and 11.30  $\mu\text{m}$  (band 14) (Sabol et al., 2009) (Figure 3.3). The 5 bands across the thermal wavelength enables peaks in different wavelengths to be identified and utilised in order to characterise the target surface in each pixel (90 m) and derive an emissivity value for that pixel (Sabol et al., 2009).

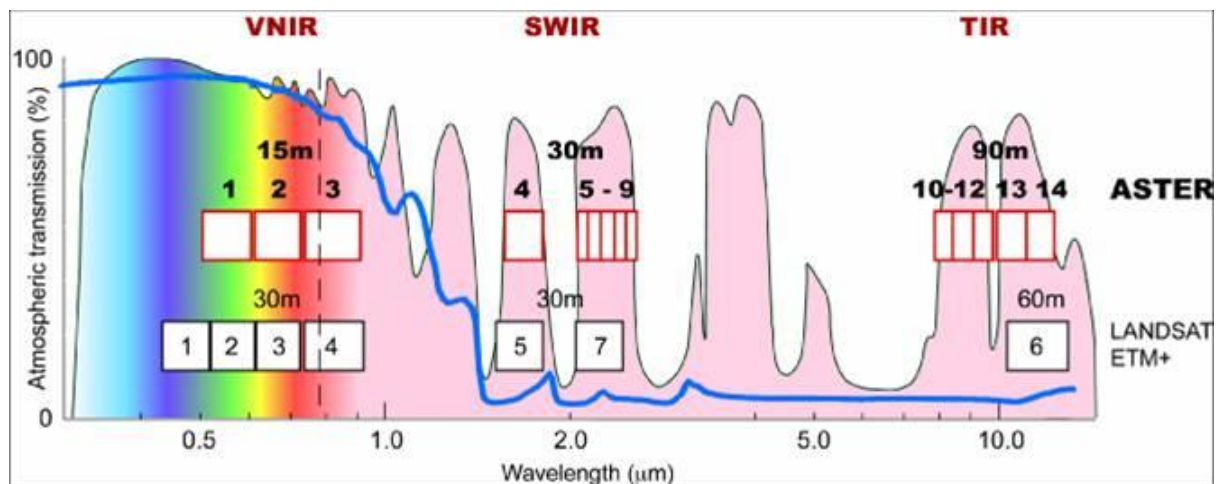


Figure 3.3 ASTER bands superimposed on model atmosphere transmission, with coloured sections denoting ‘atmospheric windows’ of wavelengths that are transmitted through a ‘typical’ atmospheric column. White sections denoting wavelengths that radiation is absorbed by the atmosphere and consequently transmission through the atmosphere is minimal. Note the trough in atmospheric transmission between ASTER bands 12 and 13, which is due to ozone content. Also note that TIR band 10 is the most affected by atmospheric absorption up to 8.5  $\mu\text{m}$  due to water content (Abrams et al., 2002).

The relatively high resolution of ASTER satellite thermal imagery (90 m) facilitates the detection of land emitted radiance of relatively small lakes (Wessels et al., 2002). The radiance emitted by the Earth's surface is related to the surface temperature, which can be calculated if several characteristics are known or estimated. The emissivity of a surface defines how efficiently it emits radiation (Gillespie et al., 1998). So if we stand close to a warm object the emission of longwave radiation will be felt more strongly from a surface with high emissivity than a surface with low emissivity (Hulley et al., 2015). Consequently it is essential to constrain the emissivity of a surface in order to calculate the surface temperature (Gillespie et al., 1998). The materials that have the highest emissivity are referred to as 'black bodies' and have an emissivity of close to 1.0 (Gustafson et al., 2006). The ASTER satellite utilises a 'black body' for sensor calibration of the thermal infrared sensor by viewing the black body (at 300°K) reference plate before each image acquisition, thus enabling short term drift in the sensor to be calibrated (Gustafson et al., 2006).

The study of Wessels et al. (2002) was one of the first to utilise ASTER thermal imagery (bands 10 to 12) to calculate mean brightness (radiant) temperatures for 2 supraglacial lakes (size unreported) on Ngozumpa glacier of 276.6 °K (3.45°C) and 282.2°K (9.05°C). The Wessels et al. (2002) study is one of the first satellite based observations of glacial lake temperatures from thermal infrared imagery and suggests they can be warmer than the uniform 1°C that has been previously assumed (Truffer and Motyka, 2016). It is important to note that the details behind the calculation of brightness (radiant) temperatures from L1B TIR imagery (with radiometric and geometric corrections applied; see Abrams et al., 2002) in Wessels et al. (2002) are unclear. This is an important omission, as the flux of radiation through the atmosphere needs to be accounted for and the correct emissivity for the surface in the pixel needs to be carefully constrained if kinetic skin surface temperatures (SST) are to be obtained (Gustafson et al., 2006). It is imperative to carefully characterise the surface emissivity, as the value for water (0.98) differs substantially from rock surfaces (~0.9 to 0.6) (Sabol et al., 2009). Indeed, the presence of rock within a pixel that is largely water will cause some thermal emission contamination. It is therefore essential when identifying lake water temperatures to ensure that the 90 m pixel purely consists of water, so areas of lake around the margins are problematic and should not be included in lake temperature analysis from satellite thermal imagery. Indeed, Wessels et al. (2002) suggest that only lakes with at least 2 full 90 m TIR pixels should be included for surface temperature analysis with ASTER. It should also be noted that the Wessels et al. (2002) was relatively soon after the launch of

ASTER (2000) so the validation of ASTER thermal imagery was relatively limited at this time.

The only other study to utilise ASTER thermal imagery for extraction of glacial lake skin surface temperatures to date (to our knowledge) is that of Watson et al. (2020). In contrast to Wessels et al. (2002) the study of Watson et al. (2020) employed a 2 pixel buffer to the margins of the lake, to minimise risk of pixels that may be subject to thermal contamination from surrounding land surfaces. The 2 pixel buffer was probably warranted under the method undertaken by Watson et al. (2020), as the geolocational mis-alignment between ASTER thermal imagery (L1B) and lake polygons derived from optical imagery was not accounted for. Pixels containing icebergs were also excluded in order to calculate an average skin surface temperature (SST) for Imja Tsho, Lower Barun and Thulagi glacial lakes in Nepal, with respective maximums of 9.6°C, 7.2°C and 10.8°C between 2000 and 2018 (Watson et al., 2020). The seasonal average SST presented by Watson et al. (2020) represent an important advance in constraining glacial lake seasonal regime through the melt season. They present a seasonal increase in glacial lake average SSTs following the spring melt of lake ice, with a plateau in temperatures during the monsoon, before decline in temperatures in the autumn before lake ice forms (Watson et al., 2020).

These glacial lake SST averages were extracted from surface temperature products derived from Landsat 8 or ASTER (AST08) satellite thermal imagery (Watson et al., 2020). The surface temperature products from both satellites are atmospherically corrected. The robustness of the Landsat 8 SSTs is questionable, particularly given there is notable ‘noise’ within the data. They suggest that this may be due to the Landsat 8 satellite only having two thermal bands, in contrast to the five bands on the ASTER satellite (which would have been confirmed by a more extensive review of the literature) (Watson et al., 2020). Crucially the 5 thermal bands of the ASTER satellite sensor enables the Temperature Emissivity Separation algorithm to be employed to derive emissivity to be calculated and derive skin surface temperature (see section 3.1.3). Watson et al. (2020) do acknowledge the uncertainties and call for more validation of satellite derived SSTs over glacial lakes.

The validation of ASTER thermal imagery over water bodies has largely been focused on a site at Lake Tahoe (USA) which has a series of automated temperature sensors on buoy moorings (Hook et al., 2007). This site was purposefully chosen as it has a dry continental climate and at an altitude of 2,000 m, therefore the atmospheric water content is relatively

low (0.5 to 1.5 cm total column) (Hook et al., 2007). Consequently the attenuation of radiation due to atmospheric water vapour is minimal and relatively constant, so the calculation of lake skin surface temperatures at Lake Tahoe is unlikely to be compromised by short term (<6 hours) fluctuations in atmospheric moisture (Hook et al., 2007). Hook et al. (2007) used the known emissivity spectra for water to calculate *radiant* temperature using Planck's law (from Aubry-Wake et al., 2015);

$$L(T) = \frac{1}{\pi} \int_{\lambda_1}^{\lambda_2} \frac{2\pi hc^2}{\lambda^5} \times \frac{1}{\frac{hc}{e^{\lambda\sigma T} - 1}} d\lambda \quad (3.3)$$

Where  $h$  is the Planck constant ( $6.626 \times 10^{-34} \text{ J s}^{-1}$ ),  $c$  is the speed of light ( $2.998 \times 10^8 \text{ m s}^{-1}$ ) in a vacuum,  $\lambda$  is the wavelength ( $\mu\text{m}$ ),  $T$  is the absolute temperature of the blackbody (K), and  $\sigma$  is the Stefan Boltzmann constant ( $5.67 \times 10^{-8} \text{ Wm}^{-2} \text{ K}^{-4}$ ) (from Aubry-Wake et al., 2015). The spectral range of interest is given by  $\lambda_1$  and  $\lambda_2$ , the spectral range for the thermal infrared is typically  $8.5 \mu\text{m}$  to  $13.5 \mu\text{m}$  (Aubry-Wake et al., 2015). Planck's law calculates radiance at a given temperature, which can therefore be used to calculate the temperature if other aspects described above are known (Aubry-Wake et al., 2015). Crucially, Planck's law assumes that the surface is a black body in thermal equilibrium, when there is no net flow of energy or matter between the body and its environment (Planck, 1901). As a black body has an emissivity of 1.0, this law needs to be adjusted to take into account varying surfaces that have different emissivities in order to calculate temperature. It is also important to remember that it refers to black bodies in thermal equilibrium, which may not be the case for water (emissivity 0.97 to 0.98) at higher temperatures ( $>290 \text{ K}$ ) that may cause change in entropy through evaporation resulting in changes of state (Gillespie et al., 2011). Furthermore, it does not account for atmospheric attenuation of the radiant energy (Aubry-Wake et al., 2015). This further emphasises the need for validation of thermal imagery over water bodies.

The validation of the ASTER TIR imagery by Hook et al. (2007) at lake Tahoe was successful and they concluded that it had met pre-flight radiometric calibration specifications of  $\pm 1.5^\circ\text{K}$  and  $\pm 0.015$  emissivity (see Gillespie et al., 1998). However, it is also essential to validate the ASTER TIR imagery at non-favourable sites with high atmospheric moisture content (such as maritime areas), particularly as Tonooka (2005) found that poor atmospheric characterisations could account for errors of 3 to  $8^\circ\text{K}$  in TIR imagery, using the Naval Research Laboratory climatology model (Gillespie et al., 2011). These large errors due to

poor atmospheric characterisation suggest that it is essential to validate ASTER TIR surface temperatures with in-situ temperature measurements of lakes ideally at the same time as an ASTER overpass (Tonooka et al., 2005).

### 3.1.3 ASTER Temperature/Emissivity Separation Algorithm used in AST05 Emissivity and AST08 Surface Temperature Products

The Temperature/Emissivity algorithm (TES) was developed for producing skin surface temperatures from ASTER thermal infrared imagery and uses the land leaving spectral radiance (AST09) as input (with atmospheric correction) (see Gillespie et al., 1998; Coll et al., 2007). The amount of radiation received by a surface (sky irradiance) was initially removed by TES using an iterative approach, which is a critical step as the amount of radiation received by a surface will affect the skin surface temperature (Coll et al., 2007; Gustafson et al., 2006). The land surface temperature (LST) and emissivity in channel  $j$  ( $\epsilon_j$ ) can be related to the at sensor radiance measured by ASTER TIR channel ( $j = 10$  to  $14$ ) by;

$$L_{s,j} = [\epsilon_j B_j(T) + (1 - \epsilon_j) F_{sky,j} / \pi] \tau_j + L_{a,j} \quad (3.4)$$

Where  $B_j$  is the Planck function for the effective wavelength of channel  $j$  (see above),  $\tau_j$  is the atmospheric transmittance,  $L_{a,j}$  is the atmospheric path radiance emitted towards the sensor and  $F_{sky,j}$  is the downwelling sky irradiance (Lambertian reflection assumed), all for channel  $j$ . (from Coll et al., 2007). If the atmospheric parameters are known (through atmospheric characterisation; discussed below), then the radiance at ground level or “land leaving” radiance,  $L_{g,i}$  [term in square brackets in equation 3.2] can be calculated from the at sensor radiance;

$$L_{g,i} = \frac{L_{s,j} - L_{a,j}}{\tau_j} \quad (3.5)$$

The TES algorithm is applied to the at ground radiances (AST09), with the principle problem that LST ( $T$ ) and emissivity ( $\epsilon$ ) are coupled (eq 3.2 from Coll et al., 2007). The 5 thermal bands of ASTER are utilised to provide 5 spectral emissivity measurements to develop an empirical relationship that is used to break down the underterminacy between LST and emissivity (Coll et al., 2007).

The Normalised Emissivity Method module (NEM; Gillespie et al., 1998) is used in TES to estimate LST initially as the maximum temperature calculated with the 5 thermal band at ground radiances (using assumed  $\epsilon = 0.97$ ) and an estimate of sky irradiance (from Coll et al., 2007). This preliminary LST is used to obtain an initial estimate of emissivity in the 5 thermal bands (Coll et al., 2007). The emissivity spectral shape and contrast (difference between maximum and minimum emissivity) is then estimated by using band ratioing in the NEM (Sabol et al., 2009). The spectral contrast in ASTER thermal imagery is represented by the maximum to minimum difference (MMD) in emissivity (Gillespie, 1998). However, this has to be scaled to relate to the known spectral minimum emissivity ( $\epsilon_{\min}$ ) of surfaces from laboratory data (Figure 3.4) (Sabol et al., 2009). This is problematic for surfaces that do not plot on the line of regression (Figure 3.4), particularly surfaces with low emissivity contrast (e.g. graybodies such as water) (Sabol et al., 2009). A gray body has an emissivity independent of radiation frequency and has a lower emissivity than a black body (Sabol et al., 2009). These new emissivity values ( $\epsilon_{\min}$ ) are then used to calculate the Land Surface Temperatures (AST08) using equation 3.2 (Coll et al., 2007).

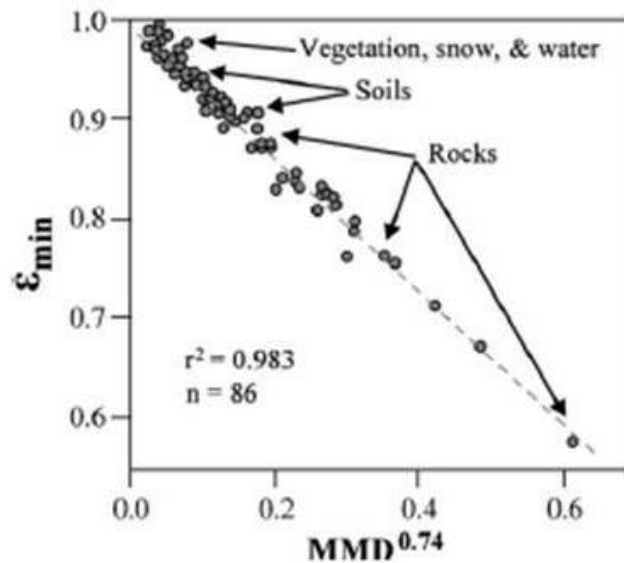


Figure 3.4 The regression line used in the TES algorithm (Gillespie et al., 1998) to scale emissivities, based on the emissivity minimum ( $\epsilon_{\min}$ ) from laboratory values used in the ASTER spectral library and Kirchhoff's law of thermal radiation (emissivity is equal to absorptivity for an arbitrary body in thermodynamic equilibrium) (Sabol et al., 2009). MMD = Maximum Minimum Difference from ASTER spectral emissivity (from Sabol et al., 2009).

### 3.1.4 Uncertainties in ASTER products (AST05 and AST08) derived from TES

The errors associated with the ASTER thermal imagery over water bodies has been investigated by several studies (Tonooka, 2005; Tonooka and Palluconi, 2005; Coll et al., 2007; Hook et al., 2007; Sabol et al., 2009; Gillespie et al., 2011). The key uncertainties in the products from the TES algorithm have been identified as being due to a) emissivity, b) atmospheric correction, c) measurement errors and d) calibration (Gillespie et al., 1998; Gustafson et al., 2006; Sabol et al., 2009; Gillespie et al., 2011). These sources of error are often intertwined due to the nature of the processing and one source may impact another, which is discussed in more detail below.

The AST05 emissivity is also produced with the TES algorithm and is used to model temperatures in the AST08 temperature product (Gillespie et al., 2011). Therefore the AST05 product is potentially a source of error in the AST08 temperatures, as it is critical to know how effectively a surface emits radiation (emissivity) to calculate the skin surface temperature (Gillespie et al., 2011). Whilst the majority of studies have found that emissivity errors with the AST05 product were within predicted limits ( $\pm 0.015$ ), it is pertinent to further explore potential sources of error within the AST05 and also AST08 products, particularly given that atmospheric conditions (particularly water content) will vary between study sites (Gillespie et al., 2011).

It should be noted that gray bodies are treated differently in different versions of TES, which may result in emissivity values for these surfaces being lower (Sabol et al., 2009). Consequently Gustafson et al. (2006) found skin surface temperatures over water produced from TES may be  $\sim 1$  K or more too high. However, both Gustafson et al. (2006) and Sabol et al. (2009) found that temperatures over water from the AST08 temperature product were within the predicted accuracy of  $\pm 1.5$  K (Gillespie et al., 1998). Although Gustafson et al. (2006) found water skin surface temperature errors of  $\sim 4$  K in 4% of the several hundred images analysed in the study of different lakes. They attribute these errors due to incomplete atmospheric correction in areas with high atmospheric temperatures and humidity (Gustafson et al., 2006). This incomplete atmospheric correction led to failure of the iterative algorithm used to remove spectral irradiance (radiant flux received by a surface), as the atmospheric composition (particularly water content) will affect the amount of down welling longwave radiation (Figure 3.2). Gustafson et al. (2006) recommended the iterative algorithm be

removed in order to improve the recovery of temperatures over gray bodies, such as water. Further emphasising the need for accurate atmospheric correction of thermal imagery.

The emissivity over water in AST05 was found to vary spatially and between different acquisition dates for a range of lakes in different locations and altitudes (Gillespie et al., 2011). This is problematic as in theory water should be a relatively uniform grey body and therefore have a relatively uniform emissivity (Gillespie et al., 2011). A potential source of error in the AST05 v 2.9 product occurs through electronic striping due to radiometric noise (Coll et al., 2007). This electronic striping may be incorrectly classified as real spectral contrast by TES and result in some water pixels having lower emissivity than surrounding water pixels (Coll et al., 2007; Gillespie et al., 2011). This would result in higher temperatures in the AST08 product, as the surface would have been characterised as emitting radiation less effectively and therefore having a higher skin temperature to account for the amount of radiation received at the satellite sensor. Whilst electronic striping was visibly detectable in the AST05 imagery analysed by Gillespie et al. (2011) they concluded that the product was still functioning at the predicted precision limits ( $\pm 0.015$ ) for water skin surface temperatures  $<290^{\circ}\text{K}$  ( $17^{\circ}\text{C}$ ). For water surfaces above  $290^{\circ}\text{K}$  ( $17^{\circ}\text{C}$ ) they found a sharp increase in emissivity errors in the AST05 product that exceeded the predicted precision limits, which they account for due to changes in sensible heat flux and increases in humidity (Gillespie et al., 2011). This again emphasises the importance of characterisation of atmospheric conditions over target surfaces.

The lake surface temperatures of 298 temperate lakes in Wisconsin (USA) were derived from the ASTER kinetic temperature product (AST08 V2.9) (Becker and Daw, 2005). The AST08 product is derived from the TES algorithm and crucially also has atmospheric correction from the United States National Centre for Environmental Protection (NCEP) and National Centre for Atmospheric Research (NCAR) reanalysis product. The NCEP NCAR reanalysis produces atmospheric characterisations every 6 hours and in  $1^{\circ} \times 1^{\circ}$  windows from interpolation of global radiosonde meteorological observations (wind, temperature, moisture and pressure) at different elevations in the atmosphere (Gustafson et al., 2006). It is important to note that the NCEP reanalysis is North American focused but also utilises observations from the World Meteorological Organisation (WMO), which may be between 1 to 4 observations daily and  $\sim 1,000\text{km}$  apart in sparsely populated areas ([http://madis.ncep.noa.gov/madis\\_raob.shtml](http://madis.ncep.noa.gov/madis_raob.shtml)). Therefore the spatial and temporal resolution

of the NCEP NCAR reanalysis product is relatively coarse when considering microclimates across a mountain range, such as around Kebnekaise.

This reanalysis data is used with MODTRAN (MODerate resolution atmospheric TRANsmittance computer program) radiative transfer model to estimate atmospheric transmissivity, path spectral radiance and down welling spectral radiance (Gustafson et al., 2006). This temporal and spatial resolution of observations and subsequent interpolation in the reanalysis, is relatively coarse compared to potential meteorological variability and unable to account for differences at the edges of air masses (Gustafson et al., 2006). This is particularly problematic in maritime areas, such as Scandinavia, where meteorological conditions may change substantially in less than 6 hours and 1,000km. So it is still crucial to validate the AST08 temperature product in order to assess atmospheric correction, ideally in the same climatic area and similar time as the image acquisition over the study site (Gillespie et al., 2011). This is a key requirement of using the AST08 temperature product in maritime areas and we present validation data of the AST08 temperature product collated by this study in section 3.3. Indeed, the study of Coll et al. (2007) used local radiosonde data for atmospheric correction of ASTER TIR data (band 13) used to calculate sea surface temperatures near the coast of Spain and reported differences of only 0.4°C compared to field validation data. They also compared contemporaneous field validation data with ASTER LST (AST08) data, which they found over estimated LSTs by 0.2°C to 1.1°C (Coll et al., 2007), which still lies within the stated accuracy of the AST08 product (+/- 1.5°C) (Sabol et al., 2009).

The strong relationship found by Becker and Daw (2005) between buoy bulk water temperatures (1cm depth) and AST08 skin surface temperatures ( $R^2=0.98$ ) suggests good atmospheric correction (from NCEP NCAR reanalysis) over Wisconsin lakes at the time of their study. It is important to note that Becker and Daw (2005) found a weaker relationship between AST08 temperatures and in situ buoy measurements ( $R^2=0.90$ ) during the daytime. Furthermore, mean difference between the two datasets was 0.9°C during the night time and 1.9°C during the daytime (Becker and Daw, 2005). They account for the stronger relationship between AST08 temperatures to buoy data during the night time due to less latent heat release from the lake surface and suggest if the air column is near the dew point then surface temperatures will be only a function of sensible heat fluxes (Becker and Daw, 2005). This emphasises the importance of the time of image capture, as it defines what part of the diurnal temperature signal is captured by the image (Becker and Daw, 2005). Consequently night

time and early morning ASTER thermal images represent a better measure of ambient lake surface temperatures due to the absence of short term surface warming during the middle of the day, which may disturb the thermal equilibrium. The depth of this solar warming will be defined by water clarity, as incoming solar radiation will penetrate deeper into clear water and result in a thicker warm surface layer (epilimnion) and greater heat storage capacity of the lake (Becker and Daw, 2005). This should be considered when interpreting lake surface temperatures, as TIR images taken during the day may capture short term diurnal warming of the surface.

### **3.1.5 Summary of Issues for Developing the AST08 Extraction Workflow**

The literature reviewed above suggests that the AST08 temperature product largely meets the stated accuracy of  $\pm 1.5^{\circ}\text{C}$ . However, there are notable exceptions where the stated accuracy is exceeded, particularly associated with emissivity errors and incorrect atmospheric characterisation. Whilst Gillespie et al. (2011) conclude that the AST08 temperature product is less affected by electronic striping and incorrect atmospheric characterisation than the AST05 emissivity product, other studies have found substantial errors in the AST08 product due to incomplete atmospheric characterisation (Tonooka, 2005). Indeed, Tonooka (2005) found that the largest source of error of skin surface temperatures calculated using the TES algorithm (used in AST08) was incorrect atmospheric characterisation that previously used the Naval Research Laboratory (NRL) climatology, particularly in humid conditions that could account for errors of between 3 to 8  $^{\circ}\text{C}$  (Gillespie et al., 2011). Again this emphasises the need for validation of the AST08 product with in situ measurements in maritime areas, where atmospheric water content may be high and potentially change in less than 6 hours.

The methodology has been developed in light of the sources of uncertainties discussed above. In light of the uncertainties discussed surrounding atmospheric correction and incomplete characterisation of clouds, the ASTER imagery was first of all filtered for cloud cover and only cloud free scenes were utilised. In addition, in situ lake near surface water temperature (<2 m depth) data were actively sought to provide ground validation of temperatures from the AST08 temperature product in maritime areas, particularly in areas adjacent to the study area in Arctic Sweden. Furthermore, a quality assessment was made from inspecting the corresponding AST05 Emissivity product imagery to assess whether the emissivity pixel values used to derive the AST08 temperatures were realistic. This is further described in the Methodology below (section 3.2).

## 3.2 Methodology

The recent (since 1996) climatic pattern in air temperatures was investigated through records of air temperature from the Tarfala research station (1,135 m) located in the study area. The surface air temperatures from the Swedish Meteorological and Hydrological Institute (SMHI) automated weather station (AWS) are measured at 2 m above the ground behind a Stevenson screen at Tarfala research station. The SMHI meteorological data are readily available for download (<https://www.smhi.se/data/meteorologi/ladda-ner-meteorologiska-observationer>) between 1996 (when the AWS was installed) and the present day. The hourly average air temperatures were downloaded between 1996 and 2018 and plotted in Excel.

The ASTER satellite thermal infrared (TIR) imagery was utilised for investigating proglacial lake skin surface temperature ( $SST_L$ ) in this study as it has the highest spatial resolution (90 m) of any freely available satellite thermal imagery. The thermal imagery from Landsat 8 was also investigated, but has a coarser resolution of 100 m. The available Landsat 8 thermal imagery is automatically sharpened using the SWIR bands to 30 m pixels, which makes it highly problematic to define whether an original 100 m TIR pixel contained 100% lake surface. This is a critical flaw as if a pixel is a mixture of lake and land surface, then the thermal signal of the lake will be subject to thermal contamination from the land surface. Therefore it was impossible to extract lake water pixel temperature values from the available Landsat 8 TIR imagery with greater than 95% confidence of no thermal contamination from surrounding land. This study therefore utilises the ASTER satellite surface temperature product (AST08; see section 3.1.2.2 and 3.1.3.3) for extraction of proglacial lake temperatures, as outlined in the workflow below (Figure 3.5).

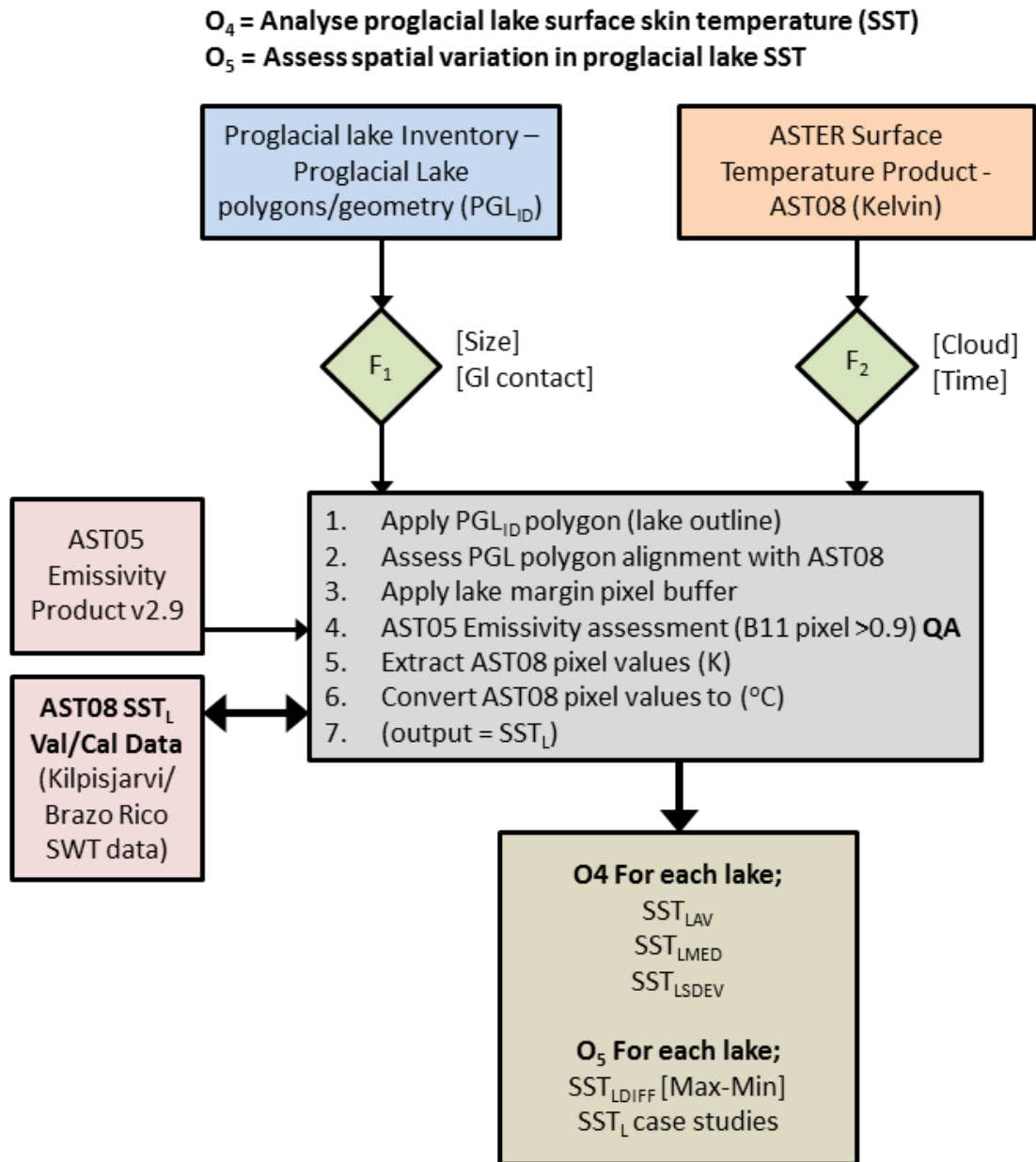


Figure 3.5 Diagram of workflow for extracting Skin Surface Temperatures (SST) for proglacial lakes ( $SST_L$ ) from ASTER surface temperature product (AST08 v2.9) over Arctic Sweden. The proglacial lake inventory ( $PGL_{ID}$ ) geometry and characteristics (including associated glacier geometry from Randolph Glacier Inventory) were used in the analysis from chapter 2. The PGL inventory was filtered for lakes  $>129,600 \text{ m}^2$  (see below) and also by classification of contact (0 = no contact, 1 = contact with glacier) with glaciers in corresponding ASTER optical imagery. The ASTER Emissivity Product (AST05) was inspected for quality assessment (QA) of emissivity data used in the production of the AST08 surface temperature product (AST08; see above). Validation/Calibration data were actively sought at conferences, with thermistor data ( $<2 \text{ m}$  depth) being kindly provided by G. Kirrilin and M. Minowa from Kilpisjarvi (Sweden) and Brazo Rico (Patagonia) respectively (see below).

### 3.2.1 Application of Proglacial lake (PGL) polygons and margin buffer

A series of 3 scenes from Arctic Sweden were downloaded for the dates of 8/8/2014

(10:46am) and 29/7/2018 (data from 2018 is not presented here). A threshold of  $129,600 \text{ m}^2$

proglacial lake area was set, which equates to a grid of 4 x 4 AST08 90 m pixels (Figure 3.6). Thus enabling the skin surface temperature to be extracted from at least 4 pixels in the centre of the lake, with a high confidence that the pixel was purely over water (Figure 3.6). This effectively leaves a 1 pixel buffer around the margin of each lake, where thermal contamination may occur due to the presence of land surface within the pixel (Figure 3.6).

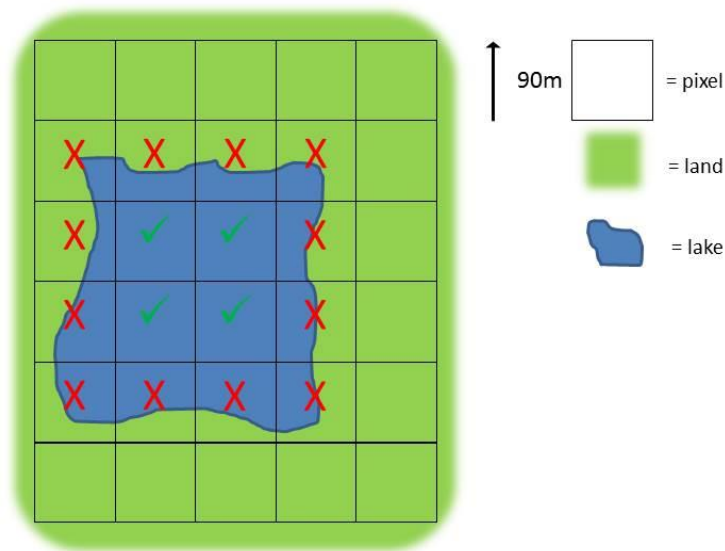


Figure 3.6 Schematic illustrating the selection of AST08 skin surface temperatures from pixels that have a high confidence (95%) of being purely from water. Mixed pixels from around the margins of the lake are not included in the analysis as they will be thermally contaminated by a temperature signal from the land within the pixel.

A total of 12 proglacial lakes in Arctic Sweden have an area greater than 129,600 m<sup>2</sup> (Chapter 2). Proglacial lake polygons from manual mapping (see Section 2.2 Methodology) of ASTER L1B were used to define proglacial lake area and crucially the pixel orientation is the same (i.e. not north to south) as the AST08 product, so errors from misalignment are minimised. Although it should be noted that geo-referencing 90 m thermal pixels is difficult due to having targets with suitably distinct thermal signatures at that spatial resolution, as effectively a square body of water (90 m) perfectly aligned with pixel orientation would be required. This potential source of error between locational mis-match of the visual and thermal imagery is accounted for in the methodology by only selecting central pixels that are 100% within the lake.

### **3.2.2 ASTER Surface Temperature Product (AST08) for Proglacial Lake Skin Surface Temperature ( $SST_L$ ) Analysis**

The skin surface temperatures of proglacial lakes ( $SST_L$ ) across Arctic Sweden were analysed through extracting pixel values from the ASTER surface temperature product (AST08 v2.9). A series of AST08 images were downloaded from the Earthdata website in geotiff format, with the NCEP NCAR reanalysis and MODTRAN radiative transfer model for atmospheric correction. The thermal imagery from Landsat was not used as it only has one single band in the thermal wavelength, which restricts the spectral signature of different surfaces and compromises the calculation of emissivity (Hook et al., 2004). In contrast the AST08 temperature product utilises the TES algorithm to analyse the spectral signature across the 5 thermal bands of ASTER imagery (discussed above in section 3.1.3).

In order to minimise potentially erroneous temperature readings due to problematic atmospheric correction, the AST08 temperature product was only downloaded for the proglacial lake analysis when corresponding optical images were cloud free. The AST08 product imagery that met these requirements was downloaded (3 scenes on each date) for 8/8/2014 and 29/7/2018. This minimises the chance of atmospheric correction affecting temperatures in the AST08 product, although presence of visibly undetectable clouds is possible (Gustafson et al., 2006). The AST05 emissivity product was downloaded for each scene and visually inspected over each proglacial lake that was analysed to assess the variability and suitability of pixel emissivity values for deriving lake surface temperature, which is discussed further below.

The skin surface temperatures (top 1 mm) were manually extracted from each AST08 pixel (excluding the margins) from each of these proglacial lakes, which will be referred to as the Skin Surface Temperature ( $SST_L$ ). Each pixel was indexed using an alpha-numeric system, to enable the spatial pattern of temperatures to be referenced and analysed in greater detail in future analysis (Figure 3.7). This spatial referencing system is particularly important for central lake pixels that may have some ice content from icebergs in the middle of the lake in some cases. These pixels were included in the analysis, as iceberg melting will have a cooling effect on  $SST_L$ , so whilst there is some thermal emission contamination from the iceberg it is still representative of  $SST_L$  at the time of image capture.

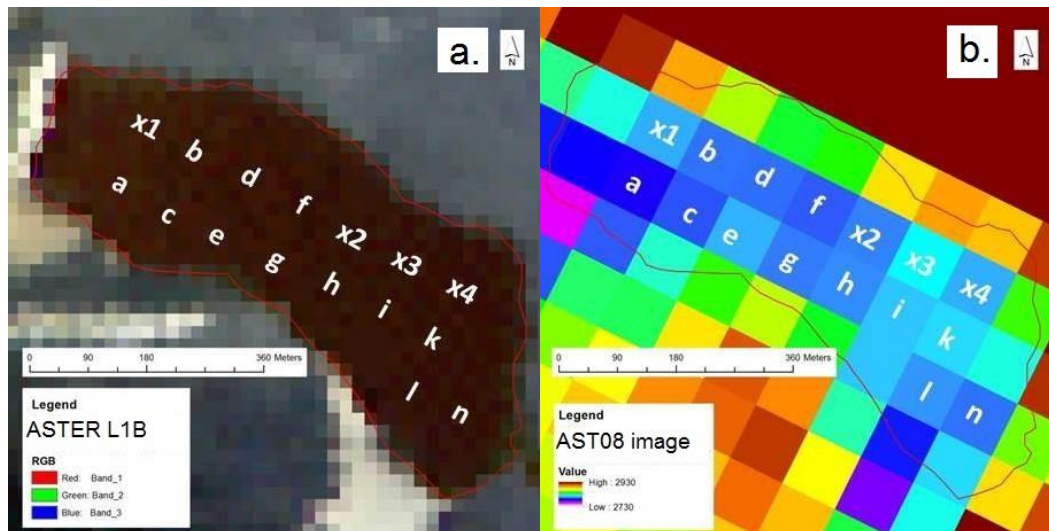


Figure 3.7 a. A composite (Green, Red and VNIR, 15 m resolution) ASTER image of proglacial lake 3, with alphanumeric numbering system for each 90 m pixel over layed across the lake. b. AST08 temperature product image for a proglacial lake (AST08<sub>ID</sub> 3) with alphanumeric referencing system for each pixel. Pixels with temperatures  $>290$  K ( $17^{\circ}\text{C}$ ) are in red and  $<273$  K ( $<0^{\circ}\text{C}$ ) are in white, with darker colours indicating colder temperatures.

The spatial referencing system also enables analysis of the contemporaneous AST05 emissivity product, which is produced in conjunction with the AST08 temperature product. Critically the AST05 product gives an indication as to whether a suitable emissivity has been used to characterise the surface of a 90 m pixel in order to calculate the skin surface temperature in the AST08 product (Sabol et al., 2009). The emissivity in each thermal band (10 to 14) is produced in the AST05 imagery, but only band 11 was analysed for simplicity as this band is least subject to atmospheric attenuation (Appendix A 6) (Sabol et al., 2009). The AST05 band 11 imagery was visually inspected and electronic striping across the scene was detected (Figure 3.8) (Gillespie et al., 2011). This appeared to produce some isolated pixels with lower (darker) emissivity values than surrounding surfaces in some areas (Appendix A 6). Consequently the AST05 emissivity imagery was subject to further analysis over proglacial lakes to assess the influence on the AST08 skin surface temperatures (Appendix A 6).

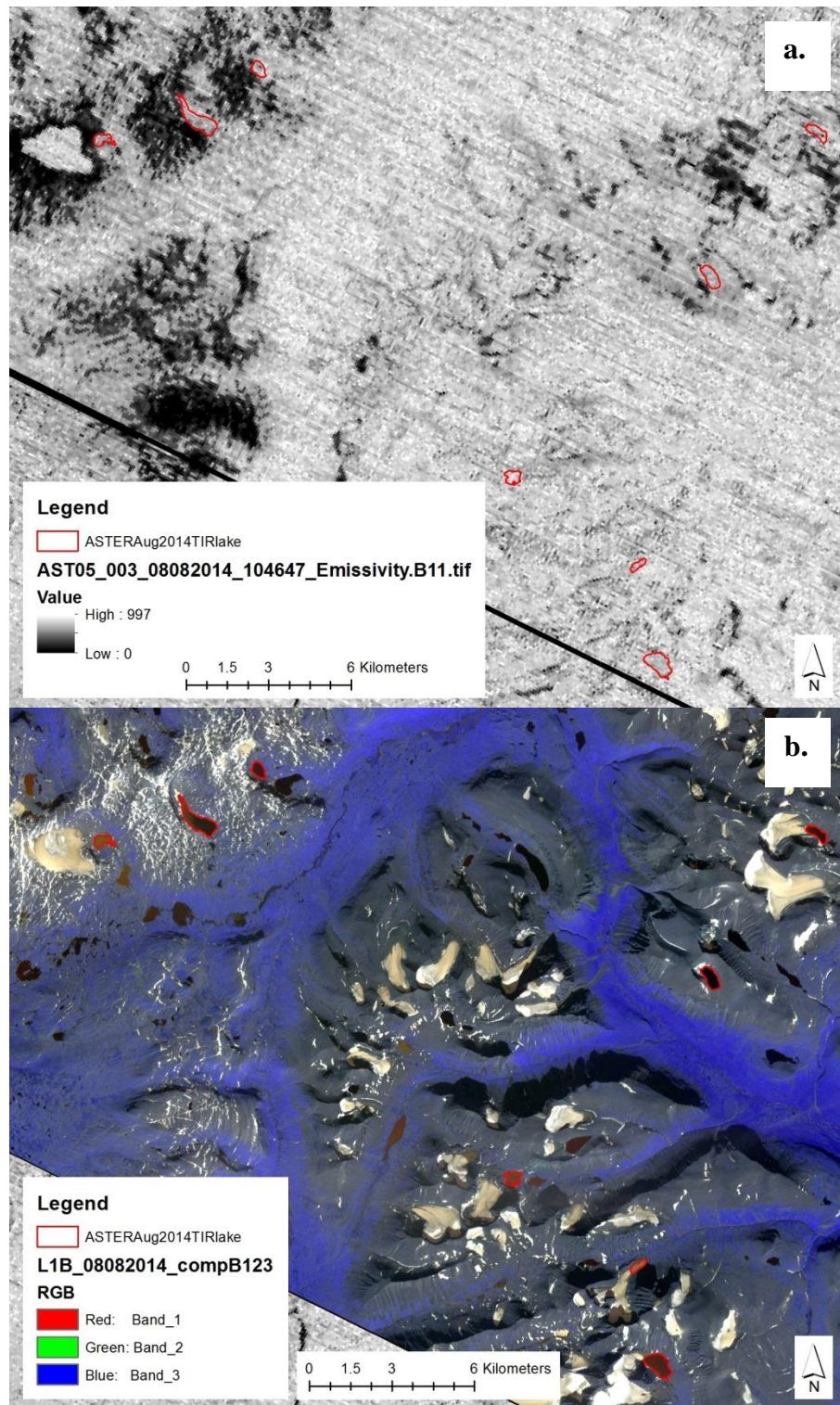


Figure 3.8 a. AST05 band 11 emissivity product image (8/8/2014) over Arctic Sweden, with outlines of proglacial lakes included in the thermal infrared (TIR) AST08 temperature analysis in red. Note the presence of electronic striping across the image orientated NW to SE, with darker pixels indicating lower emissivity values. b. A composite (Green, Red and VNIR, 15 m resolution) image of the same scene (8/8/2014) over Arctic Sweden, with outlines of proglacial lakes included in the thermal infrared (TIR) AST08 temperature analysis in red.

The emissivity values for band 11 were extracted from the AST05 product in order to assess the variability in emissivity over proglacial lakes. In theory the emissivity over water bodies should be relatively uniform and laboratory analysis values are between 0.97 to 0.98 (Sabol et al., 2009). However, it is important to consider that proglacial lakes tend to have substantial suspended sediment concentrations (SSC) associated with the input of turbid glacial meltwater (Warren and Kirkbride, 1998; Chikita et al., 1999). Consequently it seems reasonable to propose that the suspension of rock material within water will affect the thermal dynamics and consequently the emissivity of the water body (Chikita et al., 1999; Becker and Daw, 2005). Furthermore, given that the emissivity of rocks are generally lower ( $<0.9$ ) than those for water (0.97 to 0.98) (Sabol et al., 2009), it seems reasonable to propose that suspension of rock material may lower the emissivity of a water body. Although this remains an open research question and requires further validation.

### 3.3 Validation of AST08 SST against Lake Near Surface Temperatures

The AST08 temperature product has had limited validation over maritime areas (Gillespie et al., 2011). This study provides some of the first data to validate the AST08 product (particularly the atmospheric correction) for over Patagonia (see below) and Arctic Scandinavia. In situ thermistor data at 75 cm depth from buoy moorings in the central part of Kilpisjarvi (Arctic Sweden) was kindly provided by G. Kirillin for 2014 and 2017.



Figure 3.9 Satellite image (courtesy of Google Earth) over Arctic Scandinavia. The location of Tarfala Research Station has been marked, where automatic weather station data air surface temperature have been sourced. The location of Kilpisjarvi lake is also marked, where lake water temperatures were provided for 2014 and 2017 by G. Kirillin.

An extensive search of ASTER imagery over Kilpisjarvi was conducted for 2014 and 2017 in order to select and download suitable imagery with cloud free areas over the location of the buoy mooring and temperature sensor (Figure 3.9 and Table 3.1). A series of AST08 images were downloaded for 7/7/2014 (10:46am), 11/7/2014 (10:22am), 27/7/2014 (10:21am), 13/6/2017 (10:46am), 29/6/2017 (10:46am) and 4/8/2017 (10:22am). Some of these images contained clouds within the scene, but areas around the sensor location were deemed to be substantially cloud free from visual inspection. These images with clouds within the scene were included within the analysis to strengthen the validation of the AST08 product for less than nominal conditions, as localised varying humidity may not be captured by the atmospheric correction (Tonooka, 2005). The presence of undetected high cirrus clouds may also be a source of uncertainty (Gillespie et al., 2011).

The AST05 emissivity product was also downloaded and visually inspected to detect potential sources of error from poor characterisation of emissivity values over water (Sabol et al., 2009). Some isolated low (~0.90) emissivity values were detected over Kilpisjarvi, which appeared to be associated with electronic striping (Gillespie et al., 2011). However, these pixels were not in close proximity to the buoy temperature measurements and are therefore not included within the validation data.

Contemporaneous temperatures were extracted from the AST08 90 m pixel and plotted against the thermistor temperature (logging every minute) (Table 3.1 and Figure 3.10). Note that the relative proximity of Kilpisjarvi to the focus area of this study (~115 km) and data points from the same year (2014) adds strength to the validation of AST08 for this study with it being from the same climatic area and similar time period. Although it should be noted that Kilpisjarvi is not a proglacial lake as defined by this study, as it is not within the margins of a Holocene glacier extent (Figure 3.9). Furthermore, the ASTER overpass time is virtually identical for Kilpisjarvi (between 10:21am to 10:46am) as it is for the study area (10:29am to 10:46am), so the imagery is captured at the same time of the diurnal heating cycle in all images. Although preceding meteorological conditions may of course be different.

In-situ lake near surface temperature data was also kindly provided by M. Minowa and others from proglacial lake Brazo Rico in Patagonia for 2011 and 2012. An extensive search of ASTER imagery over Brazo Rico was conducted for 2011 and 2012 in order to select and download suitable imagery with cloud free areas over the location of the sensor. Only 1 image from 31/5/2011 and an image from 31/5/2012 were found to be sufficiently cloud free

for analysis. The sensor was positioned on a metal pipe in a marginal area of the lake, which may be subject to some thermal emission contamination in the AST08 pixel.

### 3.4 Results

#### 3.4.1 Validation of AST08 Skin Surface Temperatures Against Lake Near Surface Temperatures

A series of 8 AST08 surface temperature product images (between 2011 and 2017) were analysed and pixel values were extracted from the AST08 90 m pixel corresponding to the position of a thermistor with available temperature data. The AST08 pixel values were converted to Celsius and plotted against the contemporaneous thermistor temperature (logging every minute), the details of which are given in the table below (Table 1.1).

Kilpisjarvi		69.033408°N	20.77333°E	0.75m depth		
Date	AST08 time	AST08 Temp K	AST08 Temp C	Sensor Temp C	Sensor time	
07/07/2014	10:46	283.7	10.55	7.41	10:46	
11/07/2014	10:22	285.7	12.55	9.88	10:22	
27/07/2014	10:21	291.7	18.55	15.98	10:21	

Kilpisjarvi		69.02637274°N	20.8027558°E	1m depth		
Date	AST08 time	AST08 Temp K	AST08 Temp C	Sensor Temp C	Sensor time	
13/06/2017	10:46	271.5	-1.65	1.75	10:46	
29/06/2017	10:46	277.8	4.65	3.20	10:46	
04/08/2017	10:22	287.0	13.85	10.39	10:22	

Brazo Rico		50.453°S	73.023°W	<2m depth		
Date	AST08 time	AST08 Temp K	AST08 Temp C	Sensor Temp C	Sensor time	
31/05/2011	3:57	276.7	3.55	3.55	4:00	
31/05/2012	4:09	279.8	6.65	6.58	4:00	

Table 3.1 Data points compiled for this survey for validation of the AST08 temperature product. Data measured in Kilpisjarvi lake (Sweden) is from G. Kirrilin from an RBR Duo thermistor (accuracy +/- 0.002°C) temperatures (every minute) less than 1 m deep on an in-situ buoy mooring. Data Brazo Rico arm of Lago Argentino, Argentina are from Onset HOBO U20 sensor (accuracy +/- 0.5°C) mounted on a metal pole at <2 m depth kindly provided by M. Minowa and P. Skvarca.

The strong correlation (linear regression  $R^2 = 0.9365$ ) between temperatures from AST08 and those measured by thermistors <2 m deep, provides a relatively strong validation of the AST08 temperature product for the 8 data points (Figure 3.10). The strong linear relationship also suggests a strong relationship between skin surface (top 1 mm) temperature (as measured by AST08) and near surface temperature of water from in-situ thermistors (Donlon et al., 2012). Although there is a difference of up to ~3°C between the AST08 temperatures and the thermistor temperatures. It should be noted that the data point with a sensor temperature of

1.75°C and AST08 temperature of -1.65°C was due to the sensor being under ice cover. The data suggests relationship is particularly strong between 0 to 15°C and Sabol et al. (2009) also found that AST08 performs well over water up to 17°C. Although the data point with in situ temperature of 15.98°C and AST08 temperature of 18.55°C is within the stated accuracy of the AST08 temperature product ( $\pm 1.5^\circ\text{C}$ ). The limited amount of data collated by this study and the overlap between error bars from stated accuracy of sensors and the AST08 temperature product would suggest that the stated accuracy of  $\pm 1.5^\circ\text{C}$  appears to be realistic on the times and dates of image capture analysed in this study. Further data from in situ measurements at the time of ASTER overpass would further strengthen the validation of the AST08 temperature product in maritime areas, particularly if thermal infrared imagery was utilised to capture the surface temperature pattern of lake skin surface temperatures.

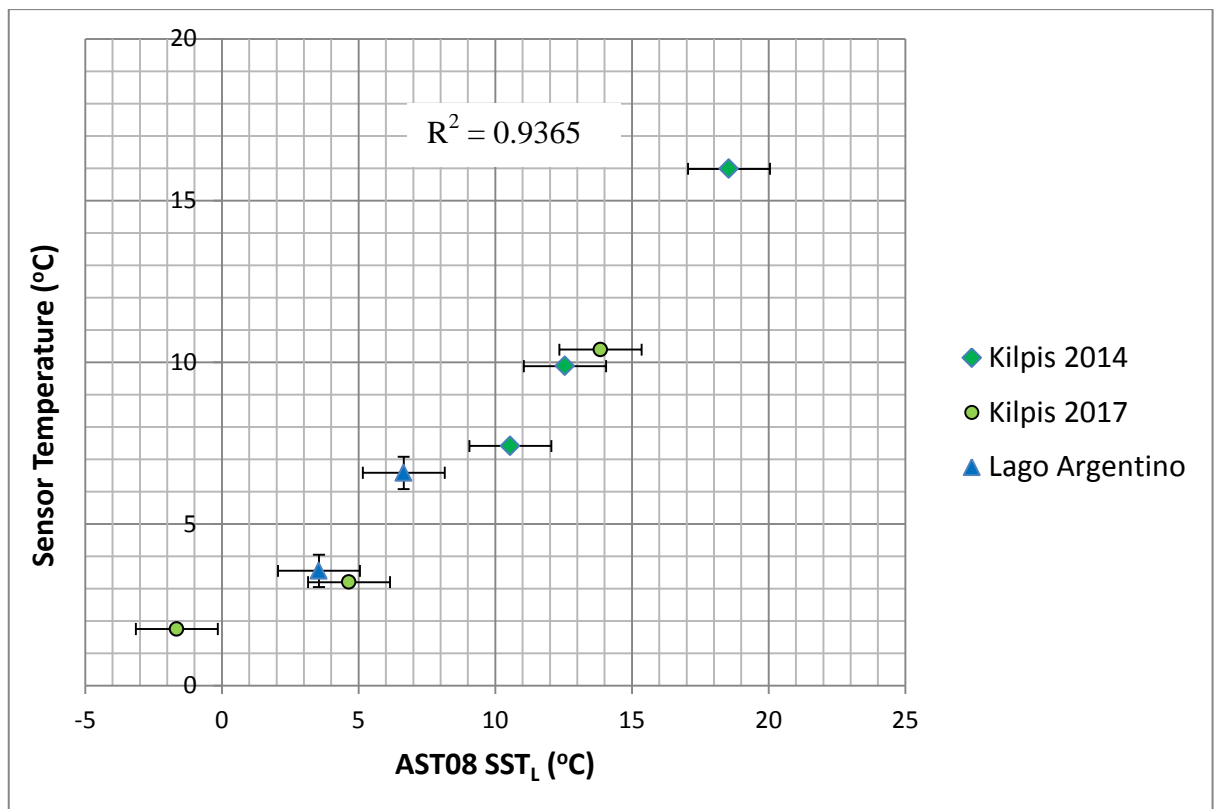


Figure 3.10 Validation of AST08 skin surface temperatures ( $\pm 1.5^\circ\text{C}$  shown as error bars) plotted against contemporaneous near surface ( $<2\text{ m}$  depth) in situ lake water temperatures. The full dataset linear regression value is  $R^2 = 0.9365$ . Green data points from an RBR Duo thermistor (accuracy  $\pm 0.002^\circ\text{C}$ ) temperatures (every minute) from in situ buoys in Kilpisjarvi lake, Sweden (from G. Kirrilin). Blue data points are from Onset HOBO U20 sensor (accuracy  $\pm 0.5^\circ\text{C}$ ) mounted on a metal pole at  $<2\text{ m}$  depth in Brazo Rico arm of Lago Argentino, Argentina (from M. Minowa).

### 3.4.2 Surface Air Temperatures from Tarfala AWS (1996 to 2018)

The available average hourly air temperature (2 m) at Tarfala Research station was downloaded and plotted in Excel for between 1996 and 2018 (Figure 3.11). The periods when the average hourly air temperature at Tarfala exceeded 20°C are circled in red (Figure 3.11), which occurred in 2003, a short event in 2007 and longer periods of warm temperatures during July 2014 and July 2018. The average hourly air temperature at Tarfala for July 2014 was 12.4°C (Figure 3.11), which is 5.4°C above the long term (1965-1994) average air temperature for July (7.0°C) (Jonsell et al., 2013). The AST08 imagery analysed in this study was taken at 10:46am on 8/8/2014, when the average hourly air temperature at Tarfala was 13.9°C at 10:00am (Figure 3.11). There is no precise definition of ‘heatwaves’ but the period of warm temperatures in 2003, 2014 and 2018 have been described as ‘heatwaves’, which provides some climatological context for this study (Kim et al., 2018). Also note that the summer of 2017 was substantially cooler, which was ‘confirmed’ by fieldwork undertaken during the summer of 2017 (Chapter 4).

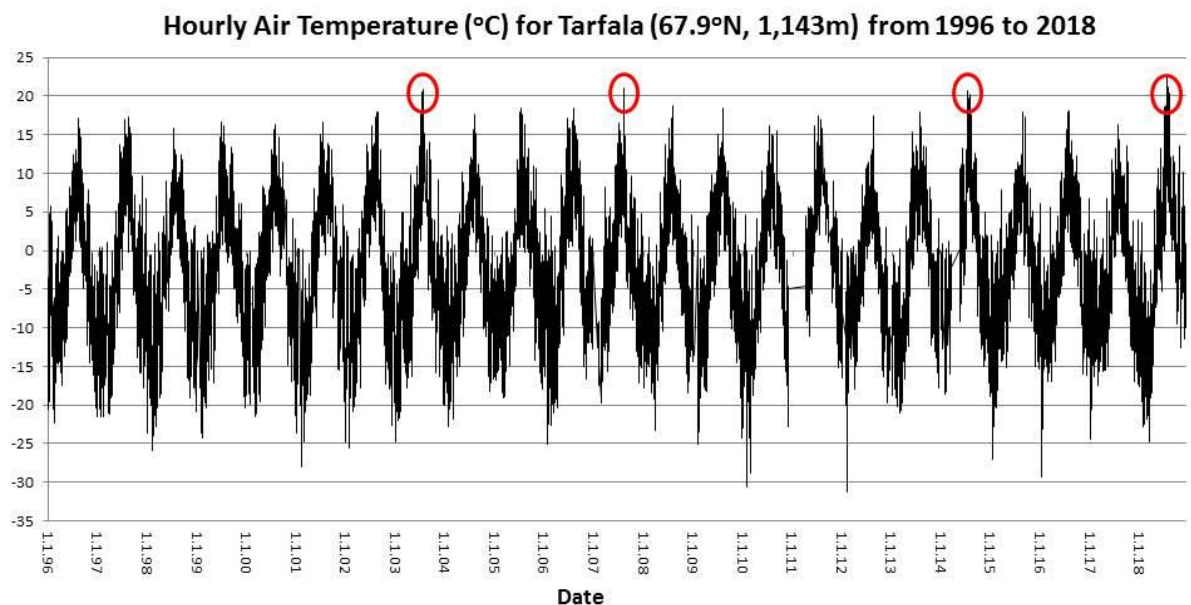


Figure 3.11 Hourly average air temperatures (°C) measured at 2 m at Tarfala research centre (67.9°N, 1,143 m) from an automated weather station (SMHI) for 1996 to 2018. Periods when air temperatures exceeded 20°C are highlighted by red circles.

### 3.4.3 Skin Surface Temperatures (SST<sub>L</sub>) for Proglacial Lakes in Arctic Sweden from AST08 Temperature Product in 2014

Temperatures were extracted from the AST08 product from 8/8/2014 for a total of 205 pixels over 12 proglacial lakes in Arctic Sweden. The average proglacial lake skin surface

temperature ( $SST_{LAV}$ ) for all 12 lakes was  $8.9^{\circ}C$ , with a median ( $SST_{LMED}$ ) of  $9.1^{\circ}C$  and a standard deviation ( $SST_{LSDEV}$ ) of  $2.0^{\circ}C$ . The table below summarises the geometry and characteristics from the Proglacial lake inventory from Chapter 2 ( $PGL_{ID}$ ), with summary statistics of the parent glacier from the Randolph Glacier Inventory (RGI) (Arendt et al., 2015) and the ID used in AST08 analysis ( $AST08_{ID}$  Figure 3.1) with  $SST_{LAV}$  and  $SST_{LSDEV}$  for each proglacial lake. The  $AST08_{ID}$  will hereafter be used as the reference ID for each proglacial lake in Chapter 3. The  $PGL_{ID}$  refers to the identification number in the Proglacial Lake Inventory as presented in Chapter 2.

PGL ID	PGL Area (m <sup>2</sup> )	Elev. (m)	Ice Cont	Glacier Area (m <sup>2</sup> )	Slope	Aspect	AST08 ID	SST <sub>LAV</sub> (C)	SST <sub>LMED</sub> (C)	SST <sub>LDIFF</sub> (C)	SST <sub>LSDEV</sub> (C)
1	157516	1267	1	265647	14.5	103	1	9.5	9.5	0.9	0.30
6	163140	1144	0	227518	23.6	92	2	11.5	11.5	0.6	0.19
14	242736	1318	1	1486665	15.5	74	3	8.3	8.3	3.0	0.67
16	346719	1382	1	105949	41.9	103	4	10.5	10.5	1.2	0.38
23	230764	1243	0	1608398	18.7	20	5	7.2	7.1	4.0	1.06
24	132172	1124	1	1533959	25.7	26	6	6.2	5.1	3.7	1.54
27	560589	1194	0	670186	22.2	73	7	8.1	7.9	4.7	1.03
39	211513	1123	0	552809	17	104	8	11.0	10.8	3.7	0.91
41	686233	1169	0	71160	16.4	110	9	9.7	9.6	4.6	1.13
42	220826	1090	0	2301468	11.3	79	10	10.6	10.7	2.8	0.84
53	149143	1227	1	398244	21.1	77	11	6.2	5.5	3.2	1.23
81	175832	1441	1	1755474	14.5	33	12	3.2	3.0	2.8	0.89

Table 3.2 Summary table of the 12 largest proglacial lakes from the inventory ( $PGL$  Chapter 2), with associated  $PGL_{ID}$  and geometry/characteristics from the ASTER 8/8/2014 manual mapping. Central columns contain geometry/characteristics of parent glaciers from the Randolph Glacier Inventory (2008). Right hand columns contain the AST08 ID (as used in Fig 1) and the  $SST_{LAV}$  ( $^{\circ}C$ ) and  $SST_{LDEV}$  ( $^{\circ}C$ ) for each lake. Elev.=elevation. Ice Cont.=Ice contact (1=yes)

The proglacial lake elevation and  $SST_L$  was investigated, as it is reasonable to assume that air temperature decreases with elevation due to the atmospheric lapse rate (Stone et al., 1979). There was no correlation between proglacial skin surface temperatures ( $SST_L$ ) and elevation ( $R^2 = 0.1254$ ) at 10:46am on 8/8/2014 (Table 1.2). The 12 largest proglacial lakes that were analysed from the AST08 product had parent glaciers with aspects between  $20^{\circ}$  and  $110^{\circ}$  (RGI, Arendt et al., 2015). These aspects were used to investigate the relationship with  $SST_{LAV}$  for the 12 lakes (Figure 3.12). There was a moderate positive correlation of  $R^2=0.5932$  between  $SST_{LAV}$  and parent glacier aspect (Figure 3.12). The temperatures described above were extracted from ice contact proglacial lakes and non-ice contact proglacial lakes.

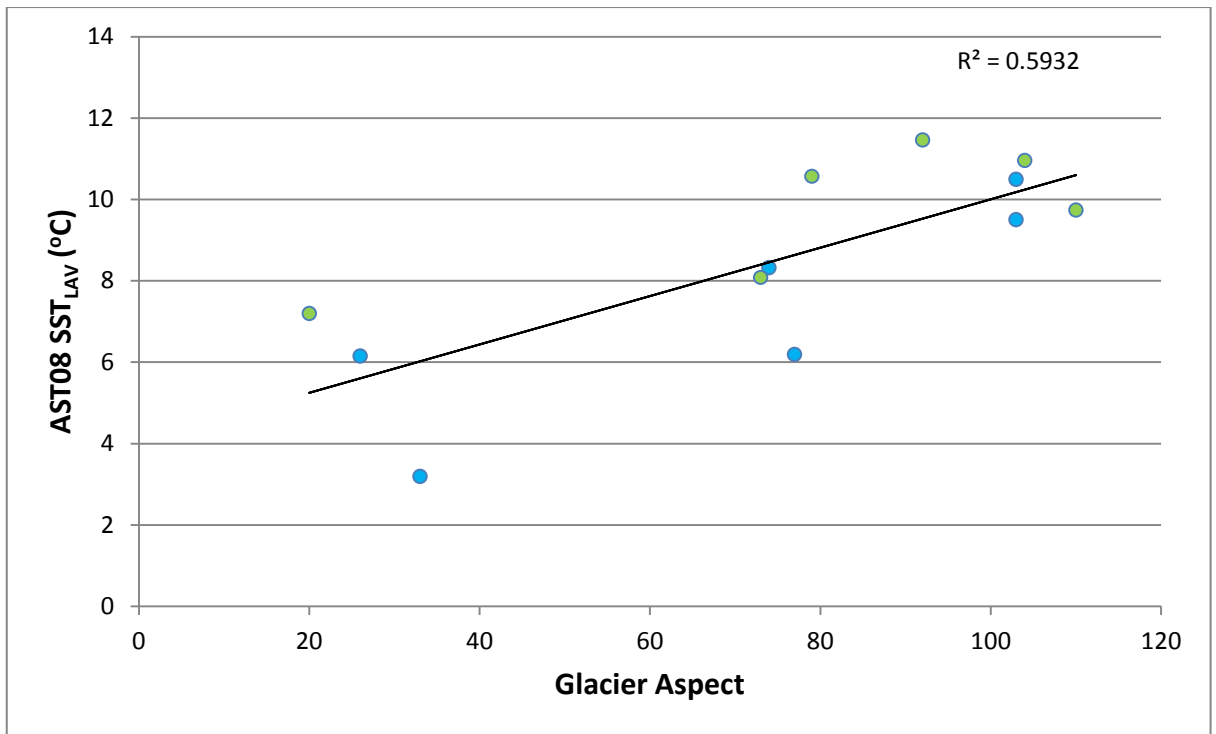


Figure 3.12 Plot of average skin surface temperature ( $SST_{LAV}$ ) for each proglacial lake from AST08 analysis (8/8/2014) against aspect of parent glacier (RGI) (Arendt et al., 2015). Blue data point = Ice-contact proglacial lake. Green data point = non-ice contact proglacial lake.

#### 3.4.4 Skin Surface Temperature ( $SST_L$ ) for Ice-Contact and Non-Ice Contact Proglacial Lakes in Arctic Sweden

The results of AST08 skin surface temperatures ( $SST_L$ ) extracted from all 205 pixels analysed in this study are presented below (Figure 3.13). The results of  $SST_L$  are presented initially as whole dataset to give an overview of  $SST_L$  from all proglacial lakes (Figure 3.13), before being separated into ice-contact and non-ice contact classifications and then further analysis of each individual proglacial lake. There were 6 ice contact proglacial lakes (AST08<sub>ID</sub> lakes 1, 3, 4, 6, 11, 12) and 6 non-ice contact proglacial lakes (AST08<sub>ID</sub> lakes 2, 5, 7, 8, 9, 10) with an area greater than 129,600 m<sup>2</sup> (Table 1.2). The AST08<sub>ID</sub> will be used in reference for each proglacial lake for analysis and discussion of the AST08 skin surface temperature results. The analysis of the spatial pattern across each proglacial lake is qualitative and therefore case studies of selected lakes are included in the discussion, due to the interpretive nature of the analysis.

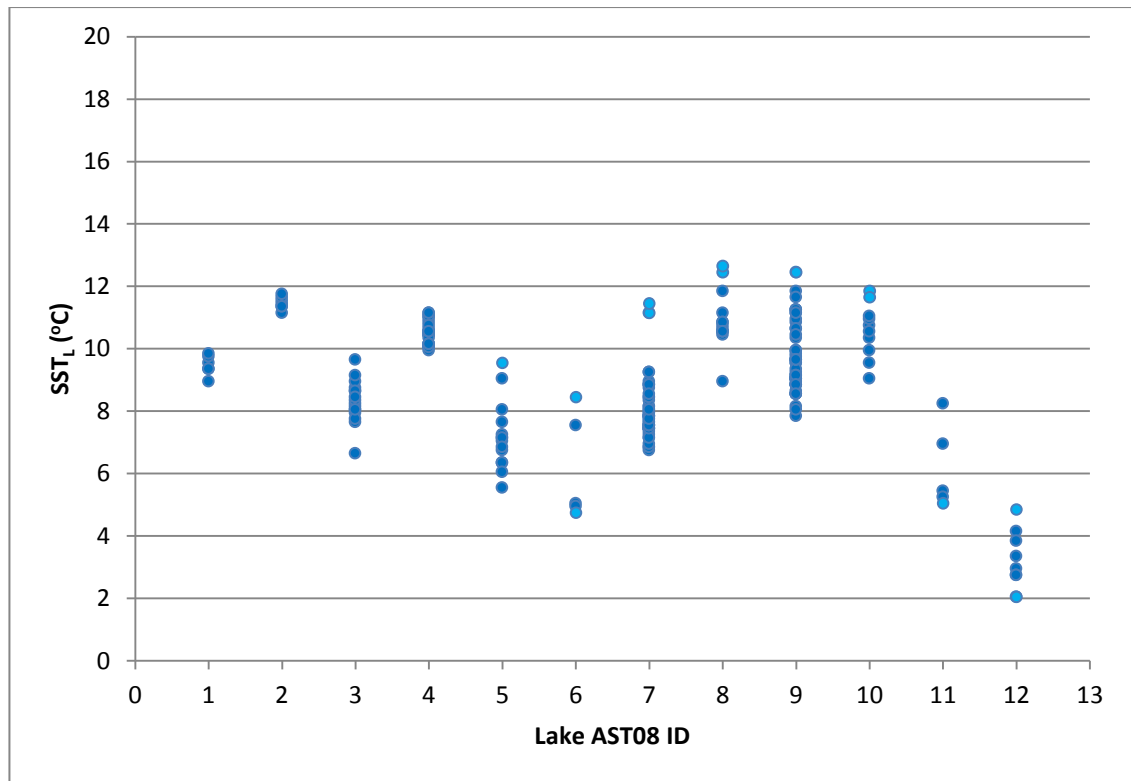


Figure 3.13 Pixel skin surface temperatures extracted from AST08 temperature product image from 10:16am on 8/8/2014. Pixels that are 100% water are shown by dark blue circles. Pixels <95% confidence of temperature are highlighted in light blue. This is due to emissivity data or where there is a risk of thermal-emission contamination from land or glacier. AST08<sub>ID</sub> lakes 1, 3, 4, 6, 11, 12 were classed as ice contact and AST08<sub>ID</sub> lakes 2, 5, 7, 8, 9, 10 were non-ice contact proglacial lakes.

A Mann Whitney U test was performed to test whether there was a significant difference in temperature between ice-contact proglacial lakes and non-ice contact. Due to the relatively large number of observations ( $n_1=65$  and  $n_2=140$ ) the critical U value ( $U_{crit}$ ) was calculated, with  $z = 1.96$  for a two tailed test at the 0.05 significance. The calculated  $U_{crit}$  for the SST<sub>L</sub> dataset was 3774.82. As the smallest U value ( $U_{stat}=3839$ ) was larger than  $U_{crit}$  the null hypothesis ( $H_0$ ), that there was no significant difference between the two datasets, is accepted. Therefore there was no significant difference in SST<sub>L</sub> between ice contact and non-ice contact proglacial lakes in Arctic Sweden on 8<sup>th</sup> August 2014. However, there are notable differences in temperature distribution between each proglacial lake, although there are also some similarities between lakes too (Figure 3.13). The results of temperature distribution for each lake are presented below (Figure 3.14).

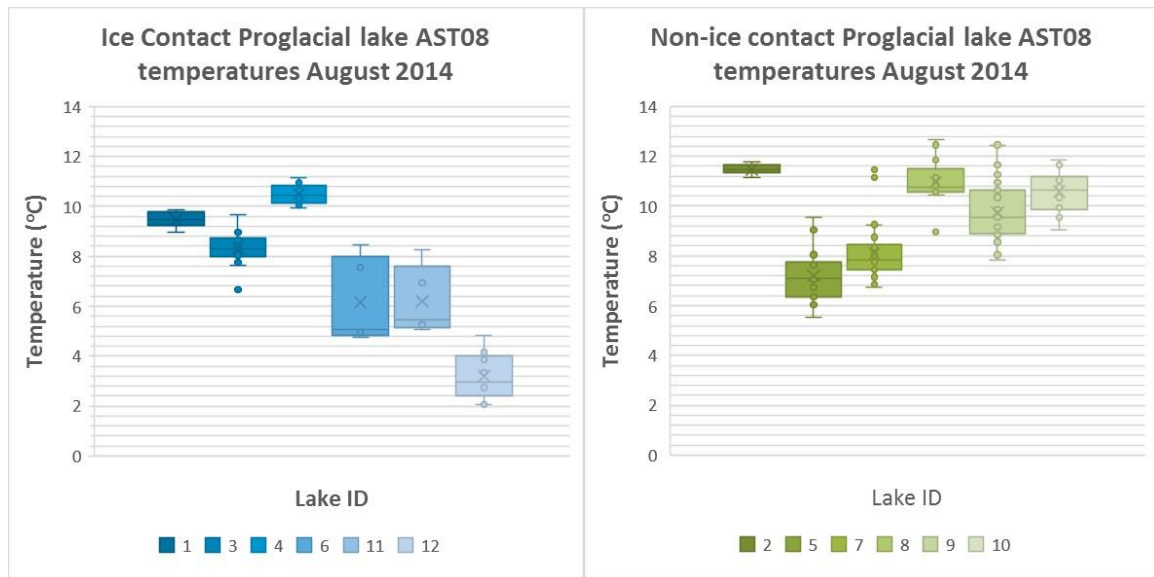


Figure 3.14 Box and whisker plot of lake surface water temperatures extracted from AST08 temperature product pixels over Arctic Sweden on 8/8/2014 at 10:46am. Whiskers extend to points within 1.5 times the interquartile range (IQR) from the upper and lower quartile. Points 1.5 times the IQR from the upper and lower quartile are plotted as outliers. With x = mean and central line = median. Lake ID = AST08 ID.

### 3.4.5 Skin Surface Temperature ( $SST_L$ ) for Ice Contact Proglacial Lakes

There were 6 ice contact proglacial lakes with an area greater than 129,600 m<sup>2</sup> from which temperatures were extracted from a total of 65 pixels (Figure 3.1, Table 1.2). The  $SST_{LAV}$  from ice contact proglacial lakes was 8.2°C, with  $SST_{LMED}$  of 8.9°C and  $SST_{LSDEV}$  of 2.6°C. There was no correlation between ice-contact proglacial lake  $SST_{LAV}$  and lake elevation ( $R^2 = 0.0012$ ) at 10:46am on 8/8/2014 (Table 1.2).

The coldest proglacial lake was lake 12, with  $SST_{LAV}$  of 3.2°C and  $SST_{LMED}$  of 3.0°C and low variation in temperature across the lake as indicated by the low  $SST_{LSDEV}$  of 0.89°C (Figure 3.14). The next coldest lakes were lake 6 and lake 11, both of which had a  $SST_{LAV}$  of 6.2°C, although lake 11 had a higher  $SST_{LMED}$  of 5.5°C compared to 5.1°C for lake 12 (Figure 3.14). Lake 6 had the highest  $SST_{LSDEV}$  of 1.54°C of any proglacial lake and had greater range ( $SST_{LDIFF}$  of 3.7°C) than lake 11 ( $SST_{LDIFF} = 3.2^\circ\text{C}$  and  $SST_{LSDEV} = 1.23^\circ\text{C}$ ) (Figure 3.14). Note that lake 6 (132,172 m<sup>2</sup>) and 11 (149,143 m<sup>2</sup>) are of a similar area. Lake 3 had a comparable range ( $SST_{LDIFF} = 3.0^\circ\text{C}$ ) to lakes 12, 11 and 6, but had a higher  $SST_{LAV}$  of 8.3°C (Figure 3.14). Lake 1 had the smallest  $SST_{LSDEV}$  (0.30°C) and  $SST_{LDIFF}$  (0.9°C) of any ice-contact proglacial lake and had the second highest  $SST_{LAV}$  of 9.5°C (Figure 3.14). The highest  $SST_{LAV}$  for any ice contact proglacial lake was 10.5°C for lake 4, which also had a low  $SST_{LDEV}$  of 0.38°C and low  $SST_{LDIFF}$  of 1.2°C (Figure 3.14).

### 3.4.6 Skin Surface Temperature (SST<sub>L</sub>) for Non-Ice Contact Proglacial Lakes

There were 6 non-ice contact proglacial lakes with an area greater than 129,600 m<sup>2</sup> from which temperatures were extracted from a total of 140 pixels (Figure 3.13). The SST<sub>LAV</sub> for non-ice contact proglacial lakes was 9.2°C, with SST<sub>LMED</sub> of 9.1°C and SST<sub>LSDEV</sub> of 1.6°C. For the 6 non-ice contact proglacial lakes SST<sub>LMAX</sub> was 12.7°C, with SST<sub>LMED</sub> of 5.6°C and a range (SST<sub>LDIFF</sub>) of 7.1°C. There was a negative correlation between non-ice-contact proglacial lake (SST<sub>LAV</sub>) and lake elevation ( $R^2 = 0.7545$ ) at 10:46am on 8/8/2014 (Table 1.2).

The lowest SST<sub>LAV</sub> and SST<sub>LMED</sub> for a non-ice contact proglacial lake was 7.2°C and 7.1°C for lake 5, which also had a large range in temperature (SST<sub>LDIFF</sub> = 4.0°C) (Figure 3.14). The next coldest non-ice contact proglacial lake was lake 7 with SST<sub>LAV</sub> of 8.1°C and SST<sub>LMED</sub> of 7.9, which had the largest range of any proglacial lake (SST<sub>LDIFF</sub> = 4.7°C) (Figure 3.14). Lake 9 had the next highest SST<sub>LAV</sub> of 9.7°C and had the second largest range in temperatures (SST<sub>LDIFF</sub> = 4.6°C) (Figure 3.14), with the largest proglacial lake area (686,233 m<sup>2</sup>) of any lake analysed in this study. Lake 8 had the maximum SST<sub>L</sub> (12.7°C) of any proglacial lake analysed in this study and a relatively large range with SST<sub>LDIFF</sub> of 3.7°C (Figure 3.14). In contrast, lake 2 had the smallest temperature variation (SST<sub>LDIFF</sub> = 0.6 and SST<sub>LSDEV</sub> = 0.19) and highest SST<sub>LAV</sub> (11.5°C) of any proglacial lake analysed in this study (Figure 3.14).

## 3.5 Discussion

The analysis of AST08 satellite surface temperature product from 8<sup>th</sup> August 2014 (10:46am) (Figure 3.13 and Figure 3.14) shows that skin surface temperatures (SST<sub>L</sub>) of 12 proglacial lakes in Arctic Sweden were widely above 1°C. The moderate resolution (90 m pixels) of the AST08 satellite thermal imagery constrained analysis to lakes greater than 129,600 m<sup>2</sup> to minimise thermal-emission contamination from surrounding land. Consequently smaller proglacial lakes (<129,600 m<sup>2</sup>) have not been included in the satellite based thermal analysis, which means that proglacial lakes in the earlier stages of evolution (following glacial retreat) have not been included in this analysis. Theoretically it seems likely that proglacial lakes emerging in the early stage of deglaciation are likely to be colder (Boyce et al., 2007; Trüssel et al., 2013). This is due to a greater proportion of the lake being dominated by the cooling influences of a relatively larger ice-contact area and influx of glacial meltwater (Boyce et al., 2007).

The 12 proglacial lakes analysed in this study are located in a similar macro-climatic region around the Kebnekaise area of Arctic Sweden (although lake 12 is in the Sarek region) (Figure 3.1). These 12 proglacial lakes are situated in a range of topographic settings across the area and represent different stages of deglaciation. These results are the first satellite derived temperatures to be reported from proglacial lakes in the Arctic. The proglacial lake average skin surface temperature ( $SST_{LAV}$ ) of  $8.9^{\circ}\text{C}$  in Arctic Sweden on 8/8/2014 is substantially higher than the  $1^{\circ}\text{C}$  commonly assumed for proglacial lakes (Chernos et al., 2016; Truffer and Motyka, 2016). The warm proglacial lake temperatures presented in this study are comparable to the maximum temperatures reported from ice-contact proglacial lakes by Roehl (2006) of  $10^{\circ}\text{C}$  in New Zealand, Watson et al (2020) of  $10^{\circ}\text{C}$  in Nepal and Minowa et al., (2017) of  $8^{\circ}\text{C}$  in Patagonia. The study of Peter and Sommaruga (2017) reported maximum temperatures of  $16^{\circ}\text{C}$  from non-ice contact proglacial lakes in the Austrian Alps. These substantially higher temperatures have substantial implications where glaciers are in contact with lakes due to thermal erosion undercutting glacier fronts and enhancing calving rates (Kirkbride, 1993; Roehl et al., 2006; Minowna et al., 2017). These warmer temperatures will also influence downstream temperatures and geochemistry, with ecological consequences, particularly for temperature sensitive species such as invertebrates (Fellman et al., 2014). The high standard deviation ( $2.0^{\circ}\text{C}$ ) and large range in proglacial lake skin surface temperatures ( $SST_L$ ) suggests there is clearly a high level of complexity for such temperatures relating to micro-climate and relationship with parent glacier (Peter and Sommaruga, 2017).

The air temperatures of July 2014 were substantially ( $5.4^{\circ}\text{C}$ ) above the long term (1965-1994) monthly average mean air temperature for July ( $7.0^{\circ}\text{C}$ ) (Jonsell et al., 2013). This difference in monthly mean air temperature gives some climatological context of the meteorological conditions preceding AST08 proglacial lake temperature results from 8/8/2014. The lack of a correlation between proglacial lake skin surface temperatures ( $SST_L$ ) and elevation, would tentatively suggest that there is also minimal correlation with proglacial lake  $SST_L$  and air temperature (if one assumes it decreases with height) at the time of image capture (10:46am), particularly for ice-contact proglacial lakes ( Stone et al., 1979). This complexity would suggest that proglacial lake  $SST_L$  at the time of image capture are more closely controlled by factors independent to each proglacial lake situation, such as proximity and coupling with neighbouring glacier and topo-climatic factors (e.g. shading from incoming solar radiation) (Richards et al., 2012; O'Reilly et al., 2015; Peter and Sommaruga,

2017). Particularly as there was a moderate positive correlation of  $R^2=0.5932$  between  $SST_{LAV}$  and parent glacier aspect (Figure 3.12).

The imagery from 8<sup>th</sup> August 2014 (10:16am) is free of visibly detectable clouds and typical of weather conditions dominated by the Scandinavian high pressure system (Sinclair et al., 2018). These clear sky conditions under a high pressure system mean that atmospheric water vapour is lower and more stable over longer time periods (> 6 hours) (Sinclair et al., 2018). Furthermore, meteorological conditions will also be more uniform across large (kilometres) areas (Kim et al., 2018). So atmospheric correction of satellite based thermal imagery products is more reliable (Gillespie et al., 2011), as atmospheric conditions persist longer than the 6 hour window of the NCEP atmospheric reanalysis product and are more uniform spatially (Gustafson et al., 2006). Therefore retrieval of  $SST_L$  is less likely to be affected by atmospheric longwave radiation transmission or emission uncertainty, due to passing clouds or increases in moisture associated with synoptic weather fronts (Sabol ety al., 2009; Aubry-Wake et al., 2015). The dominance of relatively cloud free conditions not only means that long wave radiation emitted by lakes is subject to less atmospheric attenuation, but also that lakes absorb more incoming short wave solar radiation (particularly in areas with 24 hour daylight) (Becker and Daw, 2005; O'Reilly et al., 2015). Therefore proglacial lakes with easterly aspects are likely to have higher  $SST_L$  during the morning, as they are more exposed to incoming solar radiation in the earlier part of the day that will raise temperatures quicker following the night time cooling period (see Chapter 4) (Becker and Daw, 2005; O'Reilly et al., 2015). In contrast, proglacial lakes with more northerly and westerly aspects will be subject to less incoming short wave solar radiation during the early part of the day, particularly where topography also creates substantial shading (O'Reilly et al., 2015). Therefore proglacial lakes with a NW aspect and substantial shading are likely to have lower skin surface temperatures ( $SST_L$ ) during the morning.

The influx of glacial meltwater will also lead to cooling of proglacial lakes water temperatures (Richards et al., 2012; Peter and Sommaruga, 2017). Where this cold meltwater sits in the water column will likely depend on the suspended sediment concentration (SSC), as water with high SSC content (turbid) can have a higher density than water with lower SSC at temperature density maximum ( $3.98^{\circ}C$ ) (Warren and Kirkbride, 1998; Chikita et al., 1999). Therefore the turbid glacial meltwater is likely to have a high density and sit lower down the water column, so it may not be distinctly visible as a body of water (i.e. cold pool) in lake  $SST_Ls$  (Chikita et al., 1999; Peter and Sommaruga, 2017). However, the input of turbid

glacial meltwater may have an overall cooling influence on lake water temperatures, which results in lower  $SST_L$  (Richards et al., 2012; Peter and Sommaruga, 2017). In contrast, where meltwater with low SSC has been inputted this may be present in the surface layers of the lake if it overlies denser water (either at the temperature density maximum or higher SSC) (Warren and Kirkbride, 1998; Richards et al., 2012). This input of meltwater with low turbidity is likely near glacier fronts where subaqueous melt of glacier ice occurs (where ice is relatively debris free) (Chikita et al., 1999). The level of SSC does not only control the density of the water, but will also control the depth of short wave solar penetration of water (Chikita et al., 1999). Consequently, where proglacial lakes have high SSC then light penetration will be limited, which will concentrate warming in the upper water layers (Chikita et al., 1999). This may lead to ‘super-heated’ surface layers and the formation of a relatively thin (metres) warm surface layer (hypolimnion) (Wessels et al., 2002; Chikita et al., 1999). Clearly there is a wide range of factors that may affect the temperature of proglacial lakes, particularly due to topo-climatic and glacio-hydrological factors, which are explored in greater depth below. In the next section (1.5.1) the spatial pattern of a selection of case study lakes are interpreted, starting with ice-contact proglacial lakes then non-ice contact proglacial lakes. The overall order that lakes are examined in is by relationship with the parent glacier, generally following the pattern of coldest to warmest lakes. This helps to examine the cooling influences on lakes first before exploring the spatial pattern of temperatures of lakes with less cooling influences and more dominant background climatic signal on the thermal regime.

### **3.5.1 Analysis of Spatial Pattern of Skin Surface Temperature of Ice Contact Proglacial lakes ( $SST_L$ case study)**

The variability in ice-contact proglacial lake skin surface temperatures ( $SST_L$ ) from AST08 imagery will be further explored below (with lake numbers referring to the AST08<sub>ID</sub>). It is vital to note that the spatial resolution constraints of the imagery (90 m) meant that pixel temperatures were not extracted directly proximal to the glacier, where the pixel temperature was a combination of glacier ice body and lake water. This is a notable limitation as it means the coldest proglacial lake water cannot be included within the  $SST_L$  analysis, as higher resolution thermal imagery is required to analyse uncontaminated water pixels closer to the glacier. The complexity in the results described above suggests that proglacial lake surface water temperatures ( $SST_L$ ) are highly influenced by factors independent to each proglacial lake situation, such as proximity and coupling with neighbouring glacier and topo-climatic factors.

The temperature distribution of lake 12 is notably lower than the other proglacial lakes analysed, with  $SST_{LMAX}$  of  $4.9^{\circ}C$  being similar to the  $SST_{LMIN}$  in lake 6 of  $4.8^{\circ}C$  (the next coldest lake) (Figure 3.14). Furthermore, the upper quartile of lake 12 ( $4.0^{\circ}C$ ) is  $1.0^{\circ}C$  below the lower quartile of lake 6 (Figure 3.14). Although it is important to remember the stated accuracy of the AST08 product is  $\pm 1.5^{\circ}C$  (Gillespie et al., 1998), as there is a  $3^{\circ}C$  difference between  $SST_{LAV}$  of lake 12 ( $3.2^{\circ}C$ ) and lake 6 ( $6.2^{\circ}C$ ) it would suggest this difference is at the edge of the AST08 uncertainty. The difference between  $SST_{LAV}$  for lake 12 and the other proglacial lakes (except lake 11) is greater than the uncertainty of the product ( $\pm 1.5^{\circ}C$ ) and therefore lake 12 is notably colder. It seems likely that lake 12 is relatively cold due to the N aspect and relatively small distal area (warming zone) in comparison to the large contact area (cooling zone) with the glacier terminus, as well as substantial ice bergs (Figure 3.15). Consequently the warming potential of the lake is limited due to shading and northerly aspect limiting incoming solar radiation (O'Reilly et al., 2015). The thermal regime is likely to be dominated by the cooling influence from a large contact area with a relatively large (for this study) glacier ( $1,755,474 m^2$ ) and potentially the input of large volumes of cold meltwater (Figure 3.15) (Chikita et al., 2009; Richards et al., 2012).

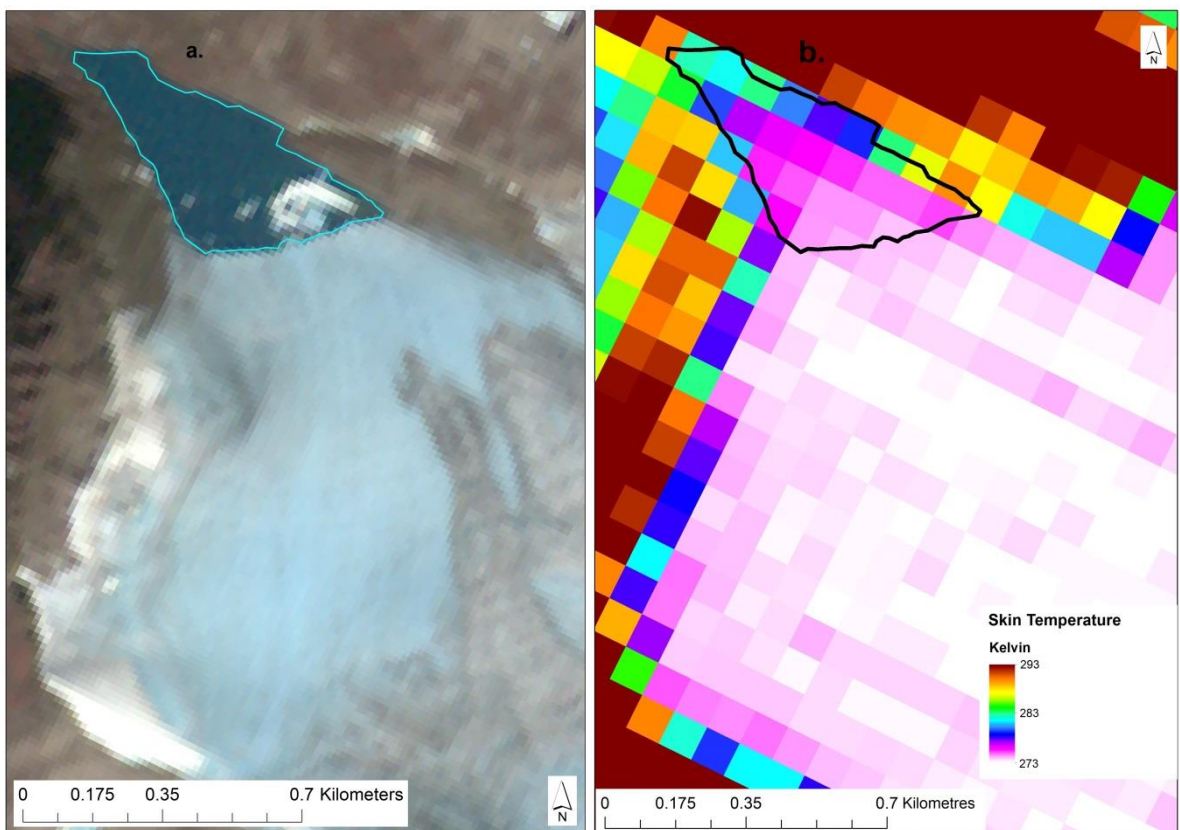


Figure 3.15 Proglacial Lake 12 a. ASTER satellite composite image (green, red and NIR) and b. ASTER surface temperature product image (AST08) at 10:46am on 8/8/2014.

Where proglacial lakes have expanded further and become more ‘established’ they will have gained more warming potential as the surface water area has increased (Becker and Daw, 2005). The geometry of the lake is also critical, such as lake 6, which has a relatively short contact point with the glacier in relation to the length of the lake (Figure 3.16). This means the distal area of lake 6 (Figure 3.16) is relatively larger than lake 12 (Figure 3.15). Therefore lake 6 has a larger area where most warming is likely to occur (O’Reilly et al., 2015), further away from the cooling influence of the glacier (Peter and Sommaruga, 2017). This is evident in the temperature gradient across lake 6 in AST08 imagery (Figure 3.16), with darker ( $SST_L$  4.8°C, 5.1°C) pixels near the terminus and lighter pixels ( $SST_L$  7.6°C, 8.5°C) at the distal end of the lake. Whilst this temperature difference is close to the stated uncertainty for the AST08 temperature product ( $\pm 1.5^\circ\text{C}$ ), field observations at the same lake during July 2017 showed a similar temperature pattern (Chapter 4 Results). With daytime maximum near surface (<1 m depth) temperatures of 8°C observed at the distal end (Chapter 4) and maximum near surface temperatures (<1 m depth) of 4.2°C were observed near the terminus (Chapter 4). Therefore proglacial lakes can have a substantial cooling influence from contact with glacier ice and meltwater (Chikita et al., 1999; Richards et al., 2012; Peter and Sommaruga., 2017). However, this cooling may be limited in spatial extent and lake area expansion may be sufficient for the distal areas to be far enough away from the terminus that they are more dominated by warming influences, as in the case of proglacial lake 6 (Figure 3.16).

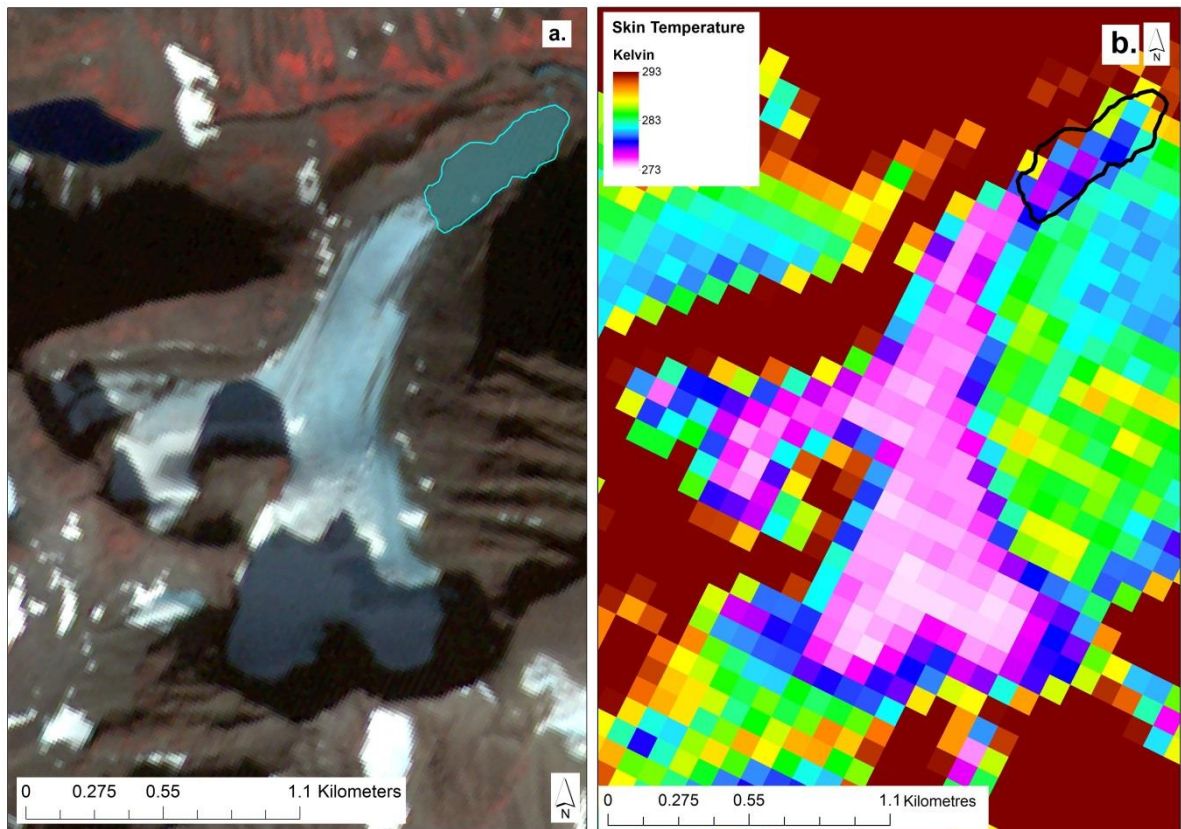


Figure 3.16 Proglacial Lake 6 a. ASTER satellite composite image (green, red and NIR) and b. ASTER surface temperature product image (AST08) at 10:46am on 8/8/2014.

The pattern of colder  $SST_L$  ( $5.1^{\circ}\text{C}$ ,  $5.3^{\circ}\text{C}$ ,  $5.5^{\circ}\text{C}$ ) proximal to the glacier is also evident in lake 11, which again has warmer distal temperatures ( $SST_L$   $7.0^{\circ}\text{C}$ ,  $8.3^{\circ}\text{C}$ ) and a similar temperature distribution to lake 6 (Figure 3.16). However, there is also a section of ice in lake 11, which may be due to iceberg calving activity (Appendix A 7). The pixel over this ice body in the lake has been included in analysis, as the presence of ice in the water body will have a direct effect on  $SST_L$  from meltwater and ice contact cooling. Lake 11 ( $149,143\text{ m}^2$ ) was also of comparable area to lake 6 ( $132,172\text{ m}^2$ ) in 2014, although lake 11 does have more complex geometry with bays and headlands (Appendix A 7). Both lake 6 and 11 have easterly aspects, so will be subject to incoming solar radiation during the morning period preceding the time of image capture (10:46am). Crucially lake 6 and 11 will therefore be at a more advanced stage of the diurnal warming cycle at 10:46am than lake 12, which will have more shade and lower levels of incoming radiation during the morning. It should also be noted that the resolution of the AST08 product (90 m) is not sufficient to constrain the extent of the cooling zone on  $SST_L$  in front of each glacier.

As proglacial lakes expand further the surface area of water increases and so the potential for absorbing incoming solar radiation also increases (O'Reilly et al., 2015). It is important to constrain the spatial extent of the cooling influence of glaciers on proglacial lakes in order to further understand their thermal regime, particularly as this is likely to change through time with increased meltwater input and also influx of icebergs (Roehl, 2006; Richards et al., 2012; Watson et al., 2020). However, this is beyond the temporal and spatial resolution of this analysis of available AST08 temperature product and calls for further high resolution thermal sensors to be launched on satellite platforms.

It is possible however to analyse proglacial lakes in more advanced stages of glacial retreat, where the large distal area dominates the overall proglacial lake thermal regime. Particularly where proglacial lakes are relatively large in comparison to the area of the neighbouring glacier that they are in contact with, such as lakes 1 (lake is 59.3% of glacier area) and 4 (lake is 327.3% of glacier area). The  $SST_{LAV}$  for lakes 1 ( $9.5^{\circ}C$ ), 3 ( $8.3^{\circ}C$ ) and 4 ( $10.5^{\circ}C$ ) are all higher than  $SST_{LAV}$  for lakes 6 ( $6.2^{\circ}C$ ), 11 ( $6.2^{\circ}C$ ) and 12 ( $3.2^{\circ}C$ ) (Figure 3.14). Furthermore, the  $SST_{LSDEV}$  is lower for lakes 1 ( $0.3^{\circ}C$ ), 3 ( $0.67^{\circ}C$ ) and 4 ( $0.38^{\circ}C$ ) than for lakes 6 ( $1.54^{\circ}C$ ), 11 ( $1.23^{\circ}C$ ) and 12 ( $0.89^{\circ}C$ ). Which would suggest that warming influences are more dominant on lakes 1,3 and 4 than for lakes 6 and 11, with relatively less warming influence on lake 12.

The locational situation of lakes 3 and 4 is similar in that they are both east facing and at altitudes of 1,318 m and 1,382 m, although it should also be noted that lake 3 has more shading from prominent topography on the southern margin (Figure 3.17; Appendix A 7). There is likely to be little climatic variability between the locations of lake 3 and 4 as they are only 6 km apart. Both lakes are of a comparable size ( $345,354\text{ m}^2$  and  $222,877\text{ m}^2$  respectively), although 24 pixels were analysed from lake 4 in comparison to 16 from lake 3 due to its geometry eliminating large sections of lake margin from analysis (Appendix A 7). It should also be noted that the curved glacier front geometry of lake 3 resulted in only 1 pixel being analysed in close proximity to the glacier front (Figure 3.17), which has a relatively cold temperature of  $6.7^{\circ}C$  and represents a prominent outlier (compared to  $SST_{LAV}$  of  $8.3^{\circ}C$  for lake 3; Figure 3.14). This suggests that the immediate cooling zone in contact with the glacier in lake 3 is relatively small, and the relatively low turbidity (appearing dark in Figure 3.17) of lake 3 would also suggest a low influx of turbid meltwater. As with other ice-contact proglacial lakes there is a temperature gradient across lake 3, with a maximum of  $9.7^{\circ}C$  at the distal end of the lake (Figure 3.14; Figure 3.17). There are also some colder

pixels (darker) at the distal end of the lake, which are in close proximity to a large snow patch and presumably associated with meltwater emanating from this (Figure 3.17).

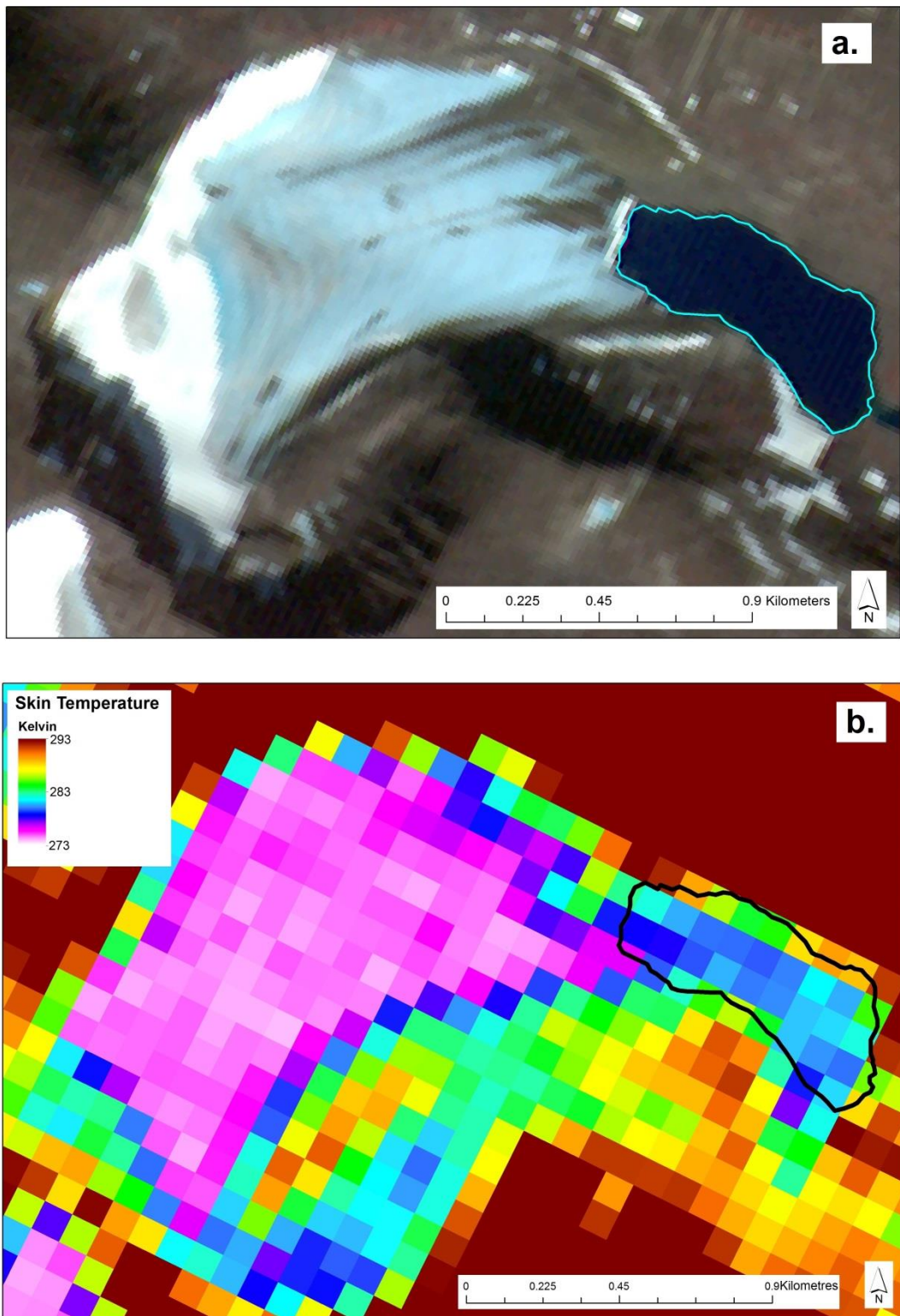


Figure 3.17 Proglacial Lake 3 a. ASTER satellite composite image (green, red and NIR) and b. ASTER surface temperature product image (AST08) at 10:46am on 8/8/2014. Pixels  $<273$  K ( $0^{\circ}\text{C}$ ) in white and  $>293$  K ( $20^{\circ}\text{C}$ ) in red and darker blue representing colder ( $<279$  K) temperatures.

The area of proglacial lake 1 (157,516 m<sup>2</sup>) is similar to the area of the glacier (265,647 m<sup>2</sup>) and snow it is in contact with, therefore the proportion of meltwater influx to ambient lake water is likely to be much smaller than the lakes discussed above that have much larger glaciers in proportion to the lake (Table 1.2) (Appendix A 7). This is partly evident through the higher SST<sub>LAV</sub> of lake 1 (9.5°C) and also lower SST<sub>LSDEV</sub> (0.3°C), which suggests minimal cooling influence on the pixels analysed. It is important to note again that pixels containing both glacier ice and lake water were not analysed due to thermal emission contamination from the glacier body. Therefore it is possible that a cooling influence from the glacier on the lake 1 SST<sub>L</sub> exists, but is smaller in spatial extent than the resolution of the imagery (90 m). The relatively high SST<sub>L</sub> of lake 1 are also likely due to the open easterly aspect meaning that there is little shading and high levels of solar radiation absorption before the time of image capture (10:46am).

### **3.5.2 Analysis of Spatial Pattern of Skin Surface Temperature of Non- Ice Contact Proglacial lakes (SSTL case study)**

The complexity in the results described above suggests that non-contact proglacial lake skin surface temperatures (SST<sub>L</sub>) are highly influenced by factors independent to each proglacial lake situation, such as proximity and coupling with neighbouring glacier and topo-climatic factors. Whilst lakes without direct contact with a glacier tend to be warmer (Figure 3.14), there is no statistically significant difference and there are notable exceptions (lake 5 and 7). Lake 7 recently (2010) lost contact with the neighbouring glacier, which has retreated ~20 m between 2010 and 2018 (Kirchner et al., 2019). The relatively short distance between the glacier terminus and proglacial lake means that there will be minimal warming of the proglacial stream before it enters lake 7 (Magnusson et al. 2012). Consequently there will be a cooling influence on the lake due to the influx of meltwater (Richards et al., 2012). This is evident in the cooler SST<sub>L</sub> near the glacier (minimum 6.8°C) represented by darker pixels in the AST08 product imagery, which appear to emanate eastwards from the glacier terminus (Figure 3.18).

There is also a temperature gradient across proglacial lake 7, with maximum temperatures of 11.5°C and 11.2°C in the margin area of the lake (Figure 3.18). These 2 pixels represent notable outliers (Figure 3.14) and the band 11 emissivity is relatively low (0.95) for these pixels, this may indicate longwave emission from the lake bed, as this is visible in optical imagery due to clear water (Figure 3.18) (Sabol et al., 2009). So the warmer pixel

temperatures at the margin could be due to warming of the water from longwave emissions from the lake bed (O'Reilly et al., 2015). It seems unlikely that emissivity errors account for the 2 colder (darker) pixels in close proximity to the lake outlet, as they both have emissivity values realistic for water of 0.97 (Gustafson et al., 2006).

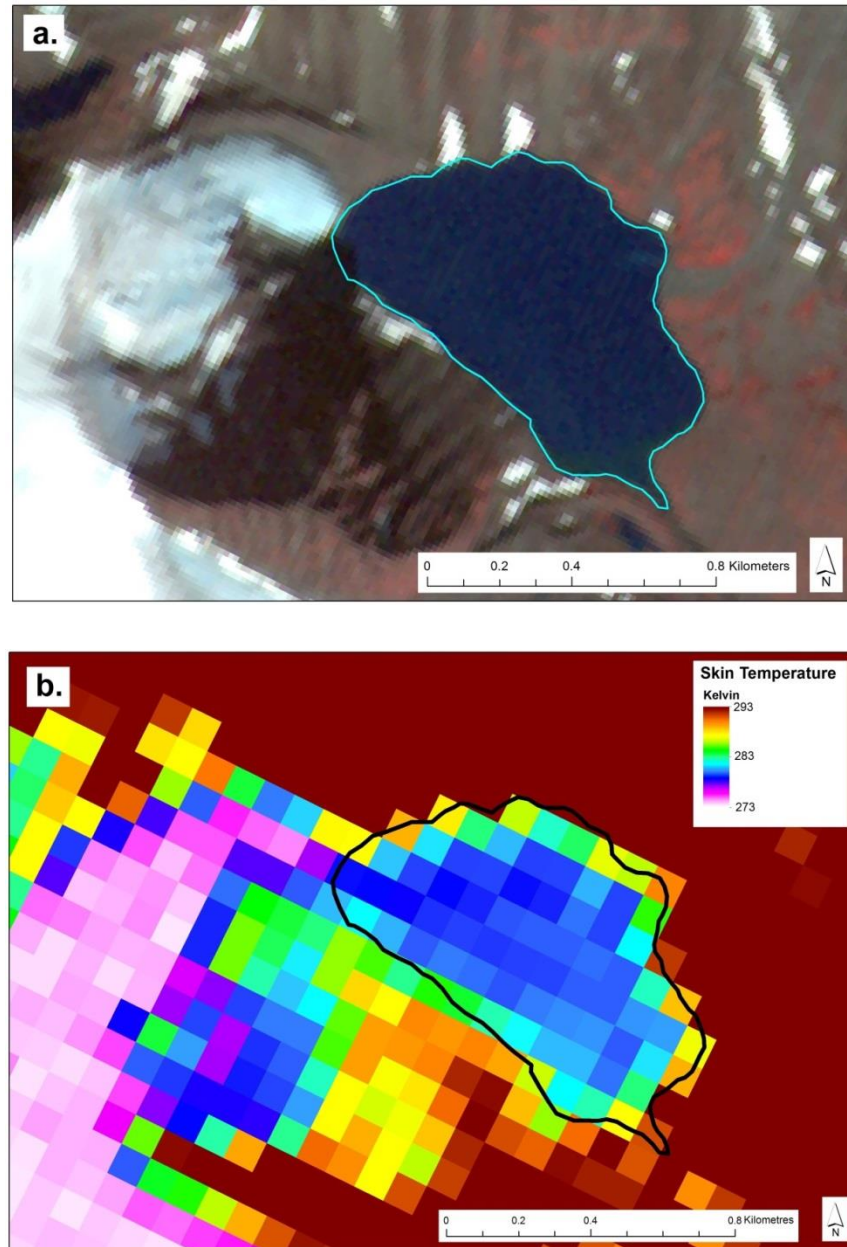
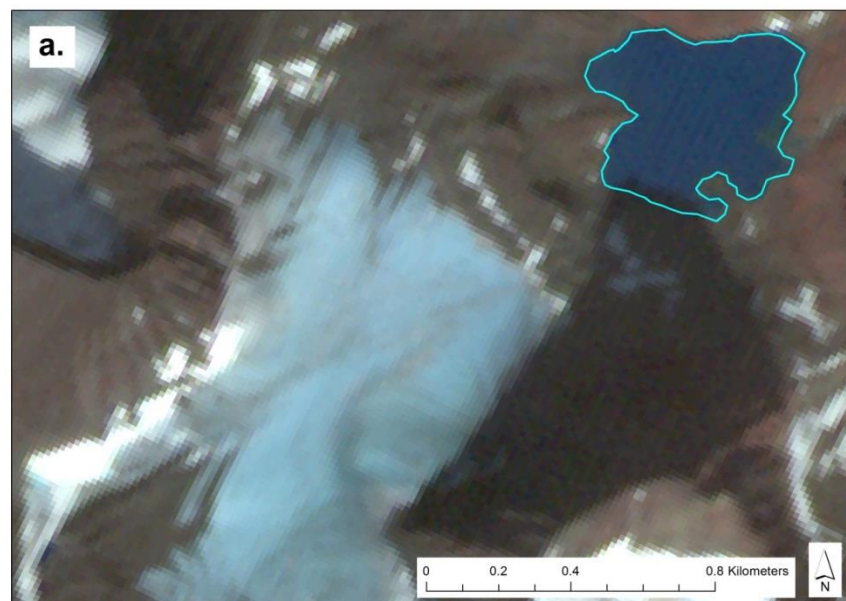


Figure 3.18 Proglacial Lake 7 a. ASTER satellite composite image (green, red and NIR) and b. ASTER surface temperature product image (AST08) at 10:46am on 8/8/2014. Pixels  $<273$  K ( $0^{\circ}\text{C}$ ) in white and  $>293$  K ( $20^{\circ}\text{C}$ ) in red and darker blue representing colder ( $<279$  K) temperatures.

The proglacial lakes 5 and 7 appear to be colder and their interquartile range lies below the other non-contact proglacial lakes analysed (Figure 3.18). The proglacial lake 5 is in a more advanced stage of glacial retreat than lake 7, as the neighbouring glacier is further away

(proglacial stream feeding into lake ~0.8 km). However, it still appears that the input of glacial meltwater into lake 5 also has a cooling influence, as the  $SST_L$  closer to the glacier are colder (minimum  $5.6^{\circ}\text{C}$ ) and the more distal pixels are warmer (maximum  $9.6^{\circ}\text{C}$ ). The  $SST_L$  of lake 5 are generally colder ( $SST_{LAV}$   $7.2^{\circ}\text{C}$ ) than lake 7 ( $SST_{LAV}$   $8.1^{\circ}\text{C}$ ). This is likely due to lake 7 having a more open easterly aspect, which results in greater warming during the morning from incoming solar radiation (Adrian et al., 2009; O'Reilly et al., 2015). In contrast lake 5 has a more northerly aspect with substantial topography around the southern margin (Figure 3.19). This creates substantial shading and reduces incoming solar radiation during the morning and results in less warming in the early part of the day than lake 7 (O'Reilly et al., 2015). The colder surface skin temperatures ( $SST_L$ ) of the glacier next to lake 5 (white  $<273^{\circ}\text{K}$ ) compared to the warmer skin surface temperatures of the glacier next to lake 7, also suggests that the aspect is a controlling factor of skin surface temperatures at the time of image capture as the glacier surface has been subject to less warming (10:46am) (Figure 3.19).



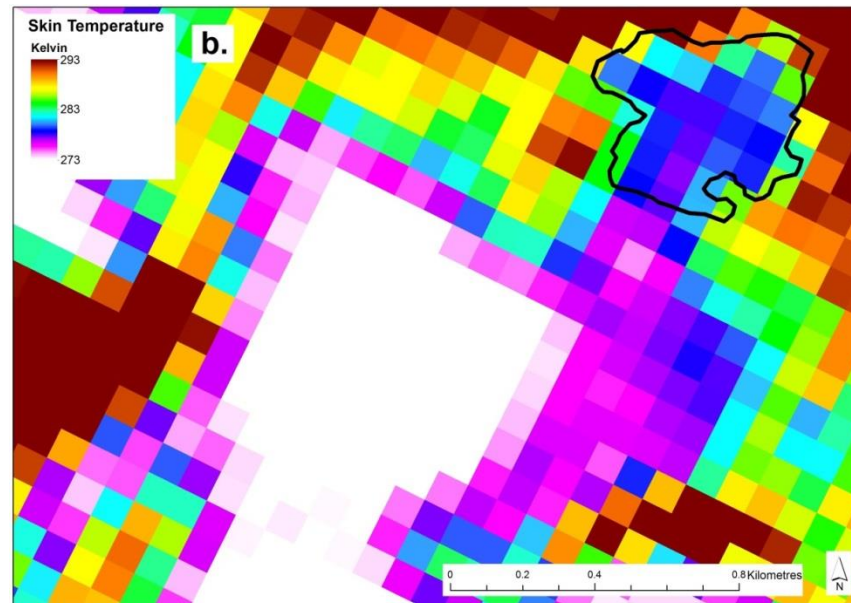


Figure 3.19 Proglacial Lake 5 a. ASTER satellite composite image (green, red and NIR) and b. ASTER surface temperature product image (AST08) at 10:46am on 8/8/2014.

The elevation and distance to neighbouring glaciers is very similar for lake 8 and 10, with both being around  $\sim 0.3$  km away from the terminus (1,123 m and 1,090 m asl respectively) (Figure 3.20). This would suggest that both proglacial streams are subject to similar amounts of warming, which is a key consideration for proglacial lake thermal regime as Magnusson et al (2012) found proglacial stream temperatures of up to  $11.4^{\circ}\text{C}$  at  $\sim 1.5$  km from a glacier terminus in Switzerland. Both proglacial lakes have a similar aspect (although lake 8 is slightly more southerly) and size (lake 8 is  $203,616 \text{ m}^2$ ; lake 10 is  $206,083 \text{ m}^2$ ). However, the size of the neighbouring glaciers is substantially different (lake 8 glacier  $552,809 \text{ m}^2$ , lake 10 glacier (Riukojekna)  $2,301,468 \text{ m}^2$ ), which has important implications for differences in meltwater input between the two lakes. Furthermore, lake 8 appears to have low turbidity, which suggests that there is a low amount of turbid meltwater influx or that suspended sediment may have been deposited before influx into lake 8 (Figure 3.20). Inspection of high resolution satellite imagery (Google Earth 2013) shows that the main meltwater influx into lake 8 is from a smaller proglacial lake ( $\sim 9,300 \text{ m}^2$ ; Chapter 2) closer to the glacier. This is likely to lead to heating of proglacial water (Richards et al., 2012), particularly as the proglacial stream then flows down a steep south facing stream into lake 8 (Magnusson et al., 2012) (Figure 3.20). Moreover the coldest pixel in lake 8 ( $9.0^{\circ}\text{C}$ , emissivity band 11 of 0.97) is actually near the outlet (Figure 3.20), which further suggests that meltwater input is not the dominant control on the cooling of  $\text{SST}_L$  in this lake.

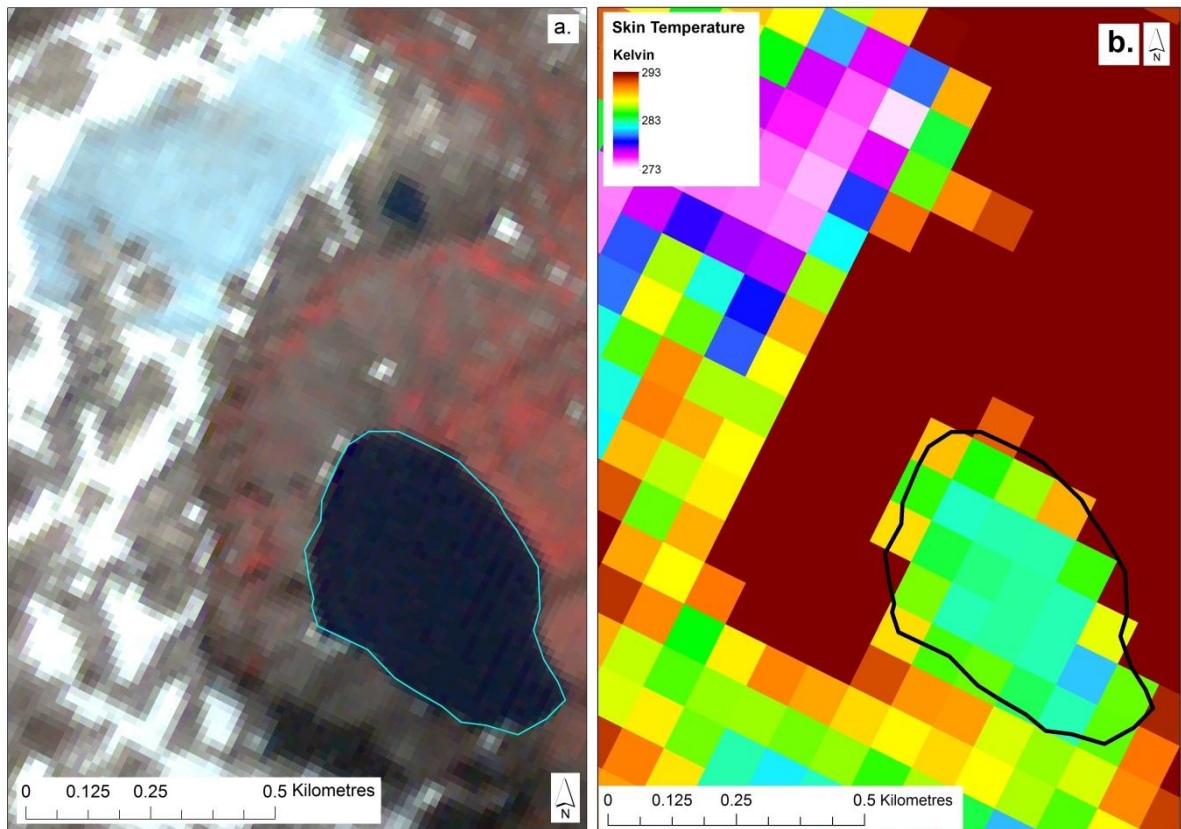


Figure 3.20 Proglacial Lake 8; a. ASTER satellite composite image (green, red and NIR) and b. ASTER surface temperature product image (AST08) at 10:46am on 8/8/2014.

In contrast, the proglacial stream flowing into lake 10 did not pass through any smaller proglacial lake (Google Earth imagery 2013) and flows along an east facing gentle slope (Appendix A 8). So it will be subject to less warming before flowing into lake 10 (Magnusson et al., 2012). Furthermore, the larger size of neighbouring glacier suggests that there will also be a greater influx of meltwater into lake 10 (glacier 2,301,468 m<sup>2</sup>) than lake 8 (glacier 552,809 m<sup>2</sup>), this cooling influence is also reflected by the colder SST<sub>LAV</sub> for lake 10 (10.6°C) than lake 8 (11.0°C). Additionally, the coldest pixel in lake 8 (9.0°C) represents a notable outlier and the location near the outlet suggests another process leading to cooling the SST<sub>L</sub> of this pixel rather than input of meltwater. The emissivity for this pixel in band 11 is 0.97, which is realistic for water (Gustafson et al., 2006; Sabol et al., 2009). There is also an area of colder (blue ~8°C) pixels near the outlet of lake 9, which are the coldest pixels in the lake (Figure 3.21). It should be noted that the pixels nearest the glacier were not analysed due to the narrow geometry of the lake potentially leading to thermal-emission contamination from surrounding land (Figure 3.21). Bearing this in mind, the pixels closest to the glacier were warmer (green) than the cold (blue) area of pixels near the outlet (Figure 3.21). The optical image would suggest that the warmer pixels are over the shallower area of lake which

appears brighter due to radiation from the lake bed and colder pixels in the darker (blue) area of lake (Figure 3.21). This lack of cold pixels nearer the glacier suggest that other limnological processes are responsible for the coldest SST<sub>L</sub> of lake 9, rather than input of cold glacial meltwater (Figure 3.21).

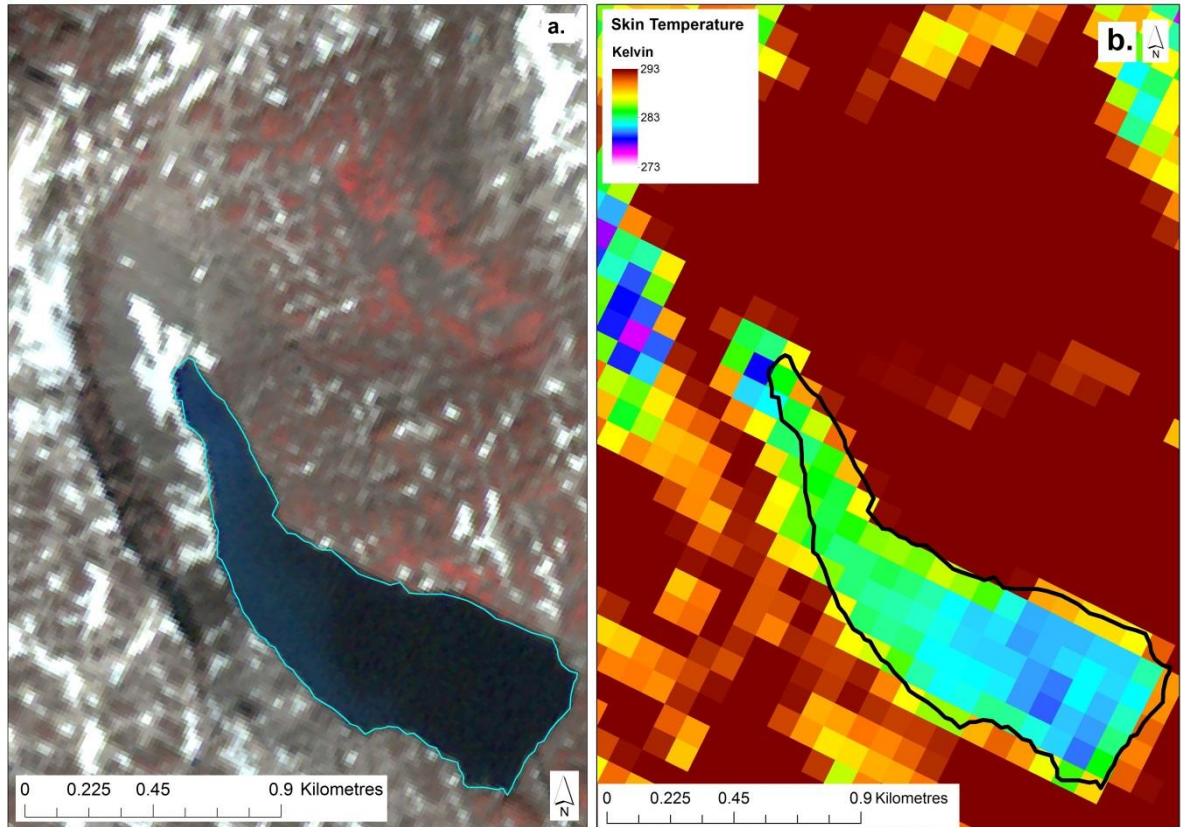


Figure 3.21 Proglacial Lake 9 a. ASTER satellite composite image (green, red and NIR) and b. ASTER surface temperature product image (AST08) at 10:46am on 8/8/2014.

There is also a large range (SST<sub>LDIFF</sub> 4.5°C) in lake 9, with a maximum of 12.5°C and the highest SST<sub>LSEV</sub> (1.13°C) of any non-ice contact proglacial lake at 10:46am on 8/8/2014 (Figure 3.14). This range in temperatures is above the stated uncertainty of the AST08 product of +/- 1.5°C (Gillespie et al., 1998). Also the emissivity band 11 values for these pixels is between ~0.96 to 0.98, which is reasonable for water and unlikely to be a source of uncertainty (Gustafson et al., 2006; Sabol et al., 2009). It should also be noted that lake 9 is of a much larger size (686,008 m<sup>2</sup>), which may enable scale dependent limnological processes to occur within this lake (Adrian et al., 2009; O'Reilly et al., 2015).

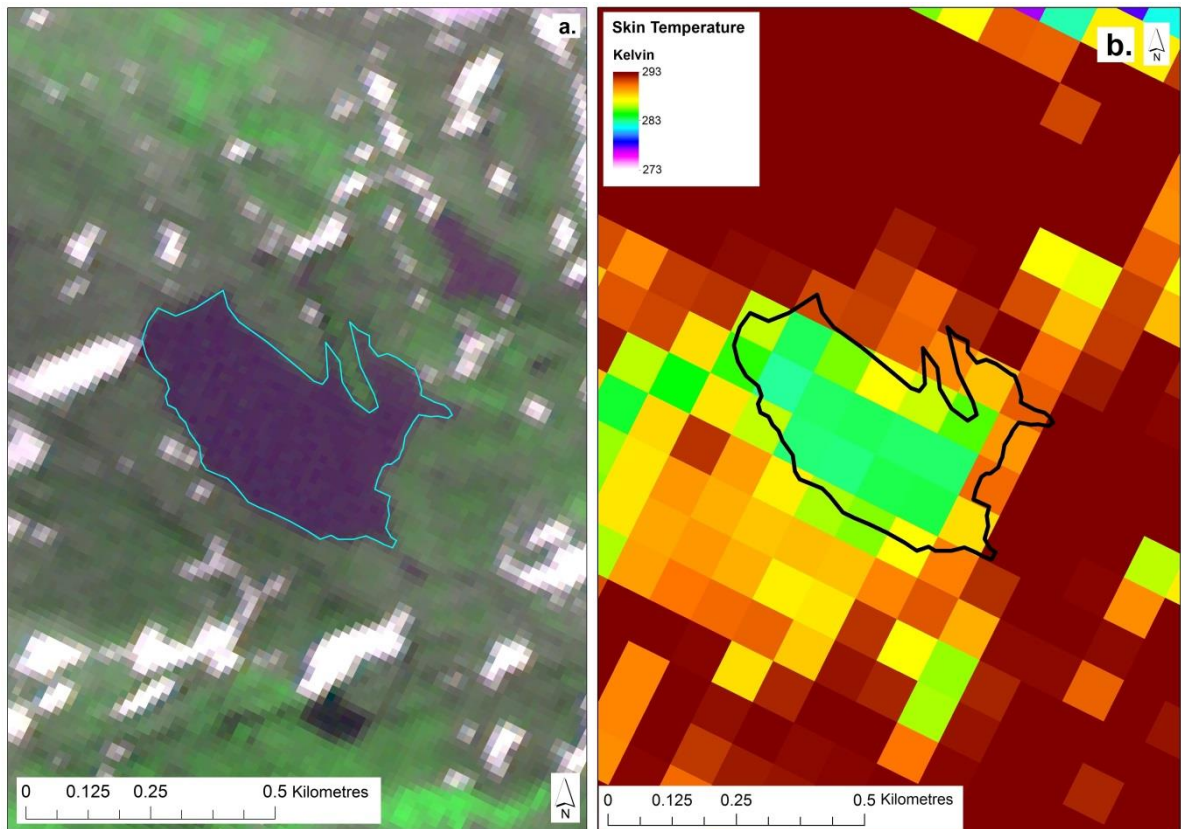


Figure 3.22 Proglacial Lake 2 a. ASTER satellite composite image (green, red and NIR) and b. ASTER surface temperature product image (AST08) at 10:46am on 8/8/2014.

The most advanced stage of deglaciation in the 12 proglacial lakes analysed is represented by lake 2, which is ~0.5 km away from the neighbouring glacier through a south east facing fore-field with a smaller proglacial lake (1,144 m asl) (Figure 3.22). Therefore diurnal warming of the proglacial stream feeding into lake 2 before image capture could be substantial, as Magnusson et al. (2012) found temperatures of up to 11.4°C ~1.5km from a glacier in Switzerland. The lack of cooling influence on the lake from meltwater input is also illustrated by it having the lowest  $SST_{LSDEV}$  (0.19°C) of any proglacial lake and also highest  $SST_{LAV}$  of (11.5°C). It is therefore suggested that lake 2 is in an advanced stage of deglaciation and essentially ‘decoupled’ from the glacier, with no evidence of meltwater cooling on the lake  $SST_L$ . It is interesting to note that lake 8 had substantially higher  $SST_{LMAX}$  (12.7°C) than lake 2 (11.8°C), which may be due to the more simple geometry of lake 8 enabling pixels to be sampled closer to the shore where solar penetration to the lake bed enhances warming of shallow water (O’Reilly et al., 2015). It should also be noted that lake 8 is surrounded by a steep east and south facing headwall, that had warm (red >293°K) skin surface temperatures (SST) at the time of image capture (10:46am). This warm

topography surrounding lake 8 may have exerted a warming influence on the lake through emission of long wave radiation (Aubry-Wake et al., 2015).

### 3.5.3 Discussion of Proglacial Lake SST<sub>L</sub> by Stage of Deglaciation

The analysis in the previous section (3.5.1 and 3.5.2) explores the relationship between proglacial lake SST<sub>L</sub> and surrounding influences through interpretation of the spatial pattern. It is evident that contact with a glacier and input of meltwater will likely lead to a cooling of the proglacial lake SST<sub>L</sub> (Magnusson et al., 2012; Peter and Sommaruga, 2017). Whereas minimal coupling with the parent glacier will lead to minimal cooling of the proglacial lake and more dominant control from surrounding climatic influences (Richards et al., 2012). Therefore the analysis of 12 proglacial lakes with different relationships with the parent glacier provides an insight as to how SST<sub>L</sub> may vary at different stages of deglaciation and climatic influences. This is conceptually illustrated in the schematic below (Figure 3.23).

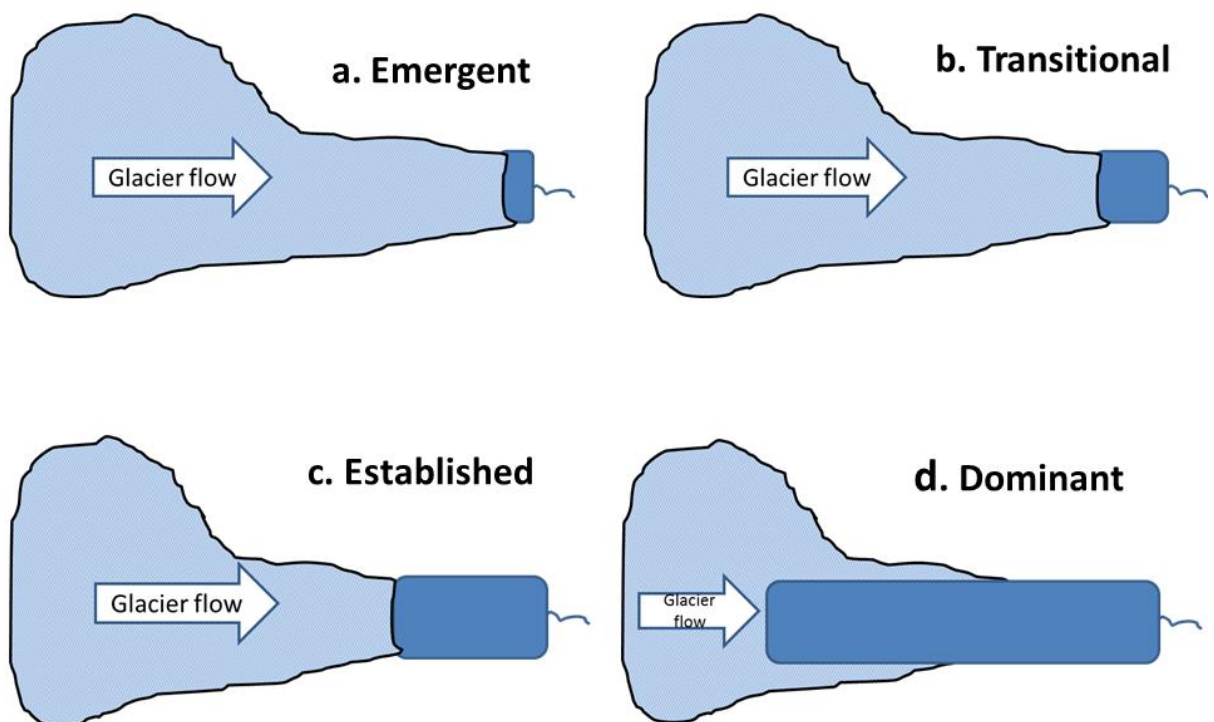


Figure 3.23 Schematic of proglacial lake thermal regime by stage of deglaciation showing a. Emergent proglacial lake due to glacier retreating into topographic basin. Lake length is less than contact width. b. Transitional proglacial lake. Lake length is proportional to glacier contact width. c. Established proglacial lake. Lake length is larger than glacier contact width d. Dominant proglacial lake. Lake length is larger than glacier length.

The first proposed stage of deglaciation for proglacial lakes is referred to as ‘Emergent’, relating to lakes that have recently emerged from glacier ice (Figure 3.23). As the length of

the Emergent proglacial lake is less than the glacier contact width, the thermal regime is dominated by cooling from contact with the glacier and input of meltwater, with water temperatures likely to be uniformly below 1°C (Figure 3.23). These lakes are relatively small in size and due to the limited resolution of the AST08 product imagery (90 m) no emergent lakes are analysed in this study. The next proposed stage of proglacial lake deglaciation thermal regime is termed 'Transitional' as the distal area of the lake may be far enough from the glacier front to be periodically dominated by warming factors before cooling dominates, due to the lake length being proportional to the glacier contact point width (Figure 3.23). When the lake length is substantially larger than the glacier contact point width, it is referred to as 'Established', as the distal area of the lake will be far enough from the glacier front to be dominated by warming factors (with some cooling periods possible in melt season) main area of the lake will be far enough from the glacier front to be dominated by warming factors, some minor cooling possible. The final stage of deglaciation for ice-contact proglacial lakes is termed 'Dominant' as the larger lake length compared to the glacier contact point width means the main area of the lake will be far enough from the glacier front to be dominated by warming factors (Figure 3.23). The different stages of deglaciation for non-contact proglacial lakes are less easily divided by geometry, but may be considered 'coupled' where cooling influences from glacial meltwater are evident. The different theoretical stages of proglacial lake deglaciation and thermal regime are now discussed below for the case studies that have been examined.

The author proposes that if the climate remains in a stable state and cooling influence from the glacier (ice-contact, iceberg input and meltwater influx) remains stable then proglacial lake 12 may continue to be in a relatively cold state (Figure 3.15). If the glacier mass balance were to remain stable, then retreat of the glacier terminus is likely to be limited, as mass loss during the summer (at the ice-cliff) will be minimal if the lake remains cold and the glacier maintains the same thickness. If the glacier mass balance were to become substantially positive (in a cooler or wetter climate) then the glacier terminus may advance and lead to a reduction in size of the lake (Nesje et al., 2008). However, if the climate were to become warmer then lake temperatures would likely rise and lead to higher rates of mass loss at the water-ice contact point through thermal undercutting and iceberg calving due to undermining of the ice-cliff (see Chapter 4) (Kirkbride, 1993; Kirkbride and Warren, 1997; Warren and Kirkbride, 1998; Roehl, 2006; Minowa et al., 2017). This increased thermal erosion would likely lead to a retreat of the ice front and expansion of the proglacial lake area (Warren and

Kirkbride, 2003; Minowna et al., 2017), which would further increase the warming potential of the proglacial lake and potentially produce a positive feedback cycle. Therefore the author argues that lake 12 represents a ‘Transitional’ stage of a proglacial lake, where a reduction or increase of proglacial lake size is finely balanced depending on climatic factors and glacier dynamic response.

The similarity in values and distribution of  $SST_L$  (Figure 3.16) in  $SST_L$  at lake 6 and 11 (see Appendix A 7) at the time of image capture supports the argument that they both have a similar relationship with cooling influence from the parent glacier (Figure 3.14). The disappearance of proglacial lake 6 or 11 due to glacier re-advance seems highly unlikely in the current climate and the warm  $SST_L$  reported in this study would suggest that glacier retreat (partly driven by thermal erosion) is more likely. Therefore both proglacial lake 6 and lake 11 are referred to as ‘established’ proglacial lakes.

The lower  $SST_{LAV}$  of lake 3 ( $8.3^{\circ}\text{C}$ ) compared to  $SST_{LAV}$  for lake 4 ( $10.5^{\circ}\text{C}$ ) would suggest that the larger glacier ( $1,486,665\text{ m}^2$ ) in contact with lake 3 than lake 4 ( $105,949\text{ m}^2$ ) exerts a stronger cooling influence on the overall lake temperatures (Table 3.2 and Figure 3.14). Therefore lake 3 should be classed as an ‘established’ proglacial lake, as warming influences on the lake were not totally dominant at 10:46am on 8/8/2014. In contrast the ‘glacier’ in contact with lake 4 is very small and whilst it was in the RGI (v6) it would be better classed as a glacieret, due to the diminutive size, and is therefore unlikely to have a substantial cooling effect on the lake. It is therefore argued that lake 4 should be classed as a ‘dominant’ proglacial lake, as the thermal regime is dominated by warming influences similar to non-glacial lakes in the area (O’Reilly et al., 2015).

The classification of non-ice contact  $SST_L$  by deglaciation is less easily defined by geometry and in cases the cooling influence of parent glaciers are less clear. Both lakes 5 and 7 appear to have strong cooling influences on  $SST_L$ , which in the case of lake 7 is likely to be due to the close proximity of the parent glacier and is effectively strongly coupled (Figure 3.18). The coupling between the parent glacier and lake 5 is less clear, as the northerly aspect and shading will also play a strong cooling influence on the lake  $SST_L$  (Figure 3.19). The lack of a cold  $SST_L$  signal from meltwater in lake 8 and 10 would suggest that they may be thermally decoupled from the parent glacier, through warming of the input meltwater stream over a steep south/east facing slopes and preceding proglacial lakes (Figure 3.20) (Richards et al., 2012; Magnusson et al., 2012).

Lake 9 is of a much larger size (686,008 m<sup>2</sup>), which may enable scale dependent limnological processes to occur within this lake (Figure 3.21) (Adrian et al., 2009; O'Reilly et al., 2015). The neighbouring 'glacier' is very small (a glacieret; 71,160m<sup>2</sup>), and the proglacial stream runs for ~0.4 km into snow patches before entering the lake so the influence of glacial meltwater on SST<sub>L</sub> is likely to be minimal (Richards et al., 2012). Therefore lake 9 represents a very advanced stage of deglaciation with minimal influence from a glacier to the extent that it could be considered 'decoupled'. The most advanced stage of deglaciation in the 12 proglacial lakes analysed is represented by lake 2, which is ~0.5 km away from the neighbouring glacier through a south east facing forefield with a smaller proglacial lake (1,144 m asl) (Figure 3.22). It is therefore suggested that lake 2 is in an advanced stage of deglaciation and essentially 'decoupled' from the glacier, with no evidence of meltwater cooling on the lake SST<sub>L</sub>.

### 3.6 Conclusion

The skin surface temperatures (SST<sub>L</sub>) presented in this study of proglacial lakes in Arctic Sweden extracted from the AST08 surface temperature product are the first satellite derived temperatures to be reported from proglacial lakes in the Arctic. The strong correlation (linear regression  $R^2 = 0.9365$ ) between temperatures from AST08 and those measured by thermistors <2 m deep, provides relatively strong (for 8 data points) validation of the AST08 temperature product and one of the first from maritime climates (Sweden and Patagonia). The strong linear relationship also suggests a strong relationship between skin surface (top 1 mm) temperature (SST) (as measured by AST08) and near surface temperature of water from in-situ thermistors at the time of image capture (Donlon et al., 2012). This study has reviewed literature on the utilisation of AST08 temperature product over water bodies to develop a robust methodology for extracting pixel SST<sub>L</sub> over proglacial lakes.

The proglacial lake average skin surface temperature (SST<sub>LAV</sub>) of 8.9°C in Arctic Sweden on 8/8/2014 is substantially higher than the 1°C commonly assumed for proglacial lakes (Chernos et al., 2016; Truffer and Motyka, 2016). The average hourly air temperature at Tarfala for July 2014 (12.4°C) was 5.4°C above the long term (1965-1994) average air temperature for July. This gives some background climatological context for the results presented in this study, with July 2014 representing a 'heatwave', which are predicted to

increase in the future (Kim et al., 2018). There was also high heterogeneity in temperatures between proglacial lakes, which suggests local factors had a strong influence on  $SST_L$  of proglacial lakes. The high standard deviation ( $2.0^{\circ}\text{C}$ ) and large range in proglacial lake skin surface temperatures ( $SST_L$ ) suggests there is clearly a high level of complexity for such temperatures relating to micro-climate and relationship with parent glacier (Peter and Sommaruga, 2017).

The temperature distribution and spatial pattern in  $SST_L$  has been reported and analysed for each of the 12 proglacial lakes for the AST08 product from 8/8/2014 (10:46am). There was a moderate positive correlation of  $R^2=0.5932$  between  $SST_{LAV}$  and parent glacier aspect, which suggests the exposure to incoming solar radiation was a strong influence on the  $SST_L$  of the 12 proglacial lakes in this study. Several lakes also had areas of cooler  $SST_L$  in close proximity to the parent glaciers, which suggests strong cooling influences from parent glaciers for some proglacial lakes. These spatial patterns in  $SST_L$  have been interpreted and used to propose a conceptual model classifying proglacial lake surface temperature by different stages of deglaciation. This conceptual model will need to be further validated by more analysis of satellite thermal imagery (ideally higher resolution) and field observations of proglacial lake temperatures.

## 4 Quantifying Proglacial Lake Temperatures and Terminus Change of Kaskapakteglaciaren in Arctic Sweden

### 4.1 Introduction

Glaciers are sensitive to changes in climate and have generally retreated in most mountain areas since the Little Ice Age cold period finished ~100 years ago (IPCC AR5, 2013). Where proglacial lakes are in contact with glacier termini, they have been shown to accelerate mass loss rates in Alaska, Patagonia, Nepal and New Zealand; through thermal and mechanical processes (Skvarca et al., 1995; Kirkbride and Warren, 1997; Warren and Kirkbride, 1998; Roehl et al., 2006; Boyce et al., 2007; King et al., 2017; Watson et al., 2020). However, despite this evidence there has been a common assumption that proglacial lakes remain at a uniform temperature of ~1°C (Boyce et al., 2007; Chernos et al., 2016). The focus of this chapter is therefore on investigating the thermal evolution of a proglacial lake in order to investigate the influence on mass loss of an Arctic glacier. A better understanding of these thermal processes is needed so as to reduce uncertainties related to future glacier retreat rate predictions, particularly given projected air and lake water temperature increases with future climate change scenarios (IPCC AR5, 2013).

The thermal influence of proglacial lakes on glacier retreat has received relatively little attention, partly due to problems of accessing the hazardous ice cliffs that are often found at the ice/water interface (Eijpen et al., 2003). However, the formation of thermally eroded notches (Figure 4.1) at the waterline on glacier termini has been observed in Alaska, Nepal, New Zealand and Patagonia throughout most of the year (except when proglacial lakes have been frozen) (Boyce et al., 2007; Sakai et al., 2009; Roehl et al., 2006; Minowa et al., 2017; Watson et al., 2020). Thermally eroded notches (Figure 4.1) undercutting subaerial ice cliffs up to 10m on the glacier terminus have been observed on Tasman Glacier (New Zealand), where iceberg calving events were observed every 4 to 8 weeks (Roehl et al., 2006). A maximum water temperature of 6.4°C was observed in the thermally eroded notches on Tasman glacier, which resulted in a maximum notch formation rate of 65 cm d<sup>-1</sup> (Roehl et al., 2006). This undercutting of the Tasman glacier ice front increased shear and tensile stresses within the ice, which resulted in failure and iceberg calving events enhancing mass loss from the glacier terminus (Roehl et al., 2006).

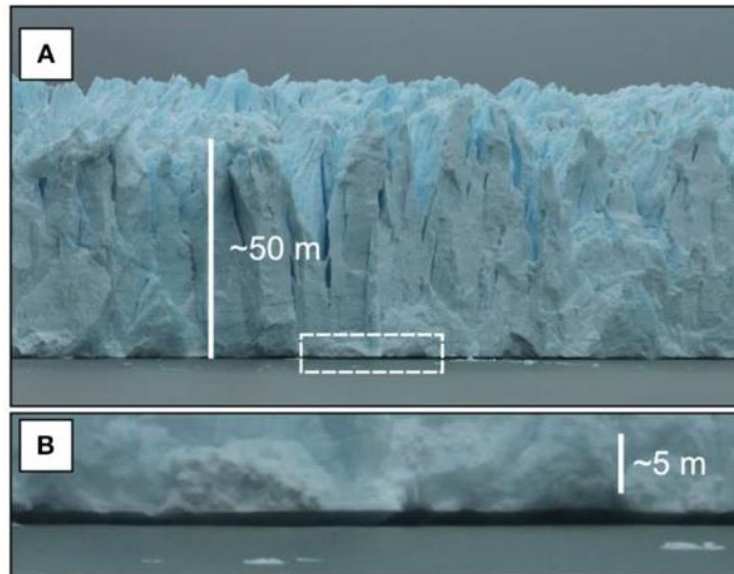


Figure 4.1 A. Image of Perito Moreno glacier front and proglacial lake (Brazo Rico). B. Thermally eroded notch from Minowa et al. (2017).

The thermal structure of proglacial lakes can clearly have a substantial influence on glacier retreat rates through thermal erosion from contact with lake water undercutting ice cliffs and leading to mass loss from ice breaking off the glacier terminus, as well as subaqueous melting (Roehl et al., 2006; Minowa et al., 2017). Furthermore, Minowa et al. (2017) found a close relationship between seasonal lake water temperature and seasonal ice front position of Glaciar Perito Moreno in Patagonia ( $r = 0.96$ ). They conclude this relationship was due to subaqueous melting undercutting the terminus, which increased calving rates and had a strong control on ice front position. However, they were unable to make temperature observations within 200 m of the glacier terminus due to the hazards of iceberg calving events, so they assume that water temperatures are the same at the ice front (Minowa et al., 2017). However there is likely to be a zone of cooler water in close proximity to the ice front (Warren and Kirkbride, 1998; Roehl et al., 2006). Therefore, there is a substantial need for observing temperature variations at the water-ice contact points between glaciers and lakes in order to advance understanding of how proglacial lakes affect glacier mass loss rates.

The temperature measurements made by Roehl (2006) and numerous observations of thermal erosion on glacier termini from other studies (Kirkbride and Warren, 1997; Chikita et al., 1999; Warren and Kirkbride, 2003; Haresign and Warren, 2005; Minowa et al., 2017; Mallalieu et al, 2020; Watson et al., 2020), clearly bring in to question the common assumption that proglacial lakes have a uniform temperature of  $<1^{\circ}\text{C}$  (Boyce et al., 2007; Chernos et al., 2016; Truffer and Motyka, 2016). These observations strongly suggests that

the thermal regime of proglacial lakes has a greater influence on glacier retreat rates than previously thought. It has previously been commonly assumed that a high iceberg flux into a proglacial lake will cool water temperatures to a uniform 1°C (Figure 4.2; Boyce et al., 2007; Chernos et al., 2016).

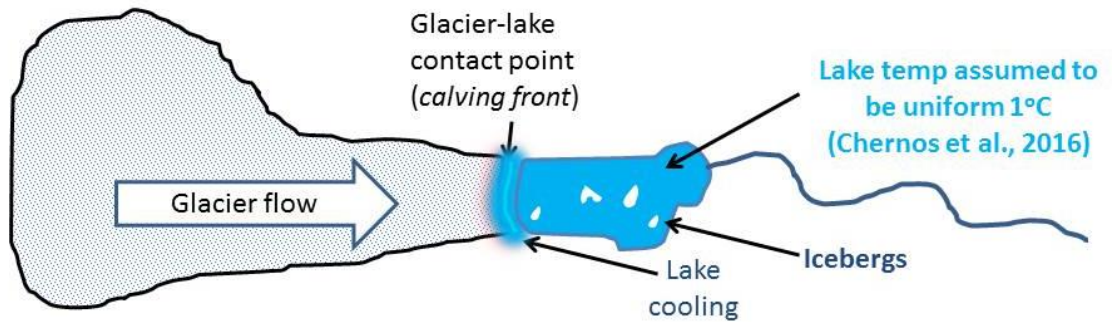


Figure 4.2 Schematic in plan view illustrating the common assumption that proglacial lakes are a uniform 1°C due to cooling at the ice front and iceberg melt (Chernos et al., 2016; Truffer and Motyka, 2016).

The null hypothesis of assuming proglacial lake temperatures are a uniform 1°C (Figure 4.2) appears to be an over simplification of proglacial lake thermal regime and is therefore tested in this study. Particularly as environmental factors such as warmer air temperatures and solar heating of water are likely to raise proglacial lake temperatures (Adrian et al., 2009; O'Reilly et al., 2015). However, rain water may also have a cooling affect depending on the rain temperature relative to the ambient lake water temperature (Peter and Sommaruga, 2017). Furthermore, as melt of glacier ice increases so too does the input of cold glacial meltwater, which will have a cooling influence on ambient lake temperatures, although this will be somewhat dependent on residence time of water in the lake (Richards et al., 2012; Fellman et al., 2014; Watson et al., 2020). The residence times of water in contact with the glacier terminus is critical in determining subaqueous melt rates, as stationary water would be cooled by the glacier ice and reduce melt rates (Warren and Kirkbride, 1998; Roehl, 2006). Conversely, lake currents (wind or circulation driven) may export cooler water away from the ice front and advect warmer water from the distal part of the lake to the ice front and increase subaqueous melt rates (Figure 4.3) (Chikita et al., 1999; Sakai et al., 2009). Consequently, it is essential to measure water temperatures through time in order to constrain the relative influence of the factors that can affect the thermal structure proglacial lakes and the influence on glacier mass loss rates.

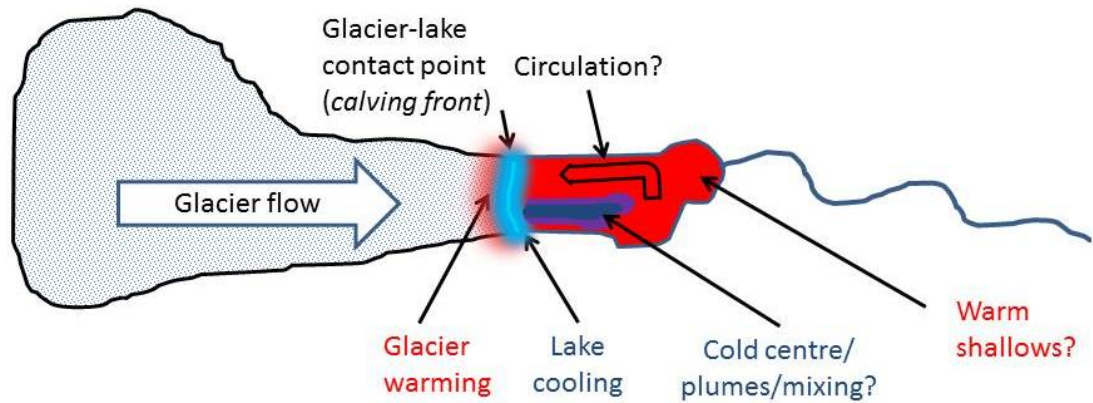


Figure 4.3 Schematic in plan view illustrating the working hypotheses of near surface water temperature patterns across a proglacial lake during the melt season. With warmer areas indicated in red.

Given that previous assumptions that iceberg melt may dominate the thermal regime of proglacial lakes and result in uniform  $1^{\circ}\text{C}$  temperatures, there now follows theoretical discussion of factors that may control the cooling influence of icebergs. Watson et al. (2020) observed a  $2^{\circ}\text{C}$  cooling of Thulagi proglacial lake skin surface temperatures following large ( $\sim 487,000 \text{ m}^3$ ) calving events and persisted for several months until temperatures returned to normal. The location of icebergs in the lake is also necessary to consider, as persistent katabatic winds may blow icebergs away from the glacier and near to the lake outlet (Warren and Kirkbride, 1998). This may result in meltwater from icebergs being rapidly exported from the lake due to proximity to the outlet, with minimal cooling influence on ambient lake temperatures. The spatial extent of the cooling influence from icebergs on ambient lake temperatures also requires consideration, as it is likely to scale with the volume and concentration of icebergs (tabular or multiple) (Warren and Kirkbride, 1998). The extent of iceberg cooling influence on ambient proglacial lake temperatures is spatially constrained in this study for the first time, using thermal infrared imagery.

The potential factors affecting proglacial lake surface temperatures discussed above are unlikely to be distributed uniformly in lakes that are large enough to have different microclimates and hydrological systems around them (Peter and Sommaruga, 2017). This is also likely to be highly controlled by topography, as shading will influence the amount of incoming direct solar radiation and therefore solar warming of the near surface water (Richards et al., 2012; O'Reilly et al., 2015; Peter and Sommaruga, 2017). The threshold in size required for a lake to develop different temperature patterns in the near surface waters is an open research question (personal communication with G.Kirillin, April 2019).

This study works towards the implementation of thermal infrared imagery for mapping the pattern of surface temperatures across a proglacial lake. This is a substantial advancement as it facilitates the pattern of lake surface temperatures to be mapped and relationship with surrounding thermal influences to be investigated. The overarching aim of this chapter is therefore to constrain the thermal structure across an Arctic proglacial lake, with particular focus on the influence of surface water temperatures on thermally eroded notch formation at an actively calving Arctic glacier terminus. The spatial pattern of proglacial lake surface temperatures are investigated over a period of several weeks.

The objectives addressed in this chapter are;

O6. Measure spatial pattern of surface temperature across a proglacial lake and analyse persistence over time.

i. Measure surface temperature spatial variations along the proglacial lake over time.

ii. Measure how surface temperature varies spatially around icebergs over time.

O7. Measure water surface temperatures directly at the glacier-lake contact point and analyse rates of change over time.

i. Measure how surface temperature varies across the glacier-lake contact point over time.

ii. Measure gradient in surface temperature towards the glacier-lake contact point over time.

## **4.2 Study Sites**

The study sites were located in Arctic Scandinavia in the region of Nordland (Norway) and Norrland (Sweden). The topography extends up to the highest point of northern Scandinavia (Kebnekaise, 2,113 m); with relief commonly of 1,000 m along the elevation axis that runs SW-NE through the study area on the Swedish side (Goodfellow et al., 2008). The climate varies across the study area, which is located on the boundary between the Arctic maritime climate of Norway to the west and the more continental climate of Sweden. The annual precipitation of 322 mm in Abisko and ~1,000mm at Tarfala (Goodfellow et al., 2008) reflects the marked gradient in precipitation across the study area from SW to NE. The Kebnekaise area is characterised by cirque glaciers whilst glaciers on the Norwegian side tend to be plateau icefields with outlet glaciers descending to lower locations. Glaciers in

both areas have been retreating since reaching the last maximum extent during the Little Ice Age (~1916) (Karlen, 1973; Paul and Andreassen, 2009).

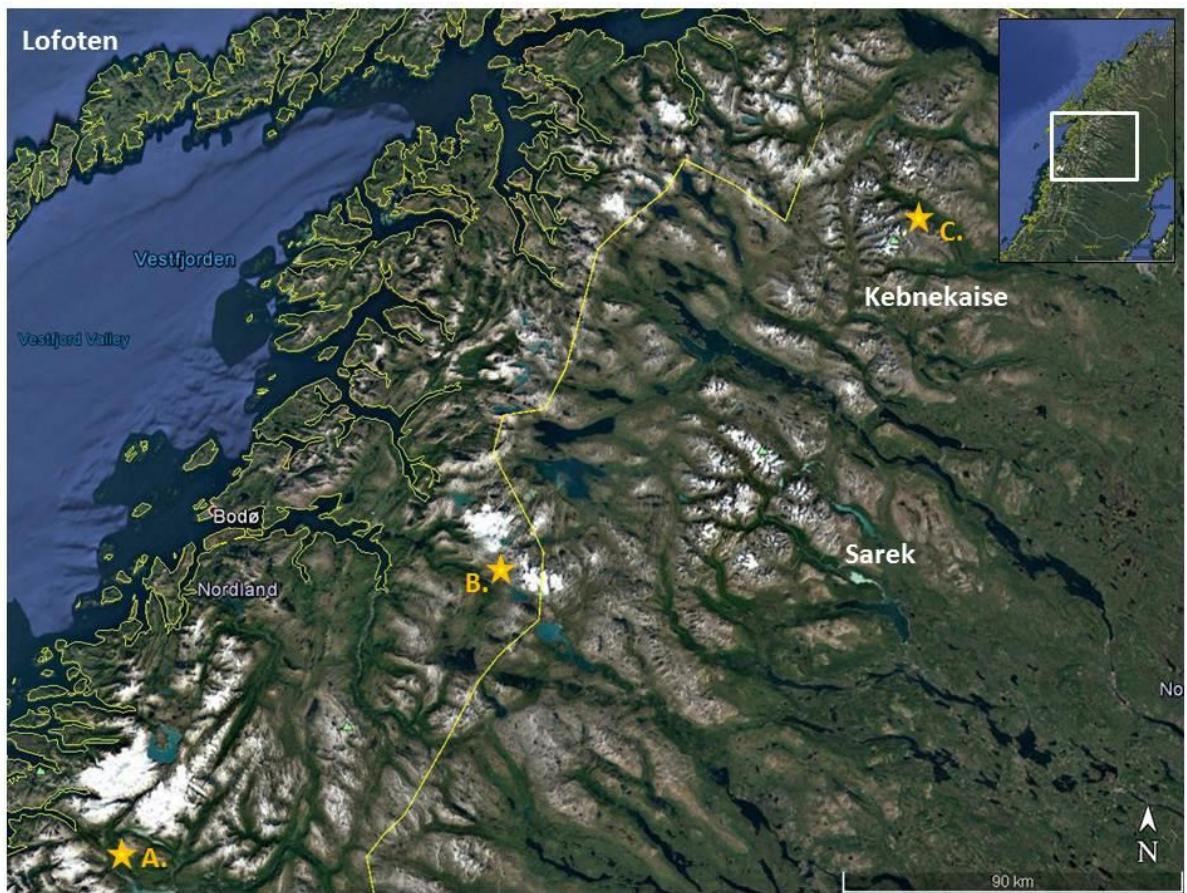


Figure 4.4 Location of study sites in Arctic Scandinavia; A. Austerdalsisen, Norway (66.517830°N, 14.088279°E) B. Blamansissen, Norway (67.230159°N, 16.149277° E) C. Kaskasapakteglaciaren, Sweden (67.954884°N, 18.561670°E).

The intended field site at Blamansissen had to be abandoned due to extensive snow and ice cover (~90%) on the approach on 10<sup>th</sup> July 2017, following the unseasonably cold and snowy spring of 2017 (see Meteorology section) (Figure 4.4). Consequently a preliminary study was conducted on 17<sup>th</sup> July at Austerdalsisen, Norway (200m asl, N 66.517674°, E 14.088271°) in order to calibrate the thermal camera measurements with thermistor data at a glacial meltwater inlet into the proglacial lake (Figure 4.4). However, the results are not presented here as Austerdalsisen glacier had lost contact with the proglacial lake.

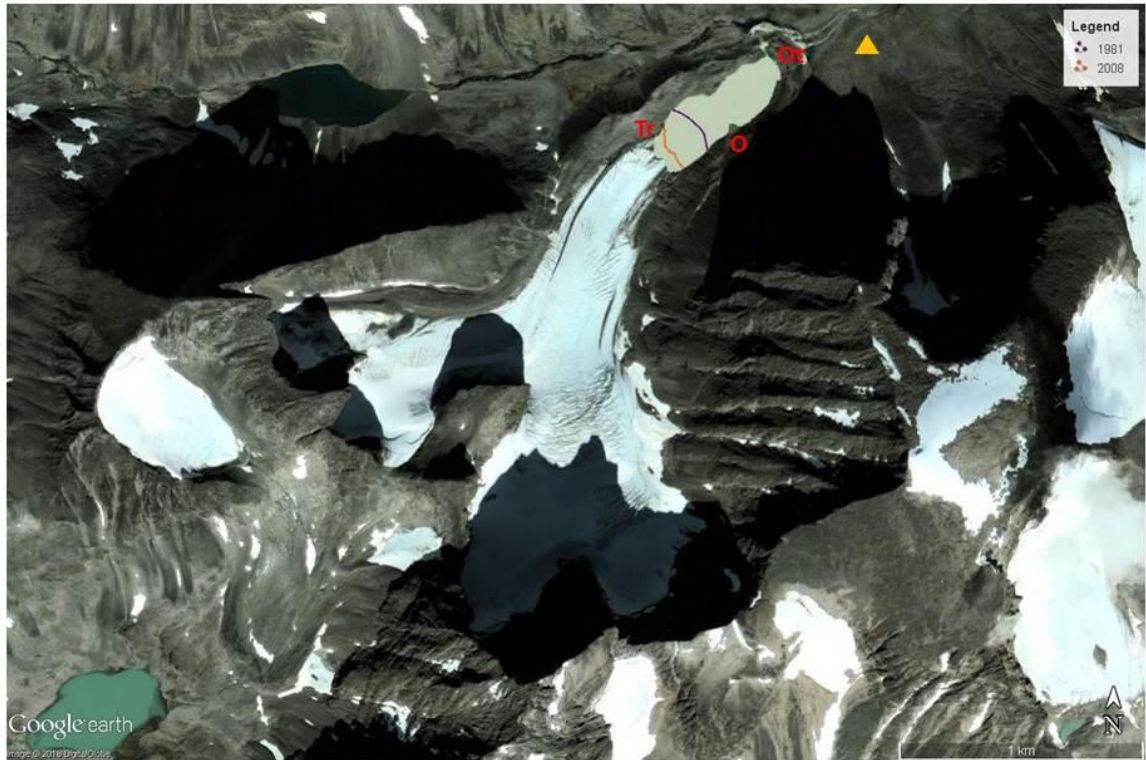


Figure 4.5 Satellite image (DigitalGlobe: 10/8/2013) of Kaskapakteglaciaren, with the peak of Norra Kaskasapakte (2,040 m) immediately to the south of the glacier (with ~500 m headwall). The previous terminus positions of 1981 (purple) mapped in Google Earth from aerial photo ([www.bolin.su.se](http://www.bolin.su.se)) and 2008 position mapped from the Swedish Lantmateriet orthophotos (September 2008). Tr = Terminus survey position. Ot = Outlet survey position. O = Owl's Nest position. Yellow triangle denotes the field camp.

The main body of fieldwork was conducted at Kaskapakteglaciaren proglacial lake (N 67.95721°, E 18.56109°) between 23<sup>rd</sup> July and 4<sup>th</sup> August 2017, with a second period of fieldwork from 29<sup>th</sup> July to 10<sup>th</sup> August 2019 (Figure 4.5). The glacier is situated in the Kebnekaise massif, with a ~500 m headwall at the southern margin and peaks of ~2,000 m to the east, south and west (Figure 4.5). The glacier flows from two main subsidiary carries into the main trunk, with a total length of ~2 km (Figure 4.5). The proglacial lake is situated at 1,100 m a.s.l. and was 670 m long, with a surface area of 132,172 m<sup>2</sup> in August 2014 (see Chapter 2 Results PGL<sub>ID</sub>24). A persistently high suspended sediment concentration was observed in the lake throughout the fieldwork and in any optical satellite imagery dating back to 2001. The proglacial lake has been expanding since the retreat of Kaskapakte glaciaren back from the Little Ice Age maximum position (~1916) (Karlen, 1973). There has been notable thinning of the glacier between 1981 and 2017 as well as ~200 m retreat of the terminus position during this period (see Figure 4.6 and Figure 4.7). The past terminus positions of Kaskapakteglaciaren were mapped from available satellite imagery and are discussed further in the next section.

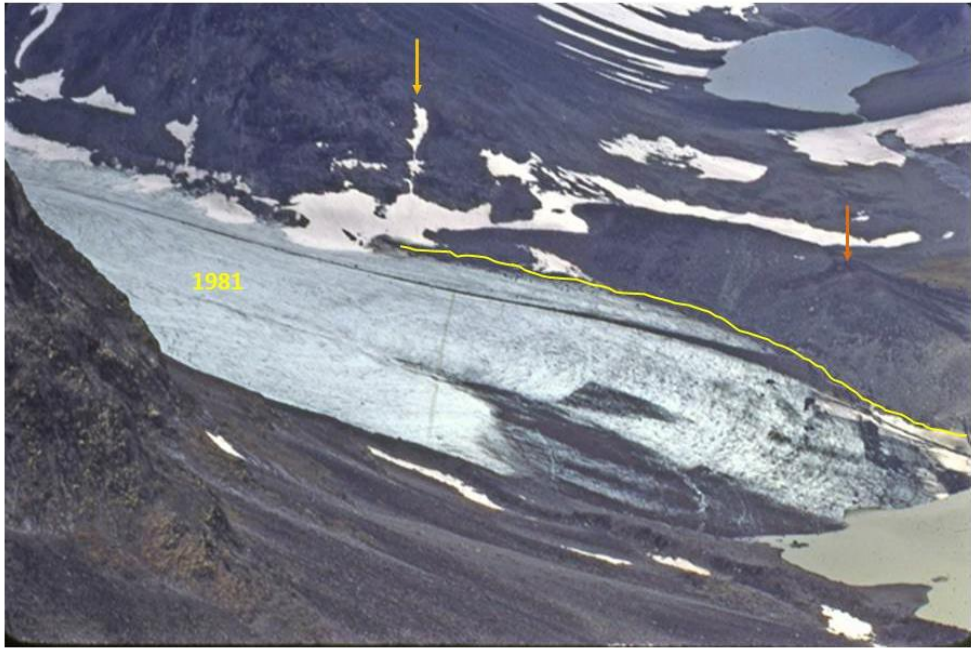


Figure 4.6 Aerial image of Kaskapakteglaciaren taken from a helicopter in 1981 ([www.bolin.su.se](http://www.bolin.su.se)). Note the general lack of a subaerial ice cliff at the terminus.

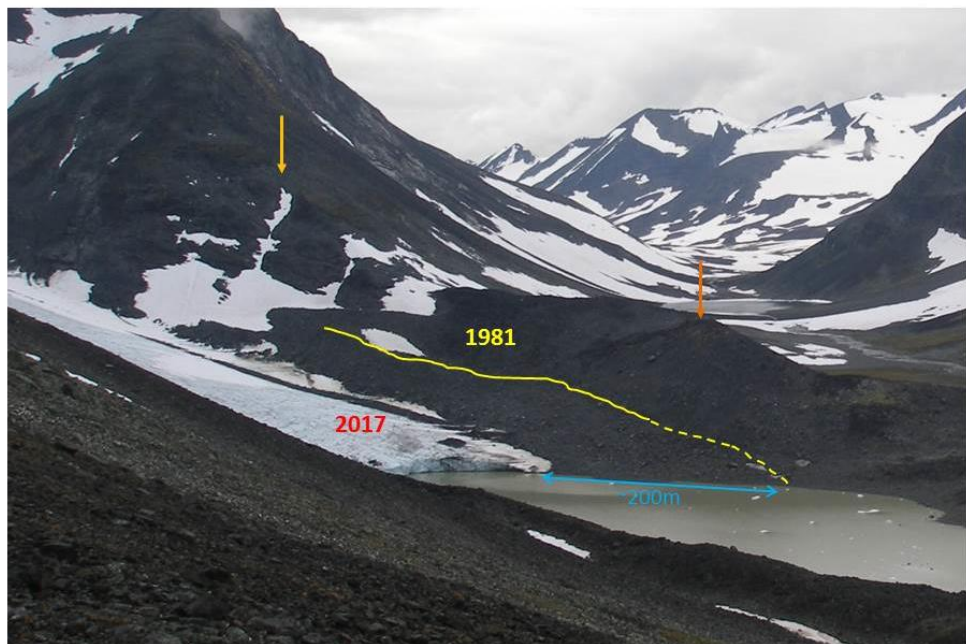


Figure 4.7 Image of Kaskapakteglaciaren taken from the slopes of Norra Kaskapakte on 4/8/2017. Note the thinning of the glacier terminus since the 1981 extent (yellow), with dashed line indicating low (<95%) confidence in exact glacier limit.

### 4.3 Methodology

The previous terminus positions of Kaskapakte glacier were mapped in ArcMAP using the available high resolution imagery (satellite and aerial) that could be obtained. A range of archives were searched for imagery with sufficiently low cloud and snow cover. An orthophoto (50 cm resolution) from September 2008 from the Swedish Lantmateriet had been purchased for a previous project. There were two Rapid Eye (5 m resolution) satellite images that were freely available from the Planet website ([www.planet.org](http://www.planet.org)), which were downloaded for July 2014 and September 2018. An imagery grant was obtained from the Digital Image Foundation for a satellite image (2 m resolution) for July 2016. A SPOT image (3 m resolution) was purchased for September 2017. These images were uploaded into ArcMAP and visually inspected for alignment between images (to detect geolocation error) before the terminus position was mapped as a polyline. This terminus position mapping was undertaken to ascertain the past retreat of Kaskapakteglaciaren and whether it was a good location for conducting fieldwork to investigate the influence of proglacial lake temperatures on glacier mass loss.

During a 2 week period from 23rd July to 4th August 2017 the change in glacier terminus geometry was monitored using a Ltl Acorn timelapse camera during fieldwork. This was positioned at A (Figure 4.5 and Figure 4.8) and programmed to capture images every minute. During this same period of fieldwork in 2017 the water temperatures of Kaskapakteglaciaren proglacial lake were investigated by a series of thermal infrared surveys (FLIR A65), combined with thermistor surveys from a remote controlled boat near the glacier terminus and near the lake outlet (sites Tr and Ot on Figure 4.5 and Figure 4.8). In situ Hobo thermistors were also installed near the glacier terminus and near the lake outlet (sites Tr and Ot on Figure 4.5 and Figure 4.8). A Campbell (CR800) automatic weather station was installed on the terminal moraine near the outlet of the lake (site Ot on Figure 4.5 and Figure 4.8) and a Kestrel 5500 was used for monitoring meteorological conditions during thermal infrared surveys. The survey sites are displayed in Figure 4.5 and Figure 4.8 and each method is further described in subsections below.

A second fieldwork campaign was conducted from 29<sup>th</sup> July to 10<sup>th</sup> August 2019 to measure proglacial lake temperatures at the calving front. Only limited results are presented here due to the relatively short time since completion of fieldwork. A 12 day temperature record is

presented from a HOBO UA-002-008 ( $\pm 0.5^{\circ}\text{C}$ ) placed at 1 m depth in proglacial lake water directly at the ice front during July and August 2019.

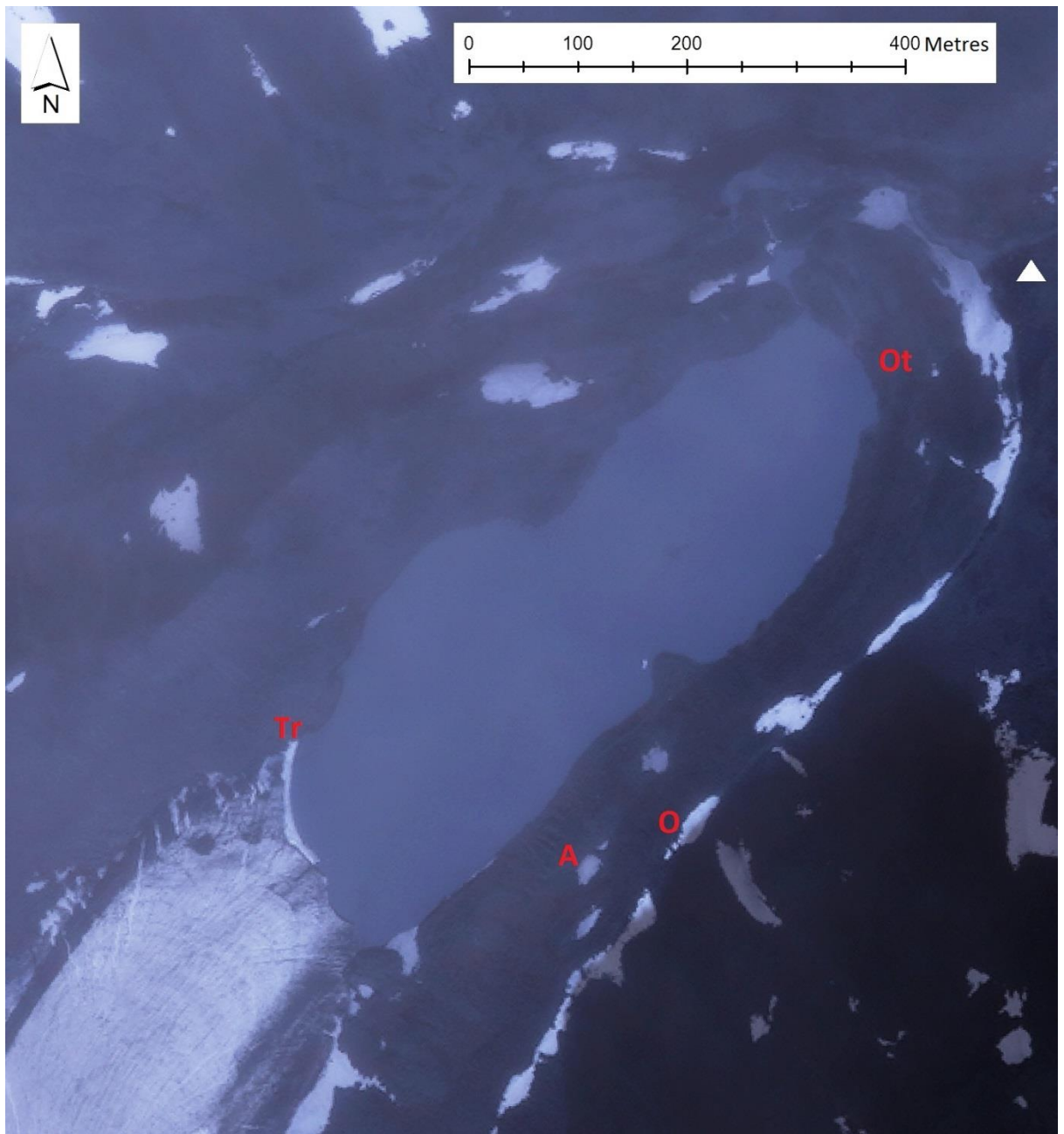


Figure 4.8 Satellite image (DigitalGlobe: July 2016) of Kaskapakte glacier, Arctic Sweden. Tr = Terminus survey position. Ot = Outlet survey position. O = Owl's Nest position. A = position of A10 Ltl Acorn (5210a) timelapse camera. White triangle denotes the field camp.

### 4.3.1 Meteorology

Air temperature, relative humidity, incoming solar radiation, wind speed and wind direction were measured using a Campbell CR800 Automatic Weather Station (AWS), which was installed on 24th July 2017 near the lake outlet (see Ot on Figure 4.8) (N  $67.95745^{\circ}$ , E

18.57486°, 1,114 m a.s.l.). Sensors measuring air temperature, relative humidity (CS215 RH and temperature sensor; +/- 0.4°C and +/- 2%), insolation (CS300 Solar radiation sensor; +/- 5%), wind speed and direction (05103-5 Young wind monitor; +/- 0.3 m s<sup>-1</sup> and +/- 0.3°), were mounted on a pole 1.5, 1.8 and 2 m above the ground respectively. On 24th July a validation was conducted between the Kestrel 5500 weather station and the Campbell CR800 weather station, by taking relative air humidity and air temperature measurements every 30 seconds for 15 minutes (Figure 4.9). The Kestrel 5500 was used for monitoring meteorological conditions, particularly air humidity, during thermal infrared surveys.

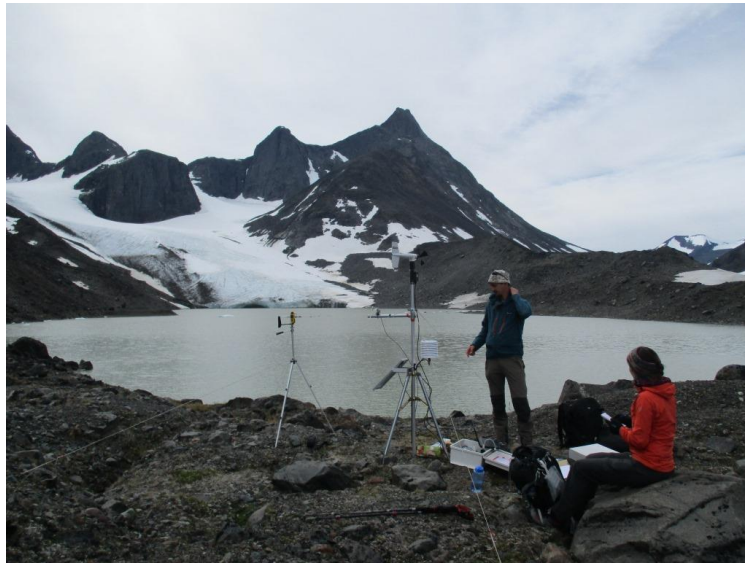


Figure 4.9 Validation of Kestrel 5500 with Campbell CR800 Automatic Weather Station (AWS) on 24/7/2017. Photo: Tom Sloan.

### 4.3.2 Lake Water Temperature and Light Intensity

The temperature of lake water was measured at the terminus of Kaskasapakteglaciaren (67.95721°N, 18.56109°E) and near to the outlet of the lake between 23rd July and 4th August 2017 (Figure 4.8). Hobo pendants (Onset, HOBO UA-002-08; resolution 0.14°C ; accuracy +/- 0.5°C) were used to measure and log temperature and light intensity (Lux), with weighting to counter their buoyancy. At both locations 1 Hobo thermistor was installed at 5 cm depth below the surface and another anchored 5 cm above the lake bed on the same line, which logged temperature data every 10 minutes for the duration of the fieldwork. The lower thermistor was anchored in water 50-80 cm deep (lake level was observed to vary ~30 cm during the period). All the temperature sensors were validated in water at different temperatures before and after the fieldwork at the University of Sheffield.



Figure 4.10 The remote controlled boat with HOBO thermistors that was used for surface temperature surveys. Note the weighting to maintain thermistor position. A further HOBO thermistor was installed on the boat deck to monitor air temperature during the survey. The boat is 40 cm long.

The spatial distribution of lake near surface temperatures was measured at the terminus and outlet using a remote controlled boat (RCB) that was operated from the shore (Figure 4.10). The near surface temperatures were measured every 30 seconds by Hobo pendant thermistors (Onset, HOBO UA-002-08; accuracy  $\pm 0.5^{\circ}\text{C}$ ), which were weighted on line to sit 5 cm below the surface on both sides and one from the front of the remote controlled boat (Figure 4.10). A further HOBO thermistor was weighted on line to sit 30 cm below the surface (Figure 4.10). One HOBO was installed on the RCB deck to measure air temperature and light intensity every 30 seconds (making 5 thermistors in total). Spatial position of the remote controlled boat was monitored using optical time lapse imagery every 30 seconds (see Figure 4.27 for boat survey routes). The remote controlled boat was then allowed to drift with the wind, in order to have more stable temperature readings and minimise disruption (mixing) of the near surface waters. It was found that trying to maintain the boat position proved problematic and required using the motor, which artificially induced water mixing as well as disrupting sensors and lead to erroneous temperature readings.

The light intensity data enables the thermistor data from the boat survey to be selected with high confidence in the quality control. The light intensity data show prominent spikes where thermistors have breached the surface of the water and become subject to higher light levels, as well as thermal contamination from background air temperature. A background light

intensity for the near surface waters was visibly denoted for each survey (Figure 4.11). The most stable thermistor readings were then selected to be plotted spatially (see red arrows in Figure 4.11). Where temperatures were consistent for 3 consecutive readings (every 30 seconds) the temperature was manually recorded into a spreadsheet. The selected temperature reading was then quality controlled against the other 4 thermistor data sets for each survey to check for agreement between sensors and eradicate anomalous readings.

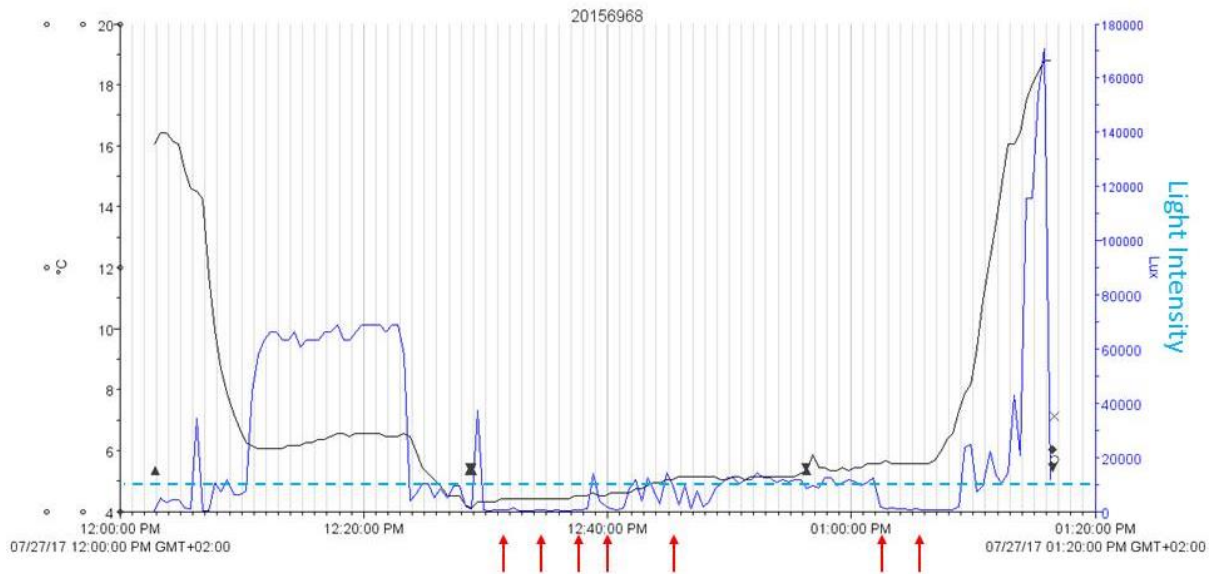


Figure 4.11 HOBO thermistor data (20156968) from the 27<sup>th</sup> July (midday) survey. Red arrows denote temperature readings that were selected for spatial plotting. The blue line denotes the background light level at 5 cm water depth during the survey, which shows some fluctuations.

The quality controlled temperature readings were then plotted in ArcMAP using the timelapse images to triangulate between prominent features (Figure 4.11), which were identified in the SPOT6 30/9/2017 image (multispectral pansharpened to 1.5 m) and Planet (3 m resolution) 25/7/2017 image. Note that the remote controlled boat was not stable enough to carry a GPS onboard, as previous tests led to capsizing. Where temperature readings were taken whilst the boat was drifting due to the wind, the horizontal extent of this temperature reading is plotted as a line for each temperature reading. The spatial positioning error for plotting the location of each temperature reading is plotted as a dashed circle (see Figure 4.31, Figure 4.32, Figure 4.33 and Figure 4.34). There is high confidence in the quality control of the remote control boat temperature surveys, as any occasions where the thermistor may have breached the surface are easily identified by a prominent spike in light intensity.



Figure 4.12 Timelapse image (GoPro Hero4) taken from the terminus survey position (Tr) showing prominent landforms used for triangulation and spatial plotting of temperature data. Note the large ice berg from the 26<sup>th</sup> July calving event, which is sitting directly in front of the section of terminus that it calved from (see Figure 4.18).

### 4.3.3 Lake Water Skin Surface Temperature (SST) from Thermal Infrared Surveys during Fieldwork in 2017

Thermal infrared sensors detect the emitted long wave radiation ( $7.5 \mu\text{m}$  to  $13 \mu\text{m}$ ) by the target surface (top 1 mm) and have been used to map radiant temperatures of glaciers and debris covered glaciers (Aubry-Wake et al., 2015; Kraaijenbrink et al., 2018). The radiant temperature of objects is also referred to as the ‘skin surface’ temperature, as it relates to the radiation emitted by the top  $\sim 1$  mm of the object (Aubdry-Wake et al., 2015). The use of thermal imagery to detect surface skin surface temperature (SST) of water bodies is discussed in more detail in Chapter 3 (section 3.2). It is critical to constrain the emissivity of the target, as knowing the efficiency that radiation is emitted by a body can enable the body temperature to be calculated using Stefan-Boltzmann’s law (Kraaijenbrink et al., 2018);

$$T_s = \sqrt[4]{\frac{\sigma T_{rad}^4 - (1-\varepsilon)LW_{\downarrow}}{\varepsilon\sigma}} \quad (6)$$

Where  $T_s$  is the surface temperature (K),  $T_{rad}$  the radiant temperature (or skin surface temperature),  $\varepsilon$  the emissivity,  $\sigma$  the Stefan Boltzmann constant ( $5.67 \times 10^{-8}$ ) and  $LW_{\downarrow}$  the incoming longwave radiation ( $W m^{-2}$ ). The incoming longwave radiation will therefore affect the relationship between skin surface temperature and body temperature of the object, with the difference between the two likely to vary depending on solar and meteorological conditions (Aubry-Wake et al., 2015; Kraaijenbrink et al., 2018). Whilst the emissivity of water is relatively well constrained (0.97 to 0.98), the atmospheric transmissivity over water bodies is more problematic and can lead to attenuation of incoming longwave radiation (Aubry-Wake et al., 2015). This is particularly salient as solar warming can increase rates of surface evaporation from water bodies and lead to attenuation of radiation between the target and the thermal infrared sensor (Aubry-Wake et al., 2015).

A further problem of utilising thermal infrared imagery to detect the skin surface temperature (SST) of water bodies, is that the reflection of long wave radiation from surrounding mountain sides can result in erroneous readings from the water surface (Aubry-Wake et al., 2015). This study starts to address these challenges through night time infrared surveys at maximum possible angles to the target ( $\sim 20^\circ$ ) from a ground based survey to capture ambient water skin surface temperature. Essentially aiming to capture temperature of the water during the period (nighttime) when surface temperatures are most stable; rather than capturing spatially isolated temperature from short term (hours) solar warming or reflection from surrounding mountainsides during the daytime.

The spatial pattern of lake water skin surface temperature (SST) was measured using a FLIR A65 thermal infrared camera every 30 seconds during surveys, with the camera mounted on a tripod in an elevated position looking at the glacier terminus or icebergs (Figure 4.13). The uncooled microbolometer sensor of the FLIR A65 has a resolution of 640 x 512 pixels and performs automatic calibrations based on the internal temperature of the shutter. A further calibration with black bodies is to be conducted by the NERC Field Spectroscopy Facility. An emissivity of 0.97 for water was used (ASTER spectral library, Gillespie et al., 1998) with atmospheric temperature and relative humidity inputted from measurements with the

Kestrel 5500 Automatic Weather Station, in order to calibrate the thermal imagery focus spot temperature for atmospheric transmissivity (Figure 4.25).



Figure 4.13 Conducting a preliminary thermal infrared survey from ‘Owl’s nest’ position on the eastern lateral moraine with FLIR A65 thermal camera (see 0Figure 4.8 for location). Photo: Tom Sloan (24/7/2017).

#### **4.3.4 Lake Water Temperature During Fieldwork in 2019**

A second field campaign was undertaken at Kaskapakteglaciaren from 29<sup>th</sup> July until 10<sup>th</sup> August 2019 to measure proglacial lake temperatures at the calving front. It was possible to access the top of the calving front directly via a wide section of stable ice on the western side of the terminus, although a relatively safe (~5 m) distance was kept from the top of the ice cliff. It was possible to cast out two Hobo pendant thermistors (Onset, HOBO UA-002-08; accuracy +/- 0.5°C) set at 1 m and 2 m depth below an inflatable buoy on a section of rope (Figure 4.14). The rope was anchored to rocks at the top of the ice cliff. A series of Automated Surface Vessel (ASV) surveys with a HOBO Temperature Pro V2 (+/-0.2°C) were conducted in conjunction with sonar surveys (Garmin Chirp Echosounder 45cv) of the ice front, but the results are not presented here due to incomplete analysis.



Figure 4.14 A GoPro (Hero4) image of Kaskapakteglaciaren terminus taken from an ASV survey on the proglacial lake at on 6/8/2019. The red Cressi buoy (~50cm tall above water) had two Hobo pendant thermistors (UA-002-08) suspended at 1 m and 2 m depth in the water underneath. Note the lake shore visible in the right side of the image.

## 4.4 Results

### 4.4.1 Mapping of Kaskapakteglaciaren Past Terminus Positions

Kaskapakteglaciaren has terminated in a lake terminating since at least 1959 (Figure 4.15). The proglacial lake (PGL<sub>ID24</sub>) expanded from 56,779 m<sup>2</sup> in 1959 to 132,172 m<sup>2</sup> in 2014 (132.8% increase) (Chapter 2 Section 2.3.5), with a centreline retreat of ~350 m (6.36 ma<sup>-1</sup>) during this period. There is also substantial thinning of Kaskapakteglaciaren between 1959 to 2014, such that the width of the glacier in 1959 was 365 m at the future 2014 position of the terminus, which was only 189 m giving an overall narrowing of 176 m. An area of 103,900.86 m<sup>2</sup> of ice was lost at Kaskapakte terminus during this period, giving a width averaged annual retreat rate of 5.17 m a<sup>-1</sup> (using 1959 terminus width) (Figure 4.15). The centreline retreat of Kaskapakte glacier between 1959 and 2018 was ~444 m, giving an average annual retreat rate of 7.53 m a<sup>-1</sup> (Figure 4.15).

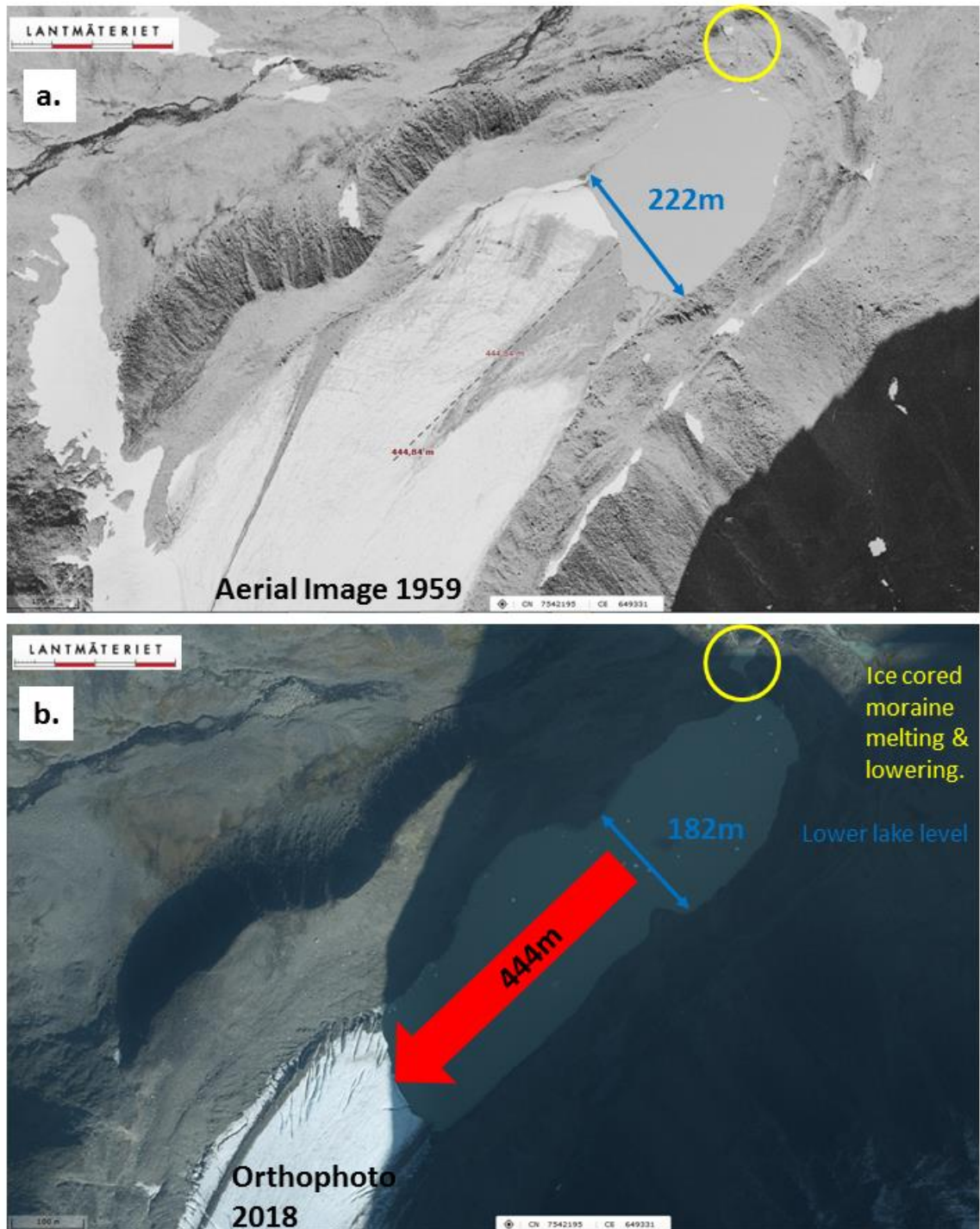


Figure 4.15 a. Aerial image (Lantmateriet, 1959) of Kaskapakteglaciaren (Sweden) showing 1959 proglacial lake width (blue arrow). Spatial resolution is unknown but estimated ~1 m. Yellow circle indicates area of small pond development in 2018 Orthophoto (scale is in lower left hand corner) b. Orthophoto from Swedish Lantmateriet (2018) showing 2018 proglacial lake width (blue arrow). Yellow circle indicates area where a pond has developed, interpreted as being due to ice cored moraine melt and lowering (Ostrem, 1964). Red arrow indicates retreat of terminus between 1959 and 2018. Glacier terminus was ~190 m wide in 2018.

The centreline retreat of Kaskapakte glacier between 2008 and 2018 was ~150 m, giving an average annual retreat rate of 15 m a<sup>-1</sup> (Figure 4.16). The terminus positions of Kaskapakteglaciaren were mapped from high resolution satellite imagery from September 2008, July 2014, July 2016, September 2017 and September 2018 (Figure 4.16). Unfortunately due to the different timings of available imagery through the melt season it is not possible to calculate the precise annual retreat rates that are truly representative for each year. The area (8,436.77 m<sup>2</sup>) of ice loss between July 2016 and 30<sup>th</sup> September 2017 was equivalent to 0.55% of the glacier area in the Randolph Glacier Inventory 2008, although note that this is effectively the area of ice lost over two melt seasons. Also note that there are several embayments in the terminus geometry, which are at slightly different locations each year, with a large embayment at the south east side of the September 2017 terminus position (Figure 4.16).

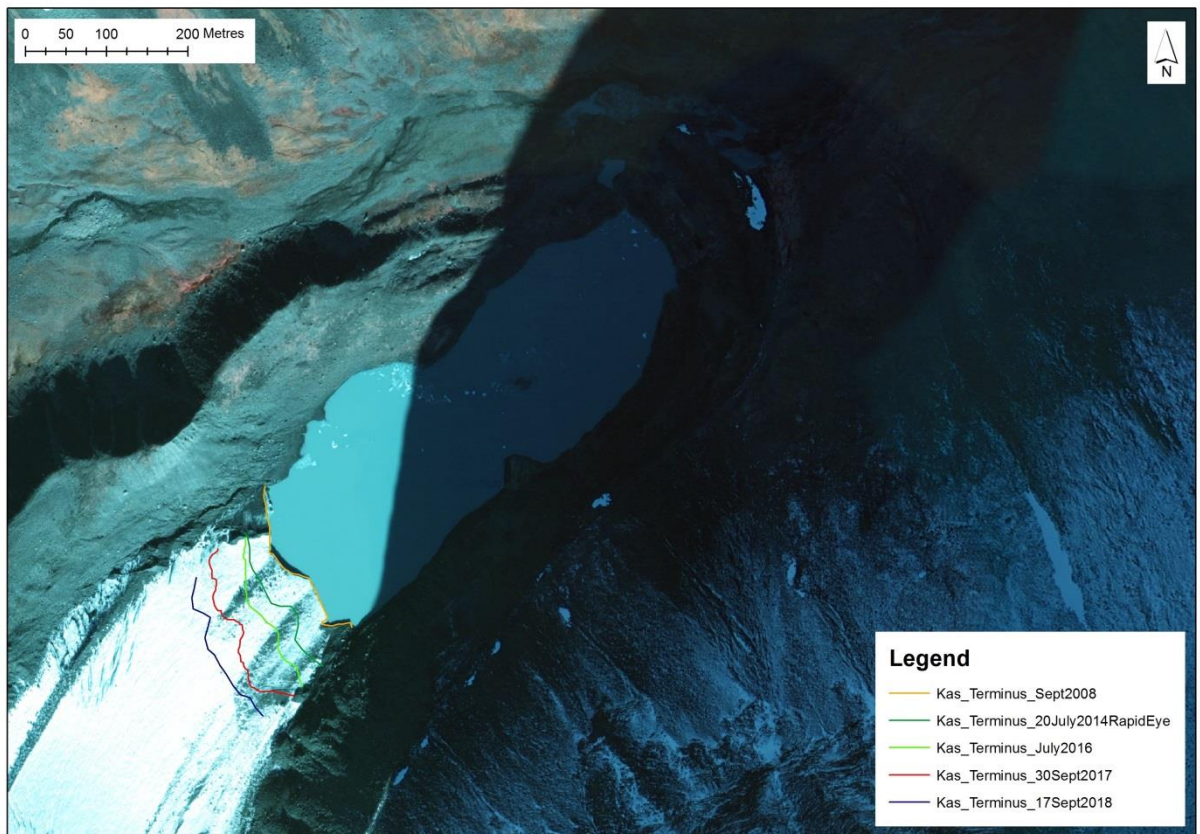


Figure 4.16 Kaskapakte glacier and proglacial lake, Arctic Sweden. Previous terminus positions have been mapped from satellite imagery from July 2014 (dark green: Rapid Eye), July 2016 (light green: Digital Globe), September 2017 (red: SPOT) and September 2018 (purple: Rapid Eye).

#### 4.4.2 Kaskapakte Terminus Geometry Change during Fieldwork in 2017

The terminus of Kaskapakte glacier had a varied geometry across the ~200 m width of the terminus on 25<sup>th</sup> July 2017 (Figure 4.17). There was a small embayment on the left hand (east) side of the terminus, with crevasses running roughly south west from the glacier front (see red box Figure 4.17). In the central section of this embayment there was a small cave feature just visible above the waterline, with a substantial section of overhanging ice at the waterline to the right (west) of this cave feature (Figure 4.17). The central section of the terminus was dominated by a large (~50 m wide) cave feature, with some limited shadowing at the waterline suggesting a slight undercut in the ice. The right hand (western) section of the terminus did not have any caves, but had an embayment shape and substantial shadowing at the waterline indicated the presence of a thermally eroded notch (see ‘Thermal notch’ Figure 4.17).

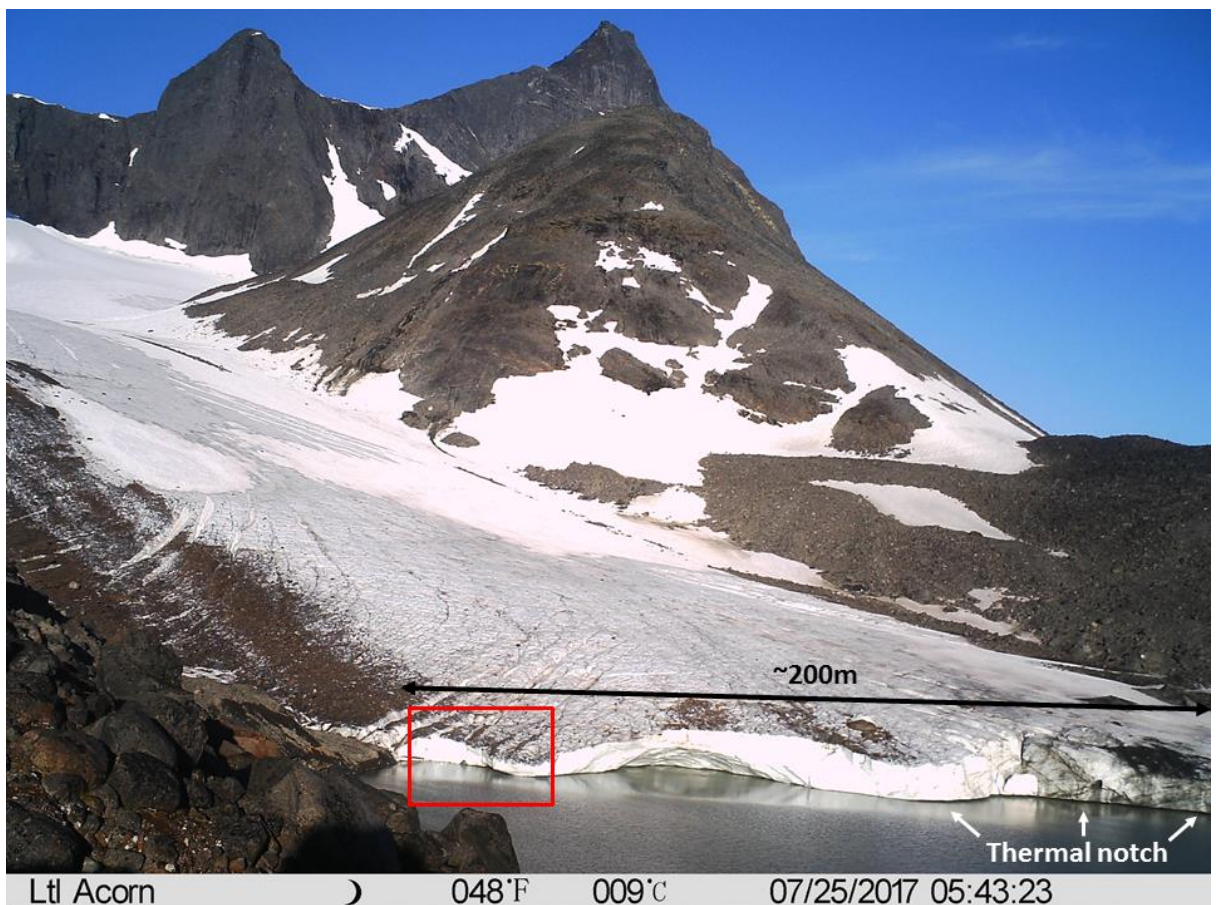


Figure 4.17 Image of Kaskapakte glacier (looking south west) taken from Ltl Acorn 5210a camera (marked A10 on Figure 4.8) taken at 5:43:23am on 25/7/2017.

During the field work in 2017 a series of calving events were observed and heard from the field camp, although not all of them were captured in time lapse imagery. Two examples are

described below, which give an indication of some of the processes of mass loss acting at the ice front. The first calving event occurred at 4:20am on 26/7/2017, when a section of the ice front in the eastern embayment collapsed (see red box Figure 4.18). The right hand section was visibly overhanging above the waterline with a short wall above this notch prior to the 4:20am calving event (see top image Figure 4.18). Following the 4:20am calving event (bottom image Figure 4.18) an overhanging cave had developed around the initially small portal, with numerous small icebergs surrounding it and waves visibly emanating out on the lake surface (Figure 4.18).

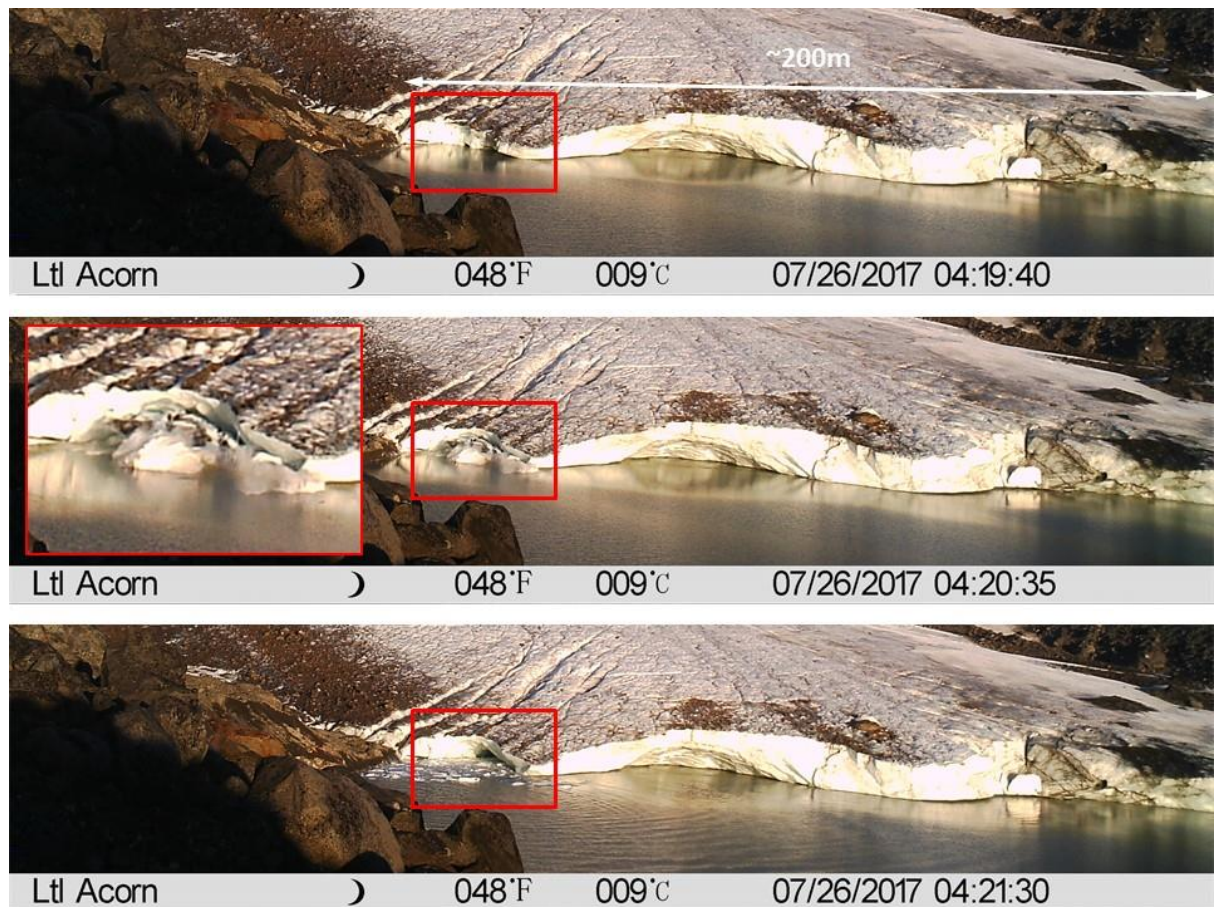


Figure 4.18 Images of Kaskapakte glacier (looking south west) taken from Ltl Acorn 5210a camera (marked A10 on Figure 4.8) taken on 26/7/2017 at 4:19:40am (top), 4:20:35am (middle) and 4:21:30am (bottom).

The next calving event captured in the time lapse imagery occurred on the right hand (west) side of the glacier terminus (Figure 4.19). At 9:40am a section of the subaerial ice cliff collapsed above a thermally eroded notch (Figure 4.19). This event produced 1 large iceberg and several smaller icebergs, whilst numerous small icebergs were also produced from the roof of the central cave in the same period (1 minute) (Figure 4.19).

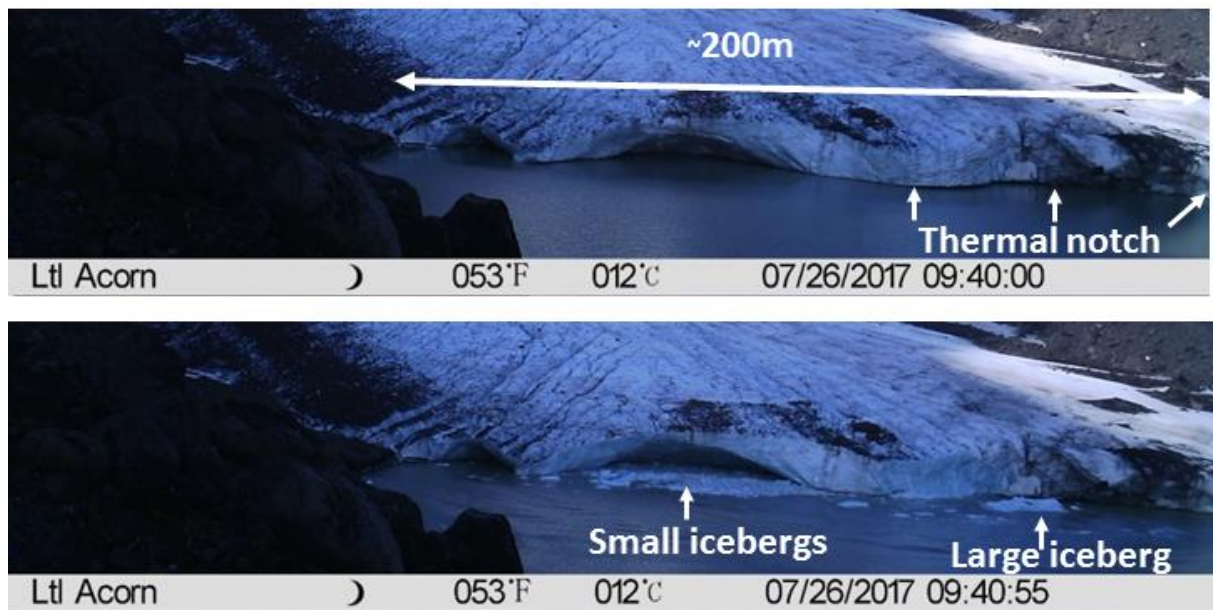


Figure 4.19 Images of Kaskapakte glacier (looking south west) taken from Ltl Acorn 5210a camera (marked A10 on Figure 4.8) taken on 26/7/2017 at 9:40:00AM (top), 9:40:55 (bottom). Note the lack of visible thermal notch above the waterline where the large iceberg calved off.

The calving of the large iceberg in the 9:40am event on 26/7/2017 resulted in no overhanging notch being visible above the waterline on this section of the western terminus (Figure 4.19). A period of inclement weather followed, during which time heavy rainfall was observed and the lake level near the outlet was observed to have risen ~30 cm. Fieldwork resumed following this period of inclement weather and a remote controlled boat survey was conducted along the western section of the terminus, although the time lapse camera failed during this period. The lake level was observed to lower following cessation of the rainfall and GoPro (Hero4) imagery was taken in close proximity to the glacier terminus on 4<sup>th</sup> August 2017 (Figure 4.20). A thermally eroded notch was visible on the glacier just above the waterline, with a sharp boundary that extended the full width of the glacier terminus (Figure 4.20). The extent of the overhang in the thermal notch was not investigated; due to likely failure of the remote controlled boat (battery compartment is situated on top with no waterproofing).



Figure 4.20 Image from GoPro Hero4 camera from remote controlled boat survey of Kaskapakte glacier, Arctic Sweden (A.Dye, 4/8/2017). Note the thermally eroded notch shadow extending along the glacier terminus at the water to ice contact point. The height of the subaerial ice cliff is estimated to be ~5 m.

#### 4.4.3 Meteorology during 2017 fieldwork

The first week of field investigations was characterised by largely clear sky conditions and light winds, with predominantly katabatic winds blowing off from the glacier and along the lake. In contrast the second week was initially characterised by heavy rainfall, low cloud and strong winds predominantly from the south west (also blowing off of the glacier and along the lake). The change in the weather pattern is clearly visible in the air temperature (Figure 4.21) and solar radiation data (Figure 4.22) from the Campbell automatic weather station data at the outlet survey point.

The first period of fieldwork was marked by strong peaks in air temperature of ~14°C (25<sup>th</sup> July), ~16°C (26<sup>th</sup> July), ~15°C (27<sup>th</sup> and 28<sup>th</sup> July) before reaching a maximum of 16.39°C (29<sup>th</sup> July) (Figure 4.210). Night time minimums of ~8°C occur throughout this period (Figure 4.210). The deterioration in weather after the 30<sup>th</sup> July is evident in the day time maximums remaining at or below 10°C and mostly fluctuating between 6 to 9°C, with a

minimum of 5.29°C on 3<sup>rd</sup> August (Figure 4.21). The incoming solar radiation followed a similar pattern during the 2 weeks, with the start of the period marked by strong diurnal cycles and daytime maximum peaks of around 0.7 Kw/m<sup>2</sup> with an overall maximum of 0.8 Kw/m<sup>2</sup> on 27<sup>th</sup> July (Figure 4.22). The following week was marked by notably lower levels of solar radiation, with daytime peaks rarely exceeding 0.2 Kw/m<sup>2</sup> from the 30<sup>th</sup> July until 1<sup>st</sup> August and can be confirmed from observations at basecamp (Figure 4.22). During this period relative air humidity remained above 80%, including several noticeably prolonged periods where it reached 100%. This was quite a contrast to the preceding period, when relative air humidity had rarely exceeded 80%. The 2<sup>nd</sup> and 3<sup>rd</sup> August were thankfully characterised by higher levels of solar radiation, with a daytime peaks of 0.45 Kw/m<sup>2</sup> and 0.64 Kw/m<sup>2</sup> respectively (Figure 4.22). Note that whilst there was 24 hour daylight, incoming solar radiation readings from the AWS reached 0 Kw/m<sup>2</sup> around midnight throughout the duration of fieldwork (Figure 4.22).

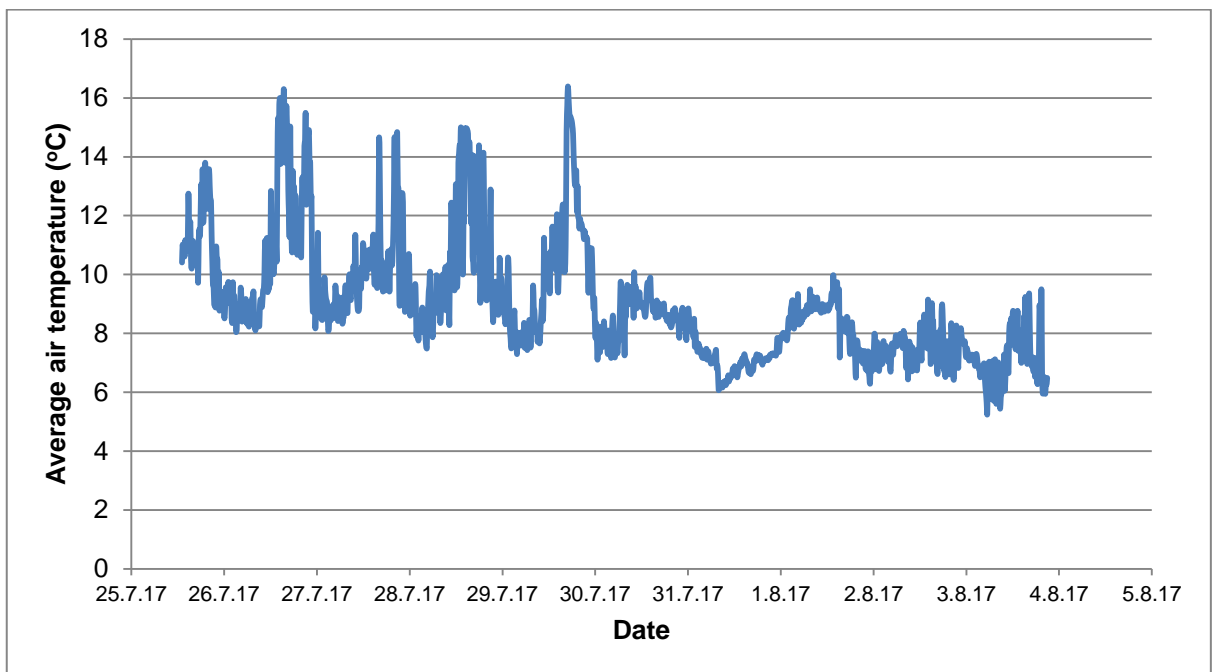


Figure 4.21 Record of air temperature from the CR800 Campbell Automatic Weather Station (AWS) installed at the outlet survey position.

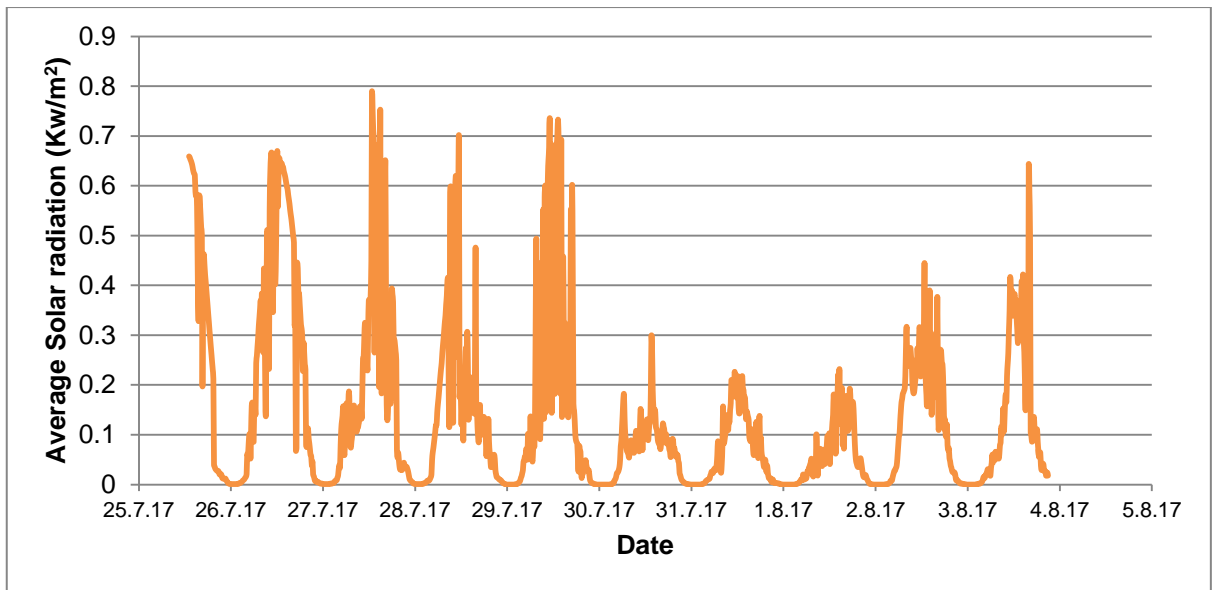


Figure 4.22 Record of average incoming solar radiation from the CR800 Campbell Automatic Weather Station (AWS) installed at the outlet survey position.

During the second week conducting field investigations became highly problematic in inclement meteorological conditions, with high rainfall and high stream levels, which resulted in a sparsity of data during the second week.

#### 4.4.4 Outlet Lake Water in situ Temperature during Fieldwork in 2017

A string of 2 HOBO thermistors were initially installed on the western bank of the lake near the outlet at ~50 cm and ~5 cm depth. However, on installation it became evident that the lake bed consisted of large boulders. The thermistor string was extracted from this initial position, as the bouldery nature was likely not representative of the wider lake bed and may result in different temperature readings from the ambient lake temperature. The particularly high spike in light intensity of 140,000 lux recorded by the HOBO thermistor sensor (serial number 20108328) at ~5 cm depth also suggests that the sensor is likely to have breached the water surface. The temperature data from 24<sup>th</sup> and 25<sup>th</sup> July at the outlet is therefore discarded.

The thermistor string was re-installed at 12:08 am on 26<sup>th</sup> July at the outlet survey position (67.95735°N, 18.57442°E) with time lapse camera to monitor the water surface conditions (Figure 4.8). A lake water temperature of 5.2°C is observed at both ~5 cm depth and ~50 cm depth from 12:19am until 12:49am (Figure 4.23). The lake water temperature then cools steadily at both depths until it reaches 4.7°C (6:39am) at ~5 cm depth and 4.6°C (7:19am) at

~50 cm depth, (Figure 4.23). Light intensity at 5 cm depth is low (<1,050 lux) until it begins to increase to 1,808 lux (06:49am) on 26<sup>th</sup> July (Figure 4.23).

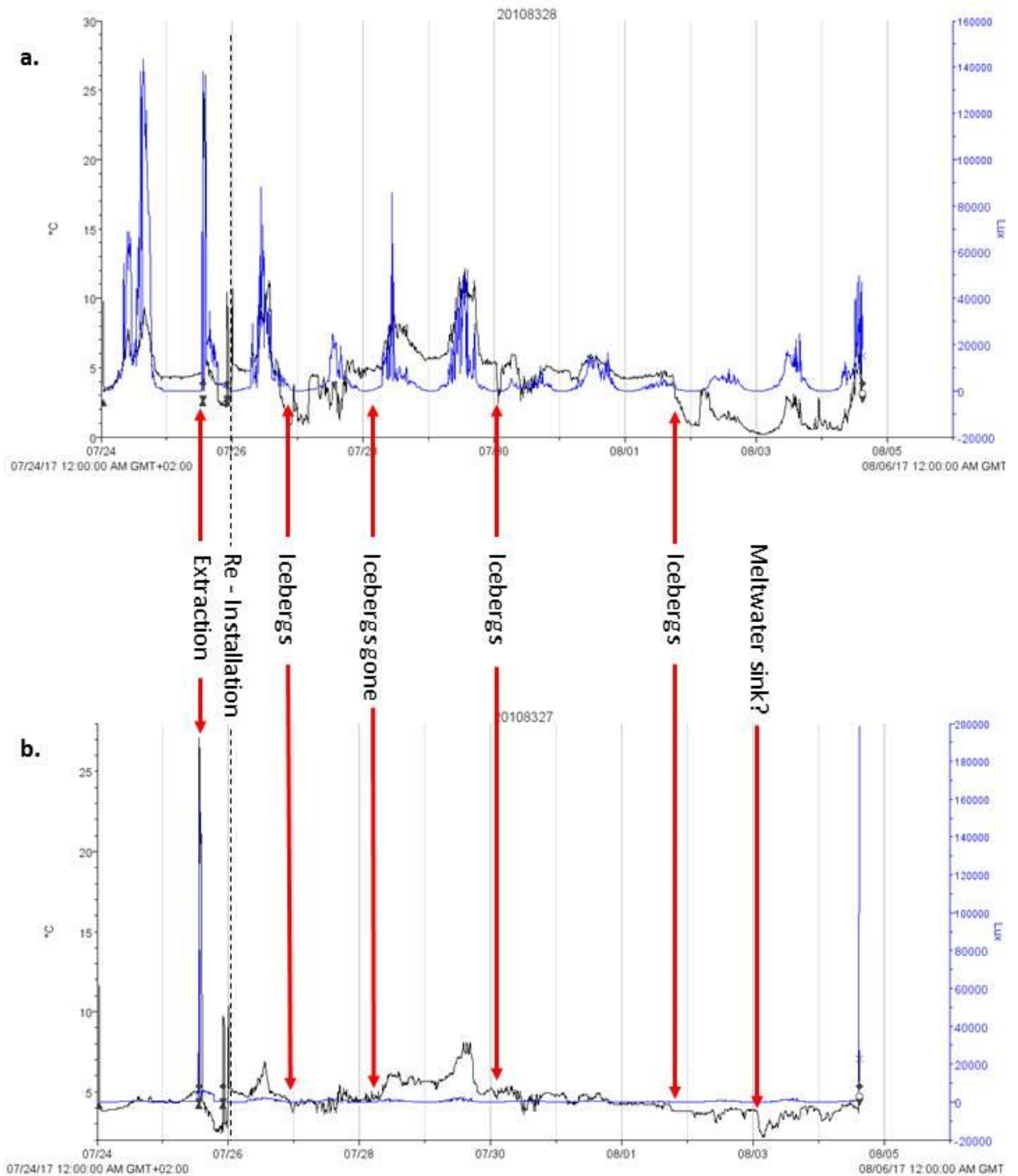


Figure 4.23 Temperature data (black) and light intensity data (blue) from HOBO thermistors situated at **a.** ~5 cm depth (sensor 20108328) and **b.** ~50 cm depth (sensor 20108327) at the outlet (Ot) survey position (67.95735°N, 18.57442°E). Note the temperature and light intensity spikes on 24/7/2017, 25/7/2017 and 4/8/2017 are due to installation/extraction of the sensors.

A substantial and rapid increase in light intensity then occurs to reach 28,933 lux (07:29am) before falling to 3,100 lux (07:39am) (likely due to clouds clearing) (Figure 4.23). There is a further rapid increase to 88,178 lux (10:29am) and remains above 10,000 Lux until it drops to 5,166 at 2:29pm on 26<sup>th</sup> July (Figure 4.23). During this period the water temperature at ~5 cm depth follows a notably similar pattern, rapidly rising to 9.0°C (10:39am) before reaching a peak of 11.2°C (1:39pm) then rapidly decreasing from 9.1°C (2:09pm) to 4.3°C at 3:39pm on 26<sup>th</sup> July (Figure 4.23). Note the lag in time between the peak of the light intensity at 10:29am and the peak in temperature at 1:39pm, likely due to the time required to heat up the near surface waters (rather than direct solar heating of the sensor which would occur within minutes) (Figure 4.23). Furthermore, the light intensity levels at ~50 cm depth remain below 2,000 lux during this period (Figure 4.23). The water temperature at ~50 cm depth increases steadily to reach a maximum temperature of 6.8°C (1:19am) before decreasing to 5.0°C (2:59pm) and again from 4.5°C (9:48pm) to 3.7°C (11:28pm) on 26<sup>th</sup> July (Figure 4.23).

The time lapse imagery video reveals the arrival of icebergs during the afternoon and evening of 26<sup>th</sup> July, which coincides with a strong cooling trend at ~5 cm depth and minimum of 0.9°C at 9:09pm (Figure 4.23). This is followed by a period of large fluctuations between 1.2°C and 5.5°C (likely due to iceberg movement away from the sensor) until the morning of 28<sup>th</sup> July, when the icebergs had fully melted (Figure 4.23). Strong diurnal patterns of daytime warming and night time cooling (down to ~5°C) are particularly evident at ~5 cm depth on the 28<sup>th</sup> and 29<sup>th</sup> July (Figure 4.23). Note that at ~50 cm depth there is a warming trend (to ~5°C) on 28<sup>th</sup> July, with a prominent peak of 8.0°C before cooling to ~5°C during 29<sup>th</sup> July (Figure 4.23). It is vital to note that light intensity remains minimal (<1,000 lux) at ~50 cm depth during this period, whilst turbidity was observed visually to remain high throughout (Figure 4.23). The remaining time between 30<sup>th</sup> July to 4<sup>th</sup> August 2017 was characterised by inclement weather with periods of heavy rainfall. There were extensive clouds during this period with low incoming solar radiation, with light intensity at ~5 cm depth remaining below 2,000 lux until 3<sup>rd</sup> August (Figure 4.23). This period was characterised by a series of calving events, with the dominant south westerly air flow exporting icebergs relatively efficiently to the lake outlet survey position as revealed in time lapse video. There is a period of cooling at ~5 cm depth during 30<sup>th</sup> July, followed by a slight increase (to ~5°C) during 31<sup>st</sup> July (Figure 4.23). A similar pattern occurs at ~50 cm depth, although note that there is a lag in troughs and peaks of temperature compared to ~5 cm

depth (Figure 4.23). During this period light intensity levels at ~50 cm depth remained minimal at below 1,000 lux (Figure 4.23).

A large calving event occurred during 1<sup>st</sup> August, which resulted in a large volume of icebergs being exported to the outlet area of the lake and captured in time lapse video. Following this event there is a rapid cooling of water temperature at ~5 cm depth from 4.5°C (5:19pm) to 2.8°C (6:19pm), then a slower cooling trend to 0.8°C at 2:19am on 2<sup>nd</sup> August (Figure 4.23). There is then a rapid increase to 3.4°C at 4:49am before a further rapid decrease to 1.2°C (9:39am), then a period of small fluctuations before water temperature slowly decreases to an overall minimum of 0.2°C at 1:19am on 3<sup>rd</sup> August (Figure 4.23). During this period water temperatures at ~50 cm depth remain relatively stable, with small fluctuations between 4.2°C and 3.0°C, followed by a rapid decrease from 3.8°C (1:28am) to an overall minimum of 2.2°C at 3:48am on 3<sup>rd</sup> August. This is a particularly prominent trough in water temperatures at ~50 cm, which occurs at a similar time to visibly high rates in iceberg melting in the time lapse imagery (Figure 4.23). Following this water temperatures at ~50 cm depth steadily increase (with some fluctuations) until reaching 4.2°C at 12:18pm on 4<sup>th</sup> August. In contrast water temperatures at ~5 cm depth fluctuate strongly during this period and follow a similar pattern to light intensity, although there is a prominent spike of 2.8°C at 10:29pm (likely associated with iceberg movement) and then rapid increase to 5.2°C (1:29pm) shortly before extraction on 4<sup>th</sup> August (Figure 4.23).

#### **4.4.5 Outlet Lake Water Spatial Temperature Survey**

The arrival of icebergs at the outlet survey position during the 26<sup>th</sup> July disrupted the diurnal cycle of daytime warming and night time cooling observed in the dataset before this point (Figure 4.23). A spatial temperature survey was conducted using remote controlled boat and thermal infrared camera (FLIR A65) at the outlet survey point on 27<sup>th</sup> July to constrain the extent of meltwater emanating from the iceberg melt (Figure 4.24 and Figure 4.25).

The FLIR thermal image taken at 10:46pm shows the horizontal extent of cold meltwater emanating from the icebergs was relatively minimal at the surface (Figure 4.25). As the wind speeds dropped from 0.01 m<sup>s</sup> (10:35pm) to 0.005 m<sup>s</sup> (11:15pm) the horizontal extent of the cold meltwater at the surface increased, as is visible in the following sequence of images at 10:55pm (Figure 4.25b), 11:00pm (Figure 4.25c) and 11:10pm (Figure 4.25d). The presence

of the cold water boundary is clearly visible in the infrared imagery and is confirmed by the remote controlled boat thermistor readings at ~5cm depth, with 2.4°C next to the icebergs initially (Figure 4.25a) and 3.9°C where the cold meltwater limit has just extended to (Figure 4.25b). The ambient lake water temperature is captured well at 11:00pm with thermistor readings of 5.0°C at ~5cm depth and ~30cm depth. Note that the temperature readings at ~50cm depth are higher (3.9°C) on the horizontal boundary of the cold water (Figure 4.25b) and also when the boat returns to the middle of the meltwater pool (3.0°C).



Figure 4.24 Optical image (GoPro Hero4) of outlet iceberg survey at 11:09pm with roughly the same extent as Figure 4.25c and Figure 4.25d.

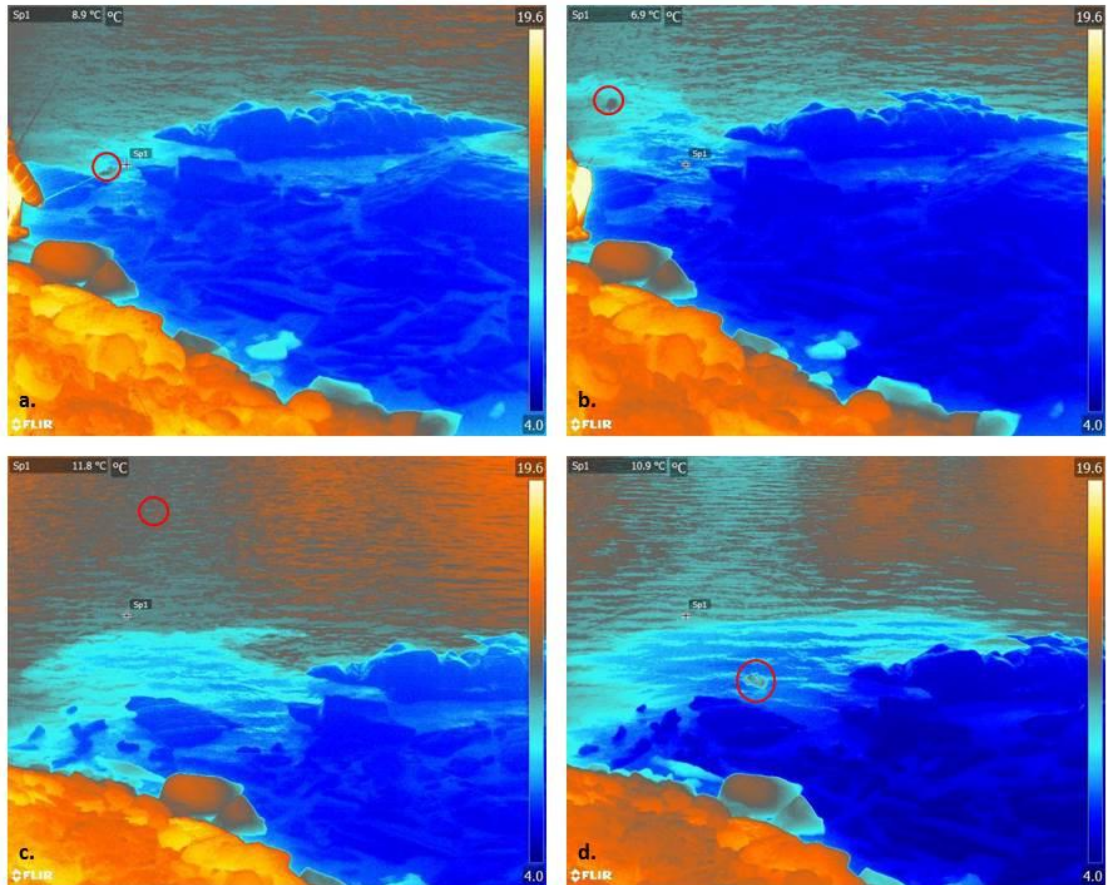


Figure 4.25 Thermal images from the FLIR A65 survey conducted from the outlet survey position on 27/7/2017 at **a.** 10:46pm **b.** 10:55pm **c.** 11:00pm and **d.** 11:10pm. With the focus spot (Sp1) skin surface temperature in the top left hand corner of each image, with an area of rocks visible in the lower left hand corner. The red circle identifies the position of the remote controlled boat during each survey, with body temperature readings of **a.** 2.4°C at ~5 cm and ~30 cm depth at 10:46pm **b.** 3.9°C at ~5 cm and 4.6°C at ~30 cm depth at 10:55pm **c.** 5.0°C at ~5 cm and ~30 cm depth at 11:00pm and **d.** 2.2°C at ~5 cm and 3.0°C at ~30 cm depth at 11:10pm. Note the changing extent in meltwater emanating from the iceberg pool during this period, which coincided in decreasing wind speed blowing in the direction from the lake onto the icebergs (evident in the reduced rippling). The viewing angle was changed to include the boat within the thermal image of **c** and **d**.

The thermal infrared imagery of the icebergs and meltwater capture the spatial pattern of water temperature boundaries with high resolution, both spatially and temporally (Figure 4.25). As the thermistor temperature readings confirm that the cold water boundary existed at the surface and this moved over a short time period of minutes (Figure 4.25). Given that the response time of the temperature sensors is ~5 minutes, the relatively rapid response time (seconds) of thermal imagery was able to capture the precise spatial pattern of the meltwater body as it emanated from the icebergs (Figure 4.25). The absolute skin surface temperature readings of 8.9°C and 6.9°C (Figure 4.25 a and b) within the meltwater pool are much higher than the thermistor readings, which may be due to the high reflection of longwave radiation in the water surface associated with the relatively high camera angle (70° from normal to the

water surface) (Aubry-Wake et al., 2015). The higher skin surface temperatures (SST) of 11.8°C and 10.9°C from outside the meltwater pool, confirm the detection of the extent of the cold water body in the thermal image (Figure 4.25).

#### **4.4.6 Near Terminus Lake Water in situ Temperature and Light Intensity during 2017 Fieldwork**

A string of 2 thermistors were installed at ~5 cm depth and ~80 cm depth within ~20 m of the terminus of Kaskapakteglaciaren at 9:54pm on 23<sup>rd</sup> July 2017 (Figure 4.8). Following settling of the sensors after installation, the water temperatures at ~5 cm depth fluctuated slightly between 3.9 to 3.5°C until 2:44am, after which they decreased to 3.2°C at 3:24am on 24<sup>th</sup> July (Figure 4.26). A period of steady increase then follows (with some fluctuations), before reaching an initial peak of 5.0°C at 9:34am followed by a period of fluctuations between 4.2°C and 4.6°C at 1:54pm (Figure 4.26). After this temperatures increase to 5.5°C (2:04pm) before reaching a maximum temperature of 6.0°C at 3:44pm on 24<sup>th</sup> July (Figure 4.26).

There is a decrease in temperatures at ~5 cm depth from 5.8°C at 4:54pm to 3.2°C at 7:14pm on 24<sup>th</sup> July (Figure 4.26). The light intensity at ~5 cm depth during this period follows a similar pattern to water temperatures initially, with a steady increase (with some fluctuations) from a minimum of 32 lux (12:24am) to 592 lux (4:04am) followed by a rapid increase to 14,466 lux at 6:24am on 24<sup>th</sup> July (Figure 4.26). This is followed by a period of fluctuating light intensity (~5 cm depth) with increasing trend between 5,000 to 15,000 lux, before reaching a maximum of 27,555 lux at 9:14am on 24<sup>th</sup> July (Figure 4.26). A further period of fluctuations between 7,000 to 16,000 lux follows this before a secondary peak of 21,355 lux is reached at 2:34pm (Figure 4.26). The light intensity then decreases from 18,600 (3:34pm) to 10,333 (3:54pm), with a further steady decline to 5,339 (6:34pm) and a further steep decline to 861 lux at 7:04pm on 24<sup>th</sup> July. It is important to note the lag between peaks in light intensity and peaks in water temperature at ~5 cm depth, particularly the decline in light intensity whilst water temperatures at ~5 cm depth remained above 5°C (Figure 4.26).

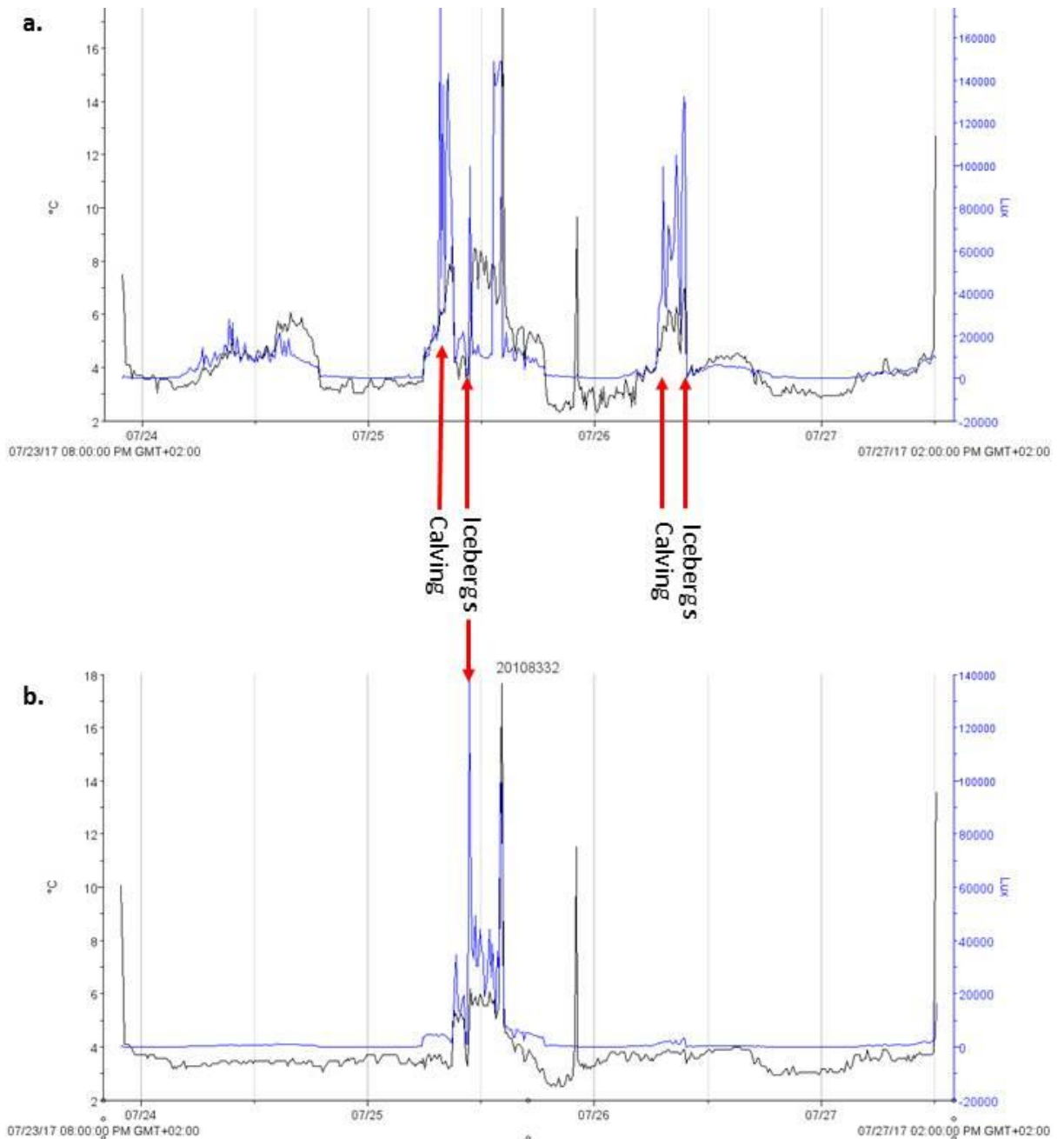


Figure 4.26 Temperature data (black) and light intensity data (blue) from HOBO thermistors situated at **a.** ~5 cm depth (20108328) and **b.** ~50 cm depth (20108332) at the terminus (Tr) survey position (67.95735°N, 18.57442°E). Note the temperature and light intensity spikes on 23/7/2017, 25/7/2017 and 4/8/2017 due to installation/extraction of the sensors.

In contrast to the near surface conditions, the light intensity at ~80 cm depth remained relatively low and below 1,120 lux throughout the period described above (24<sup>th</sup> July) (Figure 4.26). The water temperatures at ~80 cm depth initially remained around 3.6°C before decreasing to 3.1°C at 3:32am (Figure 4.26). During the middle part of the day water temperatures at ~80 cm depth fluctuated slightly around 3.4°C before a decrease from 3.5°C (6:03pm) to 3.0°C at 7:13pm on 24<sup>th</sup> July (Figure 4.26). The later part of the day is then

marked by a slight increase in water temperatures at ~80 cm depth to 3.7°C at 11:53pm, at which time light intensity levels were near the minimum at all depths (Figure 4.26). The water temperatures at ~80 cm depth decreased slightly at 3:03am (25<sup>th</sup> July) from 3.7°C to 3.4°C at 3:33am, with a period of further fluctuations (Figure 4.26).

The water temperature at ~5 cm depth also fluctuates during the ‘night time’ period of low light levels, with peaks of 3.6°C at 9:54pm, 12:14am and 1:54am and a minimum of 3.0°C at 11:14pm (Figure 4.26). There is a rapid increase from 3.4°C at 5:44am to 4.5°C at 5:54am and further increase to 5.3°C at 7:24am (Figure 4.26). The light intensity also increases rapidly at the same time from 753 lux at 5:44am to 14,466 lux at 5:54am with a further increase to 27,555 lux at 7:24am on 25<sup>th</sup> July (Figure 4.26).

After this point there is significant disruption to the sensors at both depths from iceberg calving activity, as indicated by the light intensity spiking at 176,356 lux at 7:34am on 25<sup>th</sup> July (Figure 4.26). This is likely due to waves produced by the icebergs falling into the water and subsequent moving of the sensors by icebergs drifting through the area. The sensors were subsequently recovered and reinstalled at 10:04pm on 25<sup>th</sup> July. Following this the water temperature at ~5 cm depth displayed sharper fluctuations between 2.5°C and 3.5°C (Figure 4.26). The light intensity then spikes at 99,200 at 7:14am, which coincides with further calving activity during 26<sup>th</sup> July and disruption of the sensors, which resulted in the sensors being moved ~10 metres to the north east and partially buried in sediment. Prior to this the water temperature at ~80 cm depth displays a similar trend of small fluctuations as previously described during the night of the 24<sup>th</sup> July (Figure 4.26). Interestingly, the disruption and movement of the deeper sensor is not particularly evident in the temperature or light data, which suggests the movement from the wave and/or iceberg did not result in the sensor being brought closer to the surface during the horizontal displacement (Figure 4.26). The decrease in temperature after 4:23pm from 3.9°C down to a minimum of 2.9°C at 7:23pm is likely to coincide with movement of icebergs to within metres of the sensor (Figure 4.26).

#### **4.4.7 Terminus Lake Water Temperature Spatial Surveys**

A series of temperature surveys were conducted from the terminus survey position (marked Tr on Figure 4.27) (67.95457 °N, 18.56109°E) utilising 4 HOBO thermistors suspended from the remote controlled boat and the FLIR A65 thermal camera (Figure 4.10). A GoPro Hero4 time lapse camera was used for monitoring the boat position and changing weather conditions. There was 24 hour daylight throughout the fieldwork, although the sun dropped

below the horizon from ~10.00pm to ~2.00am. The temperature surveys were predominantly conducted after 10:30pm to minimise incoming solar radiation (Figure 4.22). However, surrounding mountain slopes were emitting a notable amount of long wave radiation, particularly following days with long periods of incoming solar radiation (Figure 4.22).

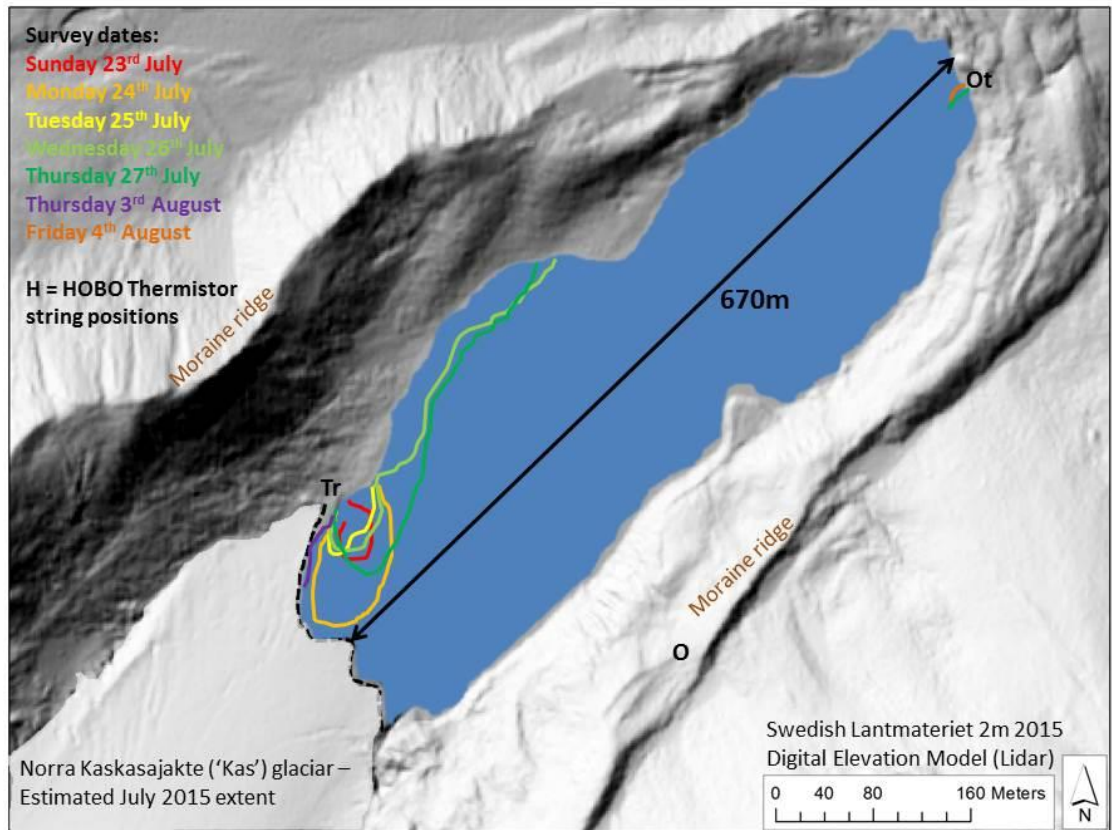


Figure 4.27 Plan of boat temperature survey routes and associated dates. Note that the calving event of 26/7/2017 restricted boat access to the ice front due to large icebergs.

A preliminary lake water temperature spatial survey was undertaken at Kas' glacier on 23<sup>rd</sup> July (Figure 4.27). The spatial pattern of temperatures has not been plotted spatially due to problems for position location with triangulation from imagery. The katabatic winds off the glacier prevented the boat getting closer to the terminus.

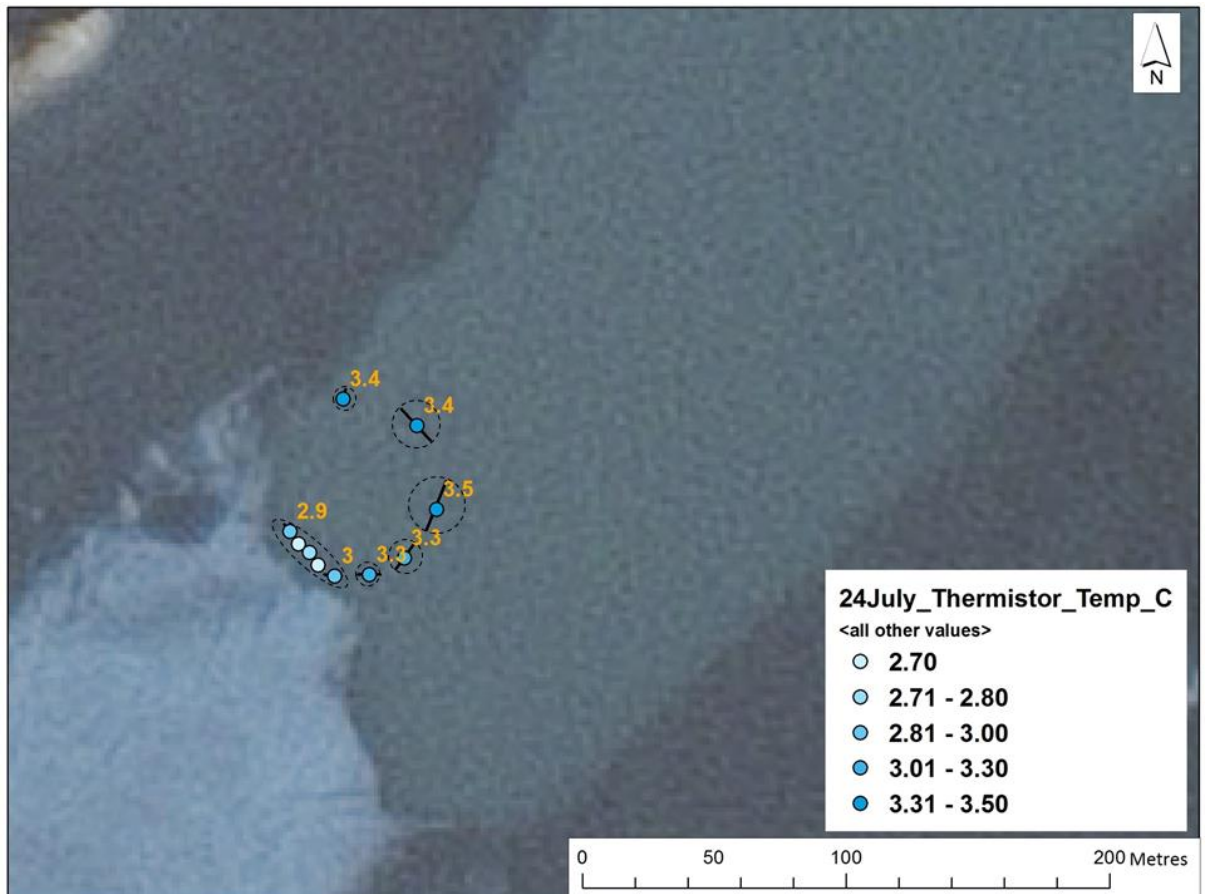


Figure 4.28 Plot of temperature measurements from HOBO thermistor (20156968) suspended from the remote control boat from 11:42pm 24/7/2017 to 12:12am 25/7/2017. With black lines representing the extent of horizontal movement of the remote controlled boat during each reading due to wind induced drift, dashed circles represent locational spatial uncertainty. Tr = Terminus survey position. At the start of the survey air temperature at Tr was 9.8°C with a relative humidity of 60.2%, at the end of the survey air temperature was 6.2°C with a relative humidity of 68.2%. Image; 30/9/2017 09:49am SPOT6 Multi Spectral (pansharpned to 1.5 m spatial resolution).

The 24<sup>th</sup> July was marked by fair weather with light winds, minimal cloud and long periods of sunshine through the day (Figure 4.21 and Figure 4.22). The lack of wind enabled the remote controlled boat to be operated to within 2 m of the ice terminus, where temperatures were observed to range between 2.7°C and 3.0°C (Figure 4.28). It is possible that the lower temperatures of 2.7°C are associated with colder meltwater emanating from a small crevasse in the subaerial ice cliff (Figure 4.29). It may also be possible that this difference represents a steep temperature gradient within metres of the ice front. However, the temperature difference of 0.3°C lies within the manufacturer’s stated accuracy of +/- 0.5°C, therefore confidence in this temperature difference remains low. A distinct temperature gradient was observed during the remote controlled boat survey moving away from the glacier terminus with readings of 2.7°C within ~2 m to readings of 3.5°C ~50 m away from the ice front (Figure 4.28).

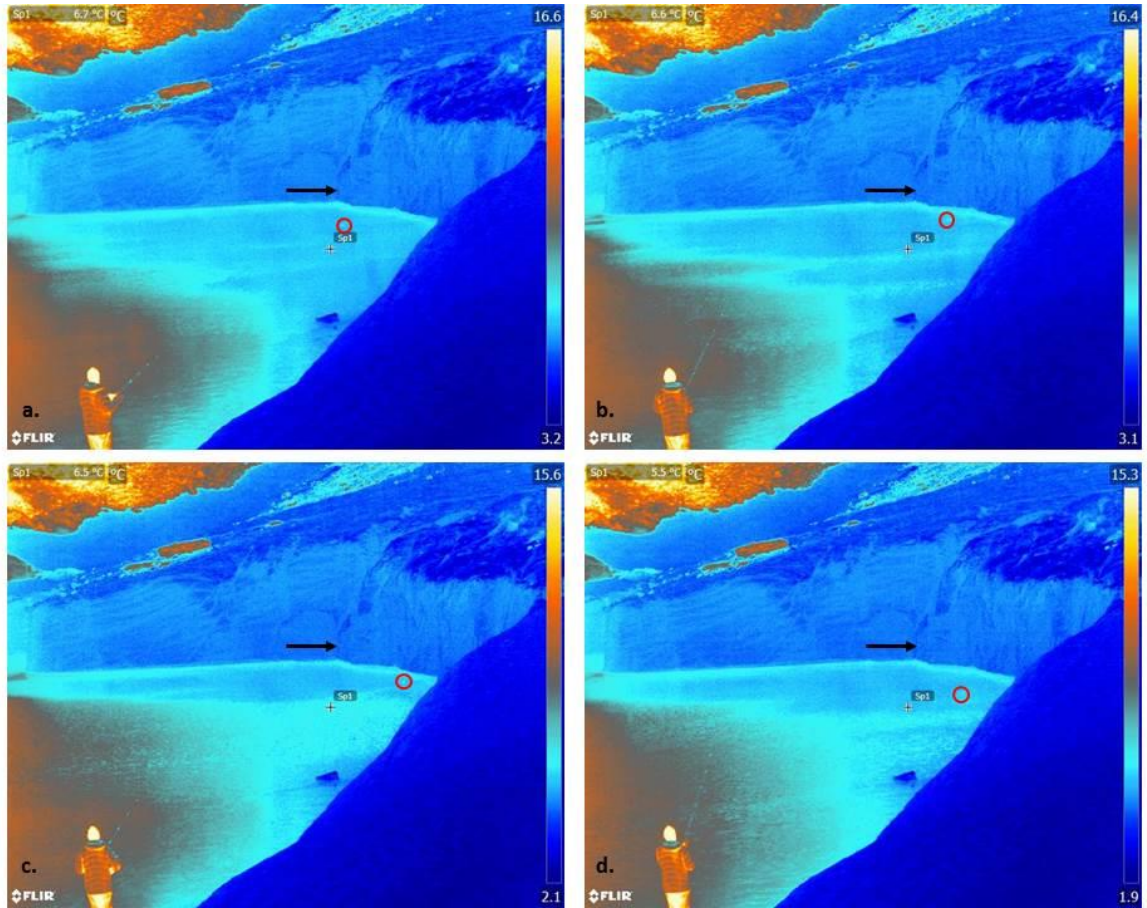


Figure 4.29 Thermal images from the FLIR A65 survey conducted from the terminus survey position on 24/7/2017 at **a.** 11:43pm **b.** 11:44pm **c.** 11:45pm and **d.** 11:46pm. With the focus spot (Sp1) skin surface temperature in the top left hand corner of each image. The red circle identifies the position of the remote controlled boat during each survey, with body temperature readings of **a.** 2.7°C at 11:43pm **b.** 2.8°C at 11:44pm **c.** 2.7°C at 11:45pm and **d.** 2.7°C at 11:46pm. The black arrow denotes the lower section of the crevasse feature. Distance to the far side of the ice cliff bay is ~100m. Note the bergy bit in the foreground.

A thermal imaging survey was conducted synchronously to the remote controlled boat survey from the terminus survey position on 24<sup>th</sup> July (Figure 4.28 and Figure 4.29). The high spatial resolution of the thermal imagery is exemplified by the prominence of debris bands (~20 cm wide) within the ice front (also see Figure 4.30 for comparable optical image) and the prominence of the crevasse feature (black arrow Figure 4.30). The bay feature in the ice cliff provides some shadowing from longwave radiation emitted by surrounding mountain slopes, which is reflected by the water surface further away from the glacier terminus and leads to erroneously high skin surface temperature readings (~12° Figure 4.29) (Aubry-Wake et al., 2015). There is some slight rippling of surface water within ~20 m of the glacier terminus (Figure 4.29). This appears to have a minimal effect on the focus spot 1 temperature readings as rippling is not present at this point in Figure 4.29c and the skin surface temperature reading of 6.5°C is in close agreement with 6.7°C in Figure 4.29a and 6.6°C

Figure 4.29b where rippling is present at the focus point in both images. Note also that the maximum skin surface temperatures in Figure 4.29a and Figure 4.29b are also higher (16.6°C and 16.4°C respectively), which suggests either changing background radiation conditions or stabilisation of the thermal infrared sensor associated with the automatic calibration process (Aubry-Wake et al., 2015). There is a temperature difference of 1.8°C between the skin surface temperature of 5.5°C (Figure 4.29d) measured by the FLIR A65 and body temperature of 2.7°C measured by the HOBO thermistors (Figure 4.28).

A small calving event occurred on 25<sup>th</sup> July as a relatively small section of the ice front collapsed above the thermally eroded notch (see Figure 4.19 and Figure 4.30a). A small iceberg became stationary in between the terminus survey position and the glacier ice front; this combined with increased wind speeds meant that it was not possible to drive the remote controlled boat further towards the ice front. The increased winds also resulted in increased surface water ripples near the glacier front, with a larger area of disrupted pixels in the thermal infrared image (Figure 4.30b). A small area of water remained sheltered by the ice front and the spot 1 skin surface temperature of 6.7°C is in agreement with a previous thermal infrared image taken at a similar time the day before (Figure 4.29c and Figure 4.30a). Note that the debris bands within the ice are less prominent in thermal images taken on 25<sup>th</sup> July (Figure 4.30) than those taken on 24<sup>th</sup> July (Figure 4.29).

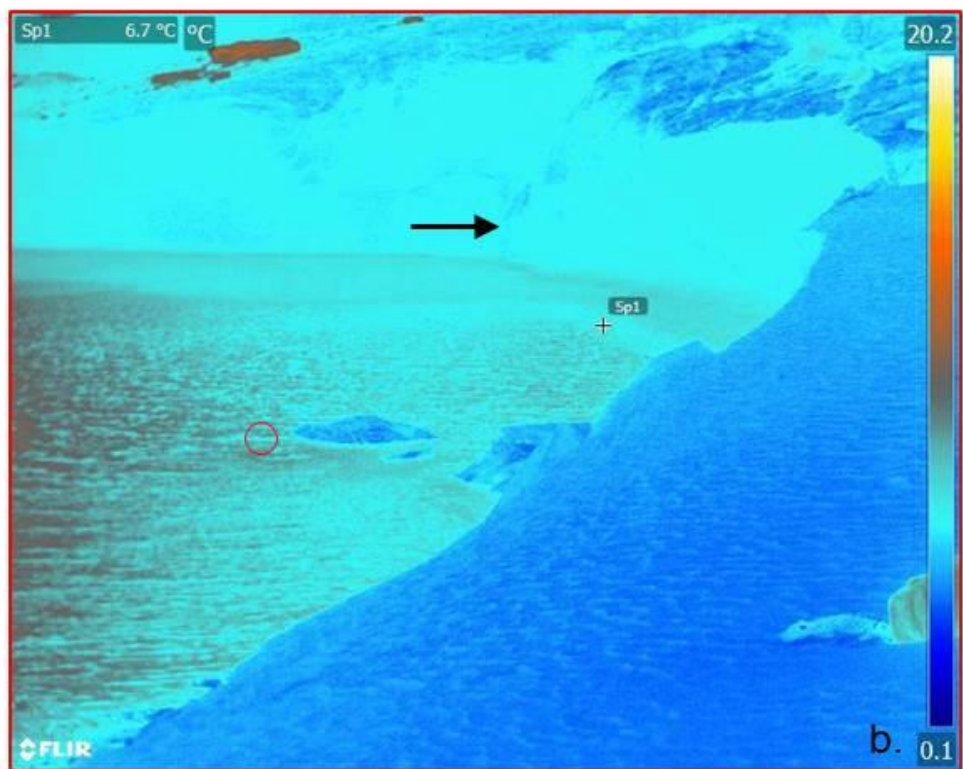


Figure 4.30 Images taken at 11:06pm 25/7/2017 from the terminus survey position. With **a.** optical image from GoPro Hero4 with red circle highlighting the boat, the black arrow points to the crevasse feature. NOTE the white arrow points to the lack of a visible thermally eroded notch following the iceberg calving event of 25/7/2017. The red boxes denote the extent of **b.** thermal infrared image (FLIR A65).

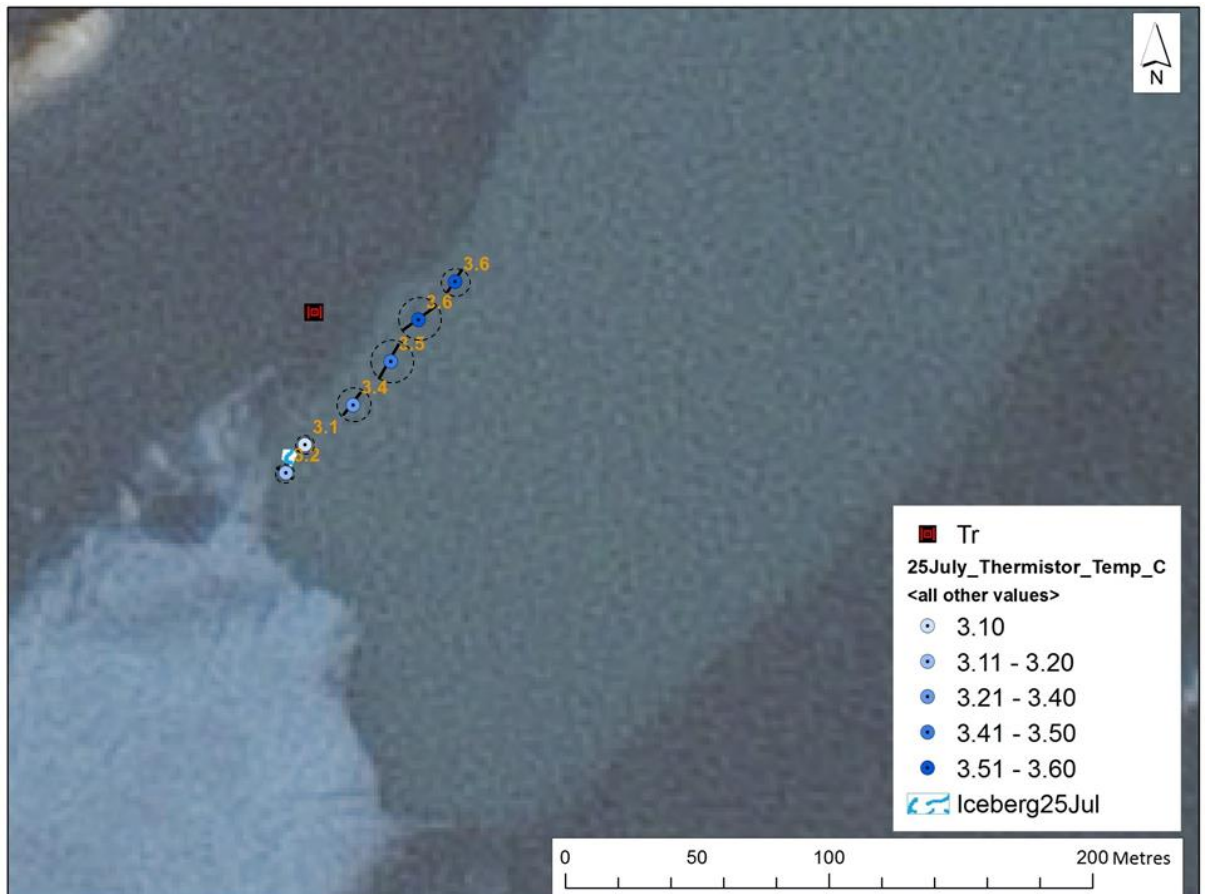


Figure 4.31 Plot of temperature measurements from HOBOT thermistor (serial no. 20110296) suspended from the remote control boat from 11:02pm to 11:31pm on 25/7/2017. With black lines representing the extent of horizontal movement of the remote controlled boat during each reading due to wind induced drift, dashed circles represent locational spatial uncertainty. Tr = Terminus survey position. At the start of the survey air temperature at Tr was 6.8°C with a relative humidity of 65.8%, at the end of the survey air temperature was 8.9°C with a relative humidity of 68.9%. Image; 30/9/2017 09:49am SPOT6 Multi Spectral (pansharpened to 1.5 m spatial resolution)

The temperature observations from the remote controlled boat survey on 25<sup>th</sup> July are similar to those taken at a similar time on 24<sup>th</sup> July (Figure 4.28 and Figure 4.31). There is a slight decrease of 0.1°C from a temperature reading of 3.1°C recorded in the lee of an iceberg, compared to a reading of 3.2°C recorded closer to the ice front although there is low confidence in these readings given the accuracy of the thermistors (+/- 0.5°C). The temperature readings of 3.5°C and 3.6°C at ~60 m and ~80 m away from the ice front on 25<sup>th</sup> July (Figure 4.31) are in agreement with temperature readings at the same distance taken on 26<sup>th</sup> July (Figure 4.32). This consistency in temperature readings between dates suggests that a relatively high confidence can be assigned to capturing the true ambient temperature gradient in proglacial lake water towards the glacier front, assuming that there had been no change between these dates due to stable meteorological conditions.

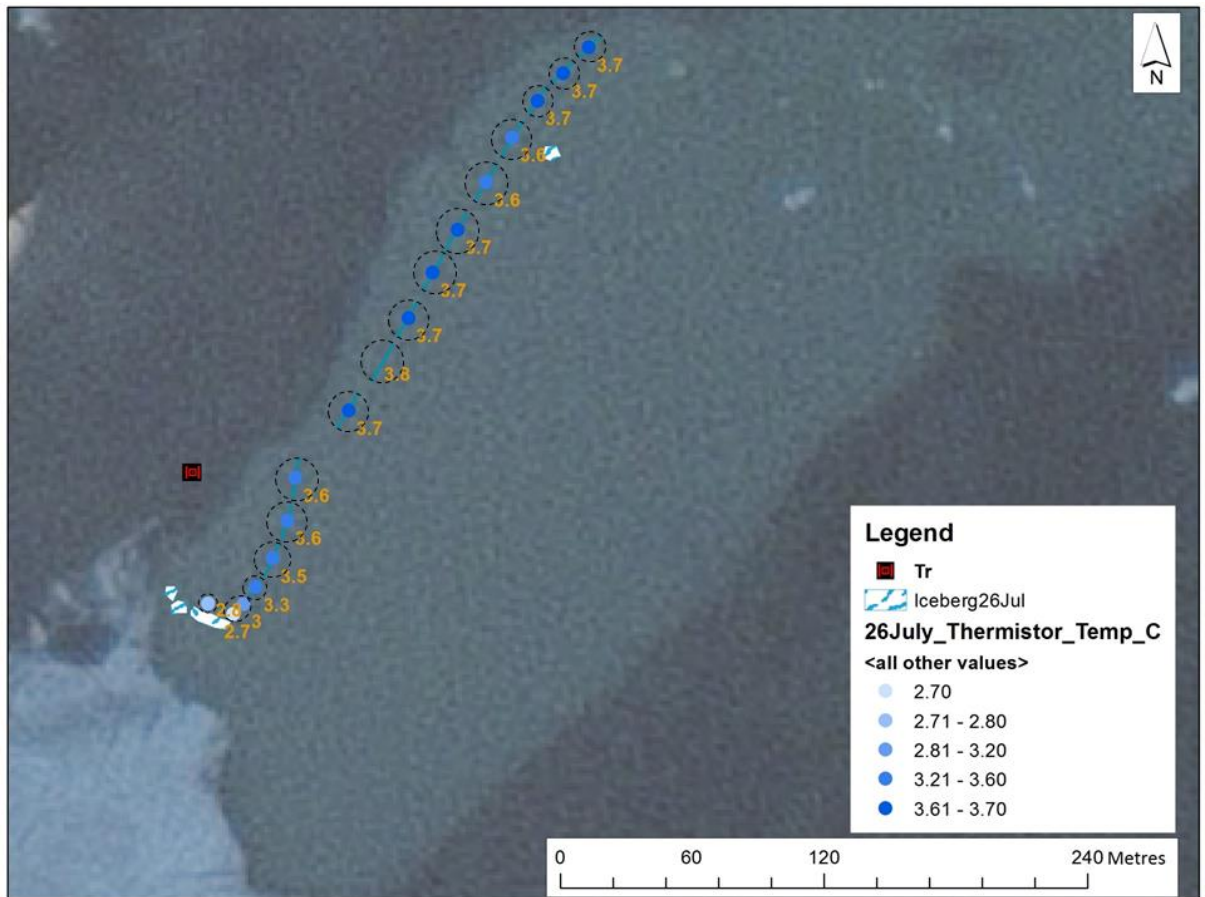


Figure 4.32 Plot of temperature measurements from HOB0 thermistor (20108329) suspended from the remote control boat from 12:17am to 01:10am on 27/7/2017. With black lines representing the extent of horizontal movement of the remote controlled boat during each reading due to wind induced drift, dashed circles represent locational spatial uncertainty. Tr = Terminus survey position. At the start of the survey air temperature at Tr was 7.0°C with a relative humidity of 74.9%, at the end of the survey air temperature was 7.4°C with a relative humidity of 74.8%. Image; 30/9/2017 09:49am SPOT6 Multi Spectral (pansharpned to 1.5 m spatial resolution)

A large section of ice from the terminus collapsed above the thermally eroded notch during 26<sup>th</sup> July (Figure 4.19). This resulted in a large iceberg becoming stationary between the terminus survey position and the ice front, which prevented the remote controlled boat being manoeuvred to the ice front (Figure 4.30). A remote controlled boat survey was conducted from the iceberg and away along the shoreline to investigate the cooling influence of icebergs on the ambient lake temperature (Figure 4.32). Temperature readings of 2.8°C and 2.7°C were made within close proximity (<2 m) of the iceberg (Figure 4.32). As the remote controlled boat was allowed to drift in the wind, temperature readings of 3.0°C and 3.3°C were made at ~15 m and ~30 m from the iceberg respectively (Figure 4.32), suggesting a relatively strong temperature gradient. This suggests the latter readings may have been made outside the cooling influence of the iceberg, although there is low confidence in this as the difference is within the error margin of the thermistors (+/- 0.5°C). The water temperatures

increased to 3.6°C ~100 m away from the glacier front and were slightly higher further away from the glacier, suggesting the immediate cooling zone in front of the glacier extended ~100 m at the time of the survey (Figure 4.32).

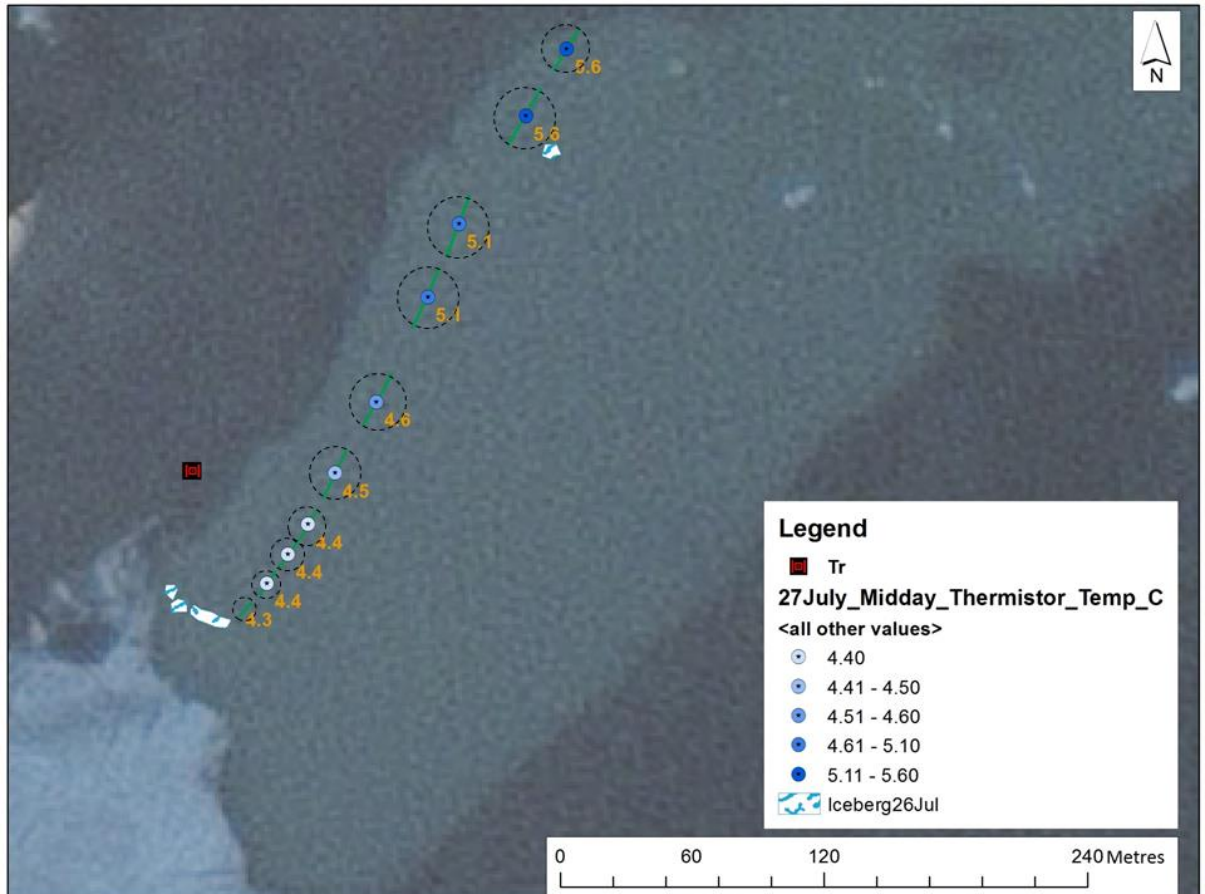


Figure 4.33 Plot of temperature measurements from HOBO thermistor (20156968) suspended from the remote control boat from 12:29pm to 1:07pm on 27/7/2017. With green lines representing the extent of horizontal movement of the remote controlled boat during each reading due to wind induced drift, dashed circles represent locational spatial uncertainty. Tr = Terminus survey position. At the start of the survey air temperature at Tr was 13.0°C with a relative humidity of 74.0%, at the end of the survey air temperature was 10.1°C with a relative humidity of 80.5%. Image; 30/9/2017 09:49am SPOT6 Multi Spectral (pansharpened to 1.5 m spatial resolution)

The survey track along the shoreline leading away from the glacier was repeated as closely as possible during the midday survey on 27<sup>th</sup> July (Figure 4.33). Although manoeuvring the boat into exactly the same position as the previous day proved challenging in the water/wind conditions. Water temperatures were overall warmer, as to be expected due to solar warming of the near surface water during the middle of the day (see Figure 4.23 and Figure 4.26). The near surface water temperatures near the glacier were notably warmer, with 4.3°C recorded ~40 m from the glacier front and within metres of the large iceberg (Figure 4.33). There was a steady increase to 4.6°C ~150 m from the glacier front (1°C higher than the previous

midnight survey) and a further increase to 5.6°C ~300 m from the glacier front (Figure 4.33). These temperatures from the midday spatial survey on the 27<sup>th</sup> July should be treated as a ‘daytime maximums’ and do not reflect the ambient temperatures of proglacial lake near the glacier front, as evidenced from short term daytime spikes in in situ lake temperatures (Figure 4.23).

This situation of elevated temperatures during the middle of the day was also likely to be the case on the 3<sup>rd</sup> August. Although the amount of incoming solar radiation was generally lower on 3<sup>rd</sup> August than during the first period of fieldwork (Figure 4.22). The lower incoming solar radiation of 3<sup>rd</sup> August (Figure 4.22) suggests that the elevation of daytime temperatures compared to night time temperatures may be less than compared to the earlier period of high incoming solar radiation (Figure 4.22).

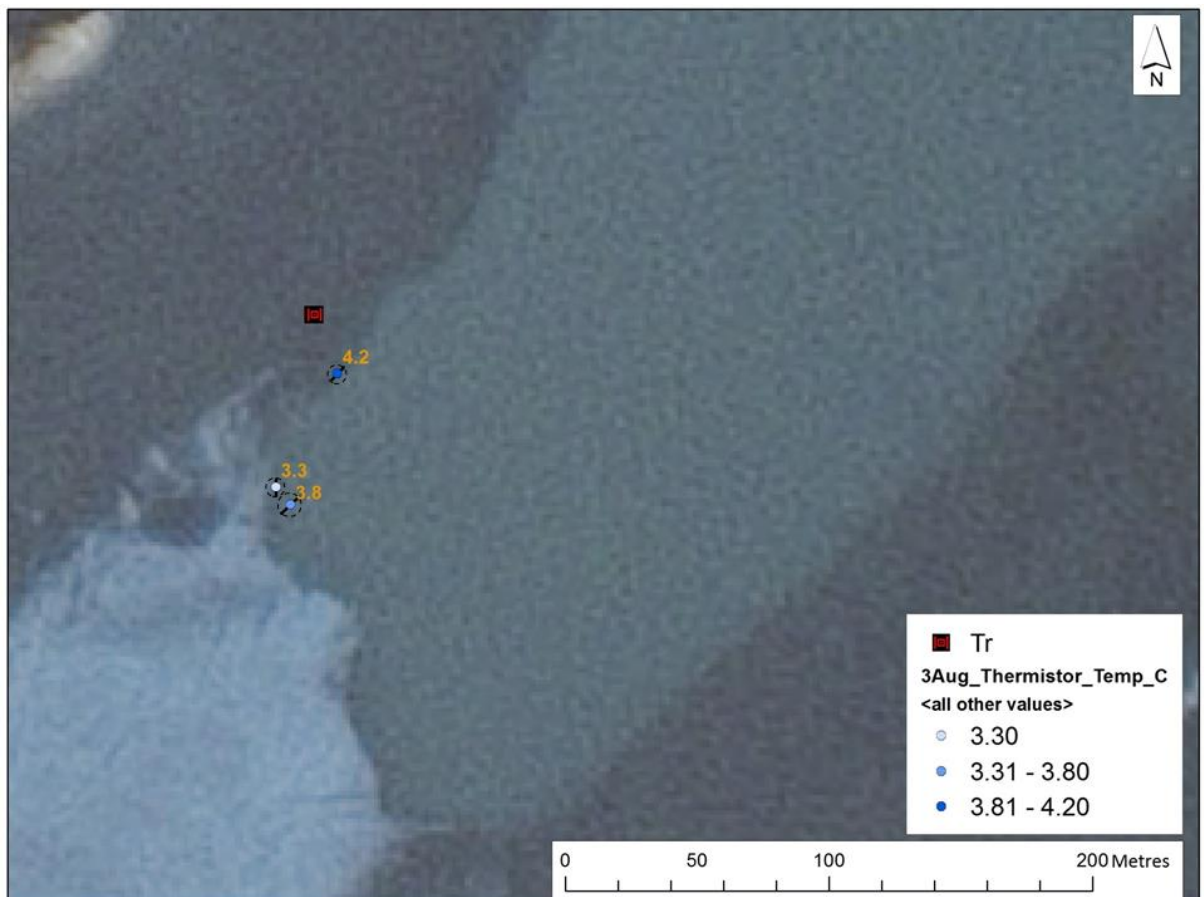


Figure 4.34 Plot of temperature measurements from HOBO thermistor (20156968) suspended from the remote control boat from 02:22 PM to 02:39 PM 3/8/2017. With black lines representing the extent of horizontal movement of the remote controlled boat during each reading due to wind induced drift, dashed circles represent locational spatial uncertainty. Tr = Terminus survey position. Air temperature on the remote controlled boat deck ranged from 9.9°C to 13.2°C (HOBO thermistor). Image; 30/9/2017 09:49AM SPOT6 Multi Spectral (pansharpened to 1.5m spatial resolution).

#### 4.4.8 Kaskapakteglaciaren Terminus Change during Fieldwork in 2019

The terminus geometry of Kaskapakte glaciär was observed to change substantially during fieldwork from 29<sup>th</sup> July to 10<sup>th</sup> August 2019. During this period of fieldwork numerous calving events were observed and captured in time lapse images, but not reported here due to the analysis being incomplete. There were several calving events that were partly recorded by handheld images (Panasonic Lumix DMC-TZ57) taken shortly after and a limited number of calving events that occurred around the temperature buoy are described here (Figure 4.35). A calving event occurred at 10:04am on 6/8/2019 and was observed by A.Dye, during which a section of the subaerial ice cliff collapsed above a thermal notch (Figure 4.35).



Figure 4.35 Image (Panasonic Lumix DMC-TZ57) of Kaskapakteglaciären taken shortly (minutes) after a calving event on 6/8/2019 (10:04am), which was observed from behind a moraine. Note the top of the red buoy (~50 cm high) is just visible behind an ice berg. The extent of undercut of the terminus is apparent in the image.

Shortly after the 10:04am calving event occurred on 6<sup>th</sup> August 2019 the top of the subaerial ice cliff was accessed and fresh crack was observed along the top of the subaerial ice cliff at 10:44am (Figure 4.36a). This crack was observed to be wider (several centimetres) by 19:54 on 6/8/2019 (Figure 4.36). The crack was observed to be wider on 7/8/2019 but the top of the subaerial ice cliff was not accessed and weather conditions were poor. On return to the top of

the subaerial ice cliff it was evident that the subsequent calving event had failed along the same section of crack.

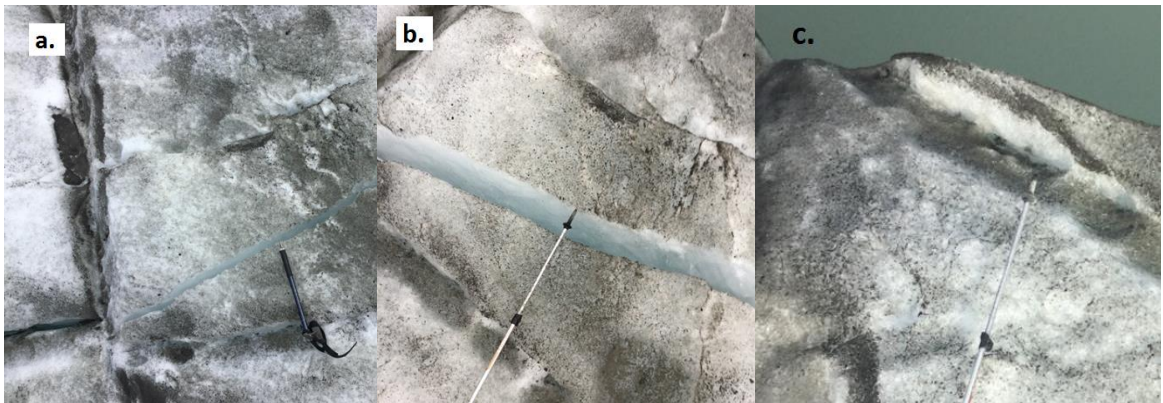


Figure 4.36 Series of images (Panasonic Lumix and iPod Touch) taken at the top of the subaerial ice cliff above the temperature buoy showing crack development following a calving event at 10:04AM on 6/8/2019. Images taken at: a. 10:44AM on 6/8/2019 b. 19:54AM on 6/8/2019 and c. 10<sup>th</sup> August with walking stick in image c pointing to the dark band also present in image b and a.

The temperature sensor buoy was left in position at the end of fieldwork on 11<sup>th</sup> August 2019 (Figure 4.37). On return to the Kaskapakteglaciaren terminus on 19<sup>th</sup> September 2019 the temperature buoy had disappeared, presumably as a result of calving events and subsequent retreat of the subaerial ice cliff.



Figure 4.37 Image (Panasonic Lumix DMC-TZ57) of Kaskapakte glacier on 11/8/2019 (10:04am), which was observed from behind a moraine. Note the red buoy (~50 cm tall).

#### 4.4.9 In Situ Lake Water Temperatures from the Calving Front during 2019

A continuous temperature and light intensity record was obtained from Kaskapakteglaciaren terminus from 29<sup>th</sup> July 2019 to 10<sup>th</sup> August 2019 (Figure 4.38). During this period a substantial calving event occurred at 10:04am on 6<sup>th</sup> August (Figure 4.35). A second calving event occurred sometime on 9<sup>th</sup> August 2019, as indicated by the large spike in light intensity from disturbance to the sensor during this event (Figure 4.38). The water temperatures at 1 m depth between 29<sup>th</sup> July to 8<sup>th</sup> August were ~4°C, with some higher and lower fluctuations that are not described further as they are within the stated error margin of the HOBO UA-002-08 (+/-0.5°C) (Figure 4.38). An exception is the decrease to 2.6°C on 29<sup>th</sup> July 2019, which is associated with passing of an iceberg near to the sensor (Figure 4.38). From 8<sup>th</sup> August to 10<sup>th</sup> August further drops in temperature were recorded following icebergs passing close to the sensor, with minimum temperatures of 1.4°C and 1.1°C (Figure 4.38). There were also periods where water temperature exceeded 4°C between 8<sup>th</sup> and 10<sup>th</sup> August 2019 (Figure 4.38).

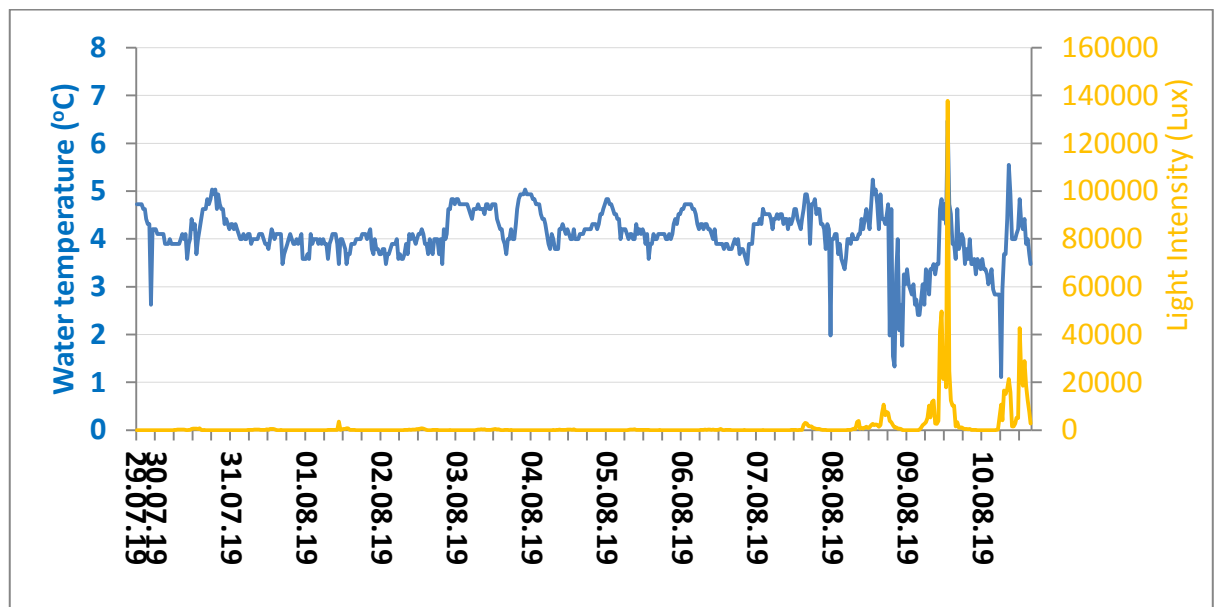


Figure 4.38 Temperature and light intensity record from HOBO Pendant (UAA 002-08 +/-0.5°C) suspended at 1 m depth in proglacial lake water from Kaskapakteglaciaren terminus (Figure 4.14 and Figure 4.37) between 29/7/2019 to 10/8/2019.

## 4.5 Discussion

The relationship between proglacial lake water temperatures and climate has received relatively little attention (Kirkbride and Warren, 1997; Richards et al., 2012; Peter and Sommaruga, 2017; Minowa et al., 2017). This is partly due to drifting icebergs disrupting or moving temperature sensors, which makes obtaining a longer time series of lake temperature data and study of thermal regime highly problematic. Whilst some previous studies have reported warm (4°C) proglacial lake temperatures from surveys during fieldwork (Kirkbride and Warren, 1998; Chikita et al., 1999; Kirkbride and Warren, 2003; Roehl, 2006; Sugiyama et al., 2016; Minowa et al., 2017; Watson et al., 2020), there has still been a common assumption that proglacial lakes tend to be a uniform 1°C (Boyce et al., 2007; Truffer and Motyka, 2016). The limited numbers of modelling studies of glacial retreat back from proglacial lakes have also assumed water temperatures of 1°C (Chernos et al., 2016). This chapter provides one of the first reports of water temperatures from an Arctic proglacial lake. These proglacial lake temperatures were measured during two periods of fieldwork in 2017 and 2019, with observations of substantial calving activity and relatively rapid thermal undercutting (Figure 4.18, Figure 4.19, Figure 4.20 and Figure 4.35).

### 4.5.1 Proglacial Lake Water Temperatures near the Outlet

The heating influence of solar radiation and air temperatures leads to elevated levels of near surface water temperatures during the daytime (Figure 4.23 and Figure 4.26) (Chikita et al., 1999; Richards et al., 2012; Peter and Sommaruga, 2017). This daytime elevation of temperatures is problematic for the timing of temperature surveys (imagery or thermistor based) in trying to capture ambient near surface lake water temperatures. This is due to solar radiation during the middle part of the day potentially warming the thermistor casing, so temperature readings of water may be subject to thermal contamination in this situation.

A close relationship between light intensity and water temperature at ~5 cm depth was observed in the in situ thermistor records at the outlet (Figure 4.23) and the terminus (Figure 4.26) during fieldwork in 2017. This suggests that the impact of solar warming on near surface waters is substantial, with a temperature maximum of 11.2°C (1.39pm) recorded by the thermistor at ~5 cm depth, before a cooling to 4.3°C on 26<sup>th</sup> July (Figure 4.23). This peak in water temperatures lagged several hours behind the peak in light intensity (10:29am), which suggests that direct solar warming of the thermistor casing was unlikely to be the

primary reason for this high temperature reading (Peter and Sommaruga, 2017). Moreover, the prominent peak of 8.0°C in temperatures at ~50 cm depth on 26<sup>th</sup> July occurs when light intensity at this depth is low (less than 1,000 lux). Therefore there is high confidence that the thermistors at ~50 cm depth captured the warming of the ambient water temperature at the outlet during 26<sup>th</sup> July, although some ‘thermal contamination’ of the sensor at ~5 cm depth is difficult to rule out conclusively. The night time cooling and mixing of near surface waters occurred throughout the study period, with temperatures at the outlet returning to around ~5°C repeatedly throughout the series of temperature observations and surveys (Figure 4.23) (Peter and Sommaruga, 2017).

The near surface water temperatures of 8°C recorded near the lake outlet in this study are higher than the ~5°C recorded in a similar position in proglacial lake Tsho Rolpa (Nepal), which is likely due to wind driven mixing of Tsho Rolpa (Chikita et al., 1999). The warmest temperatures of proglacial lakes in New Zealand recorded by the study of Warren and Kirkbride (1998) were maximums of 4.5°C in Maud Lake, which they also found to be thoroughly mixed. Warren and Kirkbride (1998) also note that temperatures of 7-9°C were recorded by Churski (1973) in the ice-distal parts of the 15 m deep proglacial lake in contact with Skeidarajokull (Iceland). Warmer (>8°C) temperatures have also been reported from distal parts of ice contact proglacial lakes in Patagonia (Warren 1994; Sugiyama et al., 2016; Minowa et al., 2017). These proglacial lake systems in Patagonia are substantially larger (kilometres long and several hundred metres deep) than Kaskapakte proglacial lake (~700 m long and maximum 20 m deep) and therefore likely to have a substantially different thermal regime (O’Reilly et al., 2015).

There have been thermal regime studies of an non-ice contact proglacial lake in Canada (Place lake max depth 12 m and 72,000 m<sup>2</sup>) that has similar dimensions to Kaskapakte proglacial lake (132,000 m<sup>2</sup>) and also smaller proglacial lakes in Austria (Faselfad Lakes, maximum 5 m deep) (Richards et al., 2012; Peter and Sommaruga, 2017). The maximum near surface water temperatures of 7°C observed in the outlet of Place lake are comparable to the maximum temperatures at 50 cm depth of 8°C measured in Kaskapakte proglacial lake (Richards et al., 2012). The study of Peter and Sommaruga (2017) recorded higher maximum temperatures of 12.69°C at 1 m depth in Faselfad lake 1 and a maximum of 16.65°C at the surface, which may be due to the Faselfad lakes being shallower and warming faster.

The observations of similar warm temperatures in the proglacial Place lake (Canada) make a useful comparison, as this lake does not have a cooling influence from direct ice contact but does have a substantial influx of meltwater (Richards et al., 2012). Furthermore, the air temperatures were similar during the study Richards et al. (2012) at Place Lake (5-15°C) as the air temperatures during the study of Kaskapakte lake (6-16°C). So similar meteorological conditions makes the comparison between thermal regimes of each lake reasonably valid, although unfortunately incoming solar radiation was not measured at Place lake. The comparison between Place lake and Kaskapakte lake thermal regimes would suggest that the area near the outlet of Kaskapakte lake is beyond the direct cooling influence of contact with the glacier terminus, as it had similar temperatures to a non-ice contact proglacial lake during 2017.

This is a key result, as it suggests the area towards the outlet of Kaskapakte proglacial lake is sufficiently far enough away from the direct cooling influence from glacier contact for the thermal regime to be dominated by meteorological thermal influences. Although periods of high fluxes of meltwater and icebergs may affect the thermal regime near the outlet. Therefore providing support for the classification of Kaskapakte proglacial lake as 'Established', under the conceptual model proposed in Chapter 3 (Section 3.5.3). Essentially the greater length of Kaskapakte lake in proportion to the width of the glacier contact point, means that ice distal areas are beyond the direct cooling influence of glacier contact.

#### **4.5.2 Proglacial Lake Water Temperatures around Icebergs**

The spatial extent of cooling from icebergs on proglacial lake temperatures is important to constrain, particularly as it forms the basis for the assumption that relatively small proglacial lakes are a uniform temperature of 1°C (Chernos et al., 2016; Truffer and Motyka, 2016). Throughout the fieldwork period icebergs were observed (in time lapse imagery) to be exported relatively efficiently towards the lake outlet area from winds blowing away from the glacier, with the notable exception of the calving event that produced the large iceberg on 26<sup>th</sup> July. A similar process of wind driven export of icebergs away from glacier termini has been reported for Hooker and Tasman proglacial lakes in New Zealand (Warren and Kirkbride, 1998). The key result of icebergs being exported efficiently from the ice front is that their cooling impact on proglacial lake water temperatures near the glacier is quickly removed from this area. Additionally, the overall cooling impact of icebergs on the proglacial water temperatures was reduced as they were exported to the warmest area of the lake where

subsequent meltwater was evacuated through the lake outlet (Warren and Kirkbride, 1998). Throughout the fieldwork period in 2017 the majority of icebergs were observed to become positioned at the lake outlet, where an in situ HOBO thermistor was placed to constrain the temporal extent of cooling influence from icebergs (Figure 4.24 and Figure 4.25). This pattern in iceberg distribution has also been evident in satellite imagery (SPOT and Planet) through the 2017 summer period, which suggests that it may be a common distribution pattern of icebergs at Kaskapakte lake during 2017 at least.

The extent of cooling influence on proglacial lake water temperatures around icebergs has not been directly constrained in the field before, although there have been numerous studies of iceberg melt in saltwater. The study of Warren and Kirkbride (1998) concludes that icebergs in lake Tasman were not the dominant cooling feature as they were insignificantly small in relation to the size of the lake, which raises the issue as to what proportion of ice berg area to lake size is required for substantial cooling. Watson et al. (2020) observed a cooling of  $\sim 2^{\circ}\text{C}$  in surface temperature of Thulagi lake, which persisted for several months following calving events that produced  $\sim 487,000\text{m}^3$  of icebergs during the melt season. Crucially they noted that lake surface temperatures returned to 'normal' before the end of the melt season, which suggests that the temporal influence of iceberg cooling may be limited to months in some situations (Watson et al., 2020).

The spatial temperature survey of icebergs at the outlet area on 27<sup>th</sup> July is one of the first to constrain the spatial extent of meltwater from icebergs with the innovative use of thermal infrared imagery (Figure 4.25). Not only does the thermal infrared imagery provide high spatial resolution for defining the spatial boundaries of different temperature water bodies on the surface (within metres), but it also provides high temporal resolution to track the movement of water bodies (within minutes) (Figure 4.25). The presence of the cold meltwater pool emanating from the icebergs near the outlet on 27<sup>th</sup> July was clearly detectable in thermal infrared imagery and confirmed by thermistor readings on board the remote controlled boat at different locations (Figure 4.25). The horizontal extent of meltwater was roughly proportional to the horizontal extent of the actual icebergs, which extended out into the lake  $\sim 5$  m from the shore. These spatial surveys near Kaskapakte lake outlet would suggest that the horizontal spatial extent of the cooling influence and meltwater from icebergs is relatively limited in calm conditions (metres) (Figure 4.25).

The temporal influence of iceberg cooling on proglacial lake temperatures is also important to consider, as this may be limited where meteorological conditions have a strong warming influence. The length of time that icebergs cooled water temperatures near the lake outlet (HOBO sensor at ~5 cm depth) was ~24 hours following the smaller 26<sup>th</sup> July calving event and ~50 hours following the larger 1<sup>st</sup> August calving, before temperatures recovered to ~4-5°C (Figure 4.23). This would suggest that the temporal cooling influence of icebergs was limited. Furthermore, there was only a relatively subdued cooling of water temperatures at ~50 cm depth (similar to previous diurnal cycles) following the 26<sup>th</sup> July event (Figure 4.23). The vertical extent of iceberg cooling influence was also limited during the first period of iceberg presence around the HOBO sensor near the lake outlet. Therefore depth of iceberg cooling also needs to be considered when constraining proglacial lake thermal structure.

There is an important potential feedback loop between proglacial lake temperature and iceberg calving. As increased iceberg production may reduce proglacial lake water temperatures and therefore reduce further mass loss at the glacier terminus (through melting or calving above thermally eroded notches) (Warren and Kirkbride, 1998). However, the observations from this study suggest that a large amount of icebergs would have been required to cool the proglacial lake of Kaskapakte down to a uniform 1°C and therefore provide further evidence for falsifying the null hypothesis.

### **4.5.3 Proglacial Lake Water Temperatures near Kaskapakte Glacier Terminus**

This study reports some of the first temperature data from ice-proximal areas of a proglacial lake in the Arctic. The 24 hour daylight period in the Arctic region results in long periods of the day when surface waters may be warmed by incoming solar radiation and relatively short periods during the ‘night time’ when cooling may occur (Figure 4.26). The temperature record from the HOBO thermistor string installed near the terminus in July 2017 provides a strong constraint on the characteristics of diurnal heating and cooling cycle of ice-proximal areas of this proglacial lake at 67°N. The period following the sun dropping below the horizon is marked by cooling of the near surface waters at ~5 cm depth (Figure 4.26). Water temperatures at ~5 cm and ~50 cm depth near the terminus remained largely stable (with some slight fluctuations) from around 10:30pm through to 3:30am (Figure 4.26). This period of time hence represents the ambient lake water temperatures during this period. Therefore there is a high confidence that the spatial remote controlled boat thermistor surveys

conducted during the night time period captured the ambient near surface water temperatures, rather than daytime temporary fluctuations in temperature.

There is a strong agreement between the in situ thermistor string installed near the glacier terminus and spatial temperature surveys undertaken during the night time of 23<sup>rd</sup>, 24<sup>th</sup>, 25<sup>th</sup> and 26<sup>th</sup> of July 2017. The temperature observations of 3.0°C taken within ~2 m of the ice front during the 24<sup>th</sup> July survey are some of the first to be reported from an Arctic glacier front. This temperature observation alone confirms the null hypothesis of uniform 1°C proglacial lake temperatures to be false. What's more, the observations of rapid thermally eroded notch formation suggest that proglacial lake temperatures were sufficiently high to facilitate this process (Eijpen et al., 2003; Roehl, 2006). The spatial pattern of proglacial lake near surface temperatures then comes into question, as the water temperatures observed at the ice front are likely to be cooler due to contact with the glacier ice and input of meltwater (Eijpen et al., 2003; Roehl, 2006).

Constraining the extent of the cooling influence from the ice front on proglacial lake water temperatures is important for understanding how proglacial lakes influence glacier melt rates (Eijpen et al., 2003; Warren and Kirkbride, 2003; Roehl, 2006). This is particularly important given the observations of increased lake water temperatures across Northern Europe of 0.08°C a<sup>-1</sup> between 1985 and 2009 and future predictions of lake temperatures increasing 2.5°C by 2080-2100 under RCP 6.0 (Hook and Schneider, 2010; Woolway et al., 2019). The spatial temperature thermistor survey of 24<sup>th</sup> July was one of the first to capture the proglacial lake temperature gradient with distance away from an Arctic glacier front, with ice-proximal temperatures of 3.0°C and temperatures of 3.6°C ~150 m from the ice front (Figure 4.31) (Warren and Kirkbride, 2003). The consistency in temperatures beyond ~150 m (~3.7°C) suggests this survey directly constrains the spatial extent of glacier front (contact) cooling influence on proglacial lake temperatures at this time (Figure 4.31). These observations further prove the null hypothesis that proglacial lake temperatures are uniformly 1°C, to be false.

The consistency and agreement in water temperature readings at similar distances from the glacier front during surveys on 23<sup>rd</sup>, 24<sup>th</sup>, 25<sup>th</sup> and 26<sup>th</sup> July 2017 gives confidence that this represents the proglacial lake ambient water temperatures during this period, given the stable meteorological conditions. The more extensive spatial surveys on 26<sup>th</sup> July suggest that water temperatures then increased to 3.7°C ~200 m from the ice front. Capturing the spatial pattern

of proglacial lake water temperatures is imperative as currents (wind or water driven) may advect this water to the ice front and lead to increased melt rates (Eijpen et al., 2003; Warren and Kirkbride, 1998; Chikita et al., 1999; Roehl, 2006). Although there will also be a cooling influence from icebergs and contact with the glacier front, which may be visible in thermal infrared imagery taken at 90° to the water surface (Kraaijenbrink et al., 2018). Unfortunately, the utilisation of thermal infrared imagery to capture this temperature gradient at the ice front was compromised by logistical constraints (low viewing angle) from the survey position (Wake et al., 2015).

The 12 day water temperature record (1 m depth) from a thermistor directly at Kaskapakteglaciaren terminus in 2019 provides the longest temperature time series from an actively calving lacustrine glacier to our knowledge. This time series recorded temperatures of ~4°C from 29<sup>th</sup> July to 10<sup>th</sup> August 2019, with periods of temperatures above this (~5°C) likely to be associated with winds blowing warmer water at the terminus (Chikita et al., 1999). These temperatures alone are sufficiently high for thermal erosional notch development to occur on a lacustrine glacier front (Eijpen et al., 2003). These temperatures from 2019 are higher than the near surface temperature observations that were made at Kaskapakteglaciaren terminus during 2017 (July/August) of ~3°C by this study and similar observations of ~3°C made in the immediate vicinity (~10 m away) of Godley/Ruth glacier in New Zealand by Warren and Kirkbride (1998). There have however been higher temperatures (maximum 6.4°C) measured in surveys of water in thermal notches on Tasman glacier in New Zealand (Roehl, 2006).

During the fieldwork in 2019 there were periods of elevated wind speeds blowing towards the glacier, which created waves in lake water observed to be a maximum of ~20 cm high that could be heard striking the glacier front. This wave action is highly likely to have further enhanced thermal undercutting of the ice front (Kirkbride and Warren, 1997; Chikita et al., 1999; Roehl, 2006). Furthermore, lateral meltwater streams were observed to be entering the proglacial lake at either side of the glacier terminus, which are likely to further drive circulation at the terminus and increase subaqueous melt rates with further enhancement of thermal undercutting (Eijpen et al., 2003; Roehl, 2006). Therefore the conditions observed during July/August 2019 promoted rapid thermal undercutting of Kaskapakteglaciaren terminus through warm proglacial lake temperatures, water circulation and wave action on the ice front.

#### 4.5.4 Changes in Kaskapakteglaciaren Terminus Position and Geometry

There has been a substantial retreat of Kaskapakteglaciaren terminus since the 1959 Lantmateriet aerial image was taken (Figure 4.15). The lack of available regular high resolution imagery across the period since 1959 makes analysis of retreat rates problematic, as the climate and response of glaciers in the study area has varied during this time (Study Area Section) (Brugger, 2007). The period of positive mass balances during the late 1980s and early 1990s is thought to have led to Rabots and Storglaciaren coming into quasi-equilibrium with the climate, so the terminus position of Kaskapakteglaciaren may have stabilised during this time (Holmlund, 1988; Brugger, 2007). However, in light of the current sparsity of high resolution imagery required to precisely constrain the relatively narrow Kaskapakteglaciaren terminus position (200 m wide) between 1959 to 2008, the centreline retreat rate is tentatively discussed based on what available imagery was acquired.

There is a greater constraint of Kaskapakteglaciaren terminus position between 2008 and 2018, due to the higher availability of higher resolution imagery. The average annual retreat rate of  $15 \text{ m a}^{-1}$  (2008 to 2018) is substantially higher than the background retreat rate of  $7.53 \text{ m a}^{-1}$  (1959 to 2018) and the retreat rate of  $7.9 \text{ m a}^{-1}$  of the nearby Kebnepakte glacier from Tarfalsjon lake (1910 to 1940) (Kirchener et al., 2019). Although the validity of calculating annual retreat rates between images over such a large time period (59 years) is questionable, it can be best considered as a background comparison with substantial caveats. Whilst it is tempting to suggest that the higher retreat rate for the latter (much shorter) period may be partly due to increase in processes of mass loss at Kaskapakteglaciaren lacustrine terminus, the wider response of the glacier (such as surface lowering and velocity) to climatic changes are currently not known. There is also only one high resolution digital surface model (DSM) (2 m) currently available for Kaskapakteglaciaren from 2015, so calculation of surface lowering by differencing of DSMs is currently not possible. The lack of regularly available high resolution imagery also made calculation of glacier velocity from tracking of surface features not possible. Therefore interpreting the relative importance of processes of mass loss at the ice-water interface on the overall mass balance and terminus position of Kaskapakteglaciaren from remote sensing based study alone is highly problematic. It should be noted though, that there are prominent embayments in the terminus geometry in 2008, 2014, 2016, 2017 and 2018, which is discussed further below.

The terminus of Kaskapakteglaciaren was observed to have a thermal notch undercutting the subaerial ice cliff along long sections during fieldwork in the summer of 2017 and 2019 (Figure 4.14 and Figure 4.17). Thermally eroded notches have been observed on numerous other lake terminating glaciers (Kirkbride and Warren, 1997; Warren and Kirkbride, 1998; Roehl, 2006; Minowa et al., 2017; Mallalieu et al., 2020; Watson et al., 2020). At the start of fieldwork in July 2017 there was an extensive section of overhanging ice along most of the terminus (Figure 4.17), with a prominent cave in the central section. The development of a cave on the south east section of the terminus captured in time lapse imagery was due to the collapse of overhanging ice around a small portal at the waterline (Figure 4.18). The proximity of this small portal to crevasses running back from the glacier front, would suggest that it may be an englacial passage, which is further supported by the efficient evacuation of icebergs from the cave during the afternoon. It is likely that the flow of water emanating from this portal/cave drove circulation in proglacial water at the ice front and enhanced thermal undercutting (Roehl, 2006). Unfortunately it was not possible to measure water temperatures in the cave due to the limited range of the boat. However, it seems likely that water temperatures near this section of the terminus were sufficiently high to facilitate further thermal erosion undercutting the sidewalls of both caves. It is proposed that this process is likely to have continued until collapse of the cave roofs produced the prominent embayment on the south east section of the terminus in September 2017 (Figure 4.16). Although unfortunately this cannot be confirmed due to the limited period of time lapse imagery.

The western section of Kaskapakteglaciaren terminus had a notably different geometry in 2017, with a distinct thermal notch overhang at the waterline but vertical subaerial ice cliff above this (Figure 4.17). The large calving event that occurred above this thermal notch on 26<sup>th</sup> July is one of the first to be reported from a lacustrine terminating glacier in the Arctic, although similar processes have been reported at Russel proglacial lake in Greenland (Mallalieu et al., 2017). Following the 26<sup>th</sup> July calving event, the subaerial ice cliff had no visible thermally eroded notch at the waterline, suggesting that the thermal undercutting had resulted in failure of the subaerial ice cliff above the notch (Kirkbride and Warren, 1997; Roehl et al., 2006). Furthermore, the remote controlled boat survey of 4<sup>th</sup> August shows the extent of thermally eroded notch development in a relatively limited time period (9 days) (Figure 4.39). The sharp boundary of the notch is interpreted to be due to the fresh thermal erosion from lake water, during the 9 day period when high rainfall led to a rise in the lake level of ~30 cm (Figure 4.39). This high rainfall is also likely to have led to a high influx of

meltwater from the glacier, which will likely have driven circulation currents at the terminus and enhanced thermal undercutting, as observed in New Zealand by Roehl (2006). Whilst the temperature of the meltwater during this 9 day period was not measured, the thermistor survey from 4<sup>th</sup> August measured temperatures of 3.8°C at the ice front, which are high enough to facilitate thermal erosion (Eijpen et al., 2003).



Figure 4.39 Image from GoPro Hero4 camera of Norra Kaskasapakte glacier, Arctic Sweden (A.Dye, 4/8/2017). Note the thermally eroded notch shadow extending along the glacier terminus at the water to ice contact point. The height of the subaerial ice cliff is estimated to be ~5 m

The observations of Kaskapakteglaciaren terminus made during fieldwork in 2019 provided further direct evidence of thermal undercutting enhancing rates of mass loss at the contact point of this glacier with proglacial lake water. At the start of fieldwork on 29<sup>th</sup> July 2019 a substantial undercut in the subaerial ice front was evident (Figure 4.14). The proglacial water temperatures of ~4°C at 1 m depth suggest that this undercutting of the subaerial ice front was due to thermal erosion from proglacial lake water, further enhanced by winds blowing warm water towards the terminus and action of waves on the ice front. The 12 day temperature series shows that ice proximal proglacial water temperatures stayed around 4°C during this period, with some isolated periods of lower temperatures due to the cooling influence of

icebergs (Figure 4.38). These icebergs were produced by the collapse of the subaerial ice cliff above the thermally eroded notch (Figure 4.38). This occurred in two stages, with an initial collapse of the subaerial ice cliff to form a prominent arch/cave feature, followed by crack development along the roof of the cave on the glacier surface, which led to the collapse of the arch/cave roof several days later. The thermistor at 1 m depth survived these calving events and the 12 day temperature series is one of the first to be recorded at an actively calving glacier front to our knowledge. This temperature time series provides important direct evidence of high proglacial lake water temperatures leading to thermal erosion of a lacustrine glacier terminus and enhancement of glacier mass loss. Therefore proving that proglacial lake temperatures can be sufficiently high ( $4^{\circ}\text{C}$ ) to enhance mass loss and contribute to the retreat of an Arctic glacier (Eijpen et al., 2003).

#### **4.5.5 Wider Implications for Proglacial Lake Temperatures and Recommendations for Future Study**

Inspection of Sentinel 2 satellite imagery suggests the proglacial lake at Kaskapakteglaciaren became totally ice free around 29<sup>th</sup> June 2017. This left a relatively short period of time of open water for meteorological conditions to influence the water temperatures of the proglacial lake before fieldwork began on 23<sup>rd</sup> July 2017. Despite this relatively short period of open water of 1 month, this study observed ambient water temperatures of  $\sim 5^{\circ}\text{C}$  at the distal end of the lake and  $\sim 3^{\circ}\text{C}$  near the ice front during fieldwork in 2017. These observations were made whilst other similarly sized lakes in the area (at Marmapakte and Tarfalasjon) still had a substantial ice cover ( $\sim 75\%$ ) in Sentinel 2 imagery, despite being only  $\sim 100$  m higher in elevation. This raises the question as to why Kaskapakteglaciaren proglacial lake became ice free and warmed up so early in comparison to other lakes.

It should be noted that Kaskapakte proglacial lake was observed to have a high turbidity throughout the fieldwork (and in satellite imagery dating back to 2001), whereas the other two lakes were observed to have lower turbidity in Sentinel 2 imagery. It is proposed that the high level of turbidity reduces the depth of solar radiation penetration into the water, as is supported by the low light intensity (below 1,000 lux) observed near the outlet and the terminus (Figure 4.23 and Figure 4.26). Consequently solar warming is concentrated in the near surface water during the day time, with a relatively short period of cooling during the nighttime period (Figure 4.23 and Figure 4.26) (Chikita et al., 1999; Richards et al., 2012; Peter and Sommaruga, 2017). Personal communications with G. Kirillin (2018) have

confirmed that the high turbidity limiting light penetration to depth is the likely reason for how near surface temperatures were able to rise to  $\sim 5^{\circ}\text{C}$  at the distal end of the lake and  $\sim 3^{\circ}\text{C}$  near the terminus of Kaskapakteglaciaren over 1 month (Chikita et al., 1999). This is a pertinent area for further research, particularly given the relatively rapid formation of thermally eroded notches on the ice front and associated iceberg calving observed in this study during summer 2017 and 2019 (Figure 4.18; Figure 4.19 and Figure 4.35). Further research should also try to install thermistor strings closer to the glacier terminus, to investigate changes in proglacial lake temperature at depth, particularly following the passing of icebergs.

The relatively short cooling period observed at night time during the summer fieldwork at Kaskapakteglaciaren proglacial lake ( $67^{\circ}\text{N}$ ) is likely to be a factor in the ambient lake water temperatures remaining relatively high (Richards et al., 2012). Also, proglacial lakes at higher latitudes that experience longer periods with the sun above the horizon may also have shorter night time cooling periods. This may result in proglacial lakes at higher latitudes having higher ambient temperatures than expected, but this may also be mitigated by the lower levels of incoming solar radiation due to the lower solar zenith angle (O'Reilly et al., 2015). The observation of enhanced retreat rates of glaciers terminating in lakes on Novaya Zemlya in the Russian Arctic as reported by Carr and others (2013), suggests that proglacial lake temperatures in areas of the Arctic may require further investigation.

A more precise constraint of the spatial pattern of proglacial lake skin surface temperatures would require a thermal camera to be mounted on an Unmanned Aerial Vehicle (UAV) (Kraaijenbrink et al., 2018). This would minimise the reflection of longwave radiation from surrounding mountainsides that results in erroneous skin surface temperature readings in the thermal imagery, due to the imagery being captured at  $90^{\circ}$  to the target surface (Aubry-Wake et al., 2015). Furthermore, the difference between body temperatures (measured by thermistors) and skin surface temperature in the thermal imagery would be reduced with a UAV based survey, particularly as the emissivity of water is 0.98 only at  $90^{\circ}$  to the surface (Kraaijenbrink et al., 2018). The use of ground control points with known emissivity, would also enable thermal imagery to be merged together to produce a map of surface temperature patterns (Kraaijenbrink et al., 2018).

Whilst any subsequently produced spatial map of skin surface temperatures would be limited by the flight time of the UAV, it would provide the opportunity for defining temperature

patterns in high resolution at particular focus points (such as at the glacier terminus). Where there is a substantial temperature gradient ( $>2^{\circ}\text{C}$ ) between meltwater and ambient lake water, this is likely to be detectable in thermal imagery given the resolution of thermal cameras. Therefore thermal imagery may be useful in spatially constraining the influx of meltwater in ice proximal areas and investigating how this drives circulation of lake water. The improved viewing angle of  $90^{\circ}$  to the water surface would also enable a more robust relationship between near surface water temperatures and skin surface temperatures from thermal imagery to be established (Donlon et al., 2012).

The upscaling of mapping proglacial lake surface temperatures from UAV based thermal imagery would provide highly valuable validation of satellite thermal imagery. Although the relatively low spatial resolution of satellite thermal imagery (ASTER TIR 90 m) would mean it would be problematic to resolve skin surface temperatures focus points at the boundary of different bodies (e.g. lake to glacier contact point). However, the ability to resolve skin surface temperatures of the main body of proglacial lakes across remote areas provides a powerful tool in assessing the potential influence of lake temperature on glacier melt rates on the larger scale. This is particularly important given the projected air temperature increases with future climate change scenarios (IPCC AR5, 2013).

## **4.6 Conclusion**

This study provides some of the first water temperatures and observations of calving to be made at the contact point between an Arctic glacier and a proglacial lake. The near surface ambient temperature observations of  $\sim 3^{\circ}\text{C}$  during 2017 and  $\sim 4^{\circ}\text{C}$  during 2019 made at the glacier front are substantially higher than the  $1^{\circ}\text{C}$  temperatures that have been assumed to be uniformly distributed across proglacial lakes (Boyce et al., 2007; Chernos et al., 2016). Furthermore, the observations of ambient near surface temperatures of  $\sim 5^{\circ}\text{C}$  at the distal end of the proglacial lake during 2017 prove that the temperature pattern across the lake is not uniform. The temperatures reported in this study are notably higher than  $1^{\circ}\text{C}$  and therefore suggest that proglacial lakes can have a greater influence on glacier melt and retreat rates than previously thought. This is also supported by the observations made in this study of rapid thermally eroded notch formation in the ice front following a period of substantial calving activity during 2017. This is further supported by observations of calving events

above thermally eroded notches during 2019 and a 12 day data series from the calving front with near surface water temperatures of 4°C for most of the period.

The precise pattern in proglacial lake near surface temperatures needs to be greater constrained in conjunction with glacier melt rates. This could be achieved using a thermal infrared camera mounted on a UAV to constrain surface temperatures more precisely spatially and temporally. This is particularly important given the future predicted increase in lake temperatures of 2.5°C under RCP 6.0 (Woolway et al., 2019). Therefore it is important to constrain proglacial lake water temperatures to improve predictions of glacier retreat rates. There are also ecological impacts of increased proglacial lake temperatures, as temperature dependent species may be affected (Fellman et al., 2014).

## 5 Discussion and Conclusions

This chapter provides an overview of all the findings from the different chapters and brings them together in the overall conclusion of the thesis. The literature review in the first chapter explores the proglacial lacustrine system and influence on neighbouring glaciers in a range of environments. This provides the reader with a background into research exploring how proglacial lakes influence the response of glaciers to changes in climate. The study area in Arctic Sweden has recently experienced an increased number of heatwaves, with positive sunshine anomalies, which makes it an important area to explore whether proglacial lake temperatures are higher than the 1°C that has previously assumed (Truffer and Motyka, 2016; Sinclair et al., 2018).

For the investigation of proglacial lake influence on glacier retreat rates, it is first of all essential to consider the spatial aspect of the problem. Therefore a proglacial lake inventory of Arctic Sweden was created from manual mapping of satellite imagery. The ASTER imagery from 8/8/2014 was utilised as it is considered to have the maximum extent of proglacial lakes in Arctic Sweden, due to the low cloud and snow cover. This inventory from 2014 was utilised to compare proglacial lake extent to those visibly present in aerial imagery from the 1950s/60s, with an increase in number and extent of proglacial lakes reported over this period. To investigate the spatial relationship between proglacial lakes and glaciers further, the retreat rates of land and lacustrine glaciers were investigated between 2010 and 2018, with the highest retreat occurring at a lake terminating glacier. The polygons of the 12 largest proglacial lakes ( $>129,600\text{m}^2$ ) from mapping presented in the second chapter were utilised for analysis of ASTER surface temperature product (AST08) to extract proglacial lake skin surface temperatures ( $SST_L$ ). The skin surface temperatures of proglacial lakes presented ( $SST_{LAV} 8.9^\circ\text{C}$ ) in this study are substantially higher than the 1°C that has previously been assumed before (Truffer and Motyka, 2016). Thus raising the question as to whether warmer proglacial lake water temperatures could lead to higher rates of mass loss at lacustrine glacier termini. Furthermore, the complex spatial patterns of  $SST_L$  reported in chapter 3 suggest a variety of factors control proglacial lake thermal regime, particularly the relationship with the parent glacier, which forms the basis of the conceptual model proposed in this chapter.

The final chapter investigates the spatial pattern of proglacial lake water temperatures and persistence through time during two field work campaigns at Kaskapakteglaciaren in 2017

and 2019. This chapter is a more in depth approach to the problem and builds on the findings of the previous two chapters, that both have a remote sensing based approach. The findings from the final chapter of warm proglacial lake temperatures (3 to 8°C), support the SST<sub>L</sub> presented in chapter 3, with a similar temperature distribution for Kaskapakte proglacial lake. The observations from time lapse imagery of rapid thermally eroded notch formation on the glacier terminus, followed by substantial iceberg calving events, gives good evidence of proglacial lake water temperatures enhancing the mass loss of an Arctic glacier. Therefore providing evidence from the field of processes contributing to the retreat rates of lacustrine terminating glaciers, as reported in chapter 2 and further supported by terminus mapping from high resolution satellite imagery. The temperature record directly from the ice-water contact point gives evidence of proglacial lake water temperatures being sufficiently high (~4°C) to enhance subaqueous melt rates for a relatively long (12 days) period of time.

The following chapter discusses the findings from research presented in Chapters 2,3 and 4 in relation to the objectives set out in Chapter 1. For a more detailed discussion and presentation of the results the reader is referred to each individual section.

### **5.1.1 Objective 1: Create a proglacial lake inventory for Arctic Sweden and analyse the spatial pattern of proglacial lakes (Chapter 2).**

To date there has been limited studies into the extent of proglacial lakes in the Arctic and only studies of isolated proglacial lakes in Scandinavia (Kennet et al., 1997; Carrivick and Quincey, 2014). Although there have been several studies focusing on the sedimentary record of isolated proglacial lakes in Norway. The first objective of this study therefore was to create a proglacial lake inventory for an area of Arctic Sweden. The study area in Arctic Sweden has a relatively diverse population of glaciers, ranging from larger plateau icefields in the western part, to larger corrie/valley glaciers in the southern part (Sarek) and a mixture of small valley and corrie glaciers in the area surrounding Kebnekaise. Therefore providing a good study area to investigate the spatial extent of proglacial lakes, across a relatively diverse range of glaciers.

The creation of a proglacial lake inventory from remote sensing required conditions with low snow cover and low cloud cover in order to capture the maximal extent of proglacial lakes. This also required relatively high resolution satellite imagery for detection and delineation of

proglacial lakes. The relatively low snow cover of August 2014 and clear sky conditions provided ideal conditions for creating a proglacial lake inventory, which was mapped manually using ASTER (15m) satellite imagery. There was a substantial proportion (29.4%) of glaciers in the study area of Arctic Sweden, which had a proglacial lake in the forefield. The total area of 4,767, 295 m<sup>2</sup> covered by the 108 proglacial lakes in the inventory represents a substantial area of water that was previously not included within the Global Lake and Wetland Database (GLWD) (Birkett et al., 1995). A large proportion (42%) of the 108 proglacial lakes mapped in Arctic Sweden were classed as being in contact with glacier termini and therefore had the potential to influence glacier retreat rates through enhancing mass loss.

The spatial distribution of proglacial lakes across Arctic Sweden was largely governed by characteristics of the parent glacier. The previous Little Ice Age maximum glacier extent (~1910) constrained the location of proglacial lakes in this study, as reflected in the relatively limited elevation band for proglacial lakes. The aspect of proglacial lake watersheds tended to be northerly through to easterly, as per the aspect of most glaciers in the area (including those without proglacial lakes). Most of the proglacial lakes in the study area were relatively small (<100,000 m<sup>2</sup>) and only 12 were >130,000 m<sup>2</sup>, the outlines of which were used with ASTER thermal imagery for analysis of surface temperature in Chapter 3.

There was a significant difference in proglacial lake size across the study area, with the southern region of Sarek having significantly smaller proglacial lakes than the Kebnekaise and surrounding areas. This is due to the style and extent of glaciers and topography in each area, as Sarek has more extensive glaciers that extend beyond corrie/valley rims into larger valley systems that results in less previously subglacial hollows for proglacial lakes to fill. In contrast the Kebnekaise and surrounding areas have numerous smaller corrie glaciers with prominent terminal moraine systems that provide proglacial lake dams. The largest proglacial lakes in the area tend to extend beyond the Little Ice Age maximum extent and some of these larger lakes are associated with the larger plateau icefield systems to the west.

### **5.1.2 Objective 2; Quantify the change in proglacial lake extent through time.**

The number of proglacial lakes in Arctic Sweden has increased since the 1950s/60s, with 45% of proglacial lakes examined previously buried under glacial ice that were that were present in 2014. There has also been an increase in area of proglacial lakes since the 1950s/60s, with an increase in mean (n=11) area from 176,091 m<sup>2</sup> in the 1950s/60s to

199,701 m<sup>2</sup> in 2014. Although this was only a relatively small sample (33 out of 108) of proglacial lakes in Arctic Sweden, it is a key result as it provides further evidence of proglacial lakes increasing in number and extent, as has been reported for the south west section of the Greenland ice sheet (Carrivick and Quincey, 2014). More high resolution imagery would enable the changing spatial pattern of proglacial lakes to be constrained more precisely through time.

### **5.1.3 Objective 3; Characterise the patterns in glacier retreat rates in Arctic Sweden.**

The relatively high snow cover in the aerial imagery from the 1950s/60s made precise quantification of glacier terminus retreat problematic, due to snow concealing margins of most glaciers. The Kaskapakteglaciaren had a relatively snow free terminus in a proglacial lake in 1959, which has undergone a centerline retreat of ~350 m up to 2014. This is a substantial retreat of a lake terminating glacier, although the land terminating Rabot's glacier underwent a higher centerline retreat of ~600 m between 1959 to 2014. Thus suggesting that as land terminating glaciers experienced greater retreat between 1959 to 2014, it seems unlikely that the proglacial lake enhanced retreat during this period. However no two glaciers are the same and the response time of each glacier needs to be taken into account, which requires fieldwork and the use of techniques such as Radar to ascertain thermal structure and bed topography of each glacier (Brugger, 2007).

The termini of 24 glaciers in the Kebnekaise area were mapped in Rapid Eye satellite images (5m) from 2010 and 2018. The relatively snow free conditions and resolution of the imagery enabled the glacier margins to be delineated and a width averaged retreat rate to be calculated (Lea et al., 2014). The glaciers were classified as lake terminating or land terminating, which was further subdivided by the presence of a proglacial lake in the forefield. The glaciers with a proglacial lake in the forefield had the highest mean retreat rate, although this was skewed by the one glacier in the small dataset (n=5), with the large retreat (122 m) of Isfallsglaciaren over a prominent icefall. Lake terminating glaciers had a higher mean retreat rate (6.63 m a<sup>-1</sup>) than land terminating glaciers with no proglacial lake (5.59 m a<sup>-1</sup>). The relatively small area of snow/cloud free available Rapid Eye satellite imagery resulted in small sample sizes of each glacier class, which makes the representativeness of this sample for the rest of Arctic Sweden questionable. In light of this problematic sample size, one lake terminating glacier was studied in detail.

The largest retreat out of the 24 glaciers, was for the lake terminating Kaskapakteglaciaren , which retreated 126 m between 2010 and 2018. This equates to an annual retreat rate of 15.75 m a<sup>-1</sup>, which is very similar to the retreat rate of 15.00 m a<sup>-1</sup> from manual mapping of terminus positions between 2008 and 2018. The mapping of previous terminus positions revealed prominent embayments along the steep ice cliff with prominent shadows along the glacier front in all images through this period. This geometry suggests that Kaskapakteglaciaren had a calving front from at least 2008 to 2018 and is further supported by icebergs in the proglacial lake visible in satellite imagery throughout this period (Kirkbride and Warren, 1997).

#### **5.1.4 Objective 5: Analyse skin surface temperatures of the 12 largest proglacial lakes across Arctic Sweden.**

This study reports some of the first surface temperatures for proglacial lakes extracted from satellite thermal imagery. The available literature for extracting skin (top mm) surface temperatures from over water bodies using the ASTER temperature product (AST08) was reviewed and used to develop a robust workflow presented in this study. The problems surrounding atmospheric correction of the AST08 product in Maritime areas were addressed through collating near surface temperature data from a lake ~50km away, with further data from a proglacial lake in Patagonia. The strong correlation between these thermistor readings ( $R^2=0.9365$ ) and the skin surface temperatures ( $SST_L$ ) extracted from the AST08 product provides a relatively strong validation. The quality control of selecting cloud free imagery for extracting pixel values from the AST08 temperature product adds further robustness to the workflow developed for extracting  $SST_L$  for proglacial lakes in maritime areas.

The proglacial lake average skin surface temperature ( $SST_{LAV}$ ) of 8.9°C in Arctic Sweden on 8/8/2014 is substantially higher than the 1°C commonly assumed for proglacial lakes (Chernos et al., 2016; Truffer and Motyka, 2016). There was also high heterogeneity in temperatures between proglacial lakes which suggests local factors had a strong influence on SST of proglacial lakes. The high standard deviation (2.0°C) and large range in proglacial lake skin surface temperatures ( $SST_L$ ) suggests there is clearly a high level of complexity for such temperatures relating to micro-climate and relationship with parent glacier (Peter and Sommaruga, 2017).

### **5.1.5 Objective 6: Assess the relationship between spatial patterns in proglacial lake skin surface temperature and factors affecting thermal regime of each proglacial lake.**

The spatial patterns of skin surface temperature were examined in relationship with surrounding topo-climatic factors and relationship with the parent glacier for 12 proglacial lakes in Arctic Sweden. There was a moderate positive correlation ( $R^2=0.5932$ ) between  $SST_{LAV}$  and parent glacier aspect, which suggests the exposure of incoming solar radiation was a strong influence on the  $SST_L$  of the 12 proglacial lakes in this study. Several lakes also had areas of cooler  $SST_L$ s in close proximity to the parent glaciers, which suggests strong cooling influences from parent glaciers for some proglacial lakes. Indeed  $SST_{LAV}$  for ice contact proglacial lakes was lower ( $8.2^\circ\text{C}$ ) than for non-ice contact proglacial lakes ( $9.2^\circ\text{C}$ ), although the difference in  $SST_{LAV}$  between the ice contact and non-ice contact proglacial lakes is not significant. This suggests that aspect and influx of meltwater may also be strong cooling influences on some non-ice contact proglacial lakes.

These spatial patterns in  $SST_L$  have been interpreted and used to propose a conceptual model classifying proglacial lake surface temperature by different stages of deglaciation. This conceptual model will need to be further validated by more analysis of satellite thermal imagery (ideally higher resolution) and field observations of proglacial lake temperatures, ideally with UAV based thermal imagery.

### **5.1.6 Objective 7: Measure spatial pattern of near surface temperature across a proglacial lake and analyse persistence over time.**

The spatial pattern in surface temperatures of Kaskapakte proglacial lake was investigated during fieldwork in July/August 2017. A series of spatial temperature surveys were undertaken with thermistors (HOBO UA-002-08) suspended under a remote controlled boat and thermal infrared imagery surveys (FLIR A65) near the terminus area of Kaskapakteglaciaren and outlet of the proglacial lake. These surveys revealed a strong temperature gradient across the proglacial lake during the first week of fieldwork in July 2017, with ambient temperatures of  $5^\circ\text{C}$  near the outlet and  $3^\circ\text{C}$  near the glacier terminus. The maximum proglacial lake water temperatures measured were also higher near the outlet

( $\sim 8^{\circ}\text{C}$  at 50cm depth) than near the glacier terminus ( $\sim 4^{\circ}\text{C}$ ), which reflects the relative cooling influence from contact with the glacier acting on the temperature gradient across the lake. Thus proving the null hypothesis that proglacial lakes are uniformly  $1^{\circ}\text{C}$ , to be false (Truffer and Motyka, 2016).

The presence of icebergs was also observed to have a cooling influence on lake temperatures, which was spatially constrained for the first time using thermal infrared imagery. This was validated from thermistor readings from a remote controlled boat, which confirmed the meltwater/cold influence of icebergs on lake temperature to be limited to be relatively small (several metres) and roughly proportional to the area of icebergs. Therefore suggesting that a large volume of icebergs would be required to sufficiently cool Kaskapakte proglacial lake to  $1^{\circ}\text{C}$ , as has been suggested for lakes in New Zealand by Warren and Kirkbride (1998). Additionally, during fieldwork in 2017 most icebergs were observed to be exported towards the lake outlet, where they melted relatively rapidly in  $\sim 5^{\circ}\text{C}$  water, which was only subject to the cooling influence of icebergs for a relatively short time ( $\sim 24$  to 48 hours).

### **5.1.7 Objective 8: Measure water surface temperatures directly at the glacier-lake contact point and analyse rates of change over time**

The lacustrine terminus of Kaskapakteglaciaren was observed to have an undercut notch at the waterline during fieldwork in 2017 and 2019. Several calving events above undercut sections of the ice front were also captured in time lapse imagery. The proglacial water temperatures observed at and around the terminus during this study in 2017 and 2019 of between  $3^{\circ}\text{C}$  to  $4^{\circ}\text{C}$  were sufficiently high for thermal erosion of the terminus to occur (Eijpen et al., 2003; Roehl, 2006). A number of spatial temperature surveys around the terminus were conducted during 2017, which observed temperatures of  $\sim 3^{\circ}\text{C}$  at the ice front and temperatures increasing to  $\sim 3.8^{\circ}\text{C}$  up to  $\sim 200$  m distance from the ice front, beyond which distance they remained stable. This temperature gradient is one of the first to be recorded directly away from an Arctic lacustrine terminating glacier and suggests that the zone of cooling (on proglacial lake water) associated with direct contact with the ice front was relatively limited at this time (July 2017).

The 12 day temperature series from a thermistor suspended (1 m depth) from Kaskapakteglaciaren terminus from 29<sup>th</sup> July to 10<sup>th</sup> August is the longest temperature record

from an active calving front to our knowledge. The period of several days of water temperatures of  $\sim 4^{\circ}\text{C}$  (and up to  $5^{\circ}\text{C}$ ) provide direct evidence of warm proglacial water temperatures persisting at an actively calving lacustrine glacier front. Furthermore, there were several calving events during this period, which had a relatively short cooling influence on proglacial lake water around the temperature sensor, as temperatures returned to  $4^{\circ}\text{C}$  following these events. These warm ice-proximal proglacial lake water temperatures and observations of calving above thermally eroded notches, provides strong evidence of a proglacial lake enhancing the mass loss of an Arctic glacier through thermal processes. This is the first report of proglacial lake temperatures enhancing the mass loss and contributing to the retreat rate of an Arctic glacier to our knowledge at this time.

## 5.2 Conclusions

The overall aim for this thesis was to investigate the temperature of proglacial lakes and the influence on glacier retreat rates in Arctic Sweden. To achieve this aim the spatial extent and changes over time of proglacial lakes in Arctic Sweden was first of all investigated through remotely mapping proglacial lakes from satellite imagery. A similar remote sensing based approach was used to map glacier termini where suitable cloud/snow free satellite imagery was available. The investigation of proglacial lake skin surface temperatures across Arctic Sweden also utilized a remote sensing based approach through extracting temperatures from the ASTER land surface temperature product (AST08). Whilst Chapter 4 reports the results from fieldwork conducted at Kaskapakte proglacial lake, with some of the first temperature measurements and observations of geometry change and calving at a lacustrine terminating Arctic glacier. The implications from all of these results are discussed below in the wider context of the overall aim of the thesis.

The proglacial lake inventory of Arctic Sweden by this study covers 108 proglacial lakes with a total area of  $4,767,295\text{ m}^2$ , which is a substantial area of lakes that were not previously included in the Global Lake and Wetlands Database (GLWD). The inventory from this study therefore spatially constrains a substantial store of freshwater that was previously not mapped, although the volume of lakes has not been calculated due to the high heterogeneity of lake geometries across the area. The recent study of Pierre et al. (2019) called for a global proglacial lake inventory as they argued that proglacial freshwaters may be a substantial sink

and store of atmospheric CO<sub>2</sub>, through chemical weathering of suspended sediments. This study has contributed to the start of a proglacial lake inventory for Scandinavia. The emergence of these proglacial lakes as glaciers recede also has implications for ecosystems and human populations downstream as they form a prominent part of the hydrological systems and may regulate water temperatures through the summer (Fellman et al., 2014).

There has been an increase in the number and extent of proglacial lakes in Arctic Sweden since the 1950s/60s. The study of Carrivick and Quincey (2014) also reported an increase in number and extent of proglacial lakes in South West Greenland since the mid 1980s, but studies into Arctic proglacial lakes currently remain limited. Note that proglacial lakes in Iceland have also been the subject of study (Churski, 1973), but are not considered directly here as they lie outside of the Arctic circle. There have also been numerous studies into proglacial lake extent in other regions of the world, but the current lack of Arctic proglacial lake inventories should be addressed.

The influence of proglacial lakes on glacier retreat rates in Arctic Sweden is difficult to address through remote sensing due to the heterogeneity in glacier responses to climate (Brugger, 2007). There can be substantial differences between glaciers in proximity that affect the response time to changes in climate, such as bed topography and thermal regime (Brugger, 2007). This heterogeneity means that in order to directly compare the responses of glaciers to climatic events, extensive fieldwork needs to be carried out with intensive methods such as Radar surveys and mass balance monitoring. Therefore it is highly problematic comparing terminus changes of a limited sample of glaciers over a short duration, as glaciers respond to climatic changes at different rates, which may be missed by a narrow time window. The classification of glaciers as land or lake terminating when investigating the influence of proglacial lakes on glacier retreat rates is also over simplistic. Other characteristics need to be taken into account, such as lake depth, temperature and amount of lateral/backstress that may be supporting the glacier from sidewalls or moraine (Boyce et al., 2007). In order to further study the influence of proglacial lakes on glacier retreat rates over time a greater extent of high resolution imagery is required to improve the sample size and also at more regular intervals, to improve exploring the relationship with climatic events.

The largest retreat out of the 24 glacier termini mapped between 2010 and 2018 was 126 m at the lake terminating Kaskapakteglaciaren (~200 m wide), which gives an annual retreat rate

of  $15.75 \text{ m a}^{-1}$ . A similar amount of retreat occurred at the land terminating Isfallsglaciaren (122 m), which has a prominent icefall at the terminus. The presence of this icefall at the terminus raises the issue as to whether Isfallsglaciaren makes a suitable comparison to a lake terminating glacier such as Kaskapakteglaciaren which does not have an icefall at the terminus. This raises the issue as to why caution should be exercised when comparing glaciers with different characteristics. There have been much higher retreat rates ( $\sim 49 \text{ m a}^{-1}$ ) of lake terminating glaciers reported in the Russian Arctic (Novaya Zemlya) by Carr et al. (2017), which is unsurprising as the wider glacier termini on Novaya Zemlya will be subject to less lateral backstress and therefore likely to experience higher calving rates (Boyce et al., 2007). Whilst the larger systems of Novaya Zemlya may not make ideal direct comparisons of lake terminating glacier retreat rates with Kaskapakteglaciaren, they do suggest that the influence of proglacial lakes on glacier retreat rates should also be more closely investigated elsewhere in the Arctic.

In light of the problems associated with comparing different glaciers from remote sensing based studies, a fieldwork campaign was undertaken at Kaskapakteglaciaren in Arctic Sweden. The aim of the fieldwork was to measure the water temperature of the proglacial lake and assess the influence on the geometry of the glacier front. At the start of fieldwork in July 2017 the subaerial ice cliff was observed to be undercut along large sections of the terminus, with a large cave in the centre of the terminus. A series of calving events were observed that were interpreted to be due to collapses of the subaerial ice front above the undercut at the waterline. The temperature observations of  $\sim 3^\circ\text{C}$  during fieldwork in 2017 are some of the first to be reported from an actively calving lacustrine Arctic glacier. The temperatures reported from the ice front support the interpretation that the undercutting of the subaerial terminus was due to thermal erosion, with further enhancement of this process by lake currents at the ice front (Eijpen et al., 2003; Roehl, 2006). A similar geometry with prominent undercutting at the waterline was observed during July/August 2019 and water temperatures of  $\sim 4^\circ\text{C}$  recorded directly at the ice front confirm that this was a thermally eroded notch. These high temperatures of  $\sim 4^\circ\text{C}$  persisted at the ice front over several days and combined with wind driven currents (and waves) towards the terminus resulted in further thermal erosion and subsequent calving events. Thereby providing direct evidence of proglacial lake temperatures directly influencing mass loss and contributing to the retreat of an Arctic glacier.

There was also a temperature gradient evident across Kaskapakte proglacial lake (AST08<sub>ID</sub> = 6) in analysis of AST08 satellite temperature product from 8<sup>th</sup> August 2014, with colder temperatures near the glacier and a warmer ice distal area. It is argued that this temperature gradient is possible as the length of the proglacial lake is substantially larger than the width of contact with Kaskapakteglaciaren. Therefore the ice-distal parts of the proglacial lake is beyond the cooling influence from direct contact with Kaskapakteglaciaren, although the lake may still be cooled by influx of meltwater from the glacier. This proglacial lake was classed as ‘Established’ under the proposed conceptual model in Chapter 3, that relates proglacial lake thermal regime to stage of deglaciation. This conceptual model was proposed through geometric considerations of the relative size of the proglacial lake in proportion to the glacier. Essentially considering whether each lake was large enough to have an ice-distal area sufficiently far enough away from the glacier terminus to be beyond the cooling influence of direct contact. This conceptual model was also developed through examining the spatial pattern of skin surface temperatures (SST<sub>L</sub>) from the ASTER temperature product (AST08) for several case studies of proglacial lakes. The analysis of the AST08 temperature product revealed a complex pattern of proglacial lake skin surface temperatures across the 12 lakes investigated. All of these 12 proglacial lakes had skin surface temperatures higher than 1°C, (SST<sub>LAV</sub> 8.9°C), which further proves the null hypothesis to be false for proglacial lakes in Arctic Sweden. Furthermore, it also shows that the relatively high temperatures measured in Kaskapakte proglacial lake are not an isolated case, as proglacial lakes across Arctic Sweden were found to have warm (>4°C) skin surface temperatures on 8<sup>th</sup> August 2014. The robust workflow used in this study for extracting skin surface temperatures from the AST08 temperature product should be utilised to investigate temperatures of proglacial lakes in other areas of the Arctic (such as Novaya Zemlya). This is particularly important given that lakes temperatures are predicted to increase by a median of 2.5°C by 2080-2100 under RCP 6.0 (Woolway et al., 2019).

Given the future predictions of increases in lake temperatures, further investigation of proglacial lake thermal regime is essential. Understanding how proglacial lake thermal regimes respond to climatic changes is not only important for predicting how lacustrine terminating glaciers will respond, but also paramount to understanding how the associated hydrological system will respond too (Warren and Kirkbride, 1998; Roehl, 2006; Fellman et al., 2014). Future study of proglacial lakes should utilise remote sensing based approaches to

assess the wider picture, as well as fieldwork based studies to identify changes on smaller scales.

The utilisation of remote sensing can enable a world inventory of proglacial lakes, particularly given the freely available Sentinel 2 imagery with high spatial, temporal and radiometric resolution. This inventory has been called for by Pierre et al. (2019) after the findings that proglacial freshwater can be a substantial sink of atmospheric carbon dioxide through chemical weathering of suspended sediment. Therefore the creation of a proglacial lake world inventory would facilitate an assessment of the role that they play in the global carbon budget. Furthermore, it would also provide some assessment of the water storage that they hold, which has substantial implications for assessing freshwater input to oceans and vital water resources in areas with high aridity. The utilisation of remote sensing enables these aims to be achieved over large and remote areas.

The development of a robust workflow in this study for obtaining proglacial lake skin surface temperatures can be utilised over proglacial lakes in other regions. Although this should be done cautiously given the technical issues discussed in chapter 4, particularly regarding the timing of image capture during the diurnal temperature cycle. This would facilitate the investigation of proglacial lake skin surface temperatures in remote regions that are difficult to access, such as the Russian Arctic, which is particularly pertinent given the Arctic Amplification of Climate Change. Furthermore, analysis of the back catalogue of the ASTER temperature product (AST08) may enable extraction of proglacial lake skin surface temperatures back to the launch of the satellite in 2000. This may facilitate the links between changes in proglacial lake skin surface temperatures and changes in climatic parameters (air temperature, incoming shortwave solar radiation) to be investigated more closely on the annual to decadal timescale. What's more it would also facilitate investigation of the evolution of non-glacial lake skin surface temperatures on annual to decadal timescale.

The precise quantification of factors controlling the thermal regime of proglacial lakes will require field studies to obtain high resolution data. This will require sustained field campaigns throughout and beyond the melt season, as it is important to capture ambient lake temperatures before warming influences occur and also after they cease. There is likely to be a high variability in characteristics of proglacial lakes; due to differences in formation (particularly those from debris covered glaciers), subglacial erosion rates and underlying geology. Therefore bathymetric surveys will be vital for ascertaining lake volume and also

the influence of lake bed geometry on circulation currents. Therefore field campaigns will need to be highly specialised to the particular field site, especially as the main challenge to extracting valuable datasets is understanding the typical production processes and transportation paths of icebergs. A reconnaissance of field sites is highly recommended before designing the field campaign and sampling strategy!

## A. Appendix

### 1. Automated Mapping of Proglacial Lakes from Remote Sensing

Where moraine-dammed proglacial lakes are present in mountainous areas with human populations downstream (such as the Alps, Andes and Himalaya) they can present a considerable hazard of glacial outburst floods (GLOFs), if the moraine dam is overtopped or becomes unstable (Lliboutry et al., 1977; Buchrothiner et al., 1982; Huggel et al., 2002). Consequently proglacial lakes in these areas were the focus of early studies and the development of remote sensing technology enabled lakes to be detected across larger remote areas using spectral analysis (Lliboutry et al., 1977; Buchrothiner et al., 1982). Proglacial lakes with suspended sediment tend to have strong reflectance in green wavelengths (0.5-0.6  $\mu\text{m}$ ) and high absorption in the near infrared (NIR) wavelengths (0.8 – 1.0  $\mu\text{m}$ ), which Buchrothiner et al. (1982) utilised in developing the use of Landsat MSS optical imagery (60 m resolution) to detect proglacial water bodies through ratios of spectral band 4 (green) and band 7 (NIR). However, areas with shadows and similar spectral reflectance are problematic with this simple ratio approach. The Normalised Difference Water Index (NDWI) aims to increase the contrast between open water bodies and surrounding rock, soil and vegetation (with high NIR reflectance) using different bands of multi-spectral imagery (McFeeters, 1996);

$$1) \text{ NDWI} = \frac{B_{\text{Green}} - B_{\text{NIR}}}{B_{\text{Green}} + B_{\text{NIR}}}$$

where  $B$  is the spectral band (or channel). Whilst the NDWI has an enhanced contrast between open water bodies and the surrounding environment, shadows remain problematic in mountainous areas (Huggel et al., 2002; Gardelle et al., 2011). The development of high resolution Digital Elevation Models (DEM) enables shadow areas misclassified as lakes to be minimised through applying shadow masks or introducing slope thresholds into decision tree algorithms for classifying proglacial lakes, although delineating lakes within shadows is then problematic (Huggel et al., 2002; Gardelle et al., 2011).

The freely available Sentinel 2 multispectral satellite imagery from the European Copernicus space programme provides a substantial advance in the detection of proglacial lakes in remote areas. The launch of the Sentinel 2A satellite with the Multispectral Instrument (MSI) in June 2015 and Sentinel 2B in March 2017 provides satellite optical imagery with a higher radiometric resolution (12-bit) compared with Advanced Spaceborne Thermal Emission and

Reflection Radiometer (ASTER) (8 bit). The greater dynamic range of the MSI on board Sentinel 2 results in a better ‘depth of colour’ and provides greater spectral contrasts between open water bodies and the surrounding environment using the NDWI technique (Eq1.). Furthermore, Sentinel 2 has an improved spatial resolution of 10 m for the visible (blue, green and red) and NIR spectral bands compared with 30 m spatial resolution for the corresponding spectral bands of Landsat 8. The higher radiometric and spatial resolution of Sentinel 2, combined with a quicker repeat time of 10 days (as opposed to 16 days for Landsat 8) provides freely available data that improves the possibilities for more precise automatic proglacial lake detection with higher spatial and temporal resolution.

## 2. Automated Detection of Proglacial Lake Extent with Sentinel 2 Multi-spectral Satellite Imagery

A multi-step approach was used to automate the initial stages of delineating lake and glacier outlines (Hanshaw and Bookhagen, 2014). Although manual intervention was required to remove misclassified lakes and glaciers as well as edit geometry where required. The proglacial lake outlines were identified first and each step as summarised in Fig.1 below.

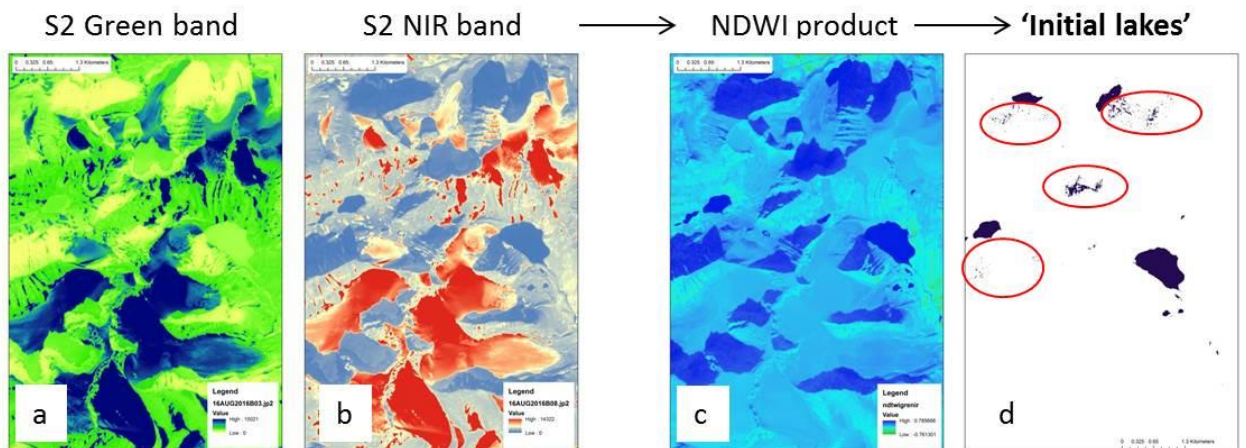


Fig.1 Summary of initial steps used in lake classification of a Sentinel 2 image from 16/8/2016. With false colour images for a. green (band 3) and b. NIR (band 8) that are used for the NDWI (equation 1) to produce image c. Spectral analysis is then applied to each scene to select a threshold to be applied (0.5 in this case) to produce d. the ‘**Initial lakes**’ dataset in purple (see Fig.2 for detail on further steps). Note that problematic shadow areas are circled in red.

### Steps used to classify Lake outlines

Pre-processing	Sentinel 2 (10 m)	ASTER (15 m)	Landsat 8 (30 m)	ASTER GDEM (30 m)	Norwegian DEM(10 m)	Swedish DEM (2 m)
	Resample SWIR		Pansharpening Clip to AOI	Filter		Change projection
	Georeference to NorDEM and SweDEM					
Lake classification	Apply LAKE classification method (NDWI)					
	Identify and apply threshold					
	Filter to create initial lake mask					
	Remove incorrectly classified lakes				Calculate shadow mask	
	Convert to polygons					
	Manually check and remove misclassified lakes using shadow mask					
	Result: Master <b>'All lakes' dataset</b>					
	Clip to within LIA moraine limits					
	Result: Master <b>'Proglacial lakes' dataset</b>					
	Manually quality control <b>'Proglacial lakes'</b> and edit geometry as required.					Calculate lake geometry
Designate ID derived from Randolph Glacier Inventory						
Perform analyses of <b>'Proglacial lakes' dataset</b>						

Fig.2 Summary of steps involved in delineating proglacial lake areas. Steps common to all imagery are combined and have a grey background. Important datasets are in bold text (modified from Hanshaw and Bookhagen, 2014).

A more detailed outline of the processing steps for classifying lakes in all imagery and DEMs is given in Fig.2. The predominant Amphibolite geology and level of suspended sediment in the proglacial lakes results in a high reflectance in the green area of the spectrum, so the normalised difference water index (NDWI; Eq.1) as outlined in McFeeters (1996). The NDWI utilising the green band (as opposed to NDWI utilising the blue band in Huggel et al., 2002) performed the best for the proglacial lakes in the study area. Furthermore, as ASTER has no blue band, utilising the green band allows comparison of the NDWI results from

Sentinel 2 and Landsat 8 imagery. Identifying lakes with low suspended sediment concentration proved to be problematic in ASTER and an extra thresholds in ratio  $R_1$  (Eq.2) and ratio  $R_2$  (Eq.3) following Wessels et al. (2002) (Gardelle et al., 2011);

$$2) R_1 = \frac{B_{Green}}{B_{NIR}}$$

$$3) R_2 = \frac{B_{NIR}}{B_{MIR}}$$

### 3. Proglacial Lake Inventory of Arctic Sweden

PGL Id	Area (m <sup>2</sup> )	Perim. (m)	Error (m <sup>2</sup> )	Error %	Elev. (m)	Ice Cont.	Icy Bord.	Mor. Dam	Glacier Area (m <sup>2</sup> )	Glacier Slope	Glacier Aspect
1	157516	1750	9019.50	5.73	1267	1	1	0	265647	14.5	103
2	3914	290	1494.66	38.19	996	1	0	0	930297	19.8	59
3	5284	290	1494.66	28.29	1006	1	0	0	930297	19.8	59
4	15562	617	3180.02	20.43	1153	0	0	0	261373	21	165
5	18696	545	2808.93	15.02	1154	0	1	0	261373	21	165
6	163140	2425	12498.45	7.66	1144	0	0	0	227518	23.6	92
7	3481	260	1340.04	38.50	1309	1	0	0	373112	25.9	68
8	11979	575	2963.55	24.74	1310	0	0	1	711778	26.3	25
9	6545	317	1633.82	24.96	1373	0	1	1	343390	28.6	54
10	19019	534	2752.24	14.47	1411	1	0	1	152658	26.5	84
11	6820	417	2149.22	31.51	1244	0	0	0	2239260	20	22
12	19206	712	3669.65	19.11	1349	1	1	1	340392	22	69
13	7606	371	1912.13	25.14	1423	0	0	1	672527	18.8	5
14	242736	2349	12106.75	4.99	1318	1	1	1	1486665	15.5	74
15	30578	739	3808.81	12.46	1359	1	0	0	3571629	12.9	84
16	346719	2519	12982.93	3.74	1382	1	1	1	105949	41.9	103
17	756	112	577.25	76.36	1273	0	1	0	183004	34	54
18	2439	213	1097.80	45.01	1305	0	0	1	1056675	15.3	5
19	24587	609	3138.79	12.77	1620	1	1	0	246051	11.6	345
20	22030	568	2927.47	13.29	1406	1	0	1	1103420	17.6	89
21	6656	346	1783.28	26.79	1406	0	0	0	1103420	17.6	89
22	88064	1938	9988.45	11.34	1304	1	1	1	1014926	25.3	37
23	230764	2372	12225.29	5.30	1243	0	0	1	1608398	18.7	20
24	132172	1717	8849.42	6.70	1124	1	0	0	1533959	25.7	26
25	6180	339	1747.21	28.27	1462	0	1	1	448759	24.7	138
26	2182	192	989.57	45.35	1420	0	1	1	1024227	23.2	91
27	560589	3297	16992.74	3.03	1194	0	1	1	670186	22.2	73
28	11026	397	2046.14	18.56	1195	0	0	0	1284257	17.6	96
29	14936	524	2700.70	18.08	1203	0	0	1	1284257	17.6	96
30	1132	138	711.25	62.83	1198	0	0	0	1284257	17.6	96
31	7575	437	2252.30	29.73	1195	0	0	0	1284257	17.6	96
32	19492	549	2829.55	14.52	1401	0	1	1	516830	21.3	8
33	5797	317	1633.82	28.18	1292	1	0	0	1693777	17.7	330

34	744	112	577.25	77.59	1292	0	0	0	1693777	17.7	330
35	6072	361	1860.59	30.64	1260	0	0	0	227322	30.2	55
36	948	127	654.56	69.05	1205	1	0	1	395579	25.5	63
37	35040	936	4824.14	13.77	1213	0	0	0	395579	25.5	63
38	5968	338	1742.05	29.19	1279	0	0	0	552809	17	104
39	211513	1791	9230.81	4.36	1123	0	1	0	552809	17	104
40	28281	696	3587.18	12.68	1267	0	1	0			
41	686233	4692	24182.57	3.52	1169	0	1	1	71160	16.4	110
42	220826	2626	13534.40	6.13	1090	0	0	0	2301468	11.3	79
43	28590	770	3968.58	13.88	1308	0	1	0	297284	21.5	81
44	7198	359	1850.29	25.71	1183	1	0	0	559112	19.1	44
45	2319	201	1035.95	44.67	1178	0	0	0	2301468	11.3	79
46	2441	229	1180.27	48.35	1316	0	0	0	2301468	11.3	79
47	6678	389	2004.91	30.02	1418	0	1	1	186759	21.9	128
48	85537	1261	6499.19	7.60	1213	0	1	0	283063	26.9	97
49	2964	252	1298.81	43.82	1214	0	0	0	1548853	16.6	170
50	41779	971	5004.53	11.98	1296	1	1	0	284076	23.3	103
51	86144	1196	6164.18	7.16	1321	1	1	1	93071	27.3	128
52	35478	860	4432.44	12.49	1378	1	1	1	349005	19.4	109
53	149143	2189	11282.11	7.56	1227	1	1	1	398244	21.1	77
54	96050	1356	6988.82	7.28	1243	1	1	1	92330	35.8	97
55	1849	164	845.26	45.71	1394	0	0	1	1359667	20.7	4
<b>56</b>	5819	289	1489.51	25.60	1366	0	1	0	1359667	20.7	4
57	24664	583	3004.78	12.18	1582	1	1	1	314808	17	111
58	4253	263	1355.50	31.87	1301	1	1	1	383786	26.1	137
59	13349	584	3009.94	22.55	1246	1	0	1	276708	32.5	45
60	14428	445	2293.53	15.90	1133	1	0	1	6627727	13.8	63
61	4560	269	1386.43	30.40	1143	1	0	0	6627727	13.8	63
62	2827	259	1334.89	47.22	1409	0	0	0	1428910	18.4	43
63	1583	150	773.10	48.84	1455	0	0	0	1428910	18.4	43
64	7647	325	1675.05	21.90	1345	0	0	0	3583619	15.3	14
65	4544	263	1355.50	29.83	1176	0	0	0	2868518	15.1	53
66	4284	278	1432.81	33.45	1418	1	1	0	3583619	15.3	14
67	1843	166	855.56	46.42	1420	0	0	0	3583619	15.3	14
68	1110	133	685.48	61.76	1216	0	0	0	2868518	15.1	53
69	520	88	453.55	87.22	1216	0	0	0	2868518	15.1	53
70	126	52	268.01	212.70	1216	0	0	0	2868518	15.1	53
71	853	120	618.48	72.51	1300	0	0	0	2807040	15.4	81
72	5064	332	1711.13	33.79	1438	1	1	0	180496	22.6	153
73	3764	239	1231.81	32.73	1350	1	0	1	1679360	13.6	354
74	21469	680	3504.72	16.32	1333	0	1	0	1679360	13.6	354
75	914	122	628.79	68.80	1362	0	0	1	1679360	13.6	354
76	5502	328	1690.51	30.73	1204	0	0	0	556380	19	144
77	14384	578	2979.01	20.71	1199	0	1	1	556380	19	144
78	5552	302	1556.51	28.04	1476	1	0	1	616688	13.3	12
79	91254	1248	6432.19	7.05	1496	1	1	1	264124	19.9	81

80	21626	629	3241.87	14.99	1275	1	0	1	816304	13.5	85
81	175832	2092	10782.17	6.13	1441	1	1	0	1755474	14.5	33
82	3227	228	1175.11	36.41	1350	1	0	0			
83	1444	172	886.49	61.39	1284	1	0	0	1804005	17.5	360
84	19879	556	2865.62	14.42	1278	1	1	1	51540	32.9	66
85	2718	210	1082.34	39.82	1359	1	1	1			
86	957	121	623.63	65.17	1309	0	0	0	788586	17.5	188
87	1072	129	664.87	62.02	1302	0	0	0	788586	17.5	188
88	875	121	623.63	71.27	1325	0	0	1	788586	17.5	188
89	53975	1125	5798.25	10.74	1499	1	1	0	1063866	16.7	141
90	11890	453	2334.76	19.64	1228	0	0	1	2978231	15.5	138
91	1231	148	762.79	61.97	1222	0	0	0	2978231	15.5	138
92	14318	469	2417.23	16.88	1269	0	0	0	2978231	15.5	138
93	18103	795	4097.43	22.63	1270	0	0	1	2978231	15.5	138
94	48522	999	5148.85	10.61	1317	1	1	0	238473	28.3	59
95	24551	600	3092.40	12.60	1339	0	0	1	2561335	17.4	322
96	55927	983	5066.38	9.06	1356	1	0	1	344628	22.9	346
97	1466	154	793.72	54.14	1341	0	0	1	344628	22.9	346
98	3495	238	1226.65	35.10	1320	0	0	0	344628	22.9	346
99	5743	320	1649.28	28.72	1331	0	0	1	344628	22.9	346
100	3134	236	1216.34	38.81	1287	0	0	1	2561335	17.4	322
101	1268	151	778.25	61.38	1343	0	0	1	2561335	17.4	322
102	9041	359	1850.29	20.47	1400	1	1	0	260503	23.9	79
103	7135	368	1896.67	26.58	1186	0	0	1	590856	24.8	42
104	1457	153	788.56	54.12	1187	0	0	1	590856	24.8	42
105	8072	423	2180.14	27.01	1435	1	1	1	276890	25.5	50
106	25314	617	3180.02	12.56	1362	1	1	1	73958	n	
107	60635	1111	5726.09	9.44	1234	0	1	1	271890	24	81
108	12047	485	2499.69	20.75	1336	1	1	1	1919289	8.3	153

Table 1: Proglacial lake inventory for Arctic Sweden from manual mapping of ASTER satellite (15 m) imagery from 8/8/2014. Where Perim.=Perimeter. Elev.=Elevation. Ice Cont.= Glacier ice contact. Icy Bord.= Icy border around lake. Mor. Dam.=Moraine Dammed lake. Glacier geometry are from the Randolph Glacier Inventory (2008) (Arendt et al., 2012)

#### 4. Spatial changes in proglacial lakes between 1950s/60s and 2014

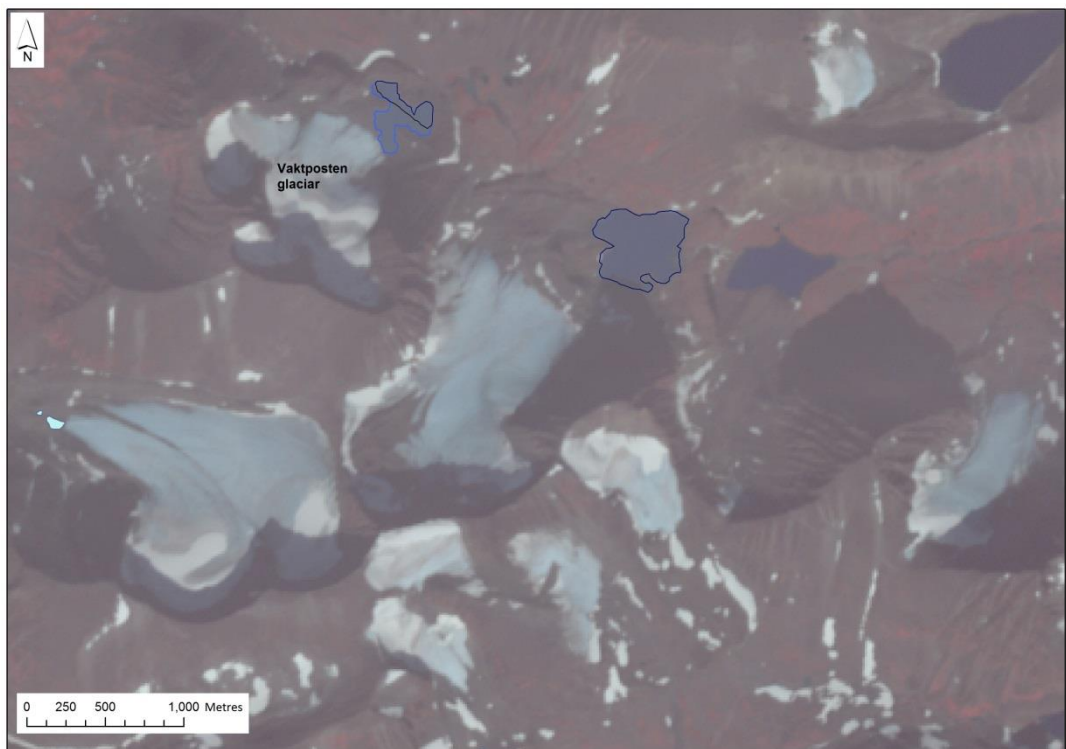
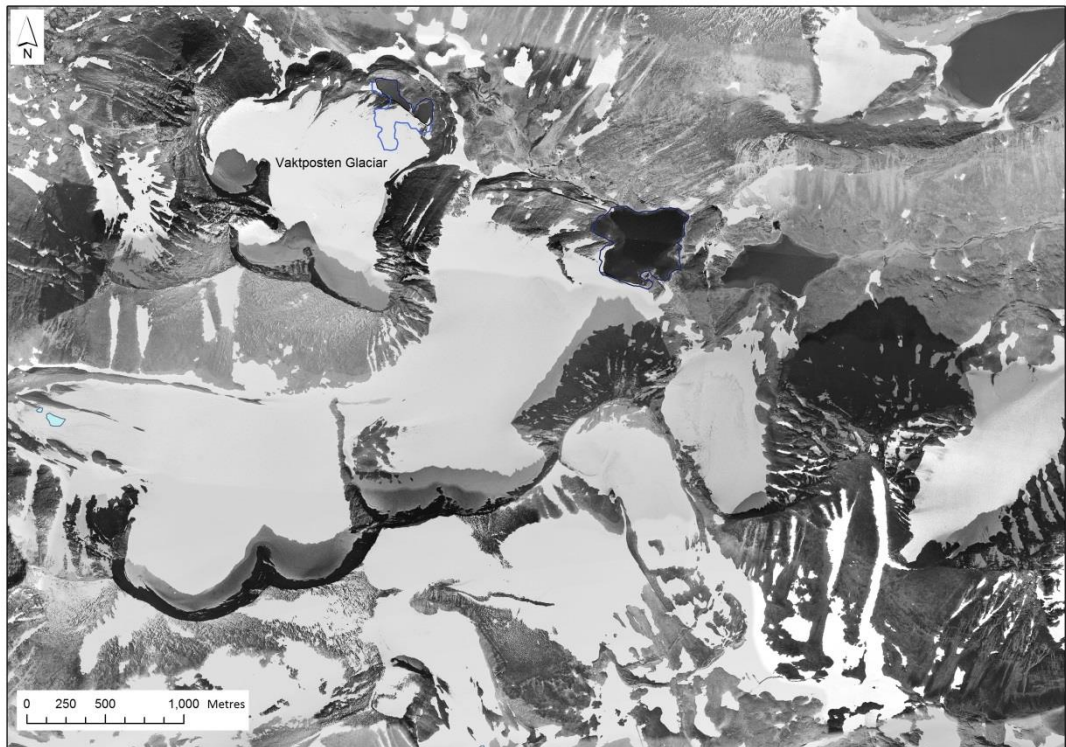


Fig.3 Top aerial image (Lantmateriet, 1959) of Vaktposten glacier showing 1959 proglacial lake outline (black) with August 2014 proglacial lake outline (blue). Spatial resolution is unknown but

estimated ~1 m. b. ASTER satellite composite image (G,R, NIR, 15 m resolution) from 8th August 2014 (10:46am) with 1960 proglacial lake outline (black) and August 2014 outline (blue).

## 5. Glacier terminus changes in Arctic Sweden from 2010 to 2018

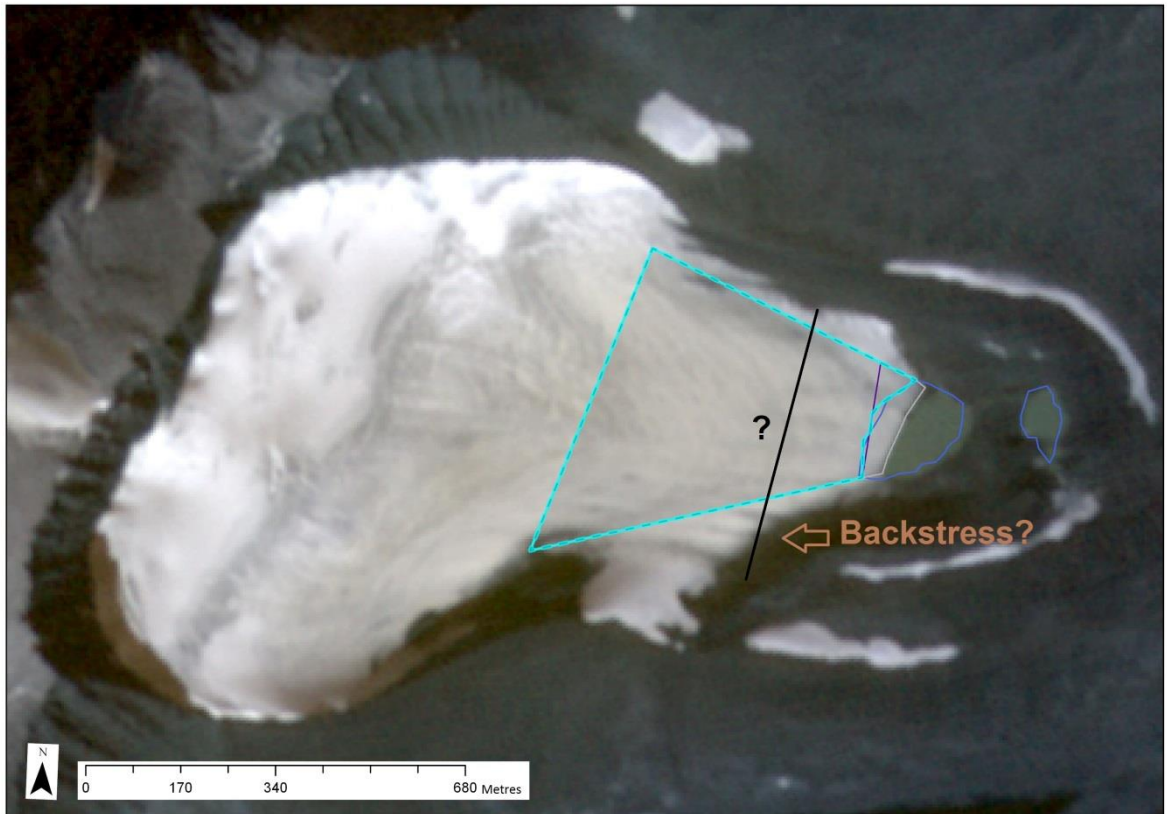


Fig.4 Rapid Eye multispectral satellite image (5 m resolution) from 27/7/2010 with; grey outline = 2010 glacier terminus area, light blue line = 2018, purple line = width, dark blue line = Aug 2014 proglacial lake outline. Under this geometry configuration the glacier terminus would be defined as having full contact with a proglacial lake. An alternative interpretation is proposed with the black line marking the possible width if defined by the area where the terminal moraine may be exerting back stress (as opposed to lateral stress at the margin). This alternative interpretation would mean only part of the terminus width is in contact with the proglacial lake.

## 6. Emissivity Values over Proglacial Lakes from AST05

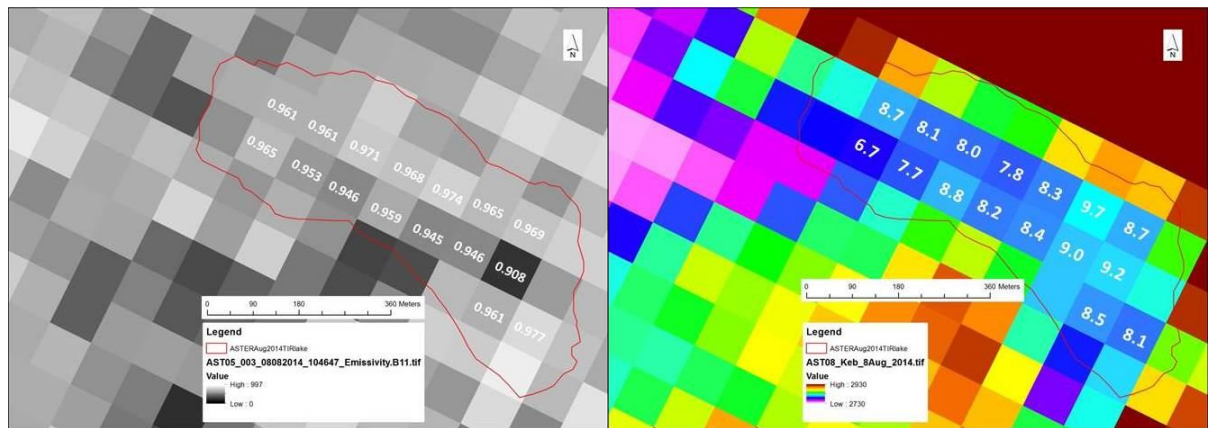


Fig.5 a. AST05 band 11 emissivity product image over Arctic Sweden (8/8/2014), with outlines of proglacial lakes included in the thermal infrared (TIR) AST08 temperature analysis in red. Note the presence of electronic striping across the image orientated NW to SE, with darker pixels indicating lower emissivity values. b. An AST08 image of the same scene over Arctic Sweden (8/8/2014), with AST08 pixel temperatures ( $^{\circ}\text{C}$ ) in white and proglacial lake outlined in red.

The inspection of AST05 band 11 emissivity values over  $\text{PGL}_{\text{ID}} 14$  reveals a range in emissivity values from 0.974 down to 0.908 (Fig.5). There are only 2 out of 16 pixels analysed that have an emissivity of  $>0.97$ , which would agree with emissivity values of water from laboratory analysis (Sabol et al., 2009). If we then consider water pixels with an emissivity of  $>0.955$ , these pixels would have reasonable agreement with laboratory emissivity values for water, considering the stated accuracy of the AST05 product ( $\pm 0.015$ ) (Sabol et al., 2009). There are 11 out of 16 pixels (69.7%) with emissivity values  $>0.955$ , with a further one pixel with a value (0.953) very close to this threshold. There are a further 3 pixels with emissivity values of 0.945 and 0.946, which lie relatively close to the stated accuracy of the AST05 product (Gillespie et al., 2011). It should also be considered as to whether these relatively low emissivity values are associated with variations in SSC, particularly given the position of these pixels next to the steep southern shore of the lake with potential sources of sediment from inflows. Although this variation is not detectable within the relatively coarse spatial (15 m) and radiometric (8 bit) resolution of optical and VNIR ASTER imagery, higher resolution sensors are required to further analyse variations in SSC.

The study of Sabol et al. (2009) identified water pixels over the Salton sea that had emissivity values of  $<0.94$  as ‘bad pixels’, although note that they did not set this as an actual threshold for identifying ‘bad pixels’. They attribute the poor emissivity recovery due to severe step discontinuities and uncertainty from the scaling with the emissivity minimum versus minimum maximum difference regression (see above) (Sabol et al., 2009). Whilst this

uncertainty is potentially a source of error within the emissivity values discussed above, it should also be remembered that the target water surface of proglacial lakes are likely to be less uniform due to variations in SSC (Becker and Daw, 2005). There is a notable outlier within the AST05 emissivity with a pixel value of 0.908, which is also the lowest AST05 emissivity value of a pixel over any proglacial lake analysed from the 8/8/2014 data in this study. This value is outside of the stated accuracy of the AST05 product and would class as a 'bad pixel' within the analysis of Sabol et al. (2009). The question about this pixel with regards to the aims of this study is how does it affect the accuracy of the AST08 surface temperature product.

Due to the lack of ground truthing data for the ASTER 8/8/2014 imagery over the proglacial lakes analysed in this study, the pattern between AST05 and AST08 pixel values is explored to give some relative comparison between pixels of different emissivity values. If the two pixels that have band 11 emissivity values in agreement with laboratory values (0.97 to 0.98) are taken as reference points, then it is possible to explore the relative accuracy of other AST08 pixel values in the context of the stated accuracy of the product. The 2 pixels with emissivity's of  $>0.97$  have AST08 temperatures of 8.0 and 8.3°C. The mean AST08 pixel value for this lake is also 8.3°C, so if this value is taken as a reference point then considering the stated accuracy of the product is  $\pm 1.5^\circ\text{C}$ , it would suggest that proximal pixels with values  $<9.8^\circ\text{C}$  are within the stated accuracy of the product. The pixel with an emissivity value of 0.908 has an AST08 value of 9.2°C and therefore falls within this relative temperature limit. This would suggest that the uncertainty arising from the emissivity value is within the stated accuracy of the AST08 product, although this analysis is only relative and other sources of uncertainty may be present. It further emphasises the need for in situ validation data of the AST08 temperature product.

Due to the lack of ground truthing data for the ASTER 8/8/2014 imagery over the proglacial lakes analysed in this study, the pattern between AST05 and AST08 pixel values is explored to give some relative comparison between pixels of different emissivity values. If the two pixels that have band 11 emissivity values in agreement with laboratory values (0.97 to 0.98) are taken as reference points, then it is possible to explore the relative accuracy of other AST08 pixel values in the context of the stated accuracy of the product. The 2 pixels with emissivity's of  $>0.97$  have AST08 temperatures of 8.0 and 8.3°C. The mean AST08 pixel value for this lake is also 8.3°C, so if this value is taken as a reference point then considering the stated accuracy of the product is  $\pm 1.5^\circ\text{C}$ , it would suggest that proximal pixels with

values  $<9.8^{\circ}\text{C}$  are within the stated accuracy of the product. The pixel with an emissivity value of 0.908 has an AST08 value of  $9.2^{\circ}\text{C}$  and therefore falls within this relative temperature limit. This would suggest that the uncertainty arising from the emissivity value is within the stated accuracy of the AST08 product, although this analysis is only relative and other sources of uncertainty may be present. It further emphasises the need for in situ validation data of the AST08 temperature product.

## 7. Spatial Pattern of Skin Surface Temperature of Ice Contact Proglacial lakes

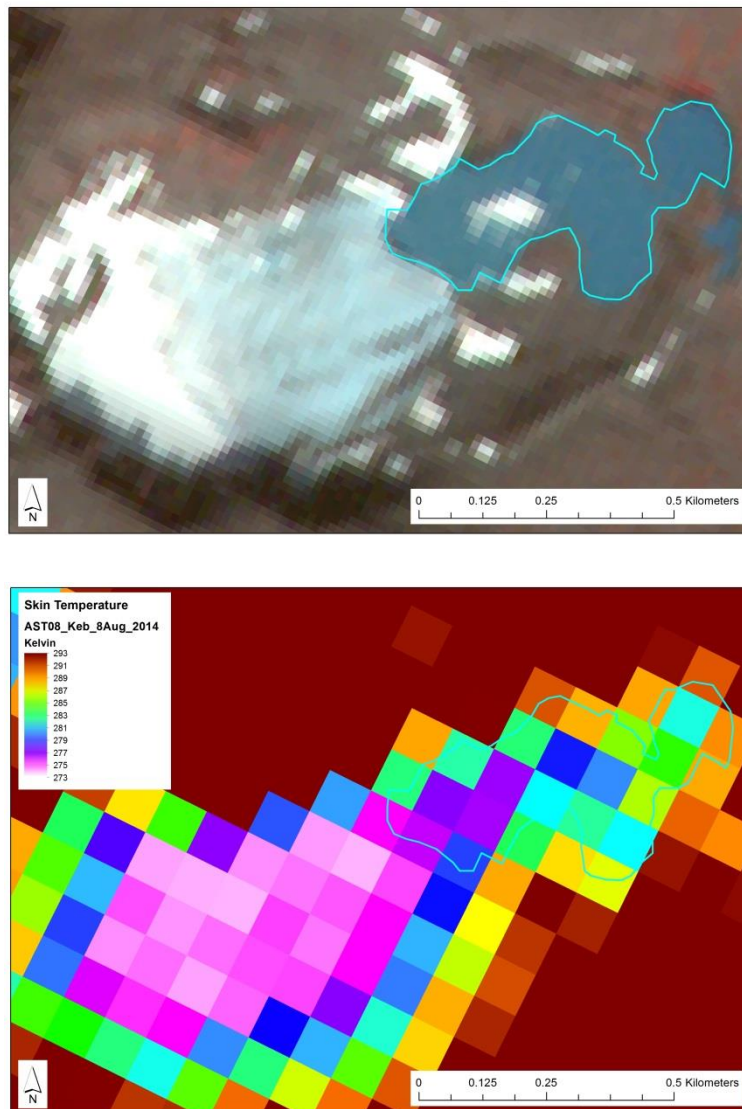


Fig.6 Proglacial Lake 11 TOP. ASTER satellite composite image (green, red and NIR) and BOTTOM. ASTER surface temperature product image (AST08) at 10:46am on 8/8/2014.

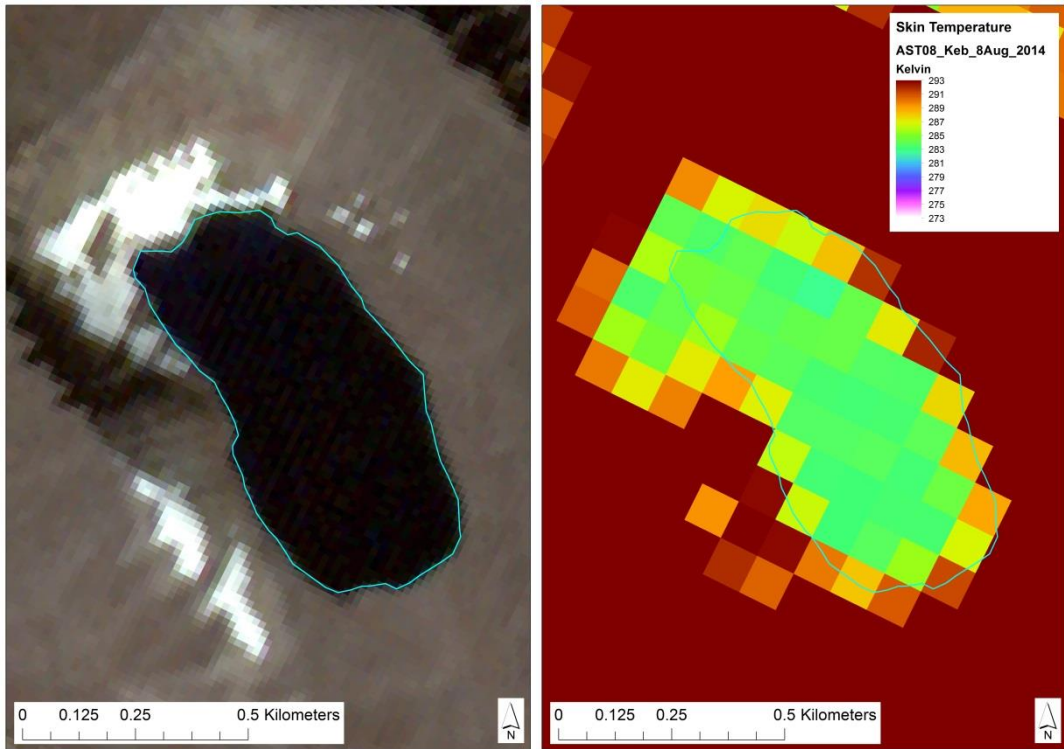


Fig.7 Proglacial Lake 4 LEFT: ASTER satellite composite image (green, red and NIR) and RIGHT: ASTER surface temperature product image (AST08) at 10:46am on 8/8/2014.

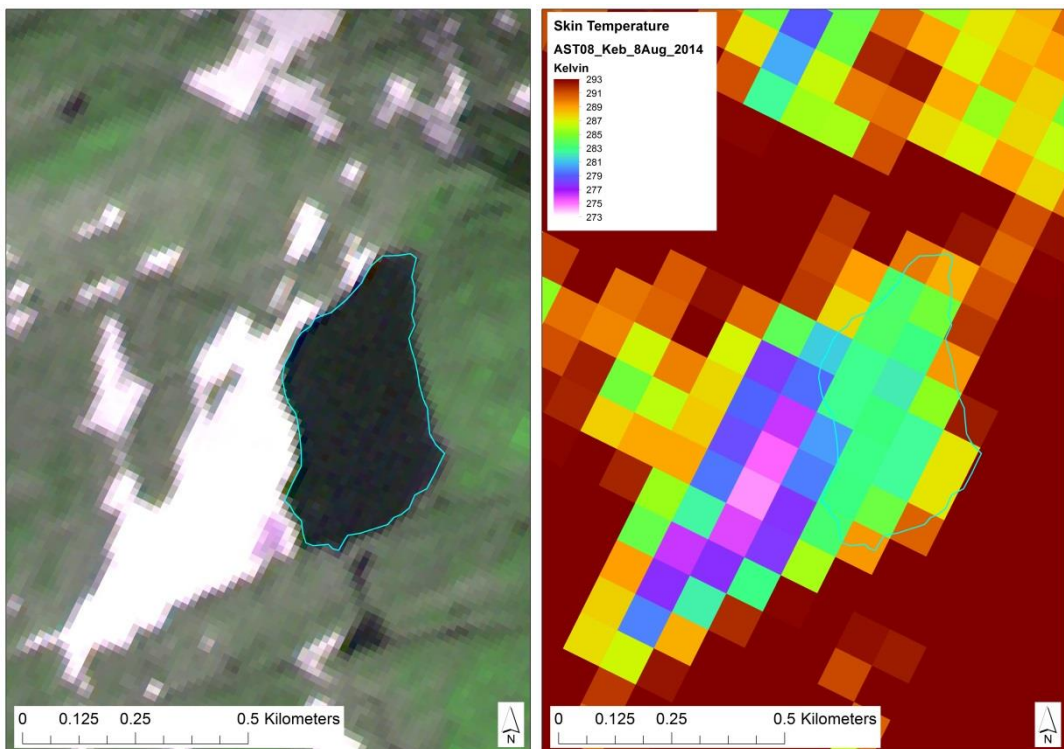


Fig.8 Proglacial Lake 1 LEFT: ASTER satellite composite image (green, red and NIR) and RIGHT: ASTER surface temperature product image (AST08) at 10:46am on 8/8/2014.

## 8. Spatial Pattern of Skin Surface Temperature of Non- Ice Contact Proglacial Lakes

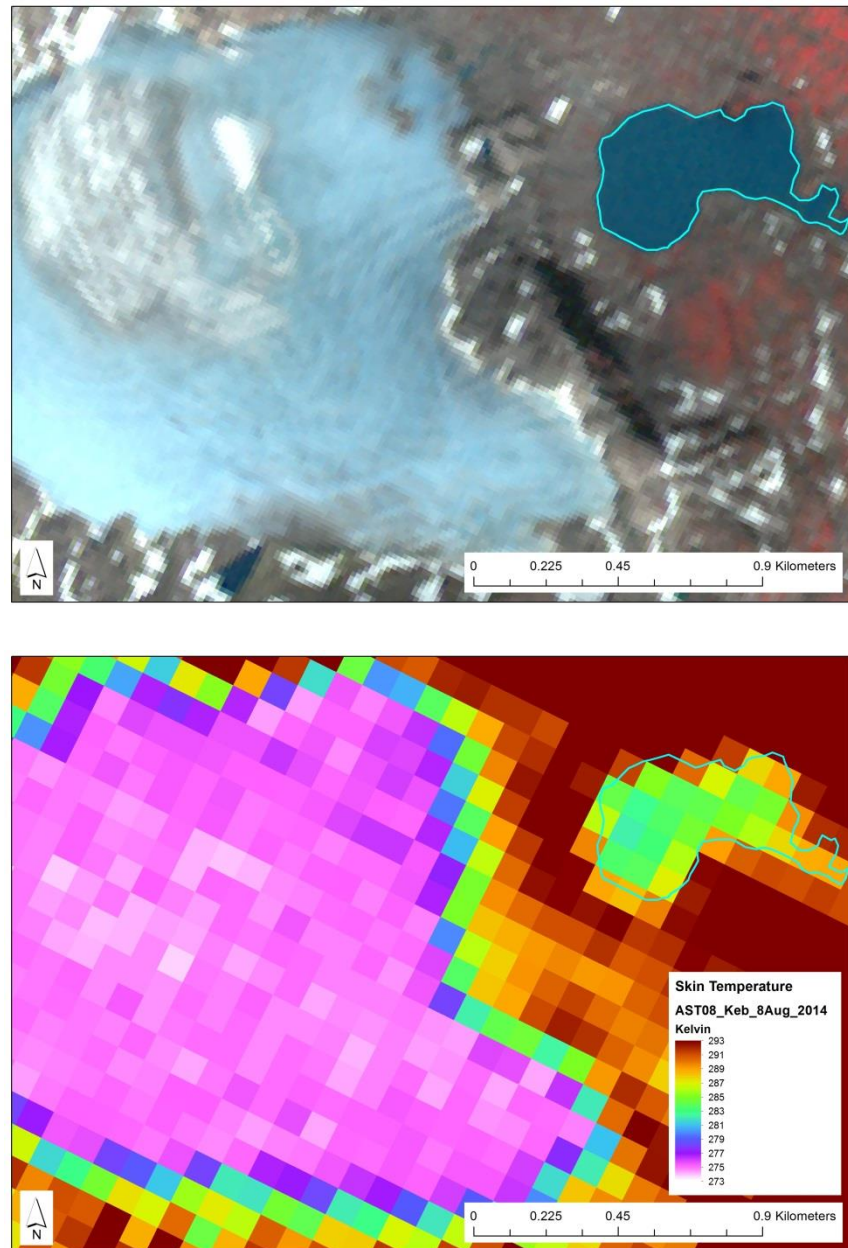


Fig.9 Proglacial Lake 10 TOP: ASTER satellite composite image (green, red and NIR) and BOTTOM: ASTER surface temperature product image (AST08) at 10:46am on 8/8/2014.



## List of References

- Abrams, M., Hook, S. and Ramachandran, B., (2002). ASTER user handbook. *Pasadena, CA: Jet Propulsion Laboratory*, pp.45-54.
- Adrian, R., O'Reilly, C.M., Zagarese, H., Baines, S.B., Hessen, D.O., Keller, W., Livingstone, D.M., Sommaruga, R., Straile, D., Van Donk, E. and Weyhenmeyer, G.A., (2009). Lakes as sentinels of climate change. *Limnology and oceanography*, 54(6 part 2), pp.2283-2297.
- Andreassen, L. M., Elvehøy, H., Kjøllmoen, B., & Belart, J. M. (2020). Glacier change in Norway since the 1960s—an overview of mass balance, area, length and surface elevation changes. *Journal of Glaciology*, 66(256), 313-328.
- Arendt, A., Bolch, T., Cogley, J.G., Gardner, A., Hagen, J.O., Hock, R., Kaser, G., Pfeffer, W.T., Moholdt, G., Paul, F. and Radic, V., (2012). Randolph Glacier Inventory [v2. 0]: A Dataset of Global Glacier Outlines, Global Land Ice Measurements from Space, Boulder Colorado, USA. *Digital Media*.
- Aubry-Wake, C., Baraer, M., McKenzie, J.M., Mark, B.G., Wigmore, O., Hellström, R.Å., Lautz, L. and Somers, L., (2015). Measuring glacier surface temperatures with ground-based thermal infrared imaging. *Geophysical Research Letters*, 42(20), pp.8489-8497.
- Baldrige, A.M., Hook, S.J., Grove, C.I. and Rivera, G., (2009). The ASTER spectral library version 2.0. *Remote Sensing of Environment*, 113(4), pp.711-715.
- Becker, M.W. and Daw, A., (2005). Influence of lake morphology and clarity on water surface temperature as measured by EOS ASTER. *Remote sensing of environment*, 99(3), pp.288-294.
- Benn, D. I., Warren, C. R., & Mottram, R. H. (2007). Calving processes and the dynamics of calving glaciers. *Earth-Science Reviews*, 82(3), 143-179.
- Birkett, C.M. and Mason, I.M., (1995). A new global lakes database for a remote sensing program studying climatically sensitive large lakes. *Journal of Great Lakes Research*, 21(3), pp.307-318.
- Bindschadler, R. (1983). The importance of pressurized subglacial water in separation and sliding at the glacier bed. *Journal of Glaciology*, 29(101), 3-19.
- Bonan, D.B., Christian, J.E. and Christianson, K., (2019). Influence of North Atlantic climate variability on glacier mass balance in Norway, Sweden and Svalbard. *Journal of Glaciology*, pp.1-15.
- Boyce, E. S., Motyka, R. J., & Truffer, M. (2007). Flotation and retreat of a lake-calving terminus, Mendenhall Glacier, southeast Alaska, USA. *Journal of Glaciology*, 53(181), 211-224.
- Box, J.E., Colgan, W.T., Christensen, T.R., Schmidt, N.M., Lund, M., Parmentier, F.J.W., Brown, R., Bhatt, U.S., Euskirchen, E.S., Romanovsky, V.E. and Walsh, J.E., (2019). Key indicators of Arctic climate change: 1971–2017. *Environmental Research Letters*, 14(4), p.045010.

- Brugger, K. A., Refsnider, K. A., & Whitehill, M. F. (2005). Variation in glacier length and ice volume of Rabots Glaciär, Sweden, in response to climate change, 1910–2003. *Annals of Glaciology*, 42, 180-188.
- Brugger, K.A., (2007). The non-synchronous response of Rabots Glaciär and Storglaciären, northern Sweden, to recent climate change: a comparative study. *Annals of Glaciology*, 46, pp.275-282.
- Buchroithner, M. F., Jentsch, G., & Wanivenhaus, B. (1982). Monitoring of recent geological events in the Khumbu area (Himalaya, Nepal) by digital processing of Landsat MSS data. *Rock Mechanics*, 15(4), 181-197.
- Carr, J. R., Stokes, C. R., & Vieli, A. (2013). Recent progress in understanding marine-terminating Arctic outlet glacier response to climatic and oceanic forcing: Twenty years of rapid change. *Progress in Physical Geography*, 37(4), 436-467.
- Carr, J. R., Stokes, C., & Vieli, A. (2014). Recent retreat of major outlet glaciers on Novaya Zemlya, Russian Arctic, influenced by fjord geometry and sea-ice conditions. *Journal of Glaciology*, 60(219), 155-170.
- Carr, J.R., Stokes, C.R. and Vieli, A., (2017). Threefold increase in marine-terminating outlet glacier retreat rates across the Atlantic Arctic: 1992–2010. *Annals of Glaciology*, 58(74), pp.72-91.
- Carrivick, J. L., & Tweed, F. S. (2013). Proglacial lakes: character, behaviour and geological importance. *Quaternary Science Reviews*, 78, 34-52.
- Carrivick, J. L., & Quincey, D. J. (2014). Progressive increase in number and volume of ice-marginal lakes on the western margin of the Greenland Ice Sheet. *Global and Planetary Change*, 116, 156-163.
- Chauché, N., Hubbard, A., Gascard, J. C., Box, J. E., Bates, R., Koppes, M., ... & Patton, H. (2014). Ice–ocean interaction and calving front morphology at two west Greenland tidewater outlet glaciers. *The Cryosphere*, 8(4), 1457-1468.
- Chernos, M., Koppes, M., & Moore, R. D. (2016). Ablation from calving and surface melt at lake-terminating Bridge Glacier, British Columbia, 1984–2013. *The Cryosphere*, 10(1), 87-102.
- Churski, Z. (1973). Hydrographic features of the proglacial area of Skeidararjokull. *Geographia Polonica*, 26, 209-254.
- Chikita, K., Jha, J., & Yamada, T. (1999). Hydrodynamics of a supraglacial lake and its effect on the basin expansion: Tsho Rolpa, Rolwaling Valley, Nepal Himalaya. *Arctic, Antarctic, and Alpine Research*, 31(1), 58-70.
- Chikita, K. A. (2007). Topographic effects on the thermal structure of Himalayan glacial lakes: Observations and numerical simulation of wind. *Journal of Asian Earth Sciences*, 30(2), 344-352.
- Christiansen, H. H., Etzelmüller, B., Isaksen, K., Juliussen, H., Farbrot, H., Humlum, O., ... & Ødegård, R. S. (2010). The thermal state of permafrost in the nordic area during the international polar year 2007–2009. *Permafrost and Periglacial Processes*, 21(2), 156-181.

- Clague, J.J. and Evans, S.G., (2000). A review of catastrophic drainage of moraine-dammed lakes in British Columbia. *Quaternary Science Reviews*, 19(17-18), pp.1763-1783.
- Cook, S. J., & Quincey, D. J. (2015). Estimating the volume of Alpine glacial lakes. *Earth Surface Dynamics*. 3, 909-940.
- Coll, C., Caselles, V., Valor, E., Niclòs, R., Sánchez, J.M., Galve, J.M. and Mira, M., (2007). Temperature and emissivity separation from ASTER data for low spectral contrast surfaces. *Remote sensing of environment*, 110(2), pp.162-175.
- Edinger, J.E., Duttweiler, D.W. and Geyer, J.C., (1968). The response of water temperatures to meteorological conditions. *Water Resources Research*, 4(5), pp.1137-1143.
- Fellman, J.B., Nagorski, S., Pyare, S., Vermilyea, A.W., Scott, D. and Hood, E., (2014). Stream temperature response to variable glacier coverage in coastal watersheds of Southeast Alaska. *Hydrological Processes*, 28(4), pp.2062-2073.
- Dahlke, H. E., Lyon, S. W., Stedinger, J. R., Rosqvist, G., & Jansson, P. (2012). Contrasting trends in floods for two sub-arctic catchments in northern Sweden-does glacier presence matter?. *Hydrology and Earth System Sciences*, 16(7), 2123.
- Denton, G.H. and Karlén, W., (1973). Lichenometry: its application to Holocene moraine studies in southern Alaska and Swedish Lapland. *Arctic and Alpine Research*, 5(4), pp.347-372.
- Donlon, C.J., Martin, M., Stark, J., Roberts-Jones, J., Fiedler, E. and Wimmer, W., (2012). The operational sea surface temperature and sea ice analysis (OSTIA) system. *Remote Sensing of Environment*, 116, pp.140-158.
- Du, J., Kimball, J. S., Duguay, C., Kim, Y., & Watts, J. D. (2017). Satellite microwave assessment of Northern Hemisphere lake ice phenology from 2002 to 2015. *The Cryosphere*, 11, 47.
- Dykes, R. C., Brook, M. S., & Winkler, S. (2010). The contemporary retreat of Tasman Glacier, Southern Alps, New Zealand, and the evolution of Tasman proglacial lake since AD 2000. *Erdkunde*, 141-154.
- Eijpen, K., Warren, C.R. and Benn, D.I., (2003). Subaqueous melt rates at calving termini: a laboratory approach. *Annals of Glaciology*, 36, pp.179-183.
- Emmer, A., Merkl, S., & Mergili, M. (2015). Spatiotemporal patterns of high-mountain lakes and related hazards in western Austria. *Geomorphology*, 246, 602-616.
- Emmer, A., (2018). GLOFs in the WOS: Bibliometrics, geographies and global trends of research on glacial lake outburst floods (Web of Science, 1979–2016). *Natural Hazards and Earth System Sciences*, 18(3), pp.813-827.
- Farinotti, D., Pistocchi, A., & Huss, M. (2016). From dwindling ice to headwater lakes: could dams replace glaciers in the European Alps?. *Environmental Research Letters*, 11(5), 054022.
- Frey, H., Haeberli, W., Linsbauer, A., Huggel, C. and Paul, F., 2010. A multi-level strategy for anticipating future glacier lake formation and associated hazard potentials. *Nat. Hazards Earth Syst. Sci*, 10(2), pp.339-352.

- Fujita, K., Suzuki, R., Nuimura, T., & Sakai, A. (2008). Performance of ASTER and SRTM DEMs, and their potential for assessing glacial lakes in the Lunana region, Bhutan Himalaya. *Journal of Glaciology*, 54(185), 220-228.
- Fujita, K., Sakai, A., Nuimura, T., Yamaguchi, S., & Sharma, R. R. (2009). Recent changes in Imja Glacial Lake and its damming moraine in the Nepal Himalaya revealed by in situ surveys and multi-temporal ASTER imagery. *Environmental Research Letters*, 4(4), 045205.
- Funk, M. and Röthlisberger, H., (1989). Forecasting the effects of a planned reservoir which will partially flood the tongue of Unteraargletscher in Switzerland. *Annals of Glaciology*, 13, pp.76-81.
- Gardelle, J., Arnaud, Y., & Berthier, E. (2011). Contrasted evolution of glacial lakes along the Hindu Kush Himalaya mountain range between 1990 and 2009. *Global and Planetary Change*, 75(1), 47-55.
- Geirsdóttir, Á., Miller, G. H., Wattrus, N. J., Björnsson, H., & Thors, K. (2008). Stabilization of glaciers terminating in closed water bodies: Evidence and broader implications. *Geophysical Research Letters*, 35(17).
- Ghimire, M., (2004). Review of studies on glacier lake outburst floods and associated vulnerability in the Himalayas. *Himalayan Review*, pp.49-64.
- Gillespie, A., Rokugawa, S., Matsunaga, T., Cothorn, J.S., Hook, S. and Kahle, A.B., (1998). A temperature and emissivity separation algorithm for Advanced Spaceborne Thermal Emission and Reflection Radiometer (ASTER) images. *IEEE transactions on geoscience and remote sensing*, 36(4), pp.1113-1126.
- Gillespie, A.R., Abbott, E.A., Gilson, L., Hulley, G., Jiménez-Muñoz, J.C. and Sobrino, J.A., (2011). Residual errors in ASTER temperature and emissivity standard products AST08 and AST05. *Remote sensing of environment*, 115(12), pp.3681-3694.
- Goodfellow, B. W., Stroeven, A. P., Hättestrand, C., Kleman, J., & Jansson, K. N. (2008). Deciphering a non-glacial/glacial landscape mosaic in the northern Swedish mountains. *Geomorphology*, 93(3), 213-232.
- Gustafson, W.T., Gillespie, A.R. and Yamada, G.J., (2006), September. Revisions to the ASTER temperature/emissivity separation algorithm. In *2nd International Symposium on Recent Advances in Quantitative Remote Sensing*. Torrent, Spain: Global Change Unit, University of Valencia.
- Hanshaw, M.N. and Bookhagen, B., (2014). Glacial areas, lake areas, and snow lines from 1975 to 2012: status of the Cordillera Vilcanota, including the Quelccaya Ice Cap, northern central Andes, Peru. *The Cryosphere*, 8(2), p.359.
- Haresign, E., & Warren, C. R. (2005). Melt rates at calving termini: a study at Glaciar León, Chilean Patagonia. *Geological Society, London, Special Publications*, 242(1), 99-109.
- Harris, P. W. V. (1976). The seasonal temperature-salinity structure of a glacial lake: Jökulsárlón, south-east Iceland. *Geografiska Annaler: Series A, Physical Geography*, 58(4), 329-336.

- Hochstein, M. P., Watson, M. I., Malengreau, B., Nobes, D. C., & Owens, I. (1998). Rapid melting of the terminal section of the Hooker Glacier (Mt Cook National Park, New Zealand). *New Zealand Journal of Geology and Geophysics*, 41(3), 203-218.
- Hock, R., Johansson, M., Jansson, P. and Barring, L., (2002). Modeling climate conditions required for glacier formation in cirques of the Rasepautasjtjåkka Massif, northern Sweden. *Arctic, Antarctic, and Alpine Research*, 34(1), pp.3-11.
- Holmlund, P., (1988). Internal geometry and evolution of moulins, Storglaciären, Sweden. *Journal of Glaciology*, 34(117), pp.242-248.
- Holmlund, P., Karlén, W. and Grudd, H., (1996). Fifty years of mass balance and glacier front observations at the Tarfala Research Station. *Geografiska Annaler: Series A, Physical Geography*, 78(2-3), pp.105-114.
- Holmlund, E.S. and Holmlund, P., (2019). Constraining 135 years of mass balance with historic structure-from-motion photogrammetry on Storglaciären, Sweden. *Geografiska Annaler: Series A, Physical Geography*, pp.1-16.
- Hook, S.J., Chander, G., Barsi, J.A., Alley, R.E., Abtahi, A., Palluconi, F.D., Markham, B.L., Richards, R.C., Schladow, S.G. and Helder, D.L., (2004). In-flight validation and recovery of water surface temperature with Landsat-5 thermal infrared data using an automated high-altitude lake validation site at Lake Tahoe. *IEEE Transactions on Geoscience and Remote Sensing*, 42(12), pp.2767-2776.
- Hook, S.J., Vaughan, R.G., Tonooka, H. and Schladow, S.G., (2007). Absolute radiometric in-flight validation of mid infrared and thermal infrared data from ASTER and MODIS on the Terra spacecraft using the Lake Tahoe, CA/NV, USA, automated validation site. *IEEE Transactions on Geoscience and Remote Sensing*, 45(6), pp.1798-1807.
- Huggel, C., Käab, A., Haeberli, W., Teyssere, P., & Paul, F. (2002). Remote sensing based assessment of hazards from glacier lake outbursts: a case study in the Swiss Alps. *Canadian Geotechnical Journal*, 39(2), 316-330.
- Hulley, G. C., Hook, S. J., Abbott, E., Malakar, N., Islam, T., & Abrams, M. (2015). The ASTER Global Emissivity Dataset (ASTER GED): Mapping Earth's emissivity at 100 meter spatial scale. *Geophysical Research Letters*, 42(19), 7966-7976.
- Jansson, P., Hock, R. and Schneider, T., (2003). The concept of glacier storage: a review. *Journal of Hydrology*, 282(1-4), pp.116-129.
- Jenkins, A., Dutrieux, P., Jacobs, S. S., McPhail, S. D., Perrett, J. R., Webb, A. T., & White, D. (2010). Observations beneath Pine Island Glacier in West Antarctica and implications for its retreat. *Nature Geoscience*, 3(7), 468-472.
- Jonsell, U., Hock, R., & Duguay, M. (2013). Recent air and ground temperature increases at Tarfala Research Station, Sweden. *Polar Research*, 32.
- Josberger, E.G., Shuchman, R.A., Meadows, G.A., Savage, S. and Payne, J., (2006). Hydrography and circulation of ice-marginal lakes at Bering Glacier, Alaska, USA. *Arctic, Antarctic, and Alpine Research*, 38(4), pp.547-560.
- Karlén, W. (1973). Holocene glacier and climatic variations, Kebnekaise mountains, Swedish Lapland. *Geografiska Annaler. Series A. Physical Geography*, 29-63.

- Kim, S., Sinclair, V.A., Räisänen, J. and Ruuhela, R., (2018). Heat waves in Finland: Present and projected summertime extreme temperatures and their associated circulation patterns. *International Journal of Climatology*, 38(3), pp.1393-1408.
- King, O., Quincey, D.J., Carrivick, J.L. and Rowan, A.V., (2017). Spatial variability in mass loss of glaciers in the Everest region, central Himalayas, between 2000 and 2015. *The Cryosphere*, 11(1), pp.407-426.
- King, O., Dehecq, A., Quincey, D. and Carrivick, J., (2018). Contrasting geometric and dynamic evolution of lake and land-terminating glaciers in the central Himalaya. *Global and planetary change*, 167, pp.46-60.
- Kirchner, N., Noormets, R., Kutteneuler, J., Erstorp, E.S., Holmlund, E.S., Rosqvist, G., Holmlund, P., Wennbom, M. and Karlin, T., (2019). High-resolution bathymetric mapping reveals subaqueous glacial landforms in the Arctic alpine lake Tarfala, Sweden. *Journal of Quaternary Science* 34 (6) pp. 452-462.
- Kirkbride, M. P. (1993). The temporal significance of transitions from melting to calving termini at glaciers in the central Southern Alps of New Zealand. *The Holocene*, 3(3), 232-240.
- Kirkbride, M. P., & Warren, C. R. (1997). Calving processes at a grounded ice cliff. *Annals of Glaciology*, 24, 116-121.
- Kirkbride, M. P., & Warren, C. R. (1999). Tasman Glacier, New Zealand: 20th-century thinning and predicted calving retreat. *Global and Planetary Change*, 22(1), 11-28.
- Komori, J., (2008). Recent expansions of glacial lakes in the Bhutan Himalayas. *Quaternary International*, 184(1), pp.177-186.
- Korup, O., & Tweed, F. (2007). Ice, moraine, and landslide dams in mountainous terrain. *Quaternary Science Reviews*, 26(25), 3406-3422.
- Kraaijenbrink, P. D. A., Shea, J. M., Litt, M., Steiner, J. F., Treichler, D., Koch, I., & Immerzeel, W. W. (2018). Mapping Surface Temperatures on a Debris-Covered Glacier with an Unmanned Aerial Vehicle. *Frontiers in Earth Science*, 6, 64.
- Lea, J.M., Mair, D.W. and Rea, B.R., (2014). Evaluation of existing and new methods of tracking glacier terminus change. *Journal of Glaciology* 220 (60) pp. 323-333.
- Loriaux, T., & Casassa, G. (2013). Evolution of glacial lakes from the Northern Patagonia Icefield and terrestrial water storage in a sea-level rise context. *Global and Planetary Change*, 102, 33-40.
- Lliboutry, L., Morales Arnao, B., Pautre, A., & Schneider, B. (1977). Glaciological problems set by the control of dangerous lakes in Cordillera Blanca, Peru. I. Historical failures of morainic dams, their causes and prevention. *Journal of Glaciology*, 18(79), 239-254.
- Magnusson, J., Jonas, T. and Kirchner, J.W., (2012). Temperature dynamics of a proglacial stream: Identifying dominant energy balance components and inferring spatially integrated hydraulic geometry. *Water Resources Research*, 48(6).

- Mallalieu, J., Carrivick, J.L., Quincey, D.J., Smith, M.W. and James, W.H., (2017). An integrated Structure-from-Motion and time-lapse technique for quantifying ice-margin dynamics. *Journal of Glaciology*, 63(242), pp.937-949.
- Mallalieu, J., Carrivick, J. L., Quincey, D. J., & Smith, M. W. (2020). Calving seasonality associated with melt-undercutting and lake ice cover. *Geophysical Research Letters*. 47(8).
- McFeeters, S. K. (1996). The use of the Normalized Difference Water Index (NDWI) in the delineation of open water features. *International journal of remote sensing*, 17(7), 1425-1432.
- Michel, R., & Rignot, E. (1999). Flow of Moreno Glaciar, Argentina, from repeat-pass Shuttle Imaging Radar images: Comparison of the phase correlation method with radar interferometry. *J. Glaciol*, 45(149), 93-100.
- Minnett, P. J., Smith, M., & Ward, B. (2011). Measurements of the oceanic thermal skin effect. *Deep Sea Research Part II: Topical Studies in Oceanography*, 58(6), 861-868.
- Minowa, M., Sugiyama, S., Sakakibara, D., & Skvarca, P. (2017). Seasonal variations in ice-front position controlled by frontal ablation at Glaciar Perito Moreno, the Southern Patagonia Icefield. *Frontiers in Earth Science*, 5, 1.
- Motyka, R. J., O'Neel, S., Connor, C. L., & Echelmeyer, K. A. (2003). Twentieth century thinning of Mendenhall Glacier, Alaska, and its relationship to climate, lake calving, and glacier run-off. *Global and Planetary Change*, 35(1), 93-112.
- O'Reilly, C.M., Sharma, S., Gray, D.K., Hampton, S.E., Read, J.S., Rowley, R.J., Schneider, P., Lenters, J.D., McIntyre, P.B., Kraemer, B.M. and Weyhenmeyer, G.A., (2015). Rapid and highly variable warming of lake surface waters around the globe. *Geophysical Research Letters*, 42(24), pp.10-773.
- Østrem, G., (1964). Ice-cored moraines in Scandinavia. *Geografiska Annaler*, 46(3), pp.282-337.
- Nesje, A., Dahl, S.O., Thun, T. and Nordli, Ø., (2008). The 'Little Ice Age' glacial expansion in western Scandinavia: summer temperature or winter precipitation?. *Climate dynamics*, 30(7-8), pp.789-801.
- O'Reilly, C.M., Sharma, S., Gray, D.K., Hampton, S.E., Read, J.S., Rowley, R.J., Schneider, P., Lenters, J.D., McIntyre, P.B., Kraemer, B.M. and Weyhenmeyer, G.A., (2015). Rapid and highly variable warming of lake surface waters around the globe. *Geophysical Research Letters*, 42(24), pp.10-773.
- Paul, F., Winsvold, S. H., Kääb, A., Nagler, T., & Schwaizer, G. (2016). Glacier Remote Sensing Using Sentinel-2. Part II: Mapping Glacier Extents and Surface Facies, and Comparison to Landsat 8. *Remote Sensing*, 8(7), 575.
- Peter, H. and Sommaruga, R., (2017). Alpine glacier-fed turbid lakes are discontinuous cold polymictic rather than dimictic. *Inland Waters*, 7(1), pp.45-54.
- Pierre, K.A.S., Louis, V.L.S., Schiff, S.L., Lehnerr, I., Dainard, P.G., Gardner, A.S., Aukes, P.J. and Sharp, M.J., (2019). Proglacial freshwaters are significant and previously unrecognized sinks of atmospheric CO<sub>2</sub>. *Proceedings of the National Academy of Sciences*, 116(36), pp.17690-17695.

- Planck, M., (1901). On the law of distribution of energy in the normal spectrum. *Annalen der physik*, 4(553), p.1.
- Pohjola, V.A. and Rogers, J.C., (1997). Atmospheric circulation and variations in Scandinavian glacier mass balance. *Quaternary Research*, 47(1), pp.29-36.
- Purdie, J., & Fitzharris, B. (1999). Processes and rates of ice loss at the terminus of Tasman Glacier, New Zealand. *Global and Planetary Change*, 22(1), 79-91.
- Richards, J., Moore, R.D. and Forrest, A.L., 2012. Late-summer thermal regime of a small proglacial lake. *Hydrological Processes*, 26(18), pp.2687-2695.
- Rippin, D. M., Carrivick, J. L., & Williams, C. (2011). Evidence towards a thermal lag in the response of Karsaglaciären, northern Sweden, to climate change. *Journal of Glaciology*, 57(205), 895-903.
- Robertson, C. M., Benn, D. I., Brook, M. S., Fuller, I. C., & Holt, K. A. (2012). Subaqueous calving margin morphology at Mueller, Hooker and Tasman glaciers in Aoraki/Mount Cook National Park, New Zealand. *Journal of Glaciology*, 58(212), 1037-1046.
- Robertson, C. M., Brook, M. S., Holt, K. A., Fuller, I. C., & Benn, D. I. (2013). Calving retreat and proglacial lake growth at Hooker Glacier, Southern Alps, New Zealand. *New Zealand Geographer*, 69(1), 14-25.
- Röhl, K. (2006). Thermo-erosional notch development at fresh-water-calving Tasman Glacier, New Zealand. *Journal of Glaciology*, 52(177), 203-213.
- Rouse, W.R., Oswald, C.J., Binyamin, J., Spence, C., Schertzer, W.M., Blanken, P.D., Bussi eres, N. and Duguay, C.R., (2005). The role of northern lakes in a regional energy balance. *Journal of Hydrometeorology*, 6(3), pp.291-305.
- Sabol Jr, D.E., Gillespie, A.R., Abbott, E. and Yamada, G., (2009). Field validation of the ASTER temperature–emissivity separation algorithm. *Remote Sensing of Environment*, 113(11), pp.2328-2344.
- Sakai, A., Nishimura, K., Kadota, T., & Takeuchi, N. (2009). Onset of calving at supraglacial lakes on debris-covered glaciers of the Nepal Himalaya. *Journal of Glaciology*, 55(193), 909-917.
- Sakakibara, D., & Sugiyama, S. (2014). Ice-front variations and speed changes of calving glaciers in the Southern Patagonia Icefield from 1984 to 2011. *Journal of Geophysical Research: Earth Surface*, 119(11), 2541-2554.
- Schaefer, M., Machguth, H., Falvey, M., Casassa, G., & Rignot, E. (2015). Quantifying mass balance processes on the Southern Patagonia Icefield. *The Cryosphere*, 9(1), 25-35.
- Schneider, P., & Hook, S. J. (2010). Space observations of inland water bodies show rapid surface warming since 1985. *Geophysical Research Letters*, 37(22).
- Schmid, M., Hunziker, S. and Wuest, A., 2014. Lake surface temperatures in a changing climate: A global sensitivity analysis. *Climatic change*, 124(1-2), pp.301-315.
- Schomacker, A., & Kj er, K. H. (2008). Quantification of dead-ice melting in ice-cored moraines at the high-Arctic glacier Holmstr mbreen, Svalbard. *Boreas*, 37(2), 211-225.

- Schomacker, A. (2010). Expansion of ice-marginal lakes at the Vatnajökull ice cap, Iceland, from 1999 to 2009. *Geomorphology*, 119(3), 232-236.
- Serreze, M.C. and Francis, J.A., 2006. The Arctic amplification debate. *Climatic change*, 76(3-4), pp.241-264.
- Sharma, S., Blagrove, K., Magnuson, J.J., O'Reilly, C.M., Oliver, S., Batt, R.D., Magee, M.R., Straile, D., Weyhenmeyer, G.A., Winslow, L. and Woolway, R.I., (2019). Widespread loss of lake ice around the Northern Hemisphere in a warming world. *Nature Climate Change*, 9(3), p.227.
- Sinclair, V.A., Mikkola, J., Rantanen, M. and Räisänen, J., (2019). The summer 2018 heatwave in Finland. *Weather*.
- Skvarca, P., Satow, K., Naruse, R., & LEIVA, J. C. (1995). Recent thinning, retreat and flow of Uppsala Glacier, Patagonia. *Bulletin of Glacier Research*, (13), 11-20.
- Somos-Valenzuela, M. A., McKinney, D. C., Rounce, D. R., & Byers, A. C. (2014). Changes in Imja Tsho in the Mount Everest region of Nepal. *The Cryosphere*, 8(5), 1661-1671.
- Steissberg, T. E., Hook, S. J., & Schladow, S. G. (2005). Characterizing partial upwellings and surface circulation at Lake Tahoe, California–Nevada, USA with thermal infrared images. *Remote Sensing of Environment*, 99(1), 2-15.
- Stokes, C. R., Popovnin, V., Aleynikov, A., Gurney, S. D., & Shahgedanova, M. (2007). Recent glacier retreat in the Caucasus Mountains, Russia, and associated increase in supraglacial debris cover and supra-/proglacial lake development. *Annals of Glaciology*, 46, 195-203.
- Stone, P.H. and Carlson, J.H., 1979. Atmospheric lapse rate regimes and their parameterization. *Journal of the Atmospheric Sciences*, 36(3), pp.415-423.
- Sugiyama, S., Skvarca, P., Naito, N., Enomoto, H., Tsutaki, S., Tone, K., ... & Aniya, M. (2011). Ice speed of a calving glacier modulated by small fluctuations in basal water pressure. *Nature Geoscience*, 4(9), 597-600.
- Sugiyama, S., Minowa, M., Sakakibara, D., Skvarca, P., Sawagaki, T., Ohashi, Y., ... & Chikita, K. (2016). Thermal structure of proglacial lakes in Patagonia. *Journal of Geophysical Research: Earth Surface*. 121 (12), 2270-2286.
- Sugiyama, S., Minowa, M. and Schaefer, M., (2019). Underwater ice terrace observed at the front of Glaciar Grey, a freshwater calving glacier in Patagonia. *Geophysical research letters*, 46(5), pp.2602-2609.
- Surdu, C. M., Duguay, C. R., Brown, L. C., & Fernández Prieto, D. (2014). Response of ice cover on shallow lakes of the North Slope of Alaska to contemporary climate conditions (1950–2011): radar remote-sensing and numerical modeling data analysis. *The Cryosphere*, 8(1), 167-180.
- Svenonius, F., Westman, J., Hamberg, A., Gavelin, A. and Enquist, F., (1910). Die Gletscher Schwedens im Jahre 1908 [The Swedish glaciers in the year 1908]: Stockholm, Kungl. boktryckeriet, PA Norstedt oh söner. *Sveriges geologiska undersökning, Series Ca (Avhandlingar och uppsatser i kvarto och folio)*, (5).

- Tonooka, H., 2005. Accurate atmospheric correction of ASTER thermal infrared imagery using the WVS method. *IEEE Transactions on Geoscience and Remote Sensing*, 43(12), pp.2778-2792.
- Tonooka, H. and Palluconi, F.D., (2005). Validation of ASTER/TIR standard atmospheric correction using water surfaces. *IEEE Transactions on Geoscience and Remote Sensing*, 43(12), pp.2769-2777.
- Trenberth, K.E., Fasullo, J.T. and Kiehl, J., (2009). Earth's global energy budget. *Bulletin of the American Meteorological Society*, 90(3), pp.311-324.
- Trenberth, K.E. and Fasullo, J.T., 2010. Tracking Earth's energy. *Science*, 328(5976), pp.316-317.
- Trenberth, K.E. and Fasullo, J.T., (2012). Tracking Earth's energy: From El Niño to global warming. *Surveys in geophysics*, 33(3-4), pp.413-426.
- Truffer, M. and Motyka, R.J., (2016). Where glaciers meet water: Subaqueous melt and its relevance to glaciers in various settings. *Reviews of Geophysics*, 54(1), pp.220-239.
- Trüssel, B. L., Motyka, R. J., Truffer, M., & Larsen, C. F. (2013). Rapid thinning of lake-calving Yakutat Glacier and the collapse of the Yakutat Icefield, southeast Alaska, USA. *Journal of Glaciology*, 59(213), 149-161.
- Tsutaki, S., Sugiyama, S., Nishimura, D., & Funk, M. (2013). Acceleration and flotation of a glacier terminus during formation of a proglacial lake in Rhonegletscher, Switzerland. *Journal of Glaciology*, 59(215), 559-570.
- Tsutaki, S., Fujita, K., Nuimura, T., Sakai, A., Sugiyama, S., Komori, J. and Tshering, P., (2019). Contrasting thinning patterns between lake-and land-terminating glaciers in the Bhutanese Himalaya. *The Cryosphere*, 13(10), pp.2733-2750.
- Vaughan, D.G., J.C. Comiso, I. Allison, J. Carrasco, G. Kaser, R. Kwok, P. Mote, T. Murray, F. Paul, J. Ren, E. Rignot, O. Solomina, K. Steffen and T. Zhang, 2013: Observations: Cryosphere. In: *Climate Change 2013: The Physical Science Basis. Contribution of Working Group I to the Fifth Assessment Report of the Intergovernmental Panel on Climate Change* [Stocker, T.F., D. Qin, G.-K. Plattner, M. Tignor, S.K. Allen, J. Boschung, A. Nauels, Y. Xia, V. Bex and P.M. Midgley (eds.)]. Cambridge University Press, Cambridge, United Kingdom and New York, NY, USA, pp. 317–382, doi:10.1017/CBO9781107415324.012.
- Wang, W., Xiang, Y., Gao, Y., Lu, A. and Yao, T., (2015). Rapid expansion of glacial lakes caused by climate and glacier retreat in the Central Himalayas. *Hydrological Processes*, 29(6), pp.859-874.
- Warren, C. R., Greene, D. R., & Glasser, N. F. (1995). Glaciar Upsala, Patagonia: rapid calving retreat in fresh water. *Ann. Glaciol*, 21, 311-316.
- Warren, C. R., & Kirkbride, M. P. (1998). Temperature and bathymetry of ice-contact lakes in Mount Cook National Park, New Zealand. *New Zealand Journal of Geology and Geophysics*, 41(2), 133-143.
- Warren, C. R., & Kirkbride, M. P. (2003). Calving speed and climatic sensitivity of New Zealand lake-calving glaciers. *Annals of Glaciology*, 36, 173-178.

- Warren, C., & Aniya, M. (1999). The calving glaciers of southern South America. *Global and Planetary Change*, 22(1), 59-77.
- Watanabe, T., Kameyama, S., & Sato, T. (1995). Imja glacier dead-ice melt rates and changes in a supra-glacial lake, 1989-1994, Khumbu Himal, Nepal: Danger of lake drainage. *Mountain Research and Development*, 293-300.
- Watson, C. S., Kargel, J. S., Shugar, D. H., Haritashya, U. K., Schiassi, E., & Furfaro, R. (2020). Mass loss from calving in Himalayan proglacial lakes. *Frontiers in Earth Science*, 7, 342.
- Wessels, R.L., Kargel, J.S. and Kieffer, H.H., (2002). ASTER measurement of supraglacial lakes in the Mount Everest region of the Himalaya. *Annals of Glaciology*, 34, pp.399-408.
- Williams, C. N., Carrivick, J. L., Evans, A. J., & Rippin, D. M. (2016). Quantifying uncertainty in using multiple datasets to determine spatiotemporal ice mass loss over 101 years at kårsaglaciären, sub-arctic sweden. *Geografiska Annaler: Series A, Physical Geography*, 98(1), 61-79.
- Woolway, R.I. and Merchant, C.J., (2019). Worldwide alteration of lake mixing regimes in response to climate change. *Nature Geoscience*, 12(4), 271.